NONLINEAR FINITE ELEMENT MODELLING OF FRP SHEAR-STRENGTHENED PRESTRESSED AND REINFORCED CONCRETE BEAMS

by

MICHAEL KEUORK QAPO

A thesis submitted to

the University of Birmingham

for the degree of

DOCTOR OF PHILOSOPHY

School of Civil Engineering

College of Engineering and Physical Sciences

University of Birmingham

May 2016

ABSTRACT

There is a global pressing need for shear strengthening of existing concrete infrastructure. Fibre reinforced polymer (FRP) composites can be effectively used to enhance the shear strength of existing concrete infrastructure but the factors influencing the shear contribution of FRP strengthening systems are still not well understood. This may be attributable to the complex behaviour of FRP shear-strengthened concrete members. As a result, the existing design guidelines for shear strengthening of concrete structures with FRP reinforcement have not gained wide acceptance as yet.

Extensive studies examining the parameters influencing the behaviour of FRP shear-strengthened concrete members are needed if the strengthened behaviour is to be fully understood. However, the high cost of physically carrying out such studies is usually prohibitive. The Finite Element Method (FEM) provides a cost-effective tool for numerically carrying out such studies. The FEM can be used to model various combinations of geometric and loading conditions. The nonlinear behaviour of FRP shear-strengthened concrete members can be taken into consideration by incorporating appropriate constitutive laws and iterative procedures.

This research provides insight into the shear behaviour of prestressed concrete (PC) and reinforced concrete (RC) girders strengthened in shear with externally bonded FRP laminates or deep embedment FRP bars, respectively. Two finite element models, incorporating a total strain rotating crack model for the concrete, were

developed. In this model, the crack direction changes with the change in the direction of the principal tensile stress. Explicit modelling of the concrete shear behaviour after cracking, e.g. via a shear retention parameter, is therefore not required as the crack plane is always a principal plane with no shear stresses. The developed models were validated using published results. Extensive parametric studies were then carried out to identify the effect of various parameters on the shear behaviour of FRP-strengthened RC and PC beams. The results suggest that FRP shear force enhancement is positively influenced by the increase in concrete compressive strength, FRP ratio and the use of inclined deep embedment FRP bars, but deteriorates with the increase in steel-to-FRP shear reinforcement ratio and change in tendon profile from straight to double-harped. The prestress in tendon, concrete precracking and shape of concrete-to-FRP bond slip model had insignificant influence. The shear span-to-effective depth ratio had a detrimental effect on shear force enhancement, except for rectangular PC girders shear-strengthened with anchored FRP laminates, where the shear force enhancement was increased by increasing the shear span-to-effective depth ratio. In general, increasing the effective beam depth resulted in an increase in shear force enhancement; however, a strong size effect was predicted for I-shaped PC girders shear-strengthened with FRP laminates, especially for girders having an effective depth of 457 mm or more.

Most importantly, the numerical results were utilised to develop a new design model for RC beams shear-strengthened with deep embedment FRP bars. Unlike current design models, the proposed design model accounts for the effect of the main influencing parameters, and hence it showed considerable accuracy.

DEDICATION

This thesis is dedicated to:

The memory of my mother

My father

My brothers and their families…

ACKNOWLEDGEMENTS

Firstly, I would like to express my sincere gratitude and appreciation to my lead supervisor Dr Samir Dirar for his guidance, advice and endless enthusiasm for this research. I am glad that I have been given the opportunity to learn from him.

Thanks are also due to my co-supervisor Dr Jian Yang as well as Prof Andrew Chan for their help.

To all my friends and colleagues from inside and outside the UK, thank you. An additional thank you goes to Wendy Sindall for proofreading this thesis.

Many thanks and appreciation also goes to the financial support of KRG.

Last, but by no means least, I would like to express my deepest gratitude to my family for their endless love, encouragement, help and support over the years. You all made so many things possible, thank you!

Michael

TABLE OF CONTENTS

LIST OF FIGURES

LIST OF TABLES

ABBREVIATIONS AND NOTATION

Abbreviations

AFRP	Arapree Fibre Reinforced Polymer
BPE	Bertero-Popov-Eligehausen
CFRP	Carbon Fibre Reinforced Polymer
DE	Deep Embedment
EB	Externally Bonded
ETS	Embedded Through-Section
FE	Finite Element
FEM	Finite Element Method
FRP	Fibre Reinforced Polymer
MCFT	Modified Compression Field Theory
NSM	Near-Surface Mounted
PC	Prestressed Concrete
RC	Reinforced Concrete
XFEM	eXtended Finite Element Method

Notation

A_{f}	Cross-sectional area of FRP bar
A_{fs}	Total area of FRP plies located within spacing s_{f}
A_{v}	Total area of steel stirrup legs
a	Shear span of the beam

a/d	Shear span-to-effective depth ratio
a_{g}	Maximum aggregate size of concrete mix
b_{f}	Width of the FRP sheet
b_{w}	Web width of the beam
C	Compression force
c_0	Empirical constant parameter can be taken as 0.2
D	Constant parameter can be found from trial and error
d	Effective depth
d_{b}	FRP bar diameter
d_{f}	Effective depth of FRP sheets
d_{fe}	Effective shear depth
E_{c}	Elastic modulus of concrete
E_{f}	Elastic modulus of FRP reinforcement
E_{fd}	Design elastic modulus of FRP reinforcement
E_{ps}	Elastic modulus of tendons
E_{s}	Elastic modulus of steel reinforcement
F_{ult}	Applied pull-out force
f	Force vector
f_1	Average principal tensile stress in concrete
f_2	Average principal compressive stress in concrete
f_{c}	Concrete compressive strength at a given strain ε_{c}
f_{c}'	Cylinder concrete compressive strength
f_{ctk}	Characteristic concrete tensile strength
f_{cu}	Cube compressive strength of concrete

f_{ext}	External force vector
f_{int}	Internal force vector
f_{ps}	Stress in tendon at a given strain $\varepsilon_{\mathrm{ps}}$
f_{pu}	Ultimate tensile strength of prestressed tendon
f_{py}	Yield stress of prestressed tendon
f_{sx}	Average stress of steel reinforcement in x-direction
f_{sxcr}	Stress of steel reinforcement in x-direction at crack location
f_{sz}	Average stress of steel reinforcement in z-direction
f_{szcr}	Stress of steel reinforcement in z-direction at crack location
f_{t}	Concrete uniaxial tensile strength
f_{u}	Ultimate strength of steel reinforcement
f_{x}	Average applied stress in x-direction
f_{y}	Yield stress of steel reinforcement
f_{yx}	Yield stress of steel reinforcement in x-direction
f_{yz}	Yield stress of steel reinforcement in z-direction
f_{z}	Average applied stress in z-direction
$f(S_{\mathrm{m}})$	Stress in the CFRP bar at slip corresponding to the bond strength
$G_{\mathrm{f}}^{\mathrm{I}}$	Fracture energy of concrete in tension
$G_{\mathrm{f,i}}^{\mathrm{II}}$	In-plane shear interfacial fracture energy
g	Out-of-balance force vector
g_0	Force vector of the initial unbalance
g_{i}	Out-of-balance force vector at certain iteration
h	Strengthened depth of the beam with FRP bars

h_c	Crack bandwidth
K_{i}	Stiffness matrix at certain iteration
k	Factor controls the post-peak part of compressive stress-strain curve
k_1	Factor accounts for the concrete strength effect on effective bond length
k_2	Factor accounts for the wrapping type on effective bond length
k_{L}	Reduction coefficient for the anchorage length of FRP bars
k_{S}	Reduction coefficient for the presence of internal steel stirrups
k_{v}	Bond reduction factor for FRP laminates
L	Span of the beam
L_{e}	Effective bond length of FRP laminates
L_{eff}	Minimum anchorage length required for FRP bars
$l_{\mathrm{b,max}}$	Required anchorage length of FRP bars
$l_{\mathrm{t,max}}$	Required anchorage length of FRP laminates
M	Maximum moment acting on the beam
M_{CR}	Critical bending moment at shear failure
M_{FL}	Full flexural capacity of the cross-section
n	Number of FRP plies
n_{s}	Parameter accounts for the type of wrapping scheme
P	Applied force
p	Parameter controls the descending branch of the bond-slip relationship
R	Reaction force
S	Concrete-to-FRP slip
S_0	Slip corresponding to the peak bond stress
S_{m}	Slip corresponding to the bond strength of FRP bars

S_{u}	Ultimate slip
S_{x}	Crack control characteristics of the reinforcement in x-direction
S_{z}	Crack control characteristics of the reinforcement in z-direction
S_{θ}	Spacing of inclined cracks
s	Stirrups spacing
s_{b}	Spacing between FRP bars
s_{f}	Spacing between FRP sheets
T	Tension force
t_{f}	Thickness of one FRP ply
u	Displacement vector
u^{c}	Predefined certain displacement increments
u_{x}	Displacement in x-direction
u_{y}	Displacement in y-direction
u_{z}	Displacement in z-direction
V	Maximum shear force acting on the beam
V_{a}	Aggregate interlock
V_{cc}	Shear stress in uncracked concrete
V_{d}	Dowel action of longitudinal reinforcing bars
V_{Exp}	Experimental shear force capacity
V_{FE}	Finite element predicted shear force capacity
V_{f}	Shear force contribution of FRP reinforcement
$V_{\mathrm{f,Eq6{\cdot}6}}$	Predicted FRP shear contribution using modified equation
$V_{\mathrm{f,Mofi}}$	Predicted FRP shear contribution according to Mofidi et al. (2012)
$V_{\mathrm{f,TR55}}$	Predicted FRP shear contribution according to TR55 (2012)

$V_{\mathrm{f,exp}}$	Experimental shear contribution due to the FRP
V_{p}	Vertical component of prestressing force in tendons
V_{R}	Summation of shear resistance components in beam-action mechanism
V_{rc}	Residual tensile stresses in concrete after cracking
V_{s}	Shear force contribution of the steel stirrups
W	Crack width
W_{eff}	Effective width over which the FRP bars may act
w_{f}	Width of FRP sheet
x, y, z	Cartesian coordinates
α	Inclination of main fibres' direction to the beam's longitudinal axis
α_{a}	Curve fitting parameter for the ascending branch of the BPE model
α_{s}	Inclination of compression struts with respect to longitudinal axis
β	Inclination of main fibres to the line perpendicular to the beam's axis
$\beta_{\sigma_{\mathrm{cr}}}$	Parameter for concrete softening in compression due to lateral cracking
γ_{A}	Partial safety factor for the adhesive material
γ_{xz}	Average shear strain relative to x-z axes
ε	Strain
ε_1	Average principal tensile strain in concrete
ε_2	Average principal compressive strain in concrete
ε_{c}	Concrete compressive strain
$\varepsilon_{\mathrm{c}}'$	Strain corresponding to the concrete cylinder compressive strength
$\varepsilon_{\mathrm{fd}}$	Design ultimate strain of FRP reinforcement
$\varepsilon_{\mathrm{fe}}$	Effective tensile strain in FRP reinforcement
$\varepsilon_{\mathrm{fe}}^{*}$	Parameter obtained using nonlinear regression and equal to $\varepsilon_{\mathrm{fe}} W_{\mathrm{eff}} / s_{\mathrm{b}}$

ε_{fu}	Ultimate tensile strain of FRP reinforcement
$\varepsilon_{l,1}$	Tensile damage in the first lateral direction
$\varepsilon_{l,2}$	Tensile damage in the second lateral direction
ε_{lat}	Average lateral damage
ε_{ps}	Strain in prestressed tendon
ε_{pu}	Ultimate strain in prestressed tendon
ε_{x}	Average strain in x-direction
ε_{z}	Average strain in z-direction
Δ_{Exp}	Experimental deflection
Δ_{FE}	Finite element predicted deflection
Δ_{T}	Distributed tensile forces along longitudinal steel reinforcement
Δu	Total displacement increment
Δu_0	Displacement vector of the initial prediction
Δu^c	Constrained displacements increment vector
Δu^u	Unconstrained displacements increment vector
δg_i	Change in out-of-balance force vector corresponding to δu_i
δu	Iterative displacement increment
δu_i	Iterative displacement increment at certain iteration
θ	Principal compressive stress direction
λ_0	Factor accounts for the shear reinforcement influence
ν	Shear stress
ν_{ci}	Shear stress on crack surfaces
ξ, η, ζ	Natural coordinates.
ρ_0	Empirical coefficient

ρ_f	FRP reinforcement ratio
ρ_s	Shear reinforcement ratio
ρ_x	Reinforcement ratio in x-direction
ρ_z	Reinforcement ratio in z-direction
σ	Stress
τ	Bond stress at a specific slip S
τ_b	Average bond stress over the anchorage length
τ_m	Bond strength of the FRP bar
τ_{max}	Bond strength of the EB CFRP sheet
$\emptyset$	Inclination of steel stirrups
$\emptyset(\lambda)$	Reduction factor for shear stress at failure
Ψ_f	Reduction factor for the shear contribution of FRP laminates

CHAPTER 1: INTRODUCTION

1.1 Background

Structural deterioration of existing concrete infrastructure is a serious problem faced by both developed and developing nations (Middleton, 1997; Nanni et al., 2004; Valerio et al., 2009). The underlying causes of this issue include heavier traffic loads, corrosion of the internal steel reinforcement, structural deterioration due to ageing, poor initial design, more stringent assessment codes, aggressive exposure conditions and natural or manmade extreme events (Valerio et al., 2009; Petty et al., 2011; Dirar et al., 2013b). In the United Kingdom, it has been estimated that there are approximately 10,000 bridges on the strategic motorway network, the majority of which are reinforced concrete (RC) or prestressed concrete (PC) structures, of which a considerable number need to be strengthened or replaced (Middleton, 2004). The estimated cost of assessing and strengthening strength-deficient structures in the United Kingdom is in excess of £4 billion (Middleton, 1997). In Europe, it has been estimated that the cost of replacing structurally deficient bridges, of which concrete bridges represent a significant percentage, is about €400 billion (Holicky et al., 2010). The international significance of the issue is further emphasised by the fact that one in nine of the 607,380 bridges in the United States of America have been rated as structurally deficient and $20.5 billion would need to be invested annually to eliminate the bridge deficient backlog by 2028 (Advisory Council of ASCE, 2013).

This high investment is partially attributed to the fact that the traditional methods of repair are labour intensive and/or time consuming. On the other hand, costs associated with bridge replacement (partially or fully) are usually unaffordable due to the associated high cost and traffic delays (Nanni et al., 2004). Imposing limits on traffic loads as a possible solution, is temporary and does not fulfil current societal needs (Schnerch, 2001). There is thus a pressing need for economic and efficient strengthening solutions.

Since it was introduced to civil engineering applications in the 1970s (Moslehy, 2010), the use of fibre reinforced polymer (FRP) composites for strengthening concrete members has been favoured over classical strengthening techniques, mainly due to their high strength-to-weight ratio, corrosion resistance, durability and ease of use, and consequently, has grown dramatically (Chaallal et al., 2011). FRP composite materials consist of fibres (e.g. carbon, glass or aramid) in a polymeric resin called the matrix. The fibres are stronger than the resin, and hence they are mainly responsible for resisting the stress applied on the composite material. The resin is used to protect and bind the fibres together, transfer the stress when adjacent fibres rupture and provide stiffness in the directions perpendicular to the fibres' direction (Kaw, 2006).

FRP flexural strengthening is well established whereas FRP shear strengthening is not fully understood. In addition to the fact that FRP flexural strengthening has received much more attention, the incomplete understanding of FRP shear strengthening may be attributable to the complex behaviour of FRP shear-

strengthened members and the significant number of influencing parameters (Teng et al., 2004; Belarbi et al., 2011; You et al., 2011). For shear strengthening, FRP composites have been mainly used in the form of externally bonded (EB) sheets or near surface mounted (NSM) bars (Mofidi et al., 2012). Although FRP composites can be easily applied by these two methods, the shear strength enhancement that can be provided by them is negatively affected by premature debonding (at a stress level of 20-30% of the FRP ultimate tensile strength), and accessibility and surface condition of the beam (You et al., 2011; Dirar et al., 2013b). Therefore, Valerio and Ibell (2003) developed the deep embedment (DE) technique, also known as the embedded through-section (ETS) (Chaallal et al., 2011; Mofidi et al., 2012; Barros and Dalfré, 2013; Qin et al., 2014; Breveglieri et al., 2015), which overcomes the shortcomings of the EB and NSM methods. The main advantage of the DE technique is that the DE bars connect the tension and compression chords, allowing truss action to take place. This is difficult in the case of EB or NSM unless they are well-anchored or fully wrapped. However, the only concern is about damaging the internal steel reinforcement during drilling of holes prior to the installation of FRP bars.

Although physical testing provides valuable information on the overall performance of beams and the local behaviour of constituent materials, high costs associated with the production of practical-scale specimens often restrict the evaluation of the parameters influencing the shear behaviour of strengthened structures (You et al., 2011). The Finite Element Method (FEM) can provide a cost-effective tool for carrying out extensive parametric studies on FRP shear-strengthened structures. However, numerical modelling of FRP shear-strengthened concrete members has not received

as much attention as physical testing, probably due to the difficulty of modelling the shear behaviour of concrete.

1.2 Scope of the Study

In the absence of widely accepted design guidelines for shear strengthening of concrete structures with FRP reinforcement (Belarbi and Acun, 2013), the FEM may be used to predict the behaviour and capacity of such structures. In the present study, finite element (FE) models incorporating appropriate constitutive relationships were developed using the commercial FE package DIANA Version 9.4.4 (DIANA user's manual, 2012) to predict the behaviour of PC and RC beams strengthened in shear with EB FRP sheets or DE FRP bars respectively. The predictions of the developed FE models were validated using experimental data from the published literature. The developed FE models were then used to carry out parametric studies to investigate the effect of influencing parameters on the shear force capacity and shear strength enhancement.

1.3 Research Objectives

The objectives of this study are:

1- To develop and validate FE models capable of simulating the behaviour of PC and RC beams shear strengthened with EB CFRP sheets or DE FRP bars respectively;

2- To use the FE models to examine the effect of the main parameters influencing shear behaviour on the shear force capacity and shear strength enhancement;

3- To examine the thoroughness of current design models for EB and DE FRP shear reinforcement (i.e. whether such models consider the main parameters influencing shear behaviour); and

4- To develop a new design equation for RC beams strengthened in shear with DE FRP bars.

1.4 Thesis Layout

Chapter Two reviews the literature related to this study. It addresses shear behaviour of unstrengthened and FRP-strengthened concrete beams, the major findings of relevant experimental investigations, shear modelling approaches, existing shear strengthening techniques and the most common design guidelines for FRP shear-strengthening. Chapter Three provides a brief introduction to the FEM, methods used for modelling the constituent materials of RC and PC beams and the main findings of relevant FE studies.

Chapter Four deals with the development and validation of the FE models. A brief description of the experimental works used for validating the developed FE models is also given in this chapter.

In Chapter Five, two parametric studies are presented for PC girders (with and without internal steel stirrups) strengthened in shear with EB FRP laminates. The FE predicted shear force gain due to EB FRP laminates is compared with the relevant results using the ACI 440.2R (2008) and TR55 design model (2012).

Chapter Six presents the parametric study carried out on RC beams strengthened in shear with DE FRP bars. A comparison between the FE-predicted shear force contribution due to DE FRP bars with the predictions of the TR55 design model (2012) and the design model developed by Mofidi et al. (2012) is presented. This chapter also deals with the development of a new design equation for determining the shear force contribution due to DE FRP bars.

Chapter Seven summarises the findings of this research and presents suggestions for future research. Finally, Appendix A presents the output of the nonlinear regression analysis used to develop the proposed design equation.

1.5 List of Publications

1.5.1 Journal Papers

1- Qapo, M., Dirar, S., Yang, J. and Elshafie, M. (2015) Nonlinear Finite Element Modelling and Parametric Study of CFRP Shear-Strengthened Prestressed Concrete Girders. Construction and Building Materials, 76: 245-255.

2- Qapo, M., Dirar, S., Jemaa, Y. (2016) Finite Element Parametric Study of Reinforced Concrete Beams Shear-Strengthened with Embedded FRP Bars. Composite Structures, 149: 93-105.

1.5.2 Conference Papers

1- Qapo, M., Dirar, S. and Chan, A.H.C. (2014) Nonlinear Finite Element Modelling of Prestressed Concrete Girders Strengthened in Shear with CFRP Reinforcement. In Proceedings of the 4th fib Congress. Mumbai, 10-14 February.

2- Qapo, M., Dirar, S., Yang, J. and Elshafie, M. (2015) Numerical Modelling of CFRP Shear-Strengthened Prestressed Concrete Beams. In Proceedings of the 7th Biennial ACIC Conference. Cambridge, 9-11 September.

CHAPTER 2: STATE-OF-THE-ART

2.1 Introduction

The development of an accurate FE model for FRP shear-strengthened beams requires an understanding of the shear behaviour of beams prior and after strengthening as well as the main factors that influence overall shear behaviour. Therefore, this chapter presents a shear behaviour review of the unstrengthened and strengthened RC and PC beams in addition to the research work that has been done so far and gaps in the knowledge in this field of study.

2.2 Shear Behaviour of RC and PC Beams without Web Reinforcement

Understanding shear behaviour of beams is essential because, unlike flexural failure which is designed to be ductile, shear failure is known to be more complicated, brittle and catastrophic in nature (Taylor, 1974). Therefore, concrete beams are designed to have greater shear strength than flexural strength at any point along the span of the beam.

The work conducted by Kani (1964, 1966) revealed that under further loading after the initiation of cracks, an RC beam turns into a comb-like structure. This structure is represented by vertical concrete teeth which develop in the tensile zone due to flexural cracks, whereas the so-called backbone of the comb, in which the concrete

teeth are anchored to it, is represented by the compressive zone as shown in Figure 2-1. It can be seen from this figure that the concrete teeth work as small cantilevers loaded horizontally by distributed tensile forces along the bonded steel reinforcement bars, ΔT.

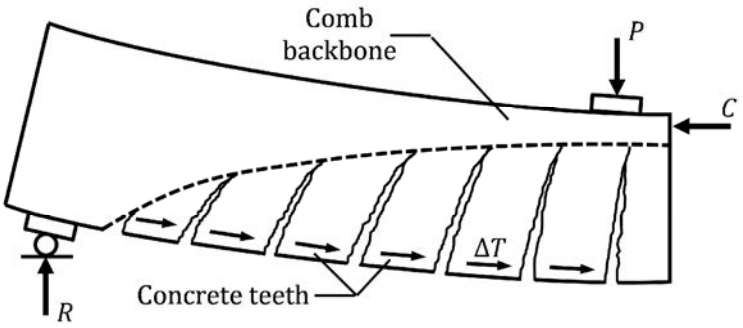

Figure 2-1: Concrete teeth in the comb-like structural system (Kani, 1964)

According to Kani's work (1964, 1966), the comb-like structural system has two different mechanisms, namely the beam-like (or beam-action) mechanism and the tied arch (arch-action) mechanism, depending whether the capacity of the concrete teeth is exceeded or not. The former mechanism (i.e. the beam-action) governs if the concrete teeth capacity is not exceeded, whilst the arch-action mechanism governs when the concrete teeth capacity is exceeded.

Figure 2-2 illustrates the variation in the capacity line of concrete teeth (i.e. the capacity provided by the beam-action mechanism) and the capacity curve of remaining arch (i.e. the capacity provided by the arch-action mechanism). The graph was extracted from work carried out by Kani (1964) and relates the ratio between M_{CR} and M_{FL}, respectively the critical bending moment at shear failure and the full

flexural capacity of the cross-section, to the shear span-to-effective depth ratio (a/d) of the beam. The shear span (a) may be defined by the ratio M/V where M is the maximum moment and V is the maximum shear force acting on the beam. Accordingly, the shear span of a beam with a uniformly distributed load may be calculated as $a = L/4$ where L is the span of the beam (Kani, 1966).

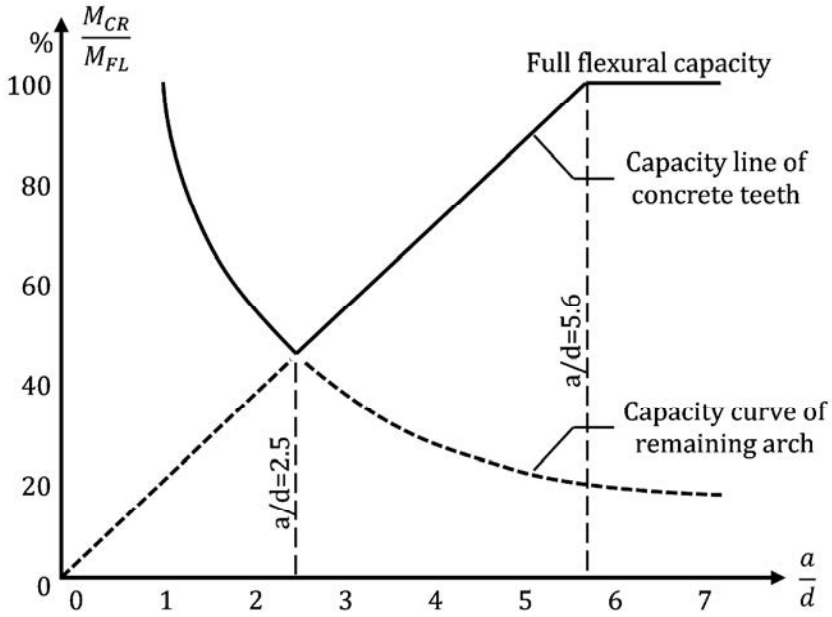

Figure 2-2: Kani's valley graph (Kani, 1964)

As can be seen in Kani's valley graph, the capacities of concrete teeth and remaining arch form three distinct zones of a/d ratio. The characteristics of each zone are:

1. *(1 < a/d < 2.5)*: The arch capacity is considerably higher than the capacity provided by concrete teeth for this range of a/d ratio; therefore the transformation from the beam-action to arch-action takes place under further loading. Hence, the failure occurs when the remaining arch capacity is exceeded.

2. *(2.5 < a/d < 5.6)*: In this range of a/d ratio, the capacity of concrete teeth is higher than the arch capacity and the failure occurs when the capacity of the concrete teeth is exceeded. A sudden collapse is expected in this region due to the brittle tensile failure of the concrete teeth as the arch capacity is lower than the applied load.

3. *(5.6 < a/d)*: For beams having a/d ratio of 5.6 and beyond, only a flexural failure is governing as the full flexural capacity of the cross-section is reached first. Therefore, a failure due to exceeding the capacity of the concrete teeth is not possible.

2.2.1 Shear Resistance Mechanisms

As mentioned in the early investigations (e.g. Kani, 1964; Taylor, 1974), the RC and PC beams can explicitly resist shear after cracking by two distinctively different mechanisms, the beam-action and the arch-action. The overall shear resistance contribution governed by each mechanism is dependent on the associated compatibility of deformations (Jeong and Kim, 2014). In the following subsections, the individual components of the shear transfer associated with the beam-action and the arch-action are given and discussed.

2.2.1.1 Beam Action

This shear resistance mechanism is predominant in RC and PC beams having a/d ratios between 2.5 to 5.6. According to the ASCE-ACI Committee 426 (1973) and ASCE-ACI Committee 445 (1998), the components of shear transfer are various in

the case of the beam-action mechanism. They can be clarified using the idealized free body diagram given in Figure 2-3 of a beam with a critical diagonal shear crack. Based on Figure 2-3, the shear transfer components due to the beam-action mechanism are as follows (ASCE-ACI Committee 426, 1973; Taylor, 1974):

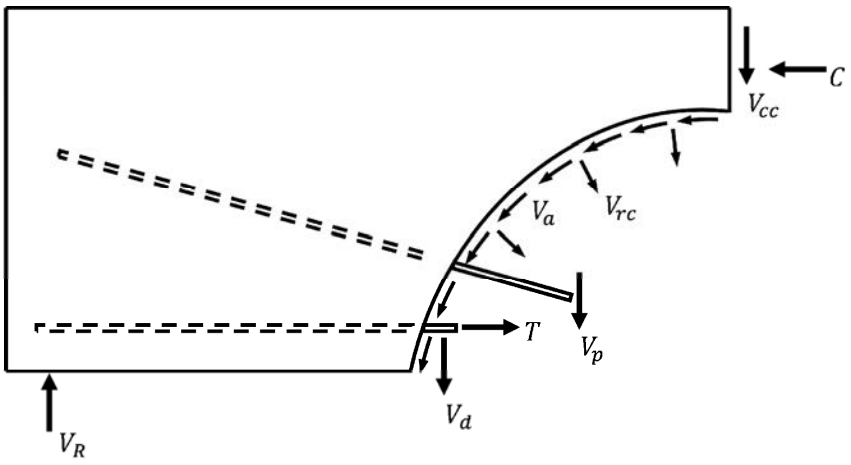

Figure 2-3: Shear resistance in beam-action mechanism

1- *Shear stress in uncracked concrete,* V_{cc}: This represents the shear stresses that can be transferred by uncracked concrete beams or the uncracked concrete portions of cracked concrete beams (i.e. the concrete in compression zone). The shear resistance provided by this mechanism is dependent upon the depth of the uncracked concrete. Its shear contribution was measured by Taylor (1974) using surface strains and found to be 20% to 40%. In the case of slender beams after cracking, the compression zone contribution to shear is insignificant as the depth is relatively small.

2- *Residual tensile stresses in concrete after cracking,* V_{rc}: It is well known that the loss of concrete tensile strength after cracking (i.e. concrete softening)

does not occur suddenly because even after cracking, tensile forces can be transmitted via small bridges of concrete pieces across the crack. These concrete bridges transmit the tensile forces when the width of crack is not greater than 0.15 mm (ASCE-ACI Committee 445, 1998). This shear resistance mechanism is normal to the crack plane.

3- *Aggregate interlock (or interface shear transfer),* V_a: Though the cracking takes place normal to the direction of principal tensile stresses where no shear stresses are expected, the redistribution of internal forces after cracking results in a tendency to slip along the crack interface. The tangential slippage resistance provided by the rough interfaces formed on the two faces of cracks gives the concrete the ability to transfer shear forces across the crack plane. This phenomenon has been noticed particularly in normal concrete strength members, where the aggregates protrude from the crack plane. The shear resistance provided by this phenomenon is dependent on the size of aggregate used in the concrete mix as well as the crack width. The magnitude of this shear resistance was found to be between 33% and 50% and it increases with the increase in aggregate size, whilst it reduces with the increase in crack width (Taylor, 1974).

4- *Dowel action of longitudinal reinforcing bars,* V_d: The intersection of a diagonal shear crack with a longitudinal steel bar results in a resistance to the shearing displacements which, in turn, produces tension forces to split the concrete directly beneath the bar. Therefore, the aforementioned shear resistance mechanism is a function of the amount of longitudinal reinforcement (i.e.

stiffness of longitudinal reinforcement), distribution of longitudinal reinforcement along the depth of the beam and tensile strength of the concrete cover surrounding longitudinal reinforcement. Around 15% to 25% of the applied shear force can be resisted by this mechanism (Taylor, 1974).

5- *The vertical component of prestressing force in tendons,* V_p: The presence of prestressing force in draped tendons provides an additional way of transmitting shear forces when compared to the traditional RC beams, which is represented in the vertical component of prestressing force as shown in Figure 2-3. Furthermore, the prestressing force prevents the formulation of shrinkage cracks and delays the initiation of web cracks, and hence it enhances the shear behaviour of PC beams (Schumacher, 1961).

2.2.1.2 Arch Action

For RC and PC beams having small a/d ratios (i.e. less than 2.5), shear forces can be directly transferred from the point of applied load into the nearest reaction by arch action mechanism, where the inclined compression strut, which is responsible for shear transfer, is coupled with the tie (i.e. the longitudinal tension reinforcement) which provides a resistance to the horizontal component of the inclined shear force as depicted in Figure 2-4.

This shear resistance mechanism is largely dependent on the compression zone depth of the beam; thus, the mechanism becomes more dominant as the a/d ratio decreases. Furthermore, it requires an essential horizontal support which may be

provided by the anchored longitudinal tension reinforcement (Park and Paulay, 1975).

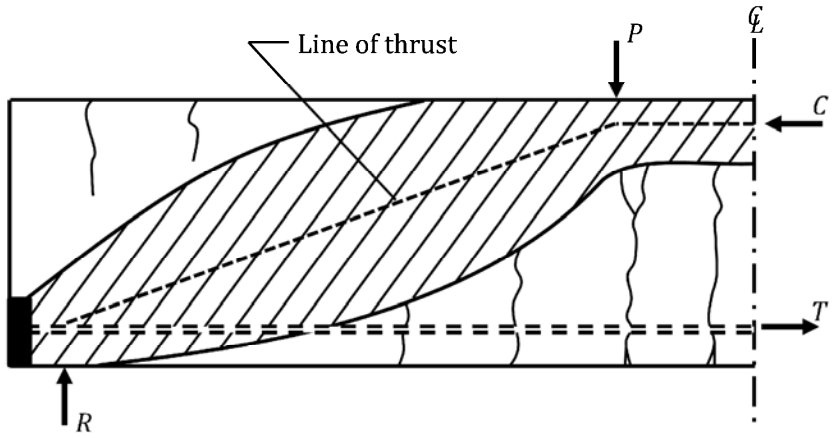

Figure 2-4: Shear resistance in arch action mechanism (Park and Paulay, 1975)

2.2.2 Factors Influencing Shear Behaviour

In addition to the a/d ratio, which plays a main role in changing the shear resistance mechanism of beams, shear behaviour of RC and PC beams is significantly influenced by the following factors (Taylor, 1974; Kesse, 2003; Punmia et al., 2007):

1- *Concrete strength*: The increase in concrete grade up to a certain limit results in a corresponding increase in the shear strength of beams. Though the importance of concrete grade becomes very pronounced in the compression zone after aggregate interlock breakdown, it also has a significant influence on the tensile strength, which in turn increases cracking load and dowel action resistance. Furthermore, it enhances the resistance of aggregate interlock requiring strong aggregates to be used in the concrete mix to prevent the development of smooth-sided cracks, as is the case in high-strength concrete.

2- *Percentage and grade of longitudinal tensile reinforcement*: Beams provided with low longitudinal tensile reinforcement ratios fail at lower shear stresses than other beams with adequate ratios. This may be attributed to the development of wider and longer flexural cracks at lower loads, which in turn reduces the compression zone and interface shear transfer. Furthermore, the reduction in the longitudinal tensile reinforcement ratio results in a corresponding reduction in the dowel action, due to the decrease in longitudinal reinforcement stiffness. For the effect of longitudinal reinforcement grade, it is well known that the use of a higher grade of steel leads to a reduction in the steel ratio required. Hence, it reduces the shear resistance of the beam (Punmia et al., 2007).

3- *Percentage of longitudinal compression reinforcement*: The results related to this parameter are contradictory. According to Kesse (2003), the effect of compression reinforcement ratio is not clear, whereas Punmia et al. (2007) suggested that the shear resistance increases with the increase in compression reinforcement percentage, which might be attributed to the enhancement in the concrete compression zone (Gale and Ibell, 2000).

4- *Axial force*: The influence of axial force corresponds to the change in diagonal cracking angle. The presence of axial compressive force at the beam's ends, due to prestressing force in tendons or applied loads, increases shear strength and cracking load of the beam, whereas shear strength and cracking load are decreased when axial tensile force is applied.

5- *Cross-section*: In comparison with rectangular beams having the same effective depth and web width, T-beams provide a better shear resistance. This can be attributed to the additional compression zone due to the beam's flange, and its magnitude depends on the dimensions of the flange.

2.3 Effect of Shear Reinforcement

It would not be safe or economical to design RC and PC beams in shear by depending only on the shear resistance provided by concrete; therefore, a minimum amount of shear reinforcement is recommended in codes of practice (Nilson, 1987).

Transverse shear stirrups resist shear forces by bridging shear cracks. The contribution takes place when a diagonal crack in the concrete crosses a shear stirrup by redistributing the internal forces which form after cracking. This contribution can be observed via a sudden development of tensile strains in the stirrups. The presence of shear stirrups can either delay or prevent the shear failure from taking place. The magnitude of the shear resistance provided by transverse reinforcement is dependent upon the yield strength, cross-sectional area and spacing between the steel stirrups.

In addition to its direct shear contribution mentioned above, shear stirrups provide a confinement to the concrete locating between the stirrups. They also can maintain the shear contribution of aggregate interlock by limiting the growth of the width of inclined cracks (results in the cracks to be more distributed along shear span), and

preventing the penetration of these cracks into the compression zone of the beam. Furthermore, it can significantly enhance the role of dowel action in shear resistance, because the stirrups can work as restraining points to hold the longitudinal reinforcement in place and prevent the tension forces from splitting the concrete cover. On the other hand, the shear capacity and the corresponding deflection of beams with internal shear stirrups is much higher than beams without internal shear stirrups, and the majority of shear resistance is carried by shear stirrups due to the wider crack openings in these beams corresponding to larger deflections near failure load. Therefore, the shear contribution due to the aggregate interlock and dowel action together as a percentage of the shear capacity was considerably reduced as reported by Swamy and Andriopoulas (1974), where the contribution was reduced from about 50-90% in beams without shear stirrups to about 30% in similar beams having web reinforcement.

Despite the provision of shear stirrups enhancing the ductility of the beam, it may not necessarily lead to a change in the mode of failure from a brittle to a ductile type of failure; and collapse may occur without adequate warning unless the flexural capacity of the beam is exceeded first (Kotsovos, 1987).

2.4 Size Effect

Due to cost and laboratory equipment limitations, the majority of experimental work on shear failure in concrete beams has been carried out on scaled beams rather than full-scale beams. Since all codes of practice are based on the results obtained from

these tests, then the effect of beam size on shear behaviour has been a field of interest.

2.4.1 Beams without Shear Reinforcement

One of the earliest research work conducted on the effect of beam size was by Kani (1967) for rectangular beams without shear reinforcement. The studied parameters were the overall depth (namely, 6, 12, 24 and 48 in) and the width (namely, 6 and 24 in) of beam. The results showed a significant influence of beam depth on the nominal shear stress at failure, which was considerably reduced when the beam depth was increased from 6 in to 48 in. However, Kani suggested a 40% reduction in the safety factor for the nominal shear stress results obtained from smaller beams, due to the lack of a conventional code formula that considers the effect of beam depth. Unlike beam depth, the influence of beam width was insignificant.

Taylor (1974) has suggested that loss of shear strength due to increase in beam size can be attributed to the fact that the aggregate size used in the concrete mix does not change proportionally with the increase in beam size. In other words, the roughness of cracks, which is responsible for aggregate interlock mechanism, does not increase proportionally with the increase in beam size. According to Walraven (1978) (cited in Walraven and Lehwalter, 1994, p.586), this conclusion does not seem valid for all cases as size effect exists even in light-weight concrete beams, in which the cracks tend to pass through the aggregate particles used in the concrete mix; therefore, it leads to form smoother crack faces. Hence, the shear contribution of aggregate interlock is small and can be ignored.

However, Walraven (1978) (cited in Walraven and Lehwalter, 1994, p.587) had compared crack patterns of beams having different depths at the same level of nominal shear stress and found that there is a positive proportional relationship between crack propagation rate (i.e. energy-release rate from the beam into cracking zone as the extension of cracking zone takes place) and size of the beam.

Based on the analysis of 296 test results from the published literature, Bažant and Kim (1984) found that the relation between the reduction in shear stress at failure and depth of the beam is nonlinear. Furthermore, the size effect became too strong when it was implied by linear elastic fracture mechanics. From these test results, a reduction factor of shear stress at failure ($\emptyset(\lambda)$) was derived using nonlinear fracture mechanics, given by:

$$\emptyset(\lambda) = \left(1 + \frac{d}{\lambda_0 a_g}\right)^{-1/2} \quad (2\text{-}1)$$

in which, d is effective depth of beam, a_g is maximum aggregate size of concrete mix and λ_0 is an empirical constant parameter. The formula given in Equation 2-1 was found to be applicable to account for the size effect in PC beams without web reinforcement (Bažant and Cao, 1986).

Later, Bažant and Sun (1987) improved the previously proposed formula, i.e. Equation 2-1, by including an additional expression to take into account the effect of maximum aggregate size distinctly. The modified formula was given by:

$$\emptyset(\lambda) = \left(1 + \left(\frac{c_0}{a_g}\right)^{1/2}\right)\left(1 + \frac{d}{\lambda_0 a_g}\right)^{-1/2} \quad (2\text{-}2)$$

where, c_0 is an empirical constant parameter and can be taken as 0.2 in. A total of 461 test results from the published literature were used to calibrate the proposed formula.

On the other hand, Collins et al. (2008) suggested that size effect is more related to the spacing between diagonal shear cracks than the depth of the beam. The spacing between the diagonal shear cracks was found to be greater in the case of larger beams, because the ability of longitudinal reinforcement in controlling crack spacing reduces as the beam depth increases, due to increase in the distance between the longitudinal reinforcement and mid-height of the beams (Zakaria et al., 2009). This in turn results in the development of wider diagonal shear cracks. However, Collins et al. (2008) reported that the distribution of longitudinal reinforcement along the overall beam depth can reduce both crack spacing and crack width, and thus it enhances the shear strength of larger beams.

2.4.2 Beams with Shear Reinforcement

The study carried out by Bažant and Sun (1987) aimed to extend the formula given in Equation 2-1 to include the influence of shear reinforcement, in addition to the effect of maximum aggregate size as mentioned in Section 2.4.1. The study showed that the influence of beam size still exists in the presence of shear reinforcement, but it is

much less than in beams without shear reinforcement. This can be attributed to the enhancement in shear contribution of concrete due to the provision of shear stirrups, where the cracks are forced to be thinner in width and closer in spacing (i.e. more distributed), in addition to its effect on dowel action explained previously.

The influence of shear reinforcement was implemented by turning (λ_0) factor of Equation 2-2 into a function of the shear reinforcement ratio as follows:

$$\lambda_0 = 25\left(1 + \frac{\rho_s}{\rho_0}\right) \quad (2\text{-}3)$$

in which, ρ_s represents the ratio of shear reinforcement, whereas ρ_0 is an empirical coefficient.

2.5 Modes of Shear Failure in RC and PC beams

In this section, shear failure modes of simply supported RC and PC beams loaded with point loads (see Figure 2-5), which have been observed in experimental tests, are presented and described. In addition to the loading pattern, the failure mode in shear is dependent on geometrical aspects of beams, including a/d ratio, beam depth, web thickness and tension chord stiffness (i.e. the ratio between longitudinal reinforcement and its bond with respect to surrounding concrete) (Rajagopalan, 2002). Therefore, modes of shear failure can be classified as follows:

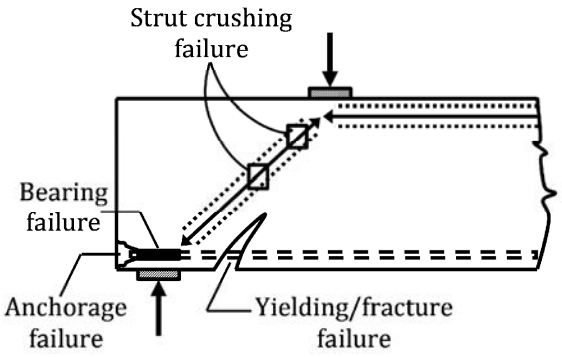

(a) Strut crushing and splitting failure

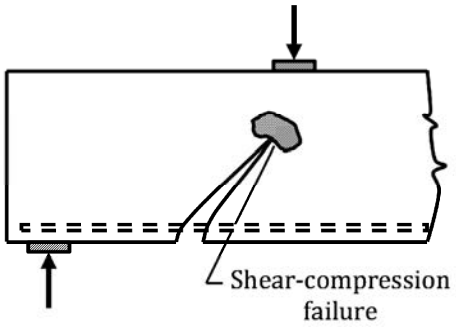

(b) Shear-compression failure

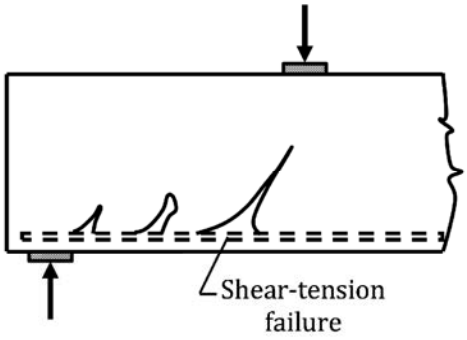

(c) Shear-tension failure

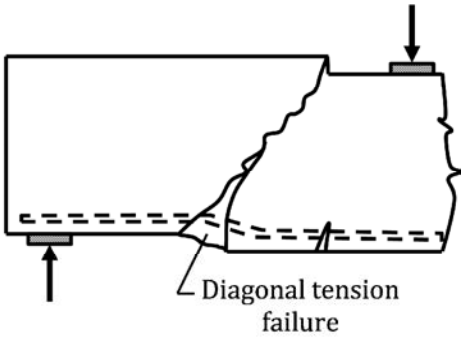

(d) Diagonal tension failure

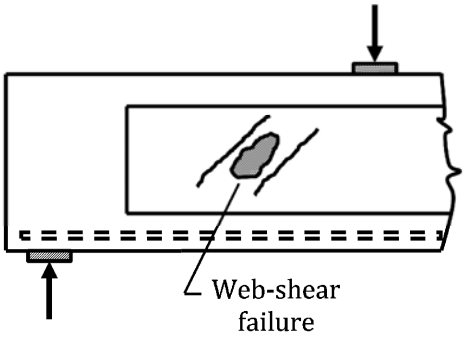

(e) Web-shear failure

Figure 2-5: Modes of shear failure

1- *Strut crushing and splitting failure*: These two modes of failure, given in Figure 2-5a, are common in deep beams with a/d < 1.0. Strut crushing or compression failure occurs due to the crushing of the concrete chord, which is responsible for the direct transition of the applied load into the nearest support, located between diagonal cracks running along the line linking loading and reaction points. However, splitting failure takes place due to yielding/fracture of longitudinal reinforcement (i.e. tension tie) at the locations of inclined cracks which develop below the concrete chord or due to anchorage/bearing failure at the beam's ends.

2- *Shear-compression/shear-tension failure*: In deep beams having a/d ratios more than 1.0 and less than 2.5, shear-compression failure can be observed when the concrete crushes at the tip of diagonal shear cracks, as the concrete chord caused by arch-action prevents the penetration of diagonal shear cracks towards the compression zone under further loading, as depicted in Figure 2-5b. Shear-tension failure takes place when the crack extends towards the tension reinforcement rather than the compression zone, until the concrete surrounding the tension reinforcement fails due to tensile splitting, as shown in Figure 2-5c.

3- *Diagonal tension failure*: This type of shear failure is commonly observed in beams with a/d ratios in the range of 2.5 to 5.6. The failure starts with a flexural crack, which under further loading turns into an inclined crack. Shortly before reaching the final failure, the crack opens widely at the bottom and

propagates rapidly towards the point loading, causing a collapse by splitting the beam into two portions (see Figure 2-5d).

4- *Web-shear failure*: For beams designed to have thin webs (such as in I-shape prestressed girders), shear failure can occur, even before the initiation of flexural cracks, due to the crushing of the concrete in the web at the location of peak stress when the compressive stress limit of the concrete is exceeded as a result of inadequate web thickness. This type of failure is known to be sudden and violent with no or very limited warning. Shortly before failure, the zone of failure (i.e. the beam web) is completely uncracked and the failure occurs in the form of a small explosion of the web immediately after the appearance of the first crack. Web-shear failure is depicted in Figure 2-5e.

2.6 Approaches for Shear Modelling in RC and PC beams

Shear problems in RC and PC beams have been the field of interest of large amounts of research and their contribution has resulted in the development of a number of models to explain the complexity of the shear transfer mechanism. The most applied approaches to shear design are described in the following sections.

2.6.1 Truss Analogies

The concept of truss analogy was initially proposed by Ritter (1899) and further developed by Morsch (1909). The concept is widely used in shear design models (Stratford and Burgoyne, 2003) in which the concrete beam with internal shear

stirrups is represented by a truss, as can be seen in Figure 2-6. The concrete in the direction of the inclined cracks and the shear reinforcement stirrups represent the compression struts and the tensile ties of the truss respectively, whereas the chords at the top and the bottom are represented by the concrete in the compression zone and tension reinforcement respectively.

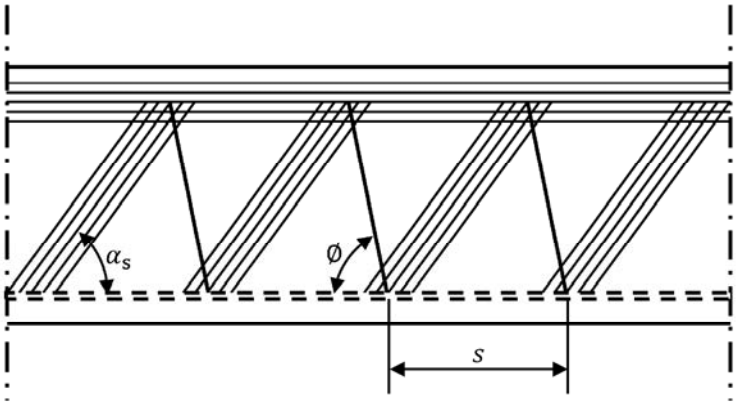

Figure 2-6: Truss analogy

The basis of this concept is that the shear in web-cracked beams is resisted by the stress that develops in the compression struts, which pushes the top and bottom chords apart, thereby causing tension force in the tensile ties (stirrups) that work to hold the components of the beam together.

In order to determine the shear capacity of the beam, Morsch (1909) assumed that the inclination angle of concrete struts is equal to 45°, as the three static equations of equilibrium are not enough to mathematically determine the variables of this approach. These variables are the stress in the concrete struts, the stress in the stirrups, the stress in the longitudinal tension reinforcement and the inclination angle

of the inclined concrete struts. However, such an assumption results in very conservative results or unsafe results respectively for concrete beams with low and high shear reinforcement ratio (Collins and Mitchell, 1980). Moreover, it may not reflect the actual stress state in the beam because, in general, the stiffness of the longitudinal reinforcement is higher than the stiffness of shear stirrups. Hence, the inclination angle of the concrete struts shall be flatter than 45°.

Nielsen et al. (1978) further modified the truss analogy based on the plasticity theory by allowing the compressive strut angle to vary. The modified model, in which both upper and lower bounds were suggested for the web crushing failure, is found to be consistent with experimental findings. However, it should be noted that approaches based on the plasticity theory cannot be applied to brittle materials such as in the case of FRP shear reinforcement (Stratford and Burgoyne, 2003).

2.6.2 Strut-and-Tie Models

The strut-and-tie model is a rational approach which was first introduced by Schlaich et al. (1987) to simulate the complex flow of forces in disturbed or discontinuity regions (i.e. regions near concentrated loads, supports and cross-section changes) of concrete structures, where the Bernoulli hypothesis is invalid because plane sections are no longer plane beyond bending (Kuchma and Collins, 1998), using a simplified truss model.

In the strut-and-tie method, there is no single or unified model for encountered design situations as can be seen in the example depicted in Figure 2-7. Therefore, the

analysis complexity is controlled by the adopted distribution of forces flow. Nevertheless, the stress distribution within the structure is simulated using a system comprising concrete compression members (struts), reinforcement tension members (ties) and nodal zones in which the concrete is subjected to high stresses. Sufficient amount and anchorage of the reinforcement are required to enable the cracked structure to support the anticipated load.

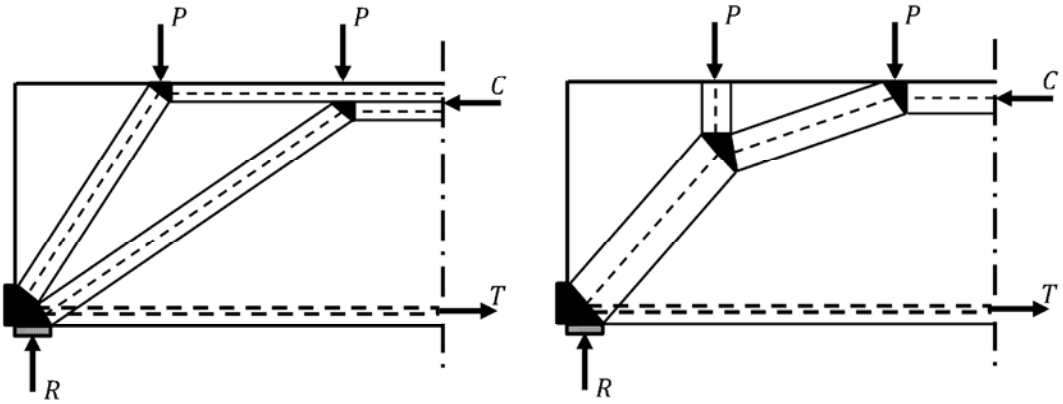

(a) Fan model (b) Arch model

Figure 2-7: Strut-and-tie models for a RC beam (Ibell et al., 1996)

Despite the fact that the plasticity theory behind the strut-and-tie method is complex, the strut-and-tie method is a straightforward method and the forces in each of its components (i.e. struts, ties and nodes) can be determined easily.

2.6.3 The Modified Compression Field Theory

The modified compression field theory (MCFT) was developed to predict the load-deformation response of RC panels (or elements) subjected to uniformly distributed

in-plane shear stresses and biaxial normal stresses (Vecchio and Collins, 1986). The analytical model uses deformations compatibility of the reinforcement (longitudinal and transverse) as well as the diagonally stressed concrete to determine the average stresses, average strains and the angle of inclination of the diagonally stressed concrete that resists shear, as illustrated in Figure 2-8.

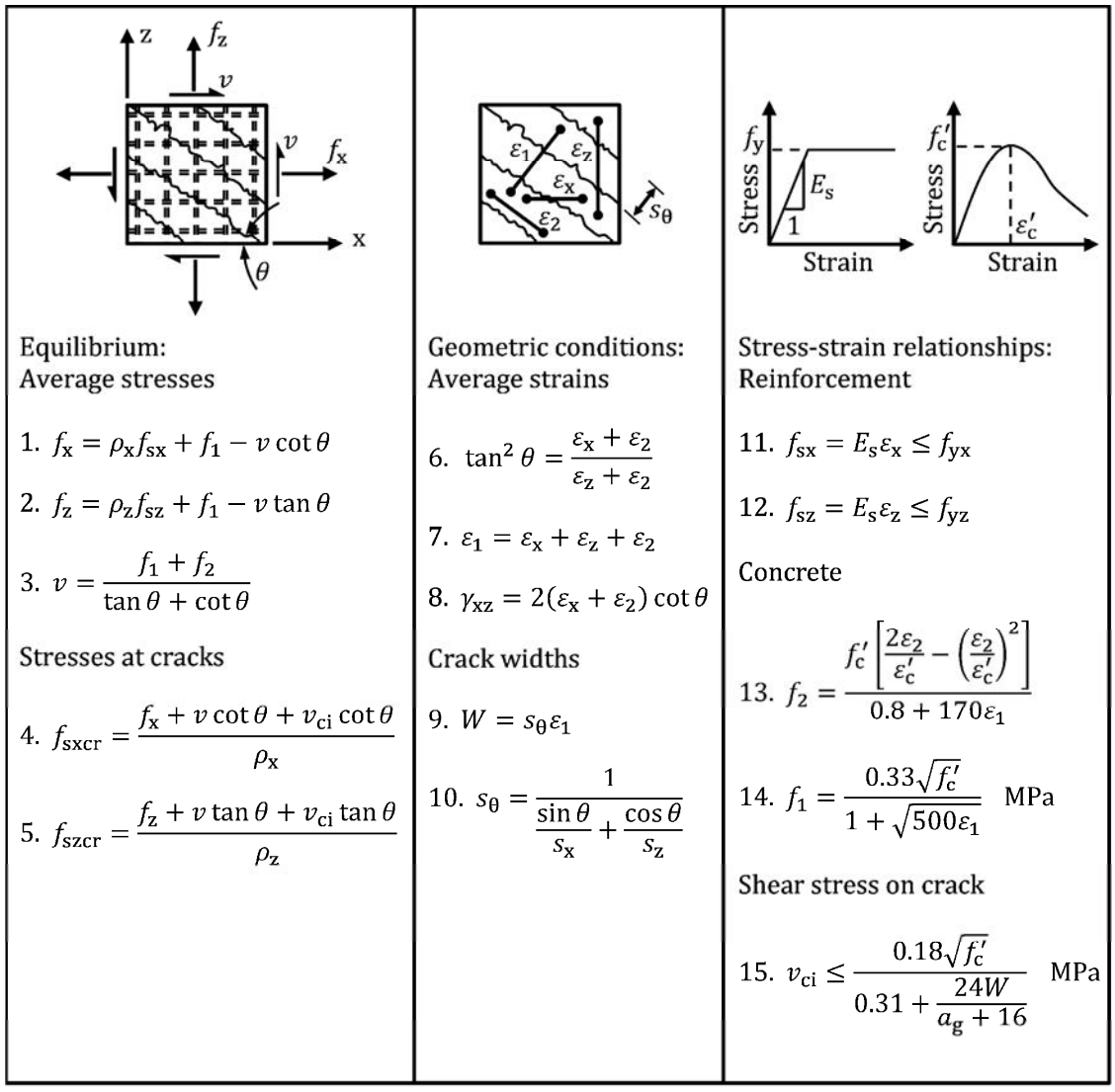

Figure 2-8: The MCFT (Bentz et al., 2006)

The MCFT permits for the concrete between the cracks to transfer tensile stresses even after extensive cracking that takes place at high average tensile strain values, whilst the compressive behaviour of the cracked concrete becomes softer when it is subjected to high lateral tensile strains (Vecchio and Collins, 1986). Due to the aforementioned interactions of complex stresses, the constitutive laws (i.e. the stress-strain relationships of concrete) derived from the results of the tested panels are different from the results that would be obtained using standard material tests.

In order to predict the shear response of a concrete beam using the MCFT, the beam is first divided into several elements, then the shear stress-shear strain relationship in each element is determined through the following process (Vecchio and Collins, 1986): determine the crack control characteristics in the longitudinal reinforcement direction (S_x) and the transverse reinforcement direction (S_z), which can be taken as 1.5 times the maximum distance between reinforcing bars in the corresponding direction; assume a value for the principal compressive stress direction (θ) to perform the calculations at the desired principal tensile strain value of concrete (ε_1); solve the equations of equilibrium, compatibility and constitutive relationship given in Figure 2-8; compare the obtained stresses and strains value to the externally applied loading to check the initial assumption accuracy; if the accuracy is not adequate, then a new assumption for θ is made and the process is iterated. An appropriate computer program is needed at each iteration to solve the MCFT equations given in Figure 2-8, because solving them by hand calculations is both a lengthy and tedious procedure.

Since predicting the shear strength of beams is more necessary in practice than the full shear-deformation response, so Bentz et al. (2006) proposed a simplified version of the MCFT for RC members suitable for hand calculations with almost the same or a very limited reduction in the accuracy. The experimental to predicted shear strength ratios, of more than 100 RC panels tested in pure shear, are 1.01 (with a coefficient of variation of 12.2%) and 1.11 (with a coefficient of variation of 13.0%) for the MCFT and the simplified MCFT respectively.

2.7 Shear Strengthening Techniques

Over the years, the shear force capacity of deficient RC and PC beams has been restored or increased by incorporating some strengthening approaches, since the cost associated with replacement of deficient beams is very high. The existing techniques for shear strengthening of RC and PC beams can be classified, according to the materials used in these techniques, into traditional and FRP shear strengthening techniques. The former techniques (i.e. the traditional) involve the use of traditional construction materials such as steel bars, steel plates and concrete; whereas more recent materials (i.e. FRP materials) are being used in the latter techniques. In the following subsection, a brief description of the most popular shear strengthening techniques is given.

2.7.1 Traditional Shear Strengthening Techniques

These methods had been developed before incorporating FRP materials into civil engineering applications, particularly for shear strengthening purposes. The most

popular traditional techniques used for shear strengthening have been addressed with their advantages and disadvantages as follows:

2.7.1.1 Steel Plate Bonding

This method has been widely used to strengthen concrete structures, particularly of concrete bridges in Europe, since the middle of the 1960s (Doran and Cather, 2014). It involves bonding steel plates or flat bars to the webs of deficient beams using epoxy adhesive to work as external shear reinforcement. The method is economical and does not change the overall dimensions of beams (Altin et al., 2005); thus, it has been considered as a convenient approach for shear strengthening and has received wide acceptance. However, it has its drawbacks including the installation, handling and transportation difficulties due to the heavy weights of steel plates, as well as the corrosion of steel plates which adversely affects the bond between concrete and steel plates (Barnes et al., 2001). Though the use of protective coatings may solve corrosion issues, it results in an increase in the maintenance costs (Hutchinson, 1999). In some cases, the use of anchorage bolts is required to enhance the bond performance.

2.7.1.2 Section Enlargement or Jacketing

In the section enlargement technique, a reinforced concrete, or shotcrete, in the form of an overlay or jacket is constructed around the existing beam's cross-section, after removal of deteriorated concrete from the beam's surfaces as well as the corrosion of the exposed reinforcement (if any is existed), to achieve the desired shear strength

(Raval and Dave, 2013). Special attention is required to ensure an appropriate bonding between the existing concrete and the casted concrete.

Though this method of shear strengthening is relatively economical, it involves several disadvantages such as, the dimensional incompatibility between the existing concrete and the casted concrete resulting in a high risk of concrete deterioration and corrosion of reinforcement, it is relatively highly labour-intensive, in addition to the reduction in the available space and increase in dead load of the beam as the cross-sectional dimensions increase.

2.7.1.3 Post-tensioning

This approach of shear strengthening has been frequently applied to RC and PC beams in the past (Taljsten, 2003). It consists of applying post-tension forces at the regions of critical shear which are delivered by means of prestressing tendons or steel rods having high tensile strength, as shown in Figure 2-9.

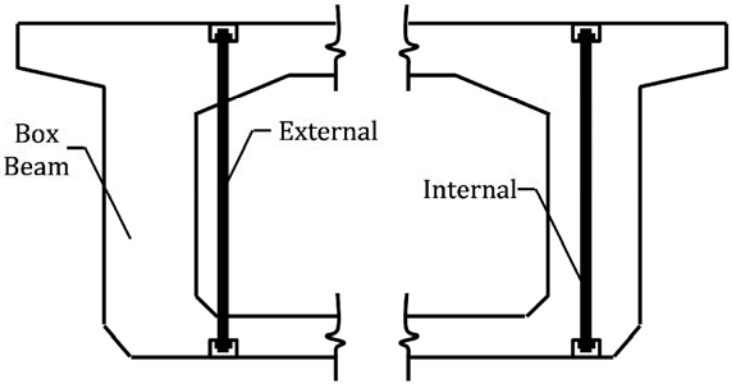

Figure 2-9: Post-tensioning technique of shear strengthening (Xanthako, 1996) (cited in Carolin, 2001, p.21)

Compared to the aforementioned traditional techniques, the post-tensioning method is efficient and much easier to carry out with less interruption to traffic. However, there is a risk that the drilling of holes through the section may damage the internal reinforcement, the prestressing tendons or steel rods are quite sensitive to corrosion, it requires stiff and efficient anchorages and the external prestressing tendons or steel rods are exposed to both impact loads and vandalism (Carolin, 2001; Taljsten, 2003).

2.7.2 Shear Strengthening with FRP Systems

The noteworthy emergence of FRP materials in the strengthening of deficient concrete elements dates back to the 1970s (Moslehy, 2010), whilst it dates back to the early 1990s for the shear strengthening applications in particular (Berset, 1992). Since then, the use of FRP systems for strengthening and retrofitting of concrete structures has increased dramatically due to their superior advantages over traditional materials, including: high strength to weight ratio, resistance to corrosion (in the case of carbon and aramid fibres), ease of use, low installation cost and exceptional formability which make them applicable to various shapes of cross-sections (ACI 440R, 2007; ACI 440.2R, 2008; Murphy et al., 2012). Though the initial cost of FRP materials is high compared to that of traditional materials, these materials can offer a considerable long-term solution and low maintenance rate (ACI 440R, 2007).

Though several studies on the FRP shear strengthening have been carried out in the last few years, the revision of published literature reveals that the numerical and

experimental studies relating to shear strengthening with FRP systems are limited compared to the studies that have been conducted on flexural and axial strengthening with FRP systems (Belarbi and Acun, 2013). Recently, several techniques of shear strengthening with FRP have been investigated. The most common techniques are given in the following subsections.

2.7.2.1 Externally Bonded (EB) FRP Laminates

This is the most common approach of FRP shear strengthening, in which unidirectional or multidirectional FRP laminates are bonded using epoxy to the of surfaces the beam (after preparation) in various configurations, either fully-wrapped or partially-wrapped depending on the accessibility of beam, to act as external shear reinforcement.

Figure 2-10 shows the three typical FRP wrapping configurations used in the externally bonded technique. Full wrapping of FRP laminates around the beam's cross-section is known to be the most efficient scheme of shear strengthening as it provides an adequate length of bond. However, this scheme is not applicable to all beams due to the inaccessibility of all the beam's sides, generally due to the existence of integral slab. When the beam is accessible from the sides and soffit or sides only, then the FRP laminates might be used in the form of a U-wrap scheme or two separate FRP laminates bonded on the two opposite beam's sides, respectively. Furthermore, the FRP laminates can be either oriented vertically to the beam's longitudinal axis or inclined with a specific angle to enhance its shear contribution (ACI 440.2R, 2008).

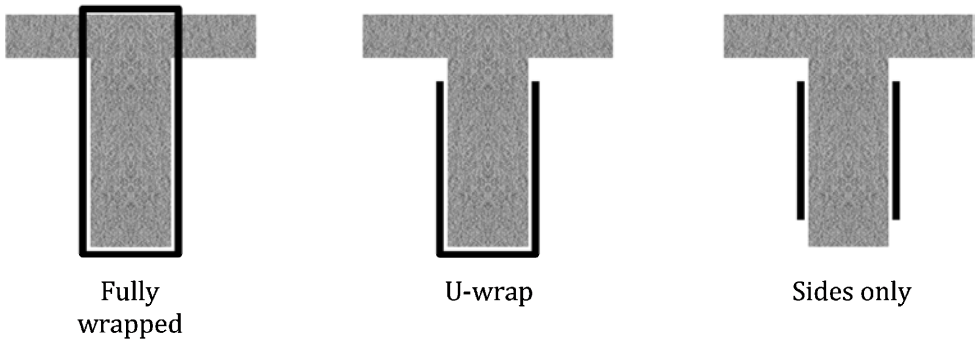

Figure 2-10: Typical wrapping schemes of FRP laminates (ACI 440.2R, 2008)

When FRP laminates are used in a U-wrap or two-side scheme, there will be a concern related to premature debonding failure of FRP at the free ends as a result of inadequate bond length being provided. Therefore, the use of a proper anchorage system is highly recommended to overcome this issue (Khalifa et al., 1999; Eshwar et al., 2008). Moreover, FRP laminates are likely to debond at the internal corners of beams with I-shape cross-sections. Hence, the method is less efficient when it is used to strengthen I-beams unless it is used along with an effective anchorage system to prevent or delay the debonding of FRP laminates at these corners (Belarbi and Acun, 2013).

2.7.2.2 Near Surface Mounted (NSM) Technique

The NSM strengthening technique consists of inserting FRP reinforcement bars, having rectangular or circular cross-section, or FRP plates into grooves cut on the concrete surface which are then filled with a suitable adhesive agent, e.g. epoxy paste or cement grout, to bond the FRP reinforcement into the grooves (ACI 440.2R, 2008; Jalali et al., 2012).

The NSM FRP technique provides numerous advantages over the EB FRP laminates as long as the concrete cover is in a good condition and thick enough to accommodate the desired groove size. These advantages include, less installation work, less tendency of the FRP reinforcement to debond due to the better bond characteristics between the FRP reinforcement and concrete, and the FRP systems are less exposed to impact loads or vandalism as they are protected by the surrounding concrete (Lorenzis and Teng, 2007). However, the efficiency of this technique is dependent upon the condition and strength of the concrete surface. Furthermore, the NSM method cannot be applied along the overall depth of concrete beams having I-shape cross-section or T-shape cross-section unless holes are created in the flange by drilling.

2.7.2.3 Deep Embedment (DE) Technique

More recent research carried out by Valerio and Ibell (2003), and followed by others (e.g. Valerio et al., 2009; Mofidi et al., 2012; Qin et al., 2014; Breveglieri et al., 2015), resulted in the development of a promising technique of shear strengthening using FRP bars called the deep embedment technique. This shear strengthening technique involves drilling vertical holes in the desired shear span, into which FRP bars are then inserted after being filled with a high viscosity epoxy resin (Valerio et al., 2009). The key strength of this technique is that it can be applied to strengthen beams accessible from one side only, i.e. either from top or soffit.

Compared to previous FRP strengthening techniques (i.e. EB sheets and NSM bars), the method does not require surface preparation and it provides better bond

characteristics between the FRP bars and surrounding concrete. Furthermore, the FRP bars in this technique, owing to the large concrete cover, are more protected from fire and other aggressive environments (Valerio, 2009; Valerio et al., 2009; Barros and Dalfre, 2013). However, the only concern is about damaging the longitudinal reinforcement during the drilling of vertical holes along the overall depth of the beam.

2.8 Shear Behaviour of Beams Strengthened with EB FRP Laminates

A careful review of the published literature reveals that the majority of the research work on concrete beams strengthened with EB FRP laminates has been experimental and focused on flexural strengthening, while much less attention has been paid to shear strengthening (Teng et al., 2004; Belarbi et al., 2011; You et al., 2011). Moreover, the research work on shear strengthening of PC beams has been carried out mainly to demonstrate the effectiveness of the EB FRP laminates for shear strengthening (or to validate the ability of the EB FRP laminates in retrieving the undamaged shear capacity of the strengthened beams) rather than to investigate the parameters influencing shear contribution of EB FRP, e.g. Hutchinson (1999), Schnerch (2001), Agapay (2003), Reed and Peterman (2004), Miller et al. (2007), Petty et al. (2011), Ary and Kang (2012), Kim et al. (2012), Murphy et al. (2012) and Zong et al. (2013). However, the successful use of the EB FRP shear strengthening technique has been demonstrated in several studies (Teng et al., 2004; Petty et al., 2011; Ary and Kang, 2012; Murphy et al., 2012).

Similar to steel stirrups in unstrengthened concrete beams, the shear contribution of FRP laminates takes place after concrete cracking. The magnitude of its contribution to shear is explicitly dependent on the FRP mechanism of failure, which can be either due to FRP rupture or FRP debonding (Bakis et al., 2002; Teng et al., 2004; Belarbi and Acun, 2013).

Failure due to FRP rupture governs when the capacity of FRP laminates is fully utilised. This type of failure has been observed in the majority of beams strengthened with fully wrapped FRP laminates, in addition to some of the beams strengthened with a U-wrap scheme, when a sufficient bond length or anchorage system was provided. The FRP laminates may rupture due to high stress concentrations along the major shear crack after local debonding or at the external corners of the beam (Triantafillou, 1998). On the other hand, the FRP debonding failure, which can occur in different modes of bond failure as shown in Figure 2-11 (fib Bulletin 14, 2001), is a major concern in beams strengthened in shear either with two-side bonding or U-wrap configuration, in which the FRP laminates tend to peel off from the concrete substrate (at the ends or around the shear cracks) before obtaining their ultimate tensile capacity. This premature type of failure takes place quickly after starting the separation of FRP from the concrete substrate with no ductility. Therefore, it is prevented as per the ACI 440.2R (2008) by setting the allowable effective tensile strain of the EB FRP laminates to a certain value, e.g. 0.004 mm/mm or a limit based on the ultimate strain of the FRP laminates.

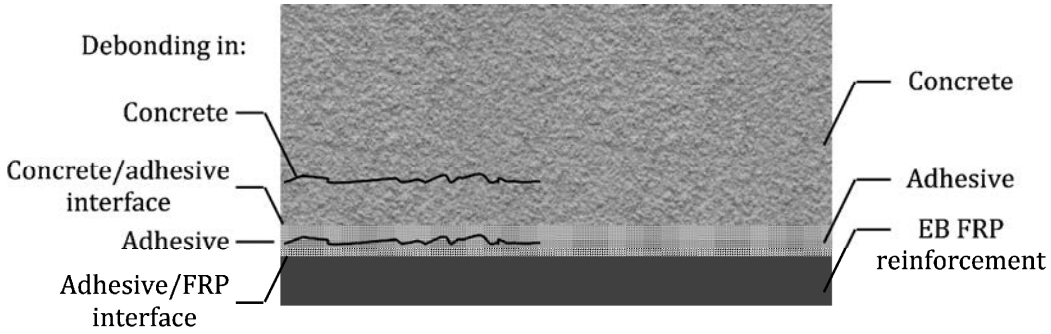

Figure 2-11: Different interfaces for bond failure (fib Bulletin 14, 2001)

In addition to the role of the FRP configuration scheme, FRP-to-concrete bond and the existence of a sufficient anchorage system, the shear contribution of EB FRP laminates is influenced by other factors (Bousselham and Chaallal, 2004; Dirar, 2010; Belarbi et al., 2011), including but not limited to:

2.8.1 Effect of Multiple FRP Layers

The influence of FRP layers number, or the FRP amount, on the shear contribution of EB FRP laminates has been investigated in several studies. In general, the shear force gain increases with the increase in the number of layers due to the associated increase in the axial rigidity of the applied FRP laminates (Chaallal et al., 2002; Adhikary and Mutsuyoshi, 2004). However, this enhancement in the shear contribution increases almost linearly up to a specific value of axial rigidity, beyond which no further increase in the shear force capacity is expected or the increase rate becomes disproportionate (Triantafillou, 1998; Bousselham and Chaallal, 2004). This can be attributed either to the premature debonding failure of the FRP from the concrete substrate (Triantafillou, 1998; Bousselham and Chaallal, 2006) or the failure

in concrete which is governed by cracking and splitting as the FRP laminates become stiffer and thicker (Adhikary and Mutsuyoshi, 2004).

Furthermore, the increase in the number of layers results in a corresponding decrease in the effective strains of the applied FRP laminates, thus preventing them from reaching their ultimate capacity before the final failure (Chaallal et al., 2002).

2.8.2 Concrete Compressive Strength

In addition to the axial rigidity (or stiffness) of the EB FRP laminates, the FRP-to-concrete bond strength is dependent on the compressive strength of concrete (Khalifa et al., 1998). When the diagonal shear cracks initiate in concrete, they result in the development of high tensile stresses in the EB FRP laminates bridging these cracks, as a result of the resistance provided to the separation of concrete along the cracks. These tensile stresses transmit along cracks via interfacial bond stresses.

If debonding is the governing mode of failure, then the shear contribution of EB FRP laminates is a function of the bond characteristics between the FRP laminates and concrete. Thus, the debonding failure mode might be delayed or even prevented in beams with higher concrete compressive strength due to the increase in the bond strength at the interface between the FRP laminates and concrete. However, the influence of concrete strength has been considered in the current design guidelines (i.e. ACI 440.2R, 2008 and Concrete Society TR55, 2012) via the determination of effective strain in the EB FRP laminates (see Section 2.10 for further details).

2.8.3 Shear Span-to-Effective Depth Ratio (a/d)

As the shear behaviour of RC and PC beams is largely influenced by the a/d ratio, therefore the effect of a/d ratio on the shear contribution of EB FRP laminates has been investigated to quantify its effect on the shear design for FRP composites.

From reviewing the published literature, it can be seen that the results concerning the influence of a/d ratio on the shear force gain due to EB FRP laminates are contradictory. According to Khalifa and Nanni (2002), Bousselham and Chaallal (2004), Bousselham and Chaallal (2006) and Ary and Kang (2012), the increase in a/d ratio results in a corresponding increase in the shear contribution of EB FRP laminates. This finding was attributed to the fact that, in deeper beams, the shear gain due to the EB FRP laminates cannot be provided beyond reaching the capacity of concrete strut. On the other hand, a more recent work carried out by Sayed et al. (2013) showed that the increase in the a/d ratio decreases the shear contribution of EB FRP laminates for beams strengthened with U-wrap or full wrap scheme.

Nevertheless, the aforementioned studies did not cover the whole range of a/d ratio (as the majority of tested beams had a/d ratio less than 3.5) suggested by Kani (1964) (see Figure 2-2), within which a concrete beam is expected to fail in shear as long as the flexural capacity is sufficiently provided. Therefore, additional investigations covering a wide range of a/d ratio is highly recommended, particularly for beams having a/d ratio greater than 2.5, to enrich the general database (Bousselham and Chaallal, 2004).

However, it should be mentioned that the current shear design guidelines for the contribution of EB FRP composites, i.e. ACI 440.2R (2008) and Concrete Society TR55 (2012), do not capture the effect of a/d ratio.

2.8.4 Size Effect

The study presented by Bousselham and Chaallal (2013) showed that more than 85% of the experimental tests, of concrete beams strengthened in shear with EB FRP laminates, have been carried out on beams with an effective depth of 450 mm or less. Hence, current shear design guidelines have been developed based on scaled beams rather than practical beam size usually being used in construction. Size effect, in turn, may result in non-conservative predictions in the cases where the shear contribution due to FRP laminates is significantly influenced by beam size.

Similar to the effect of a/d ratio, published results concerning size effect are controversial. According to Triantafillou (1998) and Dirar et al. (2012), the EB FRP laminates contribution to shear resistance is positively influenced by the increase in beam depth for beams strengthened with U-wrap scheme. This shear contribution enhancement was attributed to the longer bond transfer length provided in larger beams. On the other hand, other studies carried out on beams with and without internal shear reinforcement (Leung et al, 2007; Godat et al., 2010; Bousselham and Chaallal, 2013) revealed that the size effect can have a significant negative influence on the shear contribution of the EB FRP laminates for beams strengthened with the U-wrap configuration, where the percentage of shear gain due to the FRP tends to decrease with increasing the depth of the beam, particularly in beams with no internal

shear reinforcement (Bousselham and Chaallal, 2013). This trend was linked to the behaviour of the FRP laminates in the pull-out tests, where the maximum shear stress at the FRP-to-concrete interface shifts away from the damaged area, under further loading, rather than exhibiting an increase in its value (See Figure 2-12) (Bousselham and Chaallal, 2013). In other words, the effective bond length does not increase proportionally with the increase in beam depth.

However, the effectiveness of fully wrapped EB FRP laminates was found not only to be independent of size effect (Triantafillou, 1998; Leung et al., 2007), but can also experience shear enhancement due to the increase in the size of the beam (Leung et al., 2007).

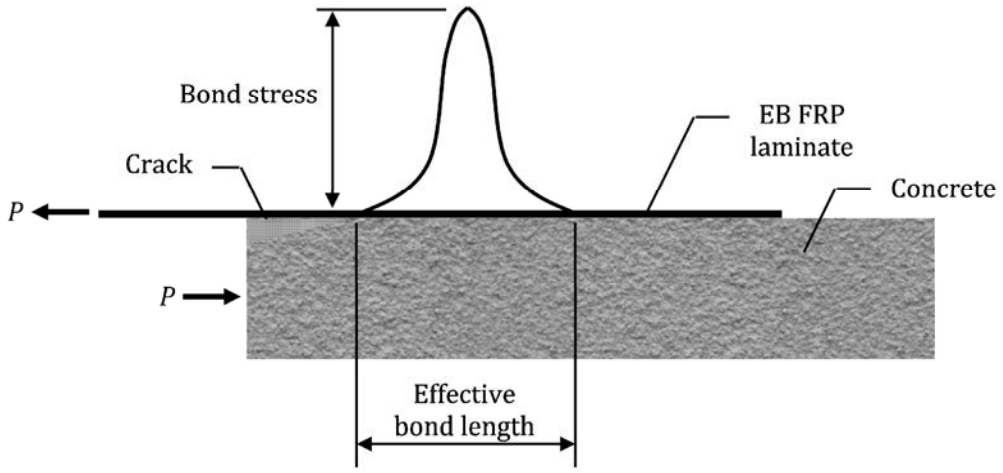

Figure 2-12: Interface shear stress transfer (Bousselham and Chaallal, 2013)

2.8.5 Interaction between Steel Stirrups and EB FRP Laminates

The presence of steel stirrups is one of the major parameters influencing the shear contribution of EB FRP sheets (Khalifa and Nanni, 2002; Ary and Kang, 2012). Thus,

investigating the interaction between internal steel stirrups and EB FRP laminates is of great importance, particularly when beams with a considerable percentage of steel stirrups require shear strengthening (Pellegrino and Modena, 2002). This interaction has been investigated in studies carried out on RC beams (Chaallal et al., 2002; Pellegrino and Modena, 2002; Bousselham and Chaallal, 2006; Bousselham and Chaallal, 2013) and the results showed that the contribution of EB FRP laminates to shear resistance is inversely proportional to the quantity $E_s\rho_s/E_f\rho_f$ (E_s and E_f are the elastic modulus of the steel stirrups and EB FRP laminates respectively, whereas ρ_s and ρ_f are the shear reinforcement ratios of the steel stirrups and EB FRP laminates respectively).

However, Bousselham and Chaallal (2004) suggested that no quantified explanation can be provided to this phenomenon due to lack of experimental data, whereas Pellegrino and Modena (2002) attributed it to the fact that cracks become more distributed as the value of $E_s\rho_s/E_f\rho_f$ increases. This more distributed crack pattern reduces the anchorage length, and consequently the contribution of the EB FRP laminates to the shear force capacity.

2.8.6 Effect of Pre-Cracking

Though most of the conducted research dealt with the shear behaviour of strengthened un-cracked beams, FRP laminates have often been used to strengthen deteriorated concrete beams. Hence, it is important to investigate the effect of pre-cracking on the shear force capacity of FRP-strengthened concrete beams. However, the experiments investigating the influence of pre-cracking, e.g. Carolin and Taljsten

(2005) and Dirar et al. (2012) for RC rectangular and T-beams, respectively, showed that pre-cracking does not influence the shear behaviour of the strengthened beams.

2.9 Shear Behaviour of Beams Strengthened with DE FRP Bars

The tests carried out using DE FRP Bars have been scarce and the majority of the work has been implemented to evaluate its effectiveness. This novel shear strengthening technique was first introduced by Valerio and Ibell (2003) in a pilot study conducted on ten RC rectangular beams without internal shear stirrups, in which six of them were strengthened in shear with Arapree (aramid-based) FRP (AFRP) bars. The studied variables were the bar diameter (7.5 mm and 10 mm bars were considered), spacing between the embedded bars and bar orientation (i.e. vertical versus 60° inclined). Their findings confirmed the validity of this shear strengthening scheme as three of the strengthened beams failed in ductile flexural mode of failure rather than the brittle shear failure mode of the unstrengthened beams, when adequate amounts of AFRP bars were used. The strengthened beams which failed in flexure exhibited 84% increase in their shear force capacity, whereas the shear force capacity gain in the other strengthened beams (with less percentage of AFRP bars) was in the range of 30-40% compared to the unstrengthened beams. However, maximum spacing of DE vertical reinforcement was suggested to be in the range of 0.5-0.75 times the effective depth to prevent shear discontinuity.

Valerio et al. (2009) used the DE FRP bar technique to strengthen rectangular beams in shear; two large-scale PC girders without internal steel stirrups, identical to

those used in short span bridges and seven small-scale beams (four RC beams including one with internal steel stirrups, and three PC beams without internal steel stirrups). For large-scale beams, the number of DE Carbon FRP (CFRP) bars placed in the cross-section was the only variable (i.e. either the use of one or two 7.5 mm CFRP bars). However, in addition to the presence of prestress force and internal steel stirrups, the variables in the case of the small-scale beams were the diameter of CFRP bars and the spacing between the CFRP bars. The results demonstrated the effectiveness of this strengthening technique, especially in the case of the small-scale beams, even with the existence of internal steel stirrups. Only two of the beams failed in shear with a remarkable increase in the shear force capacity which was in excess of 97%. Though both of the strengthened large-scale beams failed in shear, their shear force capacity was increased by about 7% and 15% over the control beam when one and two 7.5 mm CFRP bars were placed in the cross-section, respectively. Furthermore, the DE technique was found to be more efficient compared to identical beams but strengthened using the NSM method.

Mofidi et al. (2012) reported results of an experimental investigation carried out on full-scale RC T-beams strengthened in shear with DE FRP bars. The study aimed to quantify the effect of presence of steel stirrups as well as surface coating, spacing and diameter of DE CFRP bars on the shear strength enhancement of the tested beams. The findings showed that the plain-surface CFRP bars had a better contribution to shear resistance compared with the sand-coated CFRP bars due to their significant chemical bond, which led to a superior shear transfer between the CFRP-epoxy-concrete interfaces (unlike the case when no epoxy is used between

the CFRP and concrete). The shear force gain due to DE FRP bars was found to be inversely proportional to the spacing between FRP bars. Increasing the diameter of the FRP bars from 9.5 mm to 12.7 mm resulted in a 45% increase in the shear contribution. The shear resistance of the beam without internal steel stirrups increased by 122% due to the use of DE FRP bars, whereas this increase was significantly reduced when the internal steel stirrups ratio increased. Furthermore, the authors proposed a new design model for the calculation of shear contribution due to DE CFRP bars, as detailed in Section 2.10.

Qin et al. (2014) examined the effectiveness of CFRP bars as DE shear reinforcement for RC T-girders with uncorroded or corroded steel stirrups. For this purpose, they strengthened three RC T- girders with DE CFRP bars. One of the girders was uncorroded, whilst the other two had a level of corrosion in their internal steel stirrups of 7 and 12% for the second and third strengthened girders respectively. All the strengthened girders exhibited an enhancement in the shear strength over the corresponding unstrengthened girders. The shear force provided by the DE technique was adequate to retrieve the shear capacity of the beam corroded with 7% to its uncorroded shear strength, whereas it was almost but not quite enough in the case of the beam with 12% level of corrosion. The increase in the level of corrosion of the internal steel stirrups from 7% to 12% led to a decrease in the shear contribution due to DE CFRP bars from 19% to 12%. No explanation was given to the effectiveness reduction of the DE technique with increasing the corrosion level. Compared to similar beams strengthened in shear with EB CFRP laminates, the DE method was found to be more effective. Moreover, unlike the case of EB CFRP

laminates, no sign of debonding was found between the DE CFRP bars and the surrounding concrete.

Most recently, a study comprising the application of DE CFRP bars on four RC T-beams with internal steel stirrups was implemented by Breveglieri et al. (2015). In this study, the effect of internal steel stirrups ratio as well as the FRP bars orientation on the shear gain due to DE FRP bars was investigated. The obtained results demonstrated that both parameters had a great influence on shear contribution. When the internal steel stirrups ratio increased from 0.1% to 0.17%, the shear force gain due to DE FRP bars was reduced from 53% to 7% for the beams strengthened using vertically oriented DE FRP bars, whereas the shear force gain was reduced from 121% to 74% for the beams strengthened using 45° inclined DE FRP bars. However, the lower shear contribution of vertically oriented FRP bars, especially in the case of beams with a higher internal steel stirrups ratio which recorded only a 7% increase in shear contribution, was attributed to the relatively lower bond length provided by the vertically oriented bars as the main diagonal shear crack crossed the FRP bars nearly at the soffit of the beam; hence, the provided bond length was not sufficient compared with the beams strengthened with 45° inclined FRP bars which had a significant contribution to the shear resistance, even with the existence of a high internal steel stirrups ratio.

2.10 Design Guidelines for Shear Strengthening with FRP Systems

In this section, a description of the most common design approaches for shear strengthening of concrete beams using either EB FRP laminates or DE FRP bars is given in detail. The predictions of these design approaches have been assessed by comparing them with FE-predicted results, as well as experimental tests results from the published literature (see Chapters Five and Six).

2.10.1 Shear Strengthening with EB FRP laminates

Design models for determining the shear contribution of different configurations of EB FRP laminates are available in various forms (Belarbi et al., 2011). Amongst them, two of the international design guidelines are presented as follows:

2.10.1.1 ACI 440.2R (2008)

The ACI 440.2R (2008) design guidance, which is considered to be one of the most complete documents (Belarbi et al., 2011), assumes that the shear contribution of the FRP laminates can be added to that of the concrete and steel in a 45° truss analogy arrangement.

The FRP contribution to shear (V_f) was developed based on failure modes, which are most likely to be due to FRP rupture in the case of fully wrapped scheme and either FRP debonding or rupture for the U-wrap and two-side bonded scheme. It is given by:

$$\Psi_f V_f = \Psi_f \frac{A_{fs} E_f \varepsilon_{fe} (\sin\alpha + \cos\alpha) d_f}{s_f} \quad (2\text{-}4)$$

where Ψ_f is a reduction factor taken as 0.95 and 0.85 respectively for fully wrapped and U-wrap/two-side bonded, s_f is the longitudinal spacing between FRP sheets (mm), d_f is the effective FRP sheet depth which can be taken as the total FRP depth minus the distance from the beam's soffit to the centre of tension steel bars (mm), A_{fs} is the total area of FRP plies (mm^2) located within spacing s_f taken as $2nt_f w_f$ (where n is number of FRP plies, and t_f and w_f are respectively the thickness and width of one FRP ply in mm), α is the inclination of the main fibres' direction to the beam's longitudinal axis, E_f is the elastic modulus of FRP (MPa) and ε_{fe} is the effective tensile strain in FRP (mm/mm) which is calculated based on the failure mode. For fully wrapped scheme, the loss of aggregate interlock of concrete is the governing failure mode, whereas for U-wrap/two-side bonded the delamination of FRP laminates takes place before losing the aggregate interlock. Hence, ε_{fe} is given by:

$$\varepsilon_{fe} = \begin{cases} 0.004 \leq 0.75\varepsilon_{fu} & \text{(for fully wrapped)} \\ k_v \varepsilon_{fu} \leq 0.004 & \text{(for U-wrap/two-side bonded)} \end{cases} \quad (2\text{-}5)$$

where ε_{fu} is the ultimate tensile strain of the FRP reinforcement (mm/mm) and k_v is a bond-reduction factor can be determined as follows:

$$k_v = \frac{k_1 k_2 L_e}{11900\varepsilon_{fu}} \leq 0.75 \quad (2\text{-}6)$$

where L_e is the effective bond length of FRP (mm), k_1 is a factor taking into account the effect of concrete strength and k_2 is a reduction factor for the type of wrapping configuration used. These parameters are given by:

$$L_e = \frac{23300}{(nt_f E_f)^{0.58}} \tag{2-7}$$

$$k_1 = \left(\frac{f_c'}{27}\right)^{2/3} \tag{2-8}$$

$$k_2 = \begin{cases} (d_f - L_e)/d_f & \text{(for U-wrap)} \\ (d_f - 2L_e)/d_f & \text{(for two-side bonded)} \end{cases} \tag{2-9}$$

The sum of the steel stirrups (V_s) and EB FRP laminates (V_f) contributions to shear force capacity shall be limited as follows:

$$V_s + V_f \leq 0.66\sqrt{f_c'}\, b_w d \tag{2-10}$$

where b_w is the width of the beam web (mm).

2.10.1.2 Concrete Society TR55 (2012)

Similar to the ACI 440.2R (2008), the TR55 design code (2012) treats the EB FRP laminates using a 45° truss analogy, in which their contribution to the shear capacity is given by:

$$V_{\mathrm{f}} = \frac{A_{\mathrm{fs}}}{s_{\mathrm{f}}}\left(d_{\mathrm{f}} - \frac{n_{\mathrm{s}}}{3} l_{\mathrm{t,max}} \cos\beta\right) E_{\mathrm{fd}} \varepsilon_{\mathrm{fe}} (\sin\beta + \cos\beta) \qquad (2\text{-}11)$$

where s_{f} is the longitudinal spacing between the FRP sheets (mm) and equal to 1.0 in the case of continuous FRP laminates, n_{s} is a parameter accounts for type of wrapping scheme taken as 0,1 and 2 respectively for fully wrapped (or U-wrap provided with full anchorage from top), U-wrap and two-side bonded shear strengthening schemes, $l_{\mathrm{t,max}}$ is the required anchorage length (mm) which can be determined from Equation 2-12, β is the angle between the direction of the main fibres in the FRP reinforcement and the line perpendicular to that of the beam's axial axis, E_{fd} is the design elastic modulus of FRP reinforcement (MPa) and $\varepsilon_{\mathrm{fe}}$ is the effective strain in the FRP reinforcement (mm/mm) taken as the least value given by Equation 2-13.

$$l_{\mathrm{t,max}} = 0.7 \sqrt{\frac{E_{\mathrm{fd}} t_{\mathrm{f}}}{f_{\mathrm{ctk}}}} \qquad (2\text{-}12)$$

where f_{ctk} is the characteristic concrete tensile strength (MPa).

$$\varepsilon_{\mathrm{fe}} = \begin{cases} \varepsilon_{\mathrm{fd}}/2 \\ 0.5 \sqrt{\dfrac{f_{\mathrm{ctk}}}{E_{\mathrm{fd}} t_{\mathrm{f}}}} \\ 0.004 \end{cases} \qquad (2\text{-}13)$$

where $\varepsilon_{\mathrm{fd}}$ is the design ultimate strain of FRP reinforcement (mm/mm).

The guidance also limits the maximum centre-to-centre spacing of the sheets to prevent shear discontinuity due to the formation of a diagonal shear crack without intercepting an FRP sheet. Therefore, the maximum centre-to-centre spacing of the FRP sheets shall be taken as the least of the following:

- $0.8d_{\mathrm{f}}$
- $d_{\mathrm{f}} - (n_{\mathrm{s}}/3)l_{\mathrm{t,max}}\cos\beta$, and
- $b_{\mathrm{f}} + d_{\mathrm{f}}/4$

where b_{f} is the width of the FRP sheet (mm), taken as $\cos\beta$ for continuous FRP sheets.

It should be noted that Equation 2-11 is valid as long as the steel stirrups yield prior to failure, due to rupture of debonding, of the FRP reinforcement.

2.10.2 Shear Strengthening with DE FRP Bars

Unlike the case of shear strengthening with EB FRP laminates, where several design guidelines and analytical models have been proposed in the last few years, only two design procedures are available for shear strengthening with the DE technique. The first procedure is given as a set of design guidelines while the second is an analytical design model, by the TR55 design guidance (2012) and Mofidi et al. (2012) respectively.

2.10.2.1 Concrete Society TR55 (2012)

The shear contribution of the DE FRP bars, which is based on a 45° truss analogy, is given by:

$$V_{\mathrm{f}} = \frac{\varepsilon_{\mathrm{fe}} E_{\mathrm{fd}} A_{\mathrm{f}}}{s_{\mathrm{b}}} W_{\mathrm{eff}} \tag{2-14}$$

where $\varepsilon_{\mathrm{fe}}$ is the effective strain in the DE FRP (mm/mm) which conservatively taken as 0.004. A_{f} is the cross-sectional area of the DE FRP bar (mm^2), s_{b} is the spacing between the DE FRP bars (mm) and W_{eff} is the effective width over which the DE FRP bar may act (mm) and can be determined as follows:

$$W_{\mathrm{eff}} = h - 2l_{\mathrm{b,max}} \tag{2-15}$$

where h is the strengthened depth of the beam(mm), whereas $l_{\mathrm{b,max}}$ represents the required anchorage length (mm) beyond which no additional gain can be achieved in capacity. This is determined by:

$$l_{\mathrm{b,max}} = \frac{\varepsilon_{\mathrm{fe}} E_{\mathrm{fd}} A_{\mathrm{f}}}{\left(\pi d_{\mathrm{b}} \frac{\tau_{\mathrm{b}}}{\gamma_{\mathrm{A}}}\right)} \tag{2-16}$$

where d_{b} is the DE FRP bar diameter (mm), τ_{b} is the average bond stress (MPa) over the anchorage length (i.e. $l_{\mathrm{b,max}}$) which is conservatively taken as 15 MPa when no test data is available, and γ_{A} is a partial safety factor for the adhesive material

between the concrete and DE FRP bars which is taken at least equal to 4, in order to keep the stress in the adhesive less that 25% of its short-term strength.

2.10.2.2 The Design Model of Mofidi et al. (2012)

This design model was proposed to determine the shear resistance contribution of DE CFRP bars as follows:

$$V_{\mathrm{f}} = k_{\mathrm{L}} k_{\mathrm{S}} \frac{A_{\mathrm{f}} E_{\mathrm{f}} \varepsilon_{\mathrm{fe}} d_{\mathrm{fe}}}{s_{\mathrm{b}}} (\sin\alpha + \cos\alpha) \qquad (2\text{-}17)$$

where E_{f} is the Young's modulus of elasticity of the FRP bar (MPa), d_{fe} is the effective shear depth (mm) taken as the greater of 0.72 times the overall beam depth and 0.9 times the effective beam depth, and $\varepsilon_{\mathrm{fe}}$ is the effective strain in the FRP bars (mm/mm) given by:

$$\varepsilon_{\mathrm{fe}} = \sqrt{\frac{8}{d_{\mathrm{b}} E_{\mathrm{f}}} \left(\frac{\tau_{\mathrm{m}} S_{\mathrm{m}}}{1 + \alpha_{\mathrm{a}}} \right)} \leq 0.004 \qquad (2\text{-}18)$$

This equation for the calculation of the effective strain in the FRP bars was developed based on the Bertero-Popov-Eligehausen (BPE) modified bond-slip model (Cosenza et al., 1997) and pullout test results of a series of DE CFRP bars bonded using epoxy to concrete blocks (Godat et al., 2012a).

In Equation 2-18, τ_{m}, S_{m} and $\alpha_{\mathrm{a}}$are the bond strength of the FRP bar (MPa), the slip corresponding to the bond strength (mm) and curve fitting parameter controlling the ascending branch of the BPE bond-slip model, respectively. Based on the aforementioned pullout tests (Godat et al., 2012a), the parameters τ_{m}, S_{m} and α_{a}were found to be equal to 21.3 MPa, 0.176 mm and 0.125 respectively for plain-surface CFRP bars, while they were equal to 8.4 MPa, 0.08 mm and 0.09 respectively for sand-coated CFRP bars.

Furthermore, Equation 2-17 involves two additional coefficients, namely k_{S} and k_{L}. The former (i.e. k_{S}) is a reduction coefficient for the presence of internal steel stirrups (which can be taken either as 0.6 for beams with steel stirrups spaced at less than $2d/3$ or as 1.0 for other than that), whereas k_{L} is a reduction coefficient ($0 \leq k_{\mathrm{L}} \leq 1$) for the CFRP bars provided with anchorage length less than the minimum anchorage length required (L_{eff}), and can be determined from:

$$k_{\mathrm{L}} = \begin{cases} 1 & \text{for } \dfrac{d_{\mathrm{fe}}}{2} \geq L_{\mathrm{eff}} \\ \dfrac{d_{\mathrm{fe}}}{\sqrt{\dfrac{d_{\mathrm{b}} E_{\mathrm{f}}}{2} \dfrac{S_{\mathrm{m}}}{\tau_{\mathrm{m}}} \dfrac{1+\alpha_{\mathrm{a}}}{(1-\alpha_{\mathrm{a}})^2}}} & \text{for } \dfrac{d_{\mathrm{fe}}}{2} < L_{\mathrm{eff}} \end{cases} \tag{2-19}$$

$$L_{\mathrm{eff}} = \frac{f(S_{\mathrm{m}}) d_{\mathrm{b}}}{4\tau_{\mathrm{m}}} \left(\frac{1+\alpha_{\mathrm{a}}}{1-\alpha_{\mathrm{a}}} \right) \tag{2-20}$$

and $f(S_{\mathrm{m}})$ is the stress in the CFRP bar at slip corresponding to the bond strength given as follows (Cosenza et al., 2002):

$$f(S_{\mathrm{m}}) = \sqrt{\frac{8E_{\mathrm{f}}}{d_{\mathrm{b}}}\frac{\tau_{\mathrm{m}}S_{\mathrm{m}}}{1+\alpha_{\mathrm{a}}}} \qquad (2\text{-}21)$$

2.11 Concluding Remarks

This chapter has presented a comprehensive review of the shear behaviour of RC and PC beams unstrengthened and strengthened in shear with FRP materials. The review involves the shear transfer mechanisms in concrete beams, the main factors influencing the shear behaviour, modes of shear failure, the most applied shear design models, the advantages and disadvantages of shear strengthening techniques particularly the FRP strengthening techniques, the main findings of the previous tests carried out on beams strengthened in shear with EB FRP laminates and DE FRP bars, and a description of the most common design procedures for shear strengthening of concrete beams using either EB FRP laminates or DE FRP bars.

From the review it can be seen that the shear behaviour of the unstrengthened as well as FRP-strengthened RC and PC beams is complicated and can be influenced by various parameters.

In general, less attention has been paid to the FRP shear strengthening applications especially in the case of PC beams. Moreover, much of the research work on shear strengthening has been experimental and focused mainly on the effectiveness of the FRP strengthening techniques rather than the parameters influencing the shear

contribution of those techniques. Hence, Chapter Four aims to develop and validate nonlinear FE models capable of predicting the overall shear behaviour of FRP-strengthened RC and PC beams. The development of the FE models was based on the findings from the relevant previous FE work given in Chapter Three.

However, the conducted parametric studies from the published literature, if any, have not fully covered the whole range of influencing parameters, such as practical beam size or the overall range of a/d ratios in which the beams are expected to fail in shear if adequate flexural capacity is provided. Therefore, further work is needed in this area to expand available data and enrich the general understanding. Such extensive work is reported in Chapter Five and Chapter Six.

Furthermore, none of the available design guidelines for shear strengthening with FRP have received wide acceptance. Those design guidelines do not take into account the influence of all the main factors affecting the shear contribution of FRP composites; this, in turn, prevents them from being classified as fully developed guidelines. An assessment of the most common design guidelines is given in Chapters Five and Six, together with the development of a new design model for shear strengthening using DE FRP bars.

CHAPTER 3: THE FINITE ELEMENT METHOD

3.1 Introduction

Unlike the empirical and analytical models which have been usually developed for determining the shear capacity of beams strengthened with FRP composites, the FEM can provide information about the entire behaviour (e.g. stiffness, ductility and crack patterns) in addition to the predicted shear capacity of the strengthened beams. The FEM is a computer-based numerical technique used to find an approximate solution to partial differential and integral equations, in which the continuous domain of a complex problem is divided into a set of small elements (i.e. replacing the problem by a simpler one); the solution then is obtained from these elements in relation to each other (Silhavy et al., 2012). The era of the FEM was linked to the advent of computers due to the necessity of solving complicated engineering problems of elasticity and structural analysis. It can be traced back to the work carried out by Alexander Hrennikoff and Richard Courant in the early 1940s, while the term Finite Element was initially used by Clough in the 1950s (Fu, 2015).

Since the development of FEM has been in conjunction with the development of computers, the early FE work was implemented using linear-elastic analyses, in which modelling is easy to conduct with comparatively less computational costs (fib, 2008). In such analyses, however, information cannot be provided about the inelastic

behaviour of materials, including but not limited to concrete cracking, concrete crushing, aggregate interlock and yielding and buckling of reinforcement. On the other hand, the intense use of the nonlinear FE analysis framework in recent research has resulted in the development of various models that provide solutions to the complex failure process of RC and PC structures.

In the following sections, a description of the commonly used methods for FE modelling of concrete, steel and prestressed reinforcement and FRP composites is given. These methods have been used in the published FE work on RC and PC beams strengthened in shear with FRP composites.

3.2 Modelling of Concrete

3.2.1 Methods for Modelling Cracked Concrete

Modelling of cracking in concrete is amongst the significant issues in modelling of concrete structures using the FEM. The initiation and propagation of cracks in the standard FEM may be modelled using either the discrete crack approach or the smeared crack approach (ACI 446.3R, 1997). A brief description of these two approaches (i.e. the discrete crack and the smeared crack) is given in the following subsections, in addition to the crack modelling by a more recent method so-called the eXtended Finite Element Method (XFEM).

3.2.1.1 Discrete Crack Approach

In this approach, the crack in concrete is physically modelled as a geometrical discontinuity by doubling and separating the nodal points along a specific crack path to create a discrete crack in the FE mesh, as depicted in Figure 3-1.

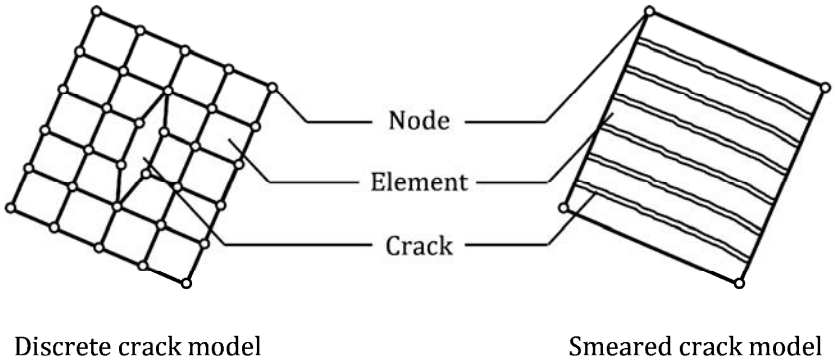

Figure 3-1: Crack modelling in FEM (Kwak and Filippou, 1990)

The concept of discrete crack was initially introduced in the FE analysis by Ngo and Scordelis (1967), who used various predefined discrete crack paths in linear-elastic analyses of identical singly-RC beams. However, their study did not take into account the crack propagation issue as they modelled cracks with traction-free surfaces. The discrete crack propagation problem was first addressed in FE modelling by Nilson (1968), who used predefined cracking criteria in a progressively increasing load model, in which the crack is defined when the average principal tensile stress in two adjacent concrete elements exceeds the concrete cracking strength. After cracking, the model topology is updated, then the model is unloaded and reloaded from zero.

The discrete crack model involves several disadvantages. First, it requires continuous change in both the topology and nodal connectivity of the FE model, and

hence it demands high computational costs to avoid numerical errors; in addition, sometimes it is difficult to apply, particularly in complex three-dimensional models. Secondly, the propagation of cracks in any FE model shall follow predefined paths; thus, it limits both the accuracy and popularity of the method when the crack orientation is hard to be predicted in advance (Rots and Blaauwendraad, 1989: Kwak and Filippou, 1990; ACI 446.3R, 1997). Despite the aforementioned shortcomings, it should be mentioned that for concrete structures with a few previously-defined dominant cracks, the discrete crack method can be used to accurately model the realistic strain discontinuities that arise from those cracks in the structure.

3.2.1.2 Smeared Crack Approach

In contrast to the previous approach, the crack in the smeared crack approach is continuum and is simulated by changing the constitutive properties of concrete elements after cracking, in terms of stress-strain relations, rather than changing the topology of the FE mesh itself, as shown in Figure 3-1. Although it is impossible to trace individual cracks using this method, the cracks are presented as regions with distributed cracking. The approach, which was initially proposed by Rashid (1968), can be categorised according to assumptions made for the direction of crack propagation into the fixed crack model and the rotating crack model (Rots and Blaauwendraad, 1989).

The research addressing which of the aforementioned approaches is more realistic is controversial (Rots and Blaauwendraad, 1989). However, in addition to the fact that the locations of cracks are not required to be known in advance in the smeared crack

approach, the approach has been found to be more convenient for two reasons (Rots and Blaauwendraad, 1989; Kwak and Filippou, 1990; ACI 446.3R, 1997; Godat, 2008; Chen, 2010). First, from the computational point of view, the smeared crack concept does not require special re-meshing algorithms to deal with the change in topology or special elements to model cracks, e.g. by means of interface elements. Secondly, unlike in metals, a fracture in composite materials such as concrete is preceded by the propagation and development of micro-cracks. This is apparent in the strain softening behaviour which is similar to the approximation used in the smeared crack model for the behaviour of concrete after cracking (i.e. modelling of a single crack using a number of paralleled and finely spaced fissures perpendicularly to the principal stress direction, see Figure 3-1).

In the fixed crack concept, the crack orientation is constant upon cracking and during the entire analysis process. If this concept is implemented, then an explicit definition of the concrete shear behaviour, usually via a shear retention model, is required. The shear retention model simulates the reduction in shear stiffness after cracking and can be defined either as a constant factor (called constant shear retention model) or a variable factor (called variable shear retention model). The value of this factor shall be less than or equal to 1 but greater than or equal to 0. The higher the shear retention factor, the higher the capability of cracked concrete to resist shear loads (Godat, 2008).

Though the fixed crack concept provides more capabilities due to the explicit modelling of shear behaviour, which is in fact an advantage, the incorporation of

crack shear models for concrete complicates the analysis. The absence of consensus on which model can accurately simulate the actual concrete shear behaviour more complicates the task. On the other hand, the rotating crack concept has a unique shear treatment which abandons the need for incorporation of a shear model for cracked concrete, and consequently assures simplicity (Rots and Blaauwendraad, 1989; and Hendriks and Rots, 2002). If the rotating crack concept is implemented for the concrete, the direction of the crack is forced to change according to the change in the principal tensile stress direction. It follows that any crack plane in this model is a principal plane and consequently there are no shear stresses acting on this plane. Thus, no explicit model for the shear behaviour of the cracked concrete, e.g. via a shear retention model, is required. Moreover, the fixed crack concept is more exposed to stress-locking than the rotating crack concept, and the severity of stress localization tends to increase with the increase of the shear retention factor of the fixed crack model (Rots and Blaauwendraad, 1989; and Hendriks and Rots, 2002).

Stress-locking phenomenon mainly occurs in the smeared crack approach due to displacement continuity and leads to a stiffer response of the structure. It occurs when the tensile straining propagates in the un-cracked elements, due to the cracking (strain softening) in adjacent elements, rather than it decreases and drops to zero (Rots and Blaauwendraad, 1989). There are two probabilities for the increasing tensile strain in the un-cracked elements (Rots and Blaauwendraad, 1989), where the tensile strength of these elements is either exceeded or not. If the tensile strength is exceeded (i.e. unrealistic cracking) then the stress-locking is

discouraged, whereas if the tensile strength is not exceeded then stress-locking (i.e. unrealistic stiffening) takes place in these elements. However, both scenarios are undesirable.

3.2.1.3 The eXtended Finite Element Method

In addition to the crack modelling approaches used in the standard FEM (i.e. the discrete crack approach and the smeared crack approach), the XFEM, a recent and advanced approach for simulating fracture in concrete, has been developed. The XFEM is a partition of unity based method (i.e. the sum of shape functions at any point is equal to one) proposed by Belytschko and Black (1999) and Moës et al. (1999), in which crack discontinuities propagate independently of the mesh. In this method, additional functions (i.e. enrichment functions) are incorporated locally (i.e. in the elements crossed by a crack) into the classical shape functions of the FEM approximation to model the discontinuities. It allows for discontinuities to arbitrarily cut through elements, hence re-meshing (or constraining the discontinuity to the element boundaries) is not required as the crack propagates. After incorporating the enrichment functions, the algebraic system of equations will involve two types of unknowns, namely classical and enriched degrees of freedom. Though the XFEM is a preferable choice for modelling localised mesh-independent fracture, its implementation results in high computational costs and requires the use of small element size at the region of interest (i.e. near crack tip) to ensure the accuracy of the solution (Asferg, 2006). Therefore, the XFEM can be advantageous in modelling the structure at micro-scale.

3.2.2 Modelling of Concrete in Compression and Tension

The experimental tests carried out on concrete cylinders and cubes under uniaxial compressive stresses showed that the behaviour of concrete in compression is highly nonlinear, as shown in Figure 3-2. However, the stress-strain curve starts with elastic behaviour whereas the inelastic deformation takes place at 30-75% (see Figure 3-2) of the concrete's compressive strength. Upon further loading, the stiffness of the stress-strain curve decreases gradually (due to the development of micro-cracks) until the concrete's compressive strength value is reached; after the peak, the stress starts to decrease until crushing failure is achieved (Mang et al., 2003).

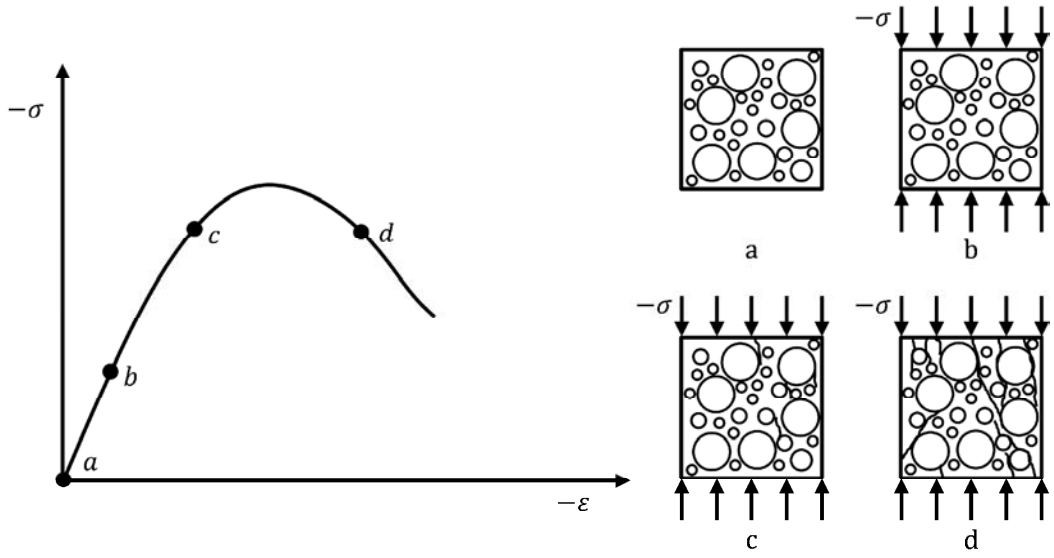

Figure 3-2: Response of concrete under uniaxial compression (Mang et al., 2003)

The behaviour of concrete under tri-axial compressive stresses exhibits a considerable level of confinement and its quantity is dependent on the lateral-to-axial compressive stress ratio. This confinement can shift the brittle behaviour of concrete

in compression into a ductile type (Mang et al., 2003). In contrast, lateral tensile strains soften the behaviour of concrete in compression (Vecchio and Collins, 1986) as mentioned earlier in Section 2.6.3.

There are several models in the literature for representing uniaxial compressive behaviour, e.g. the models developed by Thorenfeldt et al. (1987) and Mander et al. (1988) for unconfined and confined concrete respectively.

For the behaviour of concrete in tension, the uniaxial stress-strain curve comprises two phases as depicted in Figure 3-3. The pre-peak part of the stress-strain relationship is relatively linear up to approximately 60% of the concrete tensile strength value, in which the micro-cracks are negligible and distributed over the entire specimen. Upon further loading, the propagation of micro-cracks starts to concentrate in a limited zone known as the fracture process zone, which results in deterioration in the stiffness, and consequently shifts the stress-strain response into nonlinearity. In the post-peak part (or the concrete softening branch) however, the propagated micro-cracks form a band which is responsible for the rapid deterioration in the residual stress (Mang et al., 2003).

In contrast to the behaviour of concrete in compression, the failure in tension is brittle, rapid, difficult to track and caused by a much smaller number of cracks. Therefore, there is no unique relationship for concrete softening as the results obtained from experiments have been found to be scattered and contradictory

(Gopalaratnam and Shah, 1985). Moreover, the tensile response of concrete under a multi-axial state is similar to that under uniaxial tension (Mang et al., 2003).

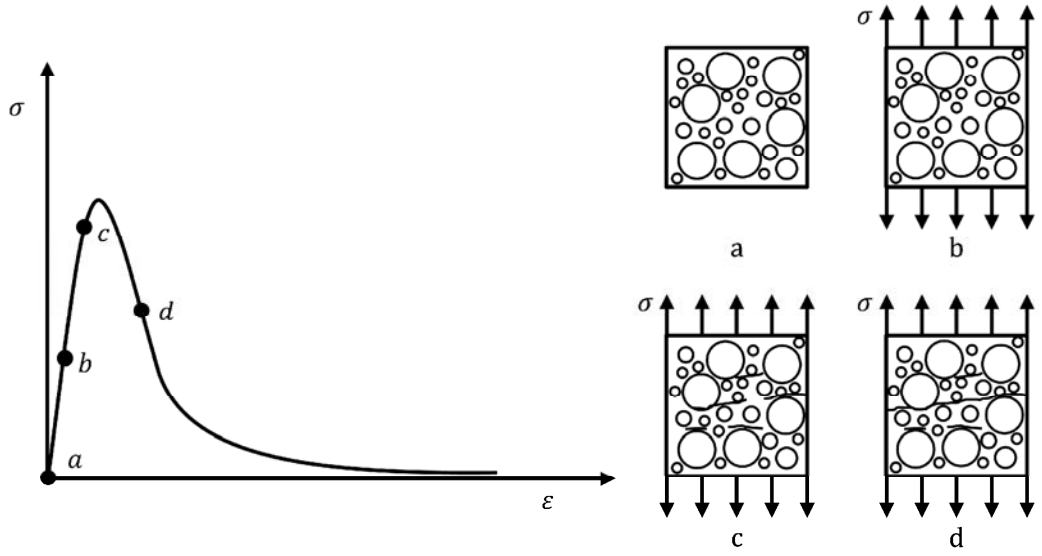

Figure 3-3: Response of concrete under uniaxial tension (Mang et al., 2003)

Constitutive models for predicting the response of concrete have been developed over the past decades on the basis of various frameworks. However, using a broader classification shows that the models can be classified into models based on elasticity-theory and models based on plasticity-theory. The elasticity and plasticity theories are briefly addressed in the following sub-sections, in addition to the total strain approach which was implemented for modelling concrete in this study.

3.2.2.1 Modelling of Concrete Using Elasticity Theory

Stress in the elastic models depends only on the strain value without accounting for the strain history (i.e. no permanent deformations occur in the concrete). The simplest concrete models are the linear-elastic models, in which the behaviour of

concrete in compression and tension is simulated by a linear-elastic stress-strain relationship until reaching defined failure criteria of concrete, such as the ultimate strength of the concrete (Chen, 2007). The failure takes place in a brittle manner, and consequently the linear-elastic models might be used to predict accurately the brittle behaviour of concrete in tension.

On the other hand, nonlinear elastic constitutive models (which are an improvement over linear-elastic models) are usually used to predict behaviour of concrete under multi-dimensional loading states (where it exhibits a significant nonlinearity), whereas the linear-elastic models fail to predict such behaviour (Chen, 2007).

3.2.2.2 Modelling of Concrete Using Plasticity Theory

The plasticity theory is used to model the behaviour of materials with permanent or irreversible deformations. In this approach, the strain is decomposed into an elastic part (reversible strain) and plastic part (irreversible strain which starts upon exceeding the yield limit). The plasticity theory was initially developed for metals and was then adjusted to fit the ductile compressive behaviour of concrete under multi-dimensional states of stress. The justification included the yield surface, the hardening rule and the flow rule (Park and Kim, 2005).

The initial yield surface specifies the level of stress at which plastic deformation takes place (i.e. elastic limit of concrete). The hardening rule is used to define the evaluation of the initial yield surface during the progress of loading, as a function between stress and plastic-strain. The flow rule is used to determine the plastic strain

direction from a given stress state by means of linking the yield surface to the stress-strain relationship (Chen and Han, 1988). Earlier research was carried out to develop suitable failure surfaces to account for the concrete response in compression, which are combined with other failure surfaces (or criteria) for concrete in tension, e.g. the combination of Drucker-Prager criterion and Rankine criterion which are respectively used to model concrete failure in compression and tension.

3.2.2.3 Modelling of Concrete Using Total Strain Models

Total strain constitutive models are nonlinear hypo-elasticity models developed along the lines of the MCFT (see Section 2.6.3), which describe the compressive and tensile behaviour of concrete with one stress-strain relationship. Later on, its applicability was extended for three-dimensional analysis by Selby and Vecchio (1997). This extension took into account the complex evolution of the concrete stress-strain response due to confinement and lateral cracking.

Total strain models can be classified, based on the smeared crack approach used for modelling cracked concrete (see Section 3.2.1.2), into total strain fixed crack model and total strain rotating crack model. In both cases, the behaviour of concrete in compression and tension can be modelled using various stress-strain relationships. For instance: brittle model, ideal model, or stress-strain model based on the fracture energy of concrete in tension and compression.

Though the elasticity-based models adopt the same loading, unloading and reloading stress-strain path; the unloading/reloading behaviour is differently implemented in the total strain models by means of secant unloading, as shown in Figure 3-4.

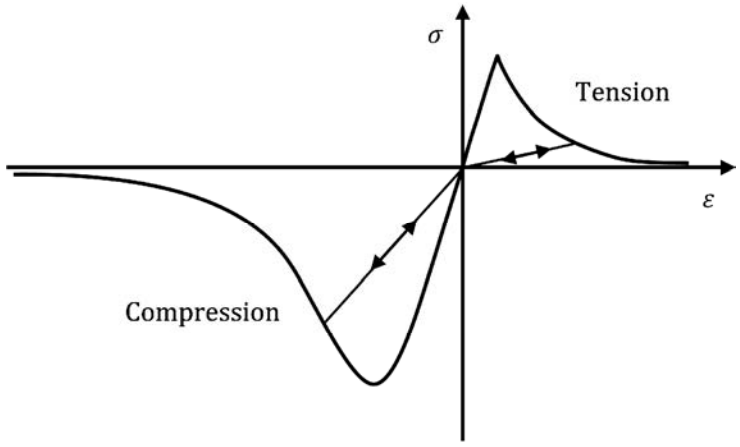

Figure 3-4: Secant unloading/reloading (DIANA user's manual, 2012)

3.3 Modelling of Non-prestressed and Prestressed Reinforcement

Compared to concrete, modelling of isotropic materials, such as non-prestressed (steel) and prestressed (tendon) reinforcement, is much simpler. Moreover, their behaviour in tension is identical to that in compression. The modelling of steel reinforcement and tendon in the FE analysis is commonly based on the theory of plasticity due to their high ductility. The Von-Mises plasticity is often employed to simulate plastic behaviour combined with one of the hardening rules, i.e. isotropic hardening (in which the yield surface expands under further loading), kinematic hardening (in which the yield surface shifts under further loading), or mixed isotropic/kinematic (Deaton, 2013).

A typical stress-strain curve for steel reinforcement is shown in Figure 3-5. Modelling of this relationship in the FE analysis is usually done by means of a bilinear elastic-perfectly plastic model or a bilinear elastic-plastic model on the basis of strain hardening. The elastic part of the model is defined by a linear stress-strain relation up to the point of yielding (f_{y}) with a slope equal to the initial elastic modulus of steel (E_{s}). After yielding, the behaviour is defined by either a horizontal line (in the case of elastic-perfectly plastic model) or an inclined line (in the case of elastic-plastic model) up to the ultimate strength (f_{u}). The slope of this line is determined according to the hardening parameter of reinforcement.

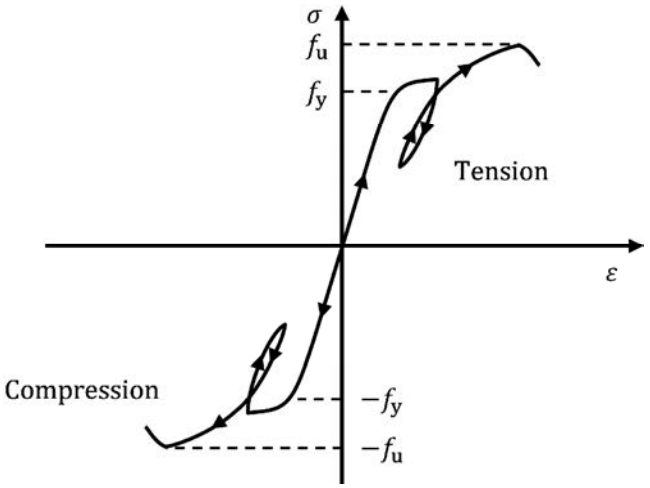

Figure 3-5: Typical stress-strain curve for steel reinforcement

Compared to the behaviour of steel reinforcement, the value of yielding stress in prestressed tendons (f_{py}) is much higher and is not well-defined (i.e. there is no plateau in the stress-strain relationship) as can be seen in Figure 3-6. Therefore, the behaviour of prestressed tendons is usually simulated using nonlinear elastic-plastic models rather than elastic-perfectly plastic models. However, the stress-strain

relationship is initially linear-elastic and extends approximately up to a stress value equal to 70% of the ultimate tensile strength (Greunen and Scordelis, 1983).

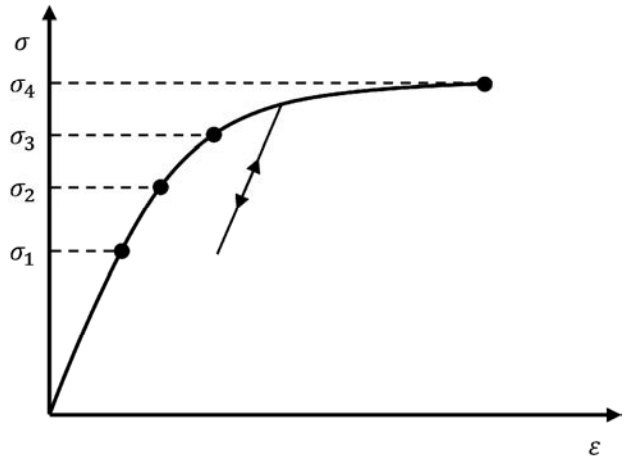

Figure 3-6: Typical stress-strain curve for tendons (Greunen and Scordelis, 1983)

3.4 Modelling of FRP Composites

As illustrated in Chapter One, FRP composites are made of fibres (e.g. carbon, glass, or aramid fibres) and a binding material called resin. A typical stress-strain relationship of FRP composites in tension is depicted in Figure 3-7. According to this figure, the behaviour of FRP composites in the FE analysis can be modelled by a linear elastic stress-strain relationship in tension with a slope equal to the elastic modulus of composite followed by brittle rupture failure. The rupture failure governs upon reaching the maximum tensile strain value of the FRP composites.

If unidirectional FRP sheets as shown in Figure 3-8 are used, then the composite is locally isotropic but is largely a material with anisotropic characteristics (or called transversely isotropic due to the same isotropic behaviour in the directions

perpendicular to the direction of the principal fibres). Consequently, special calculations are usually carried out to determine the properties of the composite in the direction of the principal fibres as well as the orthogonal directions.

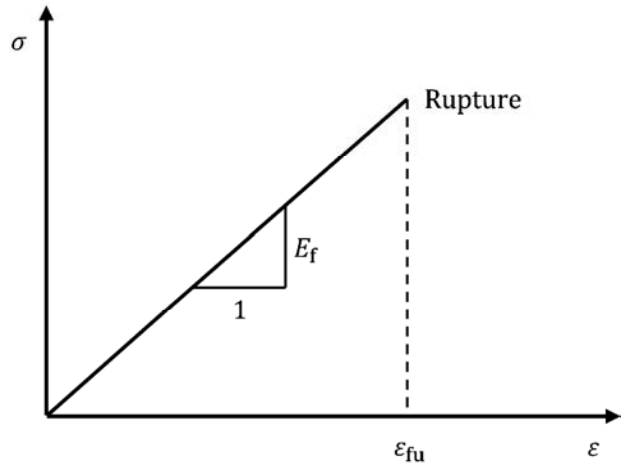

Figure 3-7: Typical stress-strain curve for FRP composites

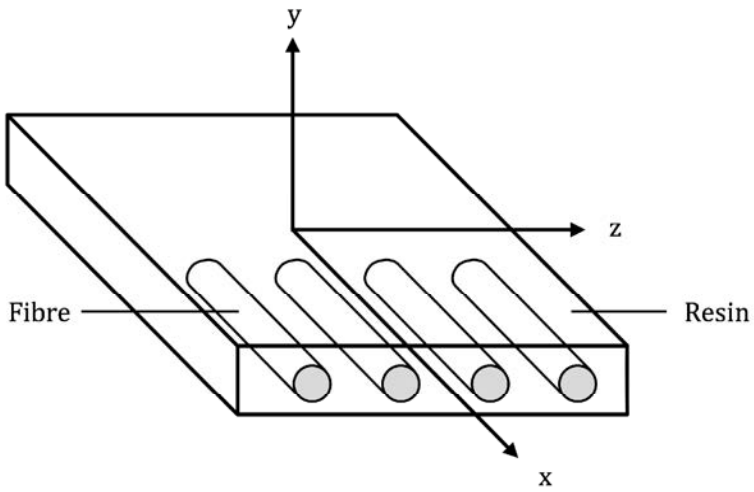

Figure 3-8: Unidirectional FRP laminate

The new composite properties, which can be determined according to Tsai (1963), include the elastic modulus of FRP composite in the principal and orthogonal

directions, in-plane and out-of plane shear modulus and Poisson's ratio for the three planes. It should be mentioned that sheets with bi-directional fibres were used in both sets of experimental work used for validation (see Section 4.2.1). Hence, the determination of aforementioned properties was not required in this study.

3.5 Nonlinear Solution Techniques

When the FE analysis is used to solve nonlinear structural problems, the relationship between the force and displacement vectors is no longer linear and the solution of algebraic equations becomes complex. The nonlinearity in RC and PC structures arises from the nonlinear behaviour of the constituent materials (e.g. due to concrete cracking, concrete crushing and yielding of reinforcement), contact nonlinearity (e.g. due to the bond-slip at the interface between concrete and reinforcement) and geometric nonlinearity due to large deformation (Madenci and Guven, 2015). The solution of nonlinear equations can be achieved either by adopting iterative technique, incremental technique or incremental-iterative technique.

The incremental-iterative solution is commonly used in nonlinear FE analysis, in which external load is applied incrementally, and in each load increment a set of successive iterations are performed to restore equilibrium. The equilibrium is achieved when the out-of-balance force vector (g), i.e. the difference between the external force vector (f_{ext}) and the internal force vector (f_{int}), is less than or equal to a pre-defined convergence criterion.

3.5.1 Iterative Procedures

The general procedure used in any iteration method is illustrated in Figure 3-9. The only difference between these methods is in the way of determining the iterative displacement increment (δu). The iterative displacement increment is used to calibrate the total displacement increment (Δu) until reaching equilibrium, as shown in Figure 3-9 (Bathe, 1996; Zienkiewicz and Taylor, 2000; DIANA user's manual, 2012).

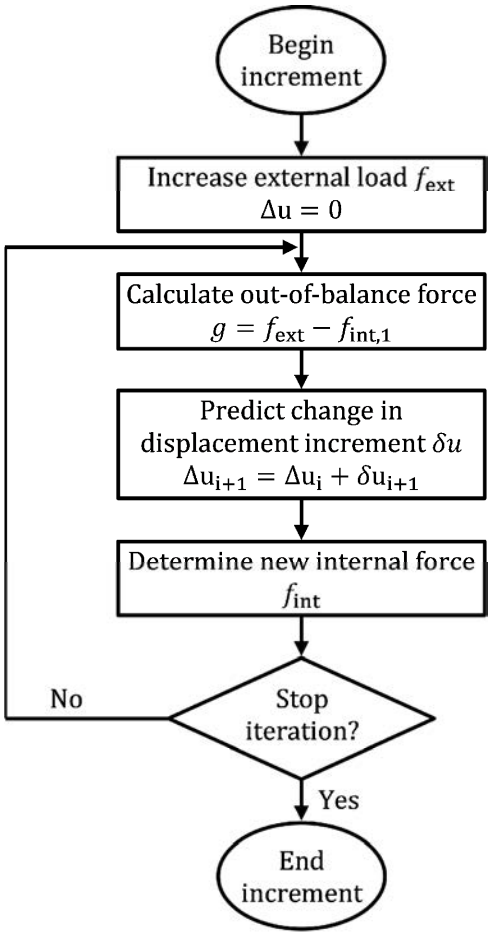

Figure 3-9: Iteration loop (DIANA user's manual, 2012)

The displacement increment at a certain iteration ($\delta \mathrm{u}_\mathrm{i}$) is determined from the stiffness matrix (K_i) and the out-of-balance force vector at the beginning of that Iteration (g_i), as follows (Zienkiewicz and Taylor, 2000; DIANA user's manual, 2012):

$$\delta \mathrm{u}_\mathrm{i} = {K_\mathrm{i}}^{-1} g_\mathrm{i} \tag{3-1}$$

3.5.1.1 Newton-Raphson Methods

The Newton-Raphson methods can be divided into the regular Newton-Raphson method and the modified Newton-Raphson method. These methods utilize the formula given in Equation 3-1 to determine the iterative displacement increment vector, in which K_i is the tangential stiffness matrix. The point of evaluating the tangential stiffness matrix in the regular Newton-Raphson method is different from that in the modified Newton-Raphson method (Zienkiewicz and Taylor, 2000).

In the regular Newton-Raphson, the tangential stiffness matrix is determined in each iteration loop, as depicted in Figure 3-10. However, the method requires a few iterations and takes time as it evaluates the tangential stiffness matrix in every iteration loop. Moreover, the prediction of current displacement increment vector is dependent on the last predicted situation, and hence divergence can easily occur when the initial solution is far from the final one (Zienkiewicz and Taylor, 2000).

In contrast, the evaluation of tangential stiffness matrix in the modified Newton-Raphson takes place only at the first iteration loop of each increment, as shown in Figure 3-11. Although convergence is achieved using more iterations compared to

the regular method, the iteration procedure is much faster in the modified Newton-Raphson method (Bathe, 1996; DIANA user's manual, 2012).

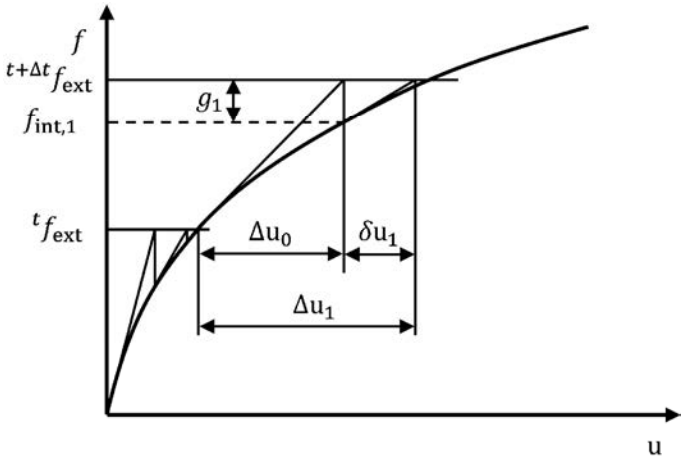

Figure 3-10: Regular Newton-Raphson method (Zienkiewicz and Taylor, 2000)

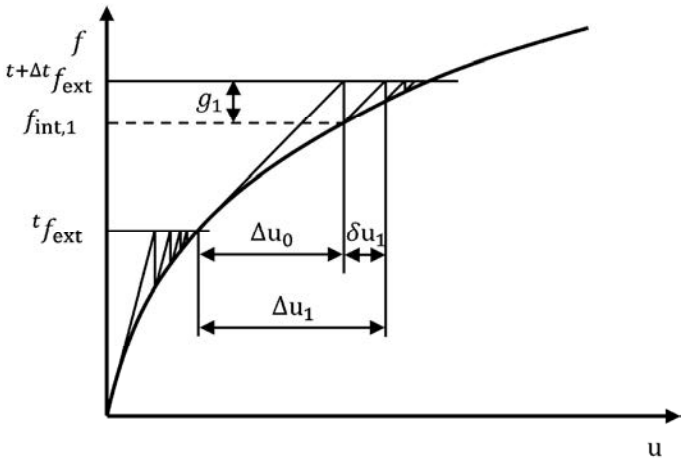

Figure 3-11: Modified Newton-Raphson method (Zienkiewicz and Taylor, 2000)

3.5.1.2 The Quasi-Newton Method (Secant Method)

During any increment of this method, a better approximation of the solution is achieved using the information of previous solution vectors as well as out-of-balance

force vectors (Rust, 2015), as illustrated in Figure 3-12. Though the secant stiffness matrix is updated in each iteration loop, the secant method does not require a complete setting up of this stiffness matrix. The secant method has a convergence rate per iteration loop between that of Newton-Raphson methods, based on the method used for assembling the stiffness matrix, and is given by (Bathe, 1996):

$$K_{i+1}\delta u_i = \delta g_i \tag{3-2}$$

$$\delta g_i = g_{i+1} - g_i \tag{3-3}$$

δg_i represents the change in out-of-balance force vector corresponding to δu_i.

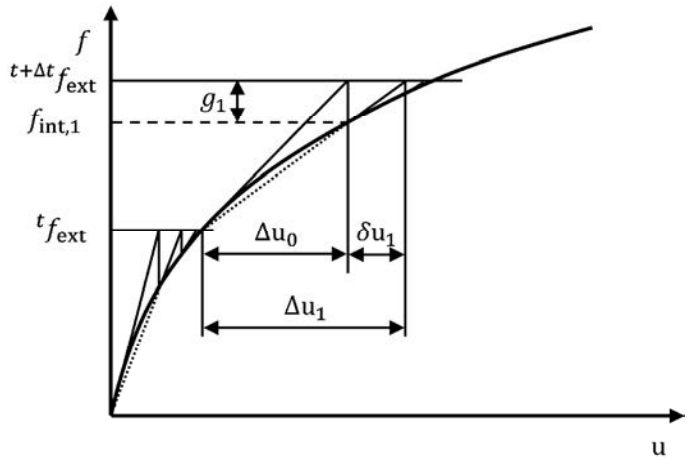

Figure 3-12: Quasi-Newton method (Zienkiewicz and Taylor, 2000)

3.5.2 Incremental Procedures

The most common procedures for applying the load incrementally are briefly given in the following subsections.

3.5.2.1 Load and Displacement Control

The load increments can be simply applied using the load control or the displacement control (Rust, 2015). In load control, the load increment is directly applied by increasing the external force vector (i.e. f_{ext}), whereas in displacement control, the load increment is indirectly applied by predefining certain displacement increments (u^{c}) as shown in Figure 3-13a and Figure 3-13b, respectively. Figure 3-13 shows that the load control fails to obtain solution for structures with snap-through behaviours.

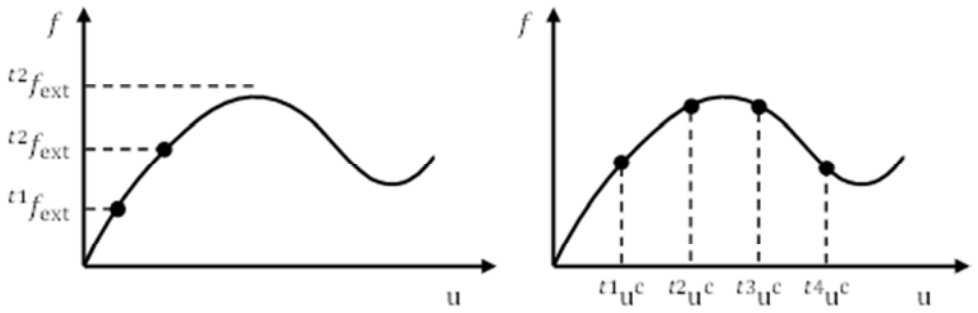

(a) Load control (b) Displacement control

Figure 3-13: Load and displacement control

As the external force is indirectly applied in displacement control, the predefined displacements are included in the external force vector at the initial iteration. Thereafter, the effective force vector, which is equivalent to the prescribed displacements, is determined by reformulating Equation 3-1 after dividing the displacement increment vector into unconstrained displacements ($\Delta\mathrm{u}^{\mathrm{u}}$) and constrained displacements ($\Delta\mathrm{u}^{\mathrm{c}}$). Both the stiffness matrix and the force vector in Equation 3-1 will be split likewise to result in (DIANA user's manual, 2012):

$$\begin{bmatrix} K^{uu} & K^{uc} \\ K^{cu} & K^{cc} \end{bmatrix}_0 \begin{Bmatrix} \Delta u^u \\ \Delta u^c \end{Bmatrix}_0 = \begin{Bmatrix} g^u \\ g^c \end{Bmatrix}_0 \quad (3\text{-}4)$$

The effective force vector is given in Equation 3-4 in the form of ($-K_0^{uc}\Delta u^c$).

3.5.2.2 Arc-length Control

If load control is used, the corresponding displacement increments to be predicted can be very large, particularly when the relationship between the load and displacement is nearly horizontal (DIANA user's manual, 2012). The arc-length control, shown in Figure 3-14, can be used to overcome such problems. In the Arc-length method, the load increment size is automatically adapted within the iteration process, depending on the current iteration results. In addition to the capability of the method in analysing structures with snap-through behaviour, which the displacement control can also do, the method can be used to analyse structures with snap-back behaviour (see Figure 3-14), which cannot be done using displacement control (Rust, 2015). However, this is not the case in this study.

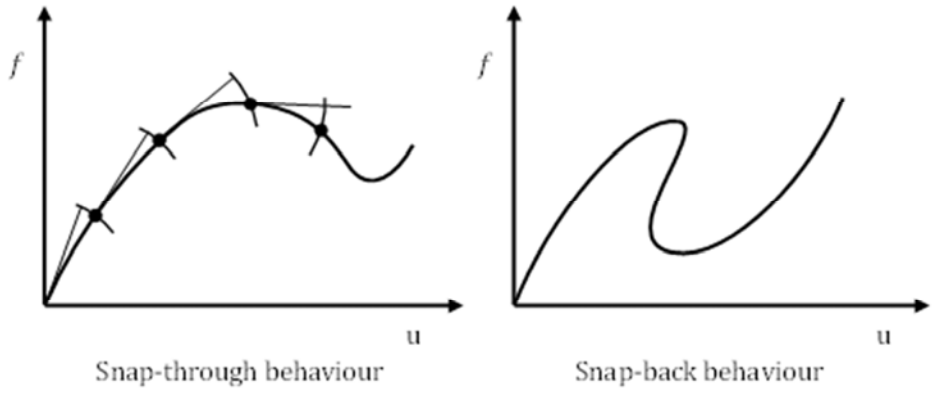

Figure 3-14: Arc-length control

3.5.3 Convergence Criteria

Convergence criteria are used to terminate the iteration process (see Figure 3-9) when results are obtained with an acceptable tolerance. Tight tolerance results in unnecessary iterations whereas loose tolerance leads to incorrect solutions. Convergence criteria are also utilized to stop the iteration process when the allowable iterations number is reached or the iteration is clearly leading to divergence. Convergence criteria can be classified into force, displacement, energy and residual criterion (DIANA user's manual, 2012; Rust, 2015). The following subsections address the force criterion and the displacement criterion illustrated in Figure 3-15.

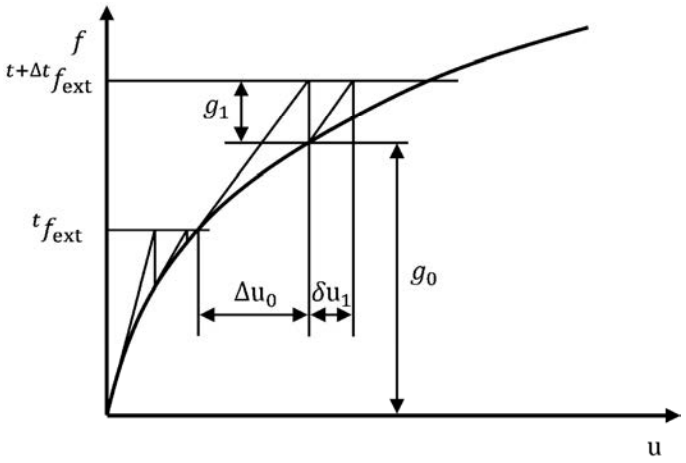

Figure 3-15: Force and displacement criterion items (DIANA user's manual, 2012)

3.5.3.1 The Force Criterion

In force criterion, the convergence is checked by comparing the out of balance force vector after the current iteration against the force vector of the initial unbalance (g_0), as follows (DIANA user's manual, 2012; Rust, 2015):

$$\text{Force criterion ratio} = \sqrt{\frac{g_i^T g_i}{g_0^T g_0}} \tag{3-5}$$

3.5.3.2 The Displacement Criterion

Similar to the force criterion, the convergence in the displacement criterion is checked by comparing the displacement vector after the current iteration against the displacement vector of the initial prediction (Δu_0), which can be expressed as follows (DIANA user's manual, 2012; Rust, 2015):

$$\text{Displacement criterion ratio} = \sqrt{\frac{\delta u_i^T \delta u_i}{\Delta u_0^T \Delta u_0}} \tag{3-6}$$

3.6 FE Studies on RC and PC Beams FRP-Strengthened in Shear

This section briefly addresses the previous work carried out on FE modelling of RC and PC beams strengthened in shear with either EB FRP laminates or DE FRP bars.

3.6.1 Beams Strengthened in Shear with EB FRP Laminates

As mentioned earlier in this chapter, the development of FEM has been in conjunction with the development of computers. Therefore, the early FE studies on shear-strengthened beams with EB FRP laminates (e.g. Kaliakin et al., 1996; Arduini et al., 1997; Vecchio and Bucci, 1999; Al-Mahaidi et al., 2001) were implemented using simpler procedures compared to the more recent studies. For instance, the

aforementioned studies assumed perfect bond between concrete and the EB FRP reinforcement, which resulted in a stiffer predicted response for the load-defection relationship (Arduini et al., 1997; Vecchio and Bucci, 1999). Moreover, the debonding mode of failure of the FRP cannot be predicted by such FE models.

Wong and Vecchio (2003) carried out FE analyses based on the rotating smeared crack approach of the MCFT to predict the debonding failure of beams strengthened in shear with EB FRP laminates. Two elementary bond-slip models were used throughout the study to simulate shear transfer and predict the debonding failure. The first model (the elastic-brittle model) was represented by a linear-brittle bond-slip model up to the bond strength value, whereas the second model (the elastic-plastic model) comprised a linear bond-slip relationship up to the bond strength value, followed by perfectly-plastic behaviour until reaching the ultimate slip value. The FRP laminates, which were simulated using truss elements, were linked to the concrete using either link elements or one dimensional contact elements.

The results obtained showed that the bond slip behaviour between concrete and FRP laminates should be considered in order to accurately predict the behaviour of strengthened beams. Moreover, there was no difference between the results obtained using link elements or contact elements. Although the developed models were able to reasonably predict the actual responses in terms of pre-yielding stiffness and load capacity, this success was limited, mainly due to the elementary bond-slip models used.

Later on, more accurate bond-slip models between the concrete and the EB FRP laminates were incorporated into the FE studies to accurately predict the debonding failure. In these studies, e.g. the work carried out by Godat et al. (2007) and Godat et al. (2010), the bilinear bond-slip model of Lu et al. (2005) was used. The fixed smeared crack concept was adopted for modelling the concrete, together with a constant shear retention factor of 0.5 to simulate the reduction in shear stiffness after cracking, as well as to indirectly account for the influence of dowel action. The concrete in tension after cracking was modelled using a linearly descending tension-stiffening model. The results showed that the numerical predictions were good compared to the load-deflection curves and failure modes of the tested beams. However the numerical predictions for post-cracking behaviour were slightly stiffer for most of the beams. This can be attributed mainly to the relatively high value adopted for the constant shear retention factor, or due to other factors such as the adopted tension-stiffening model. Moreover, the predicted strain distribution (i.e. strain profile) in the FRP laminates was not as good as would have been expected (i.e. compared to the good predictions achieved in terms of load-deflection curves and failure modes). This can be attributed to the fact that in FE models based on smeared crack approaches, the localised cracking in concrete is smeared over a finite region. It is also attributable to the stress-locking phenomenon, which is more likely to occur when the shear retention factor is relatively high (see Section 3.2.1.2).

Based on the good predictions achieved by Godat et al. (2007; 2010), the developed FE model was used to implement a numerical parametric study which was presented by Godat et al. (2012b). The study comprised the influence of stirrups ratio, concrete

grade, FRP stiffness, FRP ratio and a/d ratio on the axial strain in the FRP laminates, in addition to the influence of parameters controlling the debonding (i.e. stiffness, bond strength and fracture energy of the concrete-to-FRP bond-slip model). The numerical findings showed that the FRP axial strain increased with the increase in concrete grade, whereas it decreased with the increase in steel stirrups ratio, FRP stiffness and FRP ratio, whilst the effect of a/d ratio was not distinct. Amongst the investigated interfacial (i.e. bond-slip model) parameters, only fracture energy affected load-deflection behaviour (which increased positively with the increase in fracture energy) of the modelled beams.

A further study conducted by Godat et al. (2012c) investigated the influence of the type of element used to represent the FRP composites (i.e. shell elements which considered the in-plane orthotropic nature of the unidirectional FRP sheets versus truss elements which aligned in the direction of the fibres), the technique used for modelling the concrete-to-FRP interface and the mesh density along the depth of the FRP composites on the prediction accuracy of the FE model developed by Godat et al. (2007). The results obtained showed that the predicted load-deflection curves were flatter and less accurate when truss elements were used to model the FRP composites. For the modelling of concrete-to-FRP interface, spring, discrete truss or continuous truss elements were used. It was found that the spring elements were unable to accurately predict the debonding failure mode, which was attributed to the deficiency of spring elements in the FE package used, as opposed to the case of discrete or continuous truss elements. Finally, there was no significant difference in the results using element sizes of 25 mm or less along the depth of the FRP.

Chen et al. (2012) employed the FEM to quantify the effect of bond condition between concrete and longitudinal tension bars on the behaviour of FRP-shear strengthened RC beams. Two different assumptions for simulating bond condition were made in this study; the first was by adopting perfect bond assumption whereas the second involved using the bond-slip model of the CEB-FIP model code 90 (fib, 1993). The findings of this work suggest that the bond condition assumption can significantly change the crack patterns (i.e. the number and inclination of diagonal cracks), and consequently it affects the predicted shear behaviour. Therefore, the degree of increasing (when the number of cracks is increased but their inclination is intact) or decreasing (when the crack angle is increased) the shear capacity of the strengthened beams is dependent on the new crack patterns after including the bond-slip effect. Compared to experimental results, the FE models can more accurately predict the shear capacity and crack pattern of the tested beams when the bond-slip model is considered for the longitudinal reinforcement.

However, it should be mentioned that in other studies (e.g. Godat et al., 2007; Godat et al., 2010; Godat et al., 2012b; Dirar et al., 2013a), shear capacity was successfully predicted using perfect bond assumption between the concrete and the longitudinal reinforcement, as the mode of failure was not governed by bond failure.

Dirar et al. (2013a) compared the predictions of the commonly used constitutive models for the shear behaviour of FRP-strengthened RC beams. To this end, FE models based on the total strain rotating smeared crack approach, plasticity-based fixed smeared crack approach with a constant shear retention value of 0.1 and

plasticity-based fixed smeared crack approach with a variable shear retention factor were considered. The plasticity-based fixed crack models followed the von-Mises yield criterion for concrete in compression. A linear tension softening model was used for the behaviour of concrete in tension for all models. The unidirectional FRP composites were modelled using truss elements whereas the bilinear bond-slip model of Lu et al. (2005) was utilized for simulating the FRP-to-concrete interface behaviour. The results reveal that the FE model based on the rotating crack concept gave the best predictions in terms of the shear force-deflection response and mode of failure. However, the rotating crack model failed to predict the flexural mode of failure of one of the tested beams as a result of underestimating its shear capacity. This might be attributed to the modelling of FRP sheets, i.e. the use of truss elements, as reported by Godat et al. (2012c). Moreover, all FE models showed some discrepancies in predicting the actual strain in the EB FRP composites. Again, this can be attributed to the fact that localised cracking in concrete is smeared over a finite region. Hence, it results in a reduction in the accuracy of the model in predicting the strains of the FRP laminates.

Amongst the FE work carried out on shear strengthening with EB FRP, as far as can be ascertained, only two FE studies were conducted on PC beams. One of these studies was carried out by You et al. (2011), in which a three dimensional FE model based on the rotating smeared crack approach (which was favoured over the fixed smeared crack approach) was developed. In this study, the FRP sheets were simulated using shell elements and bond behaviour was modelled using the bilinear bond-slip model of Sato and Vecchio (2003). The modelling of mechanical

anchorages (used to anchor the FRP sheets) was implemented via adjusting the material properties of the interface elements locating along the anchorage system. The embedded reinforcement elements within the concrete were utilized to model the prestressed tendons assuming a perfect bond condition. Moreover, the phased analysis technique was used to model different loading history throughout the analysis. The developed model predicted the overall experimental responses reasonably well, especially when the effect of softening of concrete due to lateral cracking was considered. This might be attributed to the relatively coarse mesh used in the developed model.

The other FE model on PC beams shear-strengthened with EB CFRP was briefly reported by Zong et al. (2013). In this three dimensional model, perfect bond assumption was assumed between the concrete and FRP laminates. This might be accomplished due to the presence of mechanical anchorages at the free ends of the U-shape CFRP strips (see Section 4.2.1.2). Perfect bond was also assumed between the concrete and prestressed tendons, as the experimental mode of failure was not governed by bond failure along the prestressed tendons. Although the developed FE model was based on elementary modelling procedures, the results obtained (in terms of load-deflection responses, load-strain in stirrups and load-strain in EB CFRP sheets) demonstrated the capability of the model to predict the shear behaviour of strengthened PC beams.

From reviewing the published FE studies on shear strengthening with EB FRP laminates, the following might be concluded:

1. The accurate prediction of the FRP debonding failure can be only achieved when an appropriate bond-slip model for the behaviour of FRP-to-concrete interface is adopted.

2. Models based on smeared crack concepts can accurately simulate the shear force-deflection behaviour and failure mode of the FRP-strengthened beams. However, the FRP strain might not be reasonably predicted, especially in the case where the strengthened beams fail experimentally due to localised cracking.

3. In some cases, where the failure is governed by the bond along the longitudinal tension bars, considering the bond condition between the concrete and longitudinal tension bars can enhance the predictions in terms of crack patterns, and consequently load capacity.

4. The rotating smeared crack models seem to be more suitable in the modelling of concrete behaviour in shear than the fixed smeared crack models, mainly because the assumption of the shear retention factor value is sensitive and plays a substantial role on the FE model accuracy.

5. Shell elements can be used to accurately simulate the EB FRP laminates whilst the use of truss elements in modelling the EB FRP laminates results in flatter load-deflection responses.

6. The majority of the FE work has been carried out to validate the FE models rather than to numerically investigate the effect of the influencing parameters on the behaviour of beams strengthened in shear using EB FRP laminates.

7. A few FE studies have been conducted on PC shear-strengthened beams with EB FRP laminates. Therefore, further research is required in this field.

3.6.2 Beams Strengthened in Shear with DE FRP Bars

To date, as far as can be ascertained, there is only one study that addresses the FE modelling of beams strengthened in shear with DE FRP bars. The study was carried out by Godat et al. (2013) and involved the development of a nonlinear three-dimensional FE model to predict the experimental results of six beams tested by Mofidi et al. (2012), of which three were shear-strengthened with DE FRP bars, in terms of load-deflection response, strain in the DE FRP bars and failure mode. The fixed crack concept was adopted for concrete modelling with a linearly variable shear retention factor value, with a minimum of 0.5, to accommodate the influence of aggregate interlock and indirectly, the influence of steel dowel action. The FRP bars were simulated using truss element and connected directly to the concrete brick elements (i.e. perfect bond was assumed between concrete and the FRP bars) as debonding was not the governing mode of failure experimentally. The load was applied using displacement control.

Although good agreement was obtained between the FE predicted and experimental results, the strain in the FRP bars was reasonably predicted. Moreover, the predicted load-deflection responses were somewhat stiffer compared to the corresponding experimental responses in four of the modelled beams. This might be attributed to the adopted perfect bond assumption between the FRP bars and the concrete, as well as the relatively high value of the shear retention factor.

3.7 Concluding Remarks

An introduction to the development of FEM has been presented. Chapter Three has addressed FE modelling of the constitutive materials of RC and PC beams strengthened in shear with either EB or DE FRP composites. This comprised: modelling the behaviour of concrete in compression, modelling of concrete in tension, modelling of cracked concrete (i.e. the discrete crack concept and the smeared crack concept), theories behind concrete modelling in the FEM, modelling of non-prestressed and prestressed reinforcement and modelling of FRP composites.

In addition, a brief review of the most commonly applied techniques for solving the nonlinear equations of FE analysis has been presented. This included the commonly used iterative procedures, incremental procedures for applying the loads, as well as methods of achieving convergence.

In this chapter, relevant FE studies from the literature have been described, their main findings discussed and any knowledge gaps in the numerical studies have been shown. The main findings (e.g. the importance of considering bond-slip behaviour between concrete and FRP reinforcement, the suitability of the rotating smeared crack concept over the fixed smeared crack concept in modelling concrete beams in shear and the use of shell elements to accurately simulate EB FRP laminates) of these published studies were taken into account when developing the proposed FE models presented in Chapter Four.

CHAPTER 4: DEVELOPMENT AND VALIDATION OF FE MODELS

4.1 Introduction

In this study, the FE package DIANA version 9.4.4 (DIANA user's manual, 2012) was utilized to develop the three-dimensional nonlinear FE models. In addition to its extensive materials and elements library, the program provides further unique capabilities including user defined subroutines and phased analysis feature, which allows modelling of various cases using one FE model (through activating/deactivating elements and/or boundary conditions, or modifying of material properties during the analysis).

This chapter presents the constitutive models and element types used in the development of FE models. Two FE models were developed in this study, one for predicting the experimental behaviour of PC beams strengthened in shear with EB FRP laminates, and the other for RC beams strengthened in shear with DE FRP bars. The constitutive models and element types were selected carefully based on findings and recommendations of previous studies given in Chapter Three. Moreover, the developed FE models were validated against experimental results from the published literature before carrying out further FE analysis (i.e. the parametric studies presented in Chapter Five and Chapter Six).

4.2 Description of the Experimental Work

A description of experimental studies (i.e. Kang and Ary, 2012; Zong et al., 2013; Mofidi et al., 2012; Qin et al., 2014; Valerio and Ibell, 2003) used for the validation is given in the following subsection. Further details can be found in the original experimental work.

4.2.1 PC Beams Strengthened in Shear with EB FRP Laminates

Two series of FRP shear-strengthened PC beams were used for the validation of the first FE model. The first consisted of I-shape PC girders without steel stirrups tested by Kang and Ary (2012), whereas the second series comprised rectangular PC girders with internal steel stirrups tested by Zong et al. (2013).

4.2.1.1 Kang and Ary (2012)

Kang and Ary (2012) tested three I-shape PC girders in a four-point-bending configuration. The tested girders had an a/d ratio of 2.5 and were designed to fail in shear. One of the girders was used as a control specimen whereas the remaining two (i.e. IB-05 and IB-10) were strengthened using U-shaped EB bi-directional CFRP strips before testing.

The unstrengthened cross-section of the tested girders is shown in Figure 4-1. Each girder had two Ø12 mm steel bars in the compression flange. The tension flange reinforcement included two Ø25 mm bars, two Ø20 mm bars and two Ø12.5 mm tendons prestressed to 1075 MPa. Single-leg Ø10 mm steel bars were used as

stirrups within the constant moment zone whereas no internal shear reinforcement was used within the shear spans. In practice, however, prestressed concrete girders usually include at least a minimum amount of internal steel shear reinforcement. Kang and Ary (2012) reported that they excluded the shear reinforcement from the shear spans because their experimental programme was designed to study the bond behaviour between EB CFRP shear reinforcement and concrete in the absence of internal steel shear reinforcement.

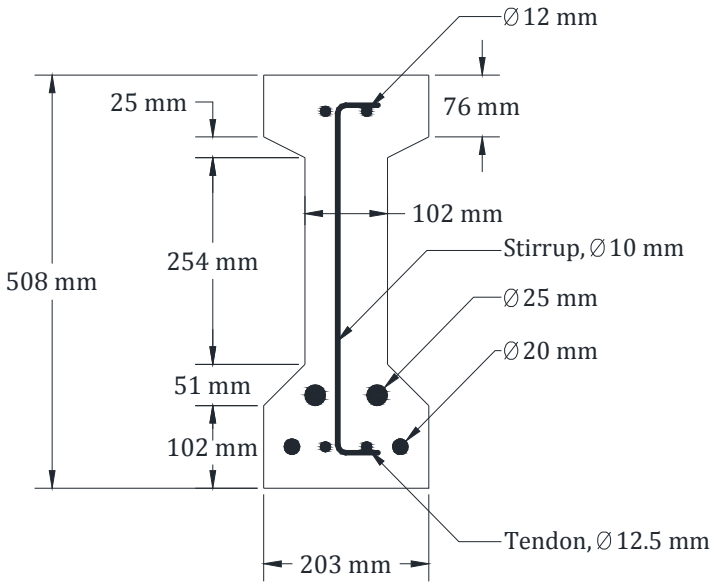

Figure 4-1: Unstrengthened cross-section of the tested PC I-girders (Kang and Ary, 2012)

The external shear reinforcement consisted of one layer (76 mm wide × 1.25 mm thick) of EB CFRP strips. Strip spacing was the only studied parameter in the experimental investigation. The centre-to-centre spacing between the EB CFRP strips was 127 mm in the case of IB-05 and 254 mm in the case of IB-10, as illustrated in Figure 4-2.

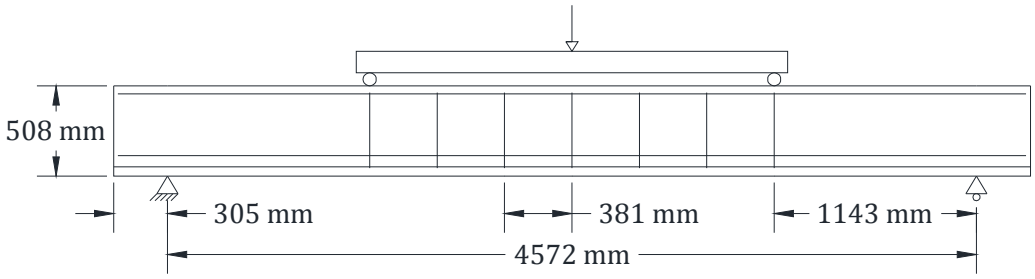

(a) Control girder

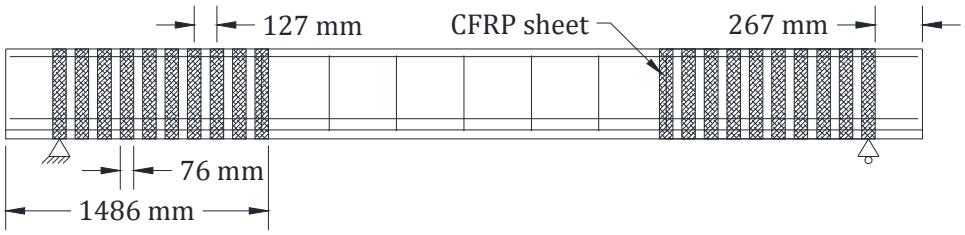

(b) IB-05

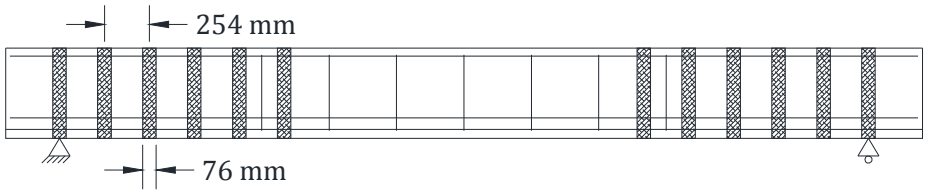

(c) IB-10

Figure 4-2: Details of the tested PC I-girders (Kang and Ary, 2012)

Table 4-1 summarises the mechanical properties of the concrete, steel reinforcement bars, seven-wire strands (tendons) and EB CFRP strips used in the experimental investigation.

Table 4-1: Material properties of the tested I-girders (Kang and Ary, 2012)

Material	Elastic modulus (MPa)	Cylinder compressive strength (MPa)	Ultimate strain (mm/mm)	Yield strength (MPa)	Ultimate strength (MPa)
Concrete	-	59.0	-	-	-
Ø10 mm stirrups	198927	-	-	439.2	699.0
Ø12 mm bars	186648	-	-	414.4	711.5
Ø20 mm bars	204547	-	-	476.4	766.0
Ø25 mm bars	192922	-	-	433.0	752.2
Ø12.5 mm tendons	200548	-	-	1656.8	1811.2
CFRP strips	6585	-	0.015	-	98.7

4.2.1.2 Zong et al. (2013)

The experimental work of Zong et al. (2012) was also used to validate the developed FE model. A total of three PC beams, i.e. an unstrengthened control beam (PPC0) together with two beams (PPC1 and PPC2) strengthened in shear with EB CFRP sheets, were considered.

The beams, which were 4,200 mm long, had a rectangular cross-section (as shown in Figure 4-3) with an overall depth, effective depth and width of 360 mm, 330 mm and 180 mm, respectively. The beams were tested in a four-point-bending configuration and had an a/d ratio of 2.42. PPC0 and PPC2 had an effective prestress of $0.42f_{\mathrm{pu}}$, where f_{pu} is the ultimate tensile strength of the prestressing tendons. The effective prestress was $0.31f_{\mathrm{pu}}$ in the case of PPC1.

For all tested girders, the compression reinforcement comprised three Ø14 mm steel bars, whereas three Ø25 mm steel bars and two Ø15.2 mm low-relaxation double-

harped prestressing tendons were used in tension, as shown in Figure 4-4. The internal shear reinforcement consisted of Ø6.5 mm steel stirrups spaced at 200 mm centre-to-centre.

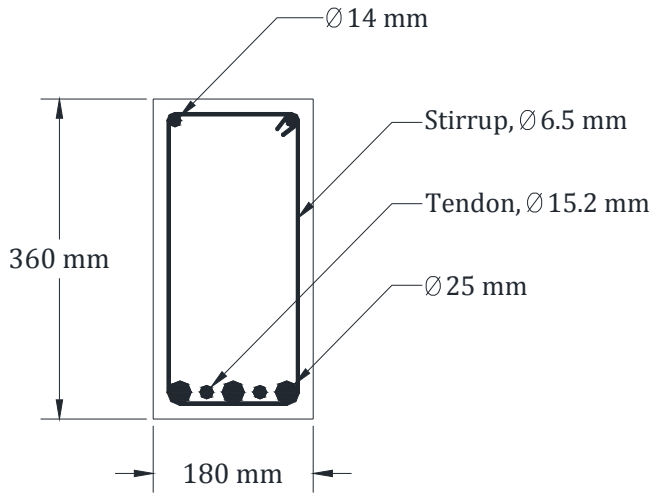

Figure 4-3: Unstrengthened cross-section of the tested PC girders (Zong et al., 2013)

The EB strengthening system, as shown in Figure 4-4, consisted of 40 mm wide × 1.4 mm thick bi-directional U-shaped CFRP sheets spaced at 200 mm centre-to-centre. In order to prevent debonding, the FRP sheets were anchored from the top. For the anchorage system, horizontal steel plates, 60 mm wide × 3 mm thick, were used to anchor the EB CFRP sheets. The horizontal steel plates were anchored to the concrete using adhesive paste and Ø8 mm bolts.

The mechanical properties of the materials used in the experimental work are presented in Table 4-2.

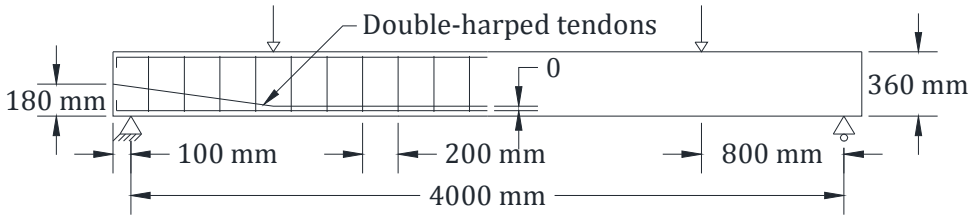

(a) Unstrengthened girder (PPC0)

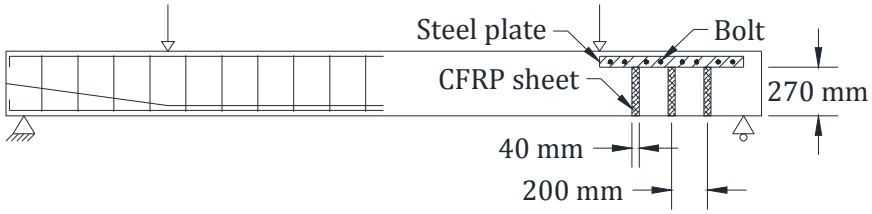

(b) Strengthened girders (PPC1 and PPC2)

Figure 4-4: Details of the tested PC girders (Zong et al., 2013)

Table 4-2: Material properties of the tested girders (Zong et al., 2013)

Material	Elastic modulus (MPa)	Cylinder compressive strength (MPa)	Ultimate strain (mm/mm)	Yield strength (MPa)	Ultimate strength (MPa)
Concrete	-	40.0	-	-	-
Ø6.5 mm stirrups	204000	-	-	350.0	531.0
Ø14 mm bars	200000	-	-	390.0	585.0
Ø25 mm bars	201000	-	-	351.0	558.0
Ø15.2 mm tendons	195000	-	-	1380.0	1860.0
CFRP strips	185000	-	0.0151	-	2800.0

4.2.2 RC Beams Strengthened in Shear with DE FRP Bars

Three of the studies mentioned previously in Section 2.9 were used for the validation of the second FE model: namely Mofidi et al. (2012), Qin et al. (2014) and Valerio and Ibell (2003). Amongst these experimentally tested beams, only the beams that failed in shear were considered in the validation. A summary of these studies is given in the following subsections.

4.2.2.1 Mofidi et al. (2012)

Four of the RC T-beams tested by Mofidi et al. (2012) were used to validate the proposed FE model. Of these, two beams were unstrengthened whereas the other two were strengthened in shear using DE FRP bars. Each beam had cross-sectional dimensions of 406 mm overall depth, 508 mm flange width, 152 mm web width and 102 mm flange thickness. The beams were reinforced in tension with four Ø25 mm steel bars, whilst six Ø10 mm steel bars were used in the compression flange, as illustrated in Figure 4-5.

One of the unstrengthened beams (S0-CON) had no internal shear reinforcement (stirrups), while the other unstrengthened beam (S1-CON) had Ø8 mm steel reinforcement stirrups placed at 175 mm centre-to-centre. For the two strengthened beams, one of them (S0-12s130d) had no internal shear reinforcement and was strengthened in shear using Ø12.7 mm sand-coated CFRP bars placed at 130 mm centre-to-centre. The other strengthened beam (S1-12d260s) had internal shear reinforcement consisting of Ø8 mm steel stirrups, which were placed at 175 mm

centre-to-centre, in addition to shear strengthening with Ø12.7 mm CFRP bars, which were placed at 260 mm centre-to-centre (see Figure 4-5d).

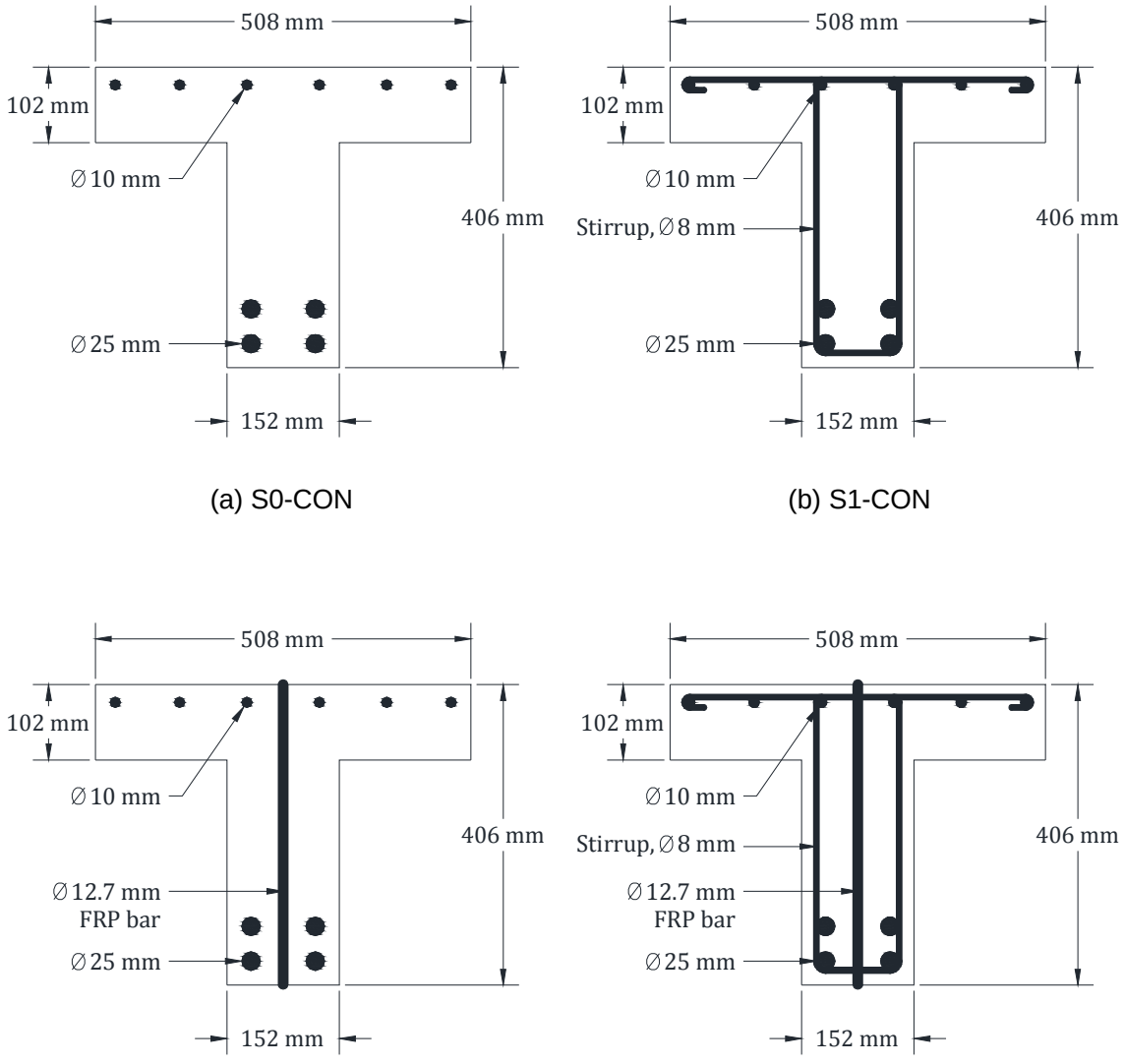

Figure 4-5: Cross-sections of the tested T-beams (Mofidi et al., 2012)

The beams were 4,520 mm long and tested in a three-point-bending test (with a/d ratio of 3.0) as depicted in Figure 4-6. The mechanical properties of the tested beams are given in Table 4-3.

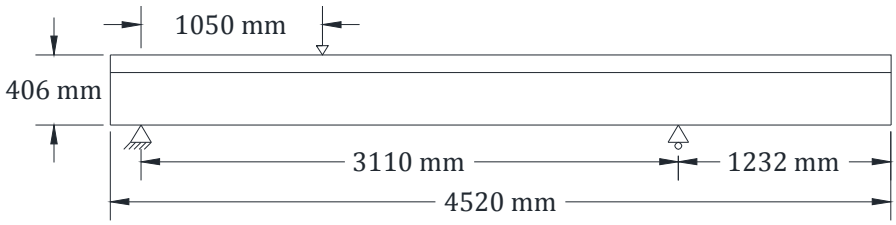

Figure 4-6: Configuration of the tested T-beams (Mofidi et al., 2012)

Table 4-3: Material properties of the tested T-beams (Mofidi et al., 2012)

Material	Elastic modulus (MPa)	Cylinder compressive strength (MPa)	Ultimate strain (mm/mm)	Yield strength (MPa)	Ultimate strength (MPa)
Concrete	-	25 *	-	-	-
Ø8 mm stirrups	200000	-	-	540.0	-
Ø10 mm bars	200000	-	-	470.0	-
Ø25 mm bars	200000	-	-	470.0	-
CFRP bars	148000	-	0.0127	-	1885.0
* The cylinder compressive strength of S1-12d260s beam was 29.6 MPa					

4.2.2.2 Qin et al. (2014)

Two of the RC T-beams, i.e. the control beam (N00) and the uncorroded strengthened beam (R00) mentioned in Section 2.9, tested by Qin et al. (2014) were used for the purpose of validation. The tested beams had cross-sectional dimensions of 360 mm total depth, 260 mm flange width, 125 mm web width and 100 mm flange

thickness as shown in Figure 4-7. The beams were 2,700 mm long with an effective depth of 295 mm and tested in a three-point-bending test (resulting in an a/d ratio of 3.05) as depicted in Figure 4-8.

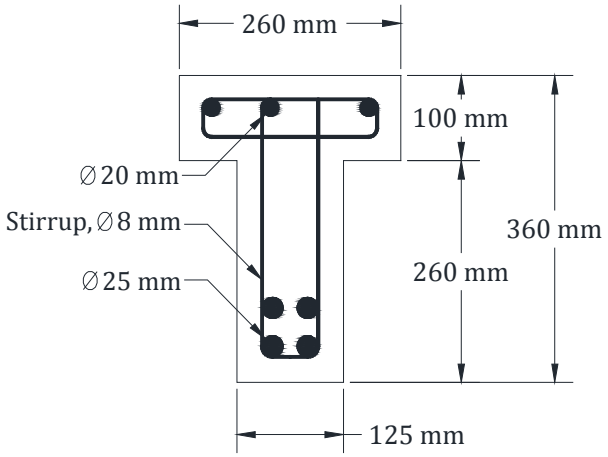

Figure 4-7: Unstrengthened cross-section of the tested T-beams (Qin et al., 2014)

The internal steel reinforcement comprised three Ø20 mm steel bars in the compression flange and four Ø25 mm bars in tension, whereas the shear reinforcement consisted of Ø8 mm steel stirrups. These stirrups were placed at 275 mm centre-to-centre within the shear span, whilst they were placed at 100 mm centre-to-centre outside the shear zone (see Figure 4-8).

For R00 beam, the shear strengthening scheme comprised Ø10 mm sand-coated DE CFRP bars placed at 275 mm centre-to-centre (see Figure 4-8b). Table 4-4 summarises the mechanical properties of the CFRP bars in additional to the mechanical properties of the other materials used by Qin et al. (2014).

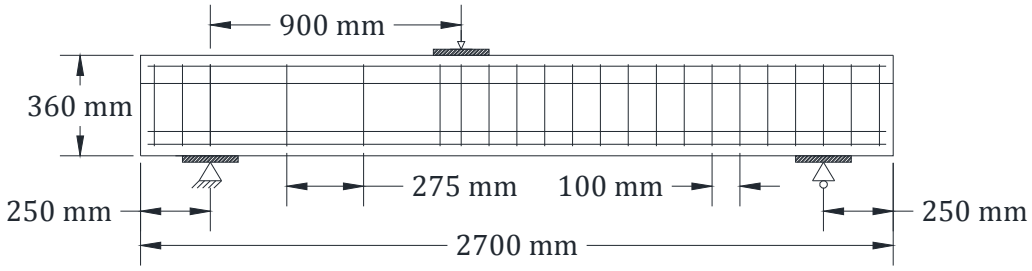

(a) Unstrengthened beam (N00)

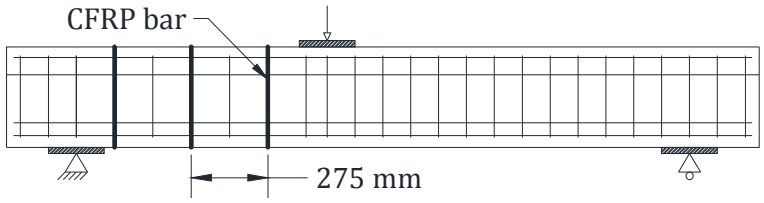

(b) Strengthened beam (R00)

Figure 4-8: Details of the tested T-beams (Qin et al., 2014)

Table 4-4: Material properties of the tested T-beams (Qin et al., 2014)

Material	Elastic modulus (MPa)	Cylinder compressive strength (MPa)	Ultimate strain (mm/mm)	Yield strength (MPa)	Ultimate strength (MPa)
Concrete	-	21 *	-	-	-
Ø8 mm (test span)	186000	-	-	542.0	664.0
Ø8 mm (other)	183000	-	-	573.0	655.0
Ø20 mm bars	179000	-	-	576.0	707.0
Ø25 mm bars	180000	-	-	537.0	669.0
CFRP bars	124000	-	0.0175	-	2172.0
* The cylinder compressive strength of R00 beam was 17.4 MPa					

4.2.2.3 Valerio and Ibell (2003)

The third set of beams used for the validation included Specimens 1, 8, 9 and 10 tested by Valerio and Ibell (2003). Specimen 1 was an unstrengthened control beam. Specimens 8, 9 and 10 were strengthened in shear with sand-coated DE Arapree bars. Each of the tested beams had a rectangular cross-section and was reinforced in tension only with two Ø12 mm steel bars. The dimensions of this cross-section were 220 mm, 189 mm and 110 mm respectively for the overall depth, effective depth and web width. Figure 4-9 illustrates the cross-sections of the tested beams.

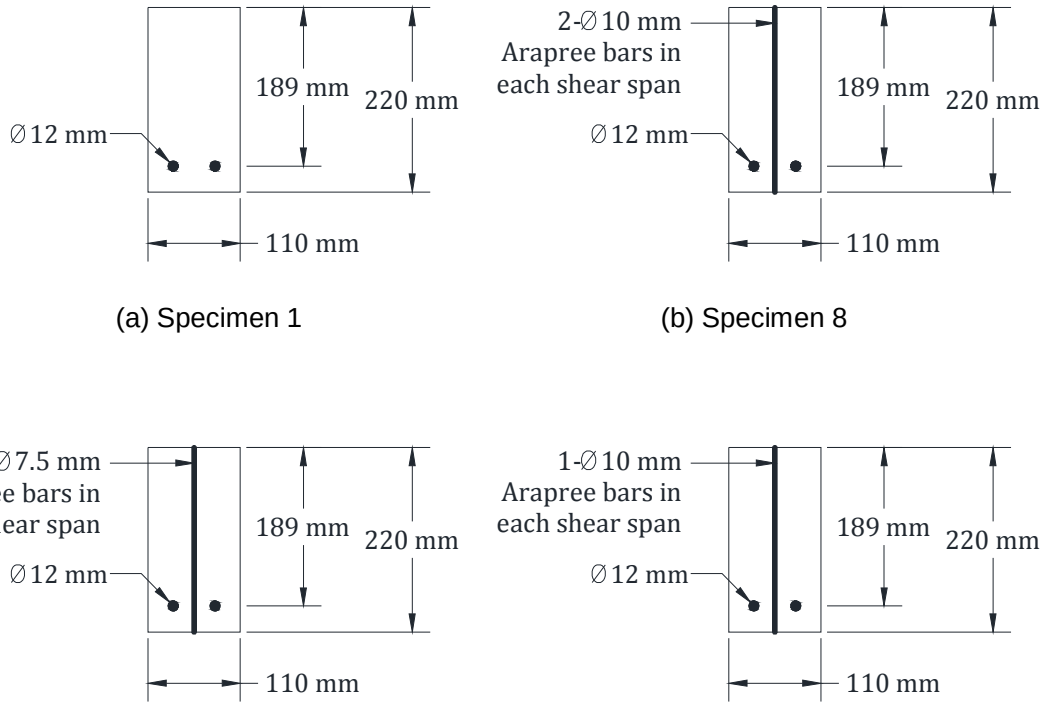

(a) Specimen 1

(b) Specimen 8

(c) Specimen 9

(d) Specimen 10

Figure 4-9: Cross-sections of the tested beams (Valerio and Ibell, 2003)

As can be seen in Figure 4-9, shear strengthening of this series involved two Ø10 mm Arapree bars (placed at 200 mm centre-to-centre), two Ø7.5 mm Arapree bars (placed at 200 mm centre-to-centre) and one Ø10 mm Arapree bar (placed in the middle) in each shear span of Specimens 8, 9 and 10, respectively.

The beams, which were 3,000 mm long, tested in a four-point-bending test with an a/d ratio of 3.17 as depicted in Figure 4-10. The mechanical properties of the materials used in the test are summarised in Table 4-4.

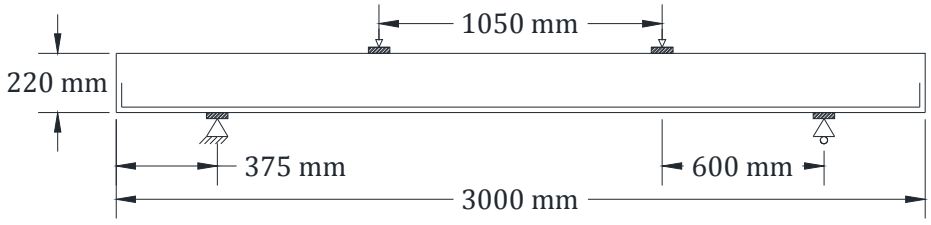

Figure 4-10: Configuration of the tested beams (Valerio and Ibell, 2003)

Table 4-5: Material properties of the tested beams (Valerio and Ibell, 2003)

Material	Elastic modulus (MPa)	Cylinder compressive strength (MPa)	Ultimate strain (mm/mm)	Yield strength (MPa)	Ultimate strength (MPa)
Concrete	-	47.2 *	-	-	-
Ø12 mm bars **	-	-	-	635.0	715.0
Ø7.5 mm Arapree bars	60000	-	0.024	-	1500.0
Ø10 mm Arapree bars	60000	-	0.024	-	1500.0

* The cylinder compressive strength of Specimen 1 was 40.8 MPa

** Elastic modulus value was assumed to be equal to 200000 MPa in the FE model

4.3 Material Modelling

Several material constitutive models from the published literature were tested. Based on the results obtained, the most appropriate ones were selected to develop the FE models. The following subsections describe the material constitutive models adopted in the FE modelling. The same constitutive models were used in both FE models unless otherwise stated.

4.3.1 Concrete

A total strain rotating crack model, based on the smeared crack concept, was used for the concrete. In this model, explicit modelling of the concrete shear behaviour after cracking is not required as the crack plane is always a principle plane with no shear stresses acting on it (see Section 3.2.1.2).

The behaviour of concrete in tension and compression in total strain models is described with one uniaxial stress-strain curve, as mentioned earlier in Section 3.2.2.3. In this study, the stress-strain curve of Thorenfeldt et al. (1987) was used for the behaviour of concrete in compression, in which both the ascending and descending branch are determined using one equation as follows (Thorenfeldt et al., 1987):

$$\frac{f_c}{f_c'} = \frac{m\left(\frac{\varepsilon_c}{\varepsilon_c'}\right)}{m - \left(1 - \left(\frac{\varepsilon_c}{\varepsilon_c'}\right)^{mk}\right)} \qquad (4\text{-}1)$$

where f_c represents the stress in concrete (MPa) at a given strain ε_c (mm/mm), f_c' is the compressive strength of concrete (given in Tables 4-1 through 4-5), ε_c' is the strain corresponding to the compressive strength of concrete (mm/mm) in the stress-strain curve (automatically calculated in DIANA), m is a parameter which can be determined as $0.18 + (f_c'/17)$ and k is a parameter to control the post-peak part of the stress-strain curve given by (Thorenfeldt et al., 1987):

$$k = \begin{cases} 1 & (\text{if } \varepsilon_c' > \varepsilon_c > 0) \\ 0.67 + (f_c'/62) & (\text{if } \varepsilon_c' \leq \varepsilon_c) \end{cases} \quad (4\text{-}2)$$

In addition, the softening of concrete in compression due to lateral cracking was taken into account by incorporating model-B, developed by Vecchio and Collins (1993), as follows (Vecchio and Collins, 1993; DIANA user's manual, 2012):

$$\beta_{\sigma_{cr}} = \frac{1}{1 + 0.27\left(-\frac{\varepsilon_{lat}}{\varepsilon_c'} - 0.37\right)} \leq 1 \quad (4\text{-}3)$$

where $\beta_{\sigma_{cr}}$ is the concrete compressive strength reduction factor and ε_{lat} represents the average lateral damage which is determined from the tensile damage in the first and second lateral direction, $\varepsilon_{l,1}$ and $\varepsilon_{l,2}$, respectively, as follows:

$$\varepsilon_{lat} = \sqrt{\varepsilon_{l,1}^2 + \varepsilon_{l,2}^2} \quad (4\text{-}4)$$

Furthermore, a Poisson's ratio value of 0.15 was adopted in this study which is consistent with the recommendation of Model Code 2010 (fib, 2012), whereas the elastic modulus value of concrete (E_c) was determined according to Wang et al. (1978) as follows:

$$E_c = 271\, f_c' + 978 \qquad (\text{in Ksi}) \tag{4-5}$$

For the behaviour of concrete in tension, two different scenarios were utilised. One of the scenarios (represented by a multi-linear quasi-brittle model) was used in the first FE model which was developed to simulate the PC beams described in Section 4.2.1. This quasi-brittle model consisted of a linear tensile stress-tensile strain relationship up to the value of the concrete uniaxial tensile strength (f_t) with a slope equal to E_c. The post-peak behaviour of concrete in tension was represented by a sharp slope drop in the tensile stress to a value just higher than zero, so as to maintain analysis stability.

The other scenario was used in the second FE model which was developed to simulate the RC beams presented in Section 4.2.2. This was implemented using a linear stress-strain relationship up to f_t with a slope equal to E_c, then followed by a linear tension stiffening model (based on fracture energy of concrete in tension G_f^I and crack bandwidth h_c) to model the gradual loss of concrete tensile strength after cracking. In this study, G_f^I was determined according to the model proposed by Remmel (1994) (cited in Deaton, 2013, p.85) as follows:

$$G_{\mathrm{f}}^{\mathrm{I}} = 0.065 \times \ln\left(1 + \frac{f_c'}{10}\right) \quad (4\text{-}6)$$

The uniaxial tensile strength of concrete was determined according to the Concrete Society TR55 (2000) as follows:

$$f_t = 0.18(f_{\mathrm{cu}})^{2/3} \quad (4\text{-}7)$$

where f_{cu} is the cube compressive strength of concrete (MPa).

4.3.2 Steel Reinforcement and Prestressing Tendons

Apart from the PC girders tested by Zong et al. (2013), all the longitudinal steel reinforcement and stirrups were modelled using an elastic-perfectly plastic model according to the experimentally measured yield strength and modulus of elasticity values (see the values reported in Tables 4-1, 4-3, 4-4 and 4-5).

For the beams tested by Zong et al. (2013), an elastic-plastic model, combined with von-Mises yield criterion (with isotropic hardening rule), was used for both the longitudinal steel reinforcement and stirrups based on the mechanical properties of the reinforcement given in Table 4-2. This exemption in steel reinforcement modelling can be justified by the fact that the internal reinforcement used by Zong et al. (2013) had relatively low yield strength values, which resulted in yielding of stirrups at earlier stages of loading before reaching failure. Due to the unavailability of full stress-strain curves for the reinforcement, the strain hardening ratio of the steel reinforcement was

taken as 2%. A similar approach was adopted by Ahmed and Gunasekaran (2014), Moradi and Alam (2015) and Van der Linde (2015). For the prestressing tendons, an elastic–plastic model combined with von-Mises yield criterion (with isotropic hardening rule) was employed. The experimental stress-strain relationship depicted in Figure 4-11 was used for the girders tested by Kang and Ary (2012).

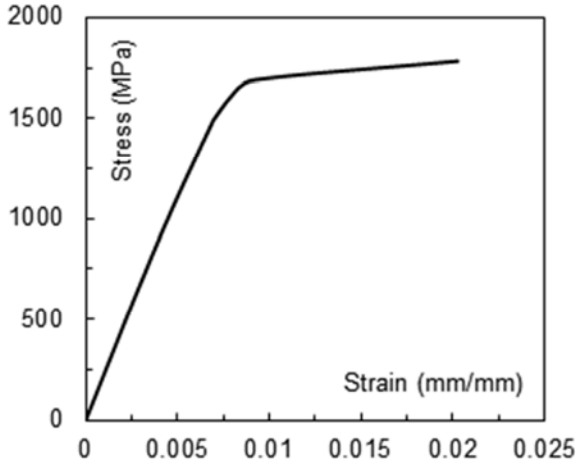

Figure 4-11: Stress-strain curve for tendons (Kang and Ary, 2012)

Due to the lack of stress-strain relationship for the tendons of the beams tested by Zong et al. (2013), the stress-strain curve of tendons was generated using the model proposed by Devalapura and Tadros (1992) which is given by:

$$f_{\mathrm{ps}} = \varepsilon_{\mathrm{ps}}\left[A + \frac{E_{\mathrm{ps}} - A}{\left(1 + \left(\frac{E_{\mathrm{ps}}\varepsilon_{\mathrm{ps}}}{1.04f_{\mathrm{py}}}\right)^{D}\right)^{1/D}}\right] \leq f_{\mathrm{pu}} \tag{4-8}$$

$$A = E_{\mathrm{ps}}\left(\frac{f_{\mathrm{pu}} - 1.04f_{\mathrm{py}}}{\varepsilon_{\mathrm{pu}}E_{\mathrm{ps}} - 1.04f_{\mathrm{py}}}\right) \tag{4-9}$$

where f_{ps} represents the stress in tendons (Ksi) at a certain strain $\varepsilon_{\mathrm{ps}}$ (in/in), E_{ps} is the modulus of elasticity of tendons (Ksi), f_{py} is the yield strength of tendons (Ksi), $\varepsilon_{\mathrm{pu}}$ is the ultimate strain (in/in) corresponding to the tensile strength of tendons f_{pu} (Ksi), and D is a constant parameter which can be found from solving Equation 4-8 at f_{ps} equal to f_{py} and $\varepsilon_{\mathrm{ps}}$ equal to 0.01.

Similar to previous studies (e.g. Godat et al. 2007; Godat et al. 2010; Godat et al. 2012b; Dirar et al., 2013a; Zong et al., 2013), bond failure was not the governing failure mode; hence, perfect bond was assumed between the concrete and the ordinary steel reinforcement and tendons.

4.3.3 FRP Composites

As mentioned earlier in Section 3.4, FRP sheets with bi-directional fibres were used in both experimental works (i.e. Kang and Ary, 2012; Zong et al., 2013). Thus, the tensile behaviour of the FRP laminates in the in-plane directions can be modelled by a linear elastic stress-strain relationship, up to the ultimate tensile strength values of the FRP laminates given in Table 4-1 and Table 4-2, with a slope equal to the elastic modulus of the FRP laminates, then followed by a brittle rupture type of failure (see Figure 3-7).

As with the FRP sheets, the behaviour of the FRP bars in the axial direction was modelled by a linear-brittle stress-strain relationship up to the ultimate tensile strength with a slope equal to the elastic modulus of the FRP bars. The

experimentally measured values of the ultimate tensile strength and elastic modulus of the FRP bars (as given in Tables 4-3, 4-4 and 4-5) were used. A Poisson's ratio of 0.35 was assumed for the FRP composites (Kaliakin et al., 1996).

4.3.4 FRP-to-Concrete Interface

The bond zone between the concrete and EB CFRP laminates was modelled by the bi-linear bond-slip model developed by Sato and Vecchio (2003). This model assumes that bond failure occurs within a thin layer of the concrete adjacent to the concrete-to-adhesive interface because the adhesive is usually stronger than the concrete. Hence, the bond-slip model simulates the overall behaviour of the CFRP-to-concrete interface rather than the adhesive material itself. The adopted bond-slip model, which is shown in Figure 4-12, is given by:

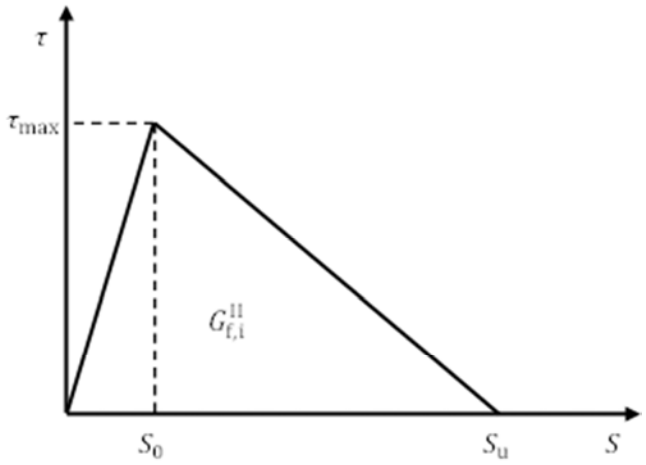

Figure 4-12: EB CFRP-to-concrete bond-slip model (Sato and Vecchio, 2003)

$$\tau_{max} = (54 f_c')^{0.19} \quad (4\text{-}10)$$

$$S_0 = 0.057\sqrt{G_{\mathrm{f,i}}} \tag{4-11}$$

$$S_{\mathrm{u}} = \frac{2G_{\mathrm{f,i}}}{\tau_{\max}} \tag{4-12}$$

$$G_{\mathrm{f,i}}^{\mathrm{II}} = \left(\frac{\tau_{\max}}{6.6}\right)^2 \tag{4-13}$$

where $\tau_{\max}$ is the bond strength (MPa), S_0 is the slip (mm) corresponding to $\tau_{\max}$, S_{u} is the ultimate slip (mm) and $G_{\mathrm{f,i}}^{\mathrm{II}}$ is the mode II (in-plane shear) interfacial fracture energy (N/mm). Debonding starts when the slip value exceeds S_0 and complete debonding occurs when the slip value reaches S_{u}.

On the other hand, the two-part bond-slip model developed by Mofidi et al. (2012) was adopted to simulate the interface behaviour between the concrete and FRP bars. This model, which is depicted in Figure 4-13, was developed based on the modified BPE bond-slip (Cosenza et al., 1997) and pullout test results of a series of DE FRP bars carried out by Godat et al. (2012a).

As can be seen from Figure 4-13, the ascending branch of this model is defined by a parabolic relationship between the bond stress and slip, up to the value of bond shear strength τ_{m}, as follows:

$$\tau = \tau_{\mathrm{m}}\left(\frac{S}{S_{\mathrm{m}}}\right)^{\alpha_{\mathrm{a}}} \tag{4-14}$$

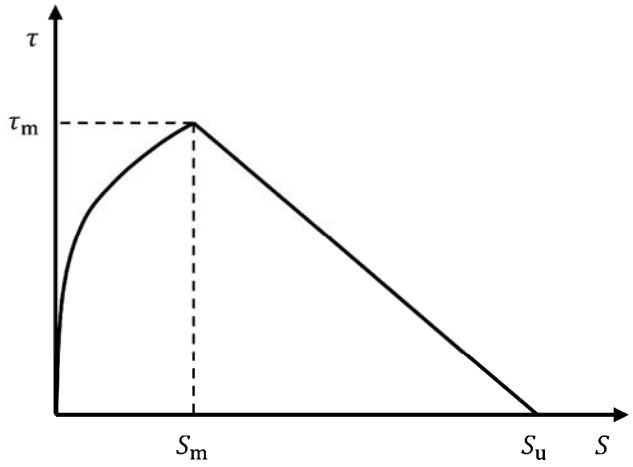

Figure 4-13: FRP bar-to-concrete bond-slip model (Mofidi et al., 2012)

then it is followed by a linear descending branch which continues until it reaches zero, given by:

$$\tau = \tau_m \left(1 + p - p\frac{S}{S_m}\right) \quad (4\text{-}15)$$

where τ is the bond stress at a specific slip S, p is a parameter to control the descending branch of the bond-slip relationship (can be taken as 0.07 for sand-coated CFRP bars), whereas the definition of other parameters (i.e. τ_m, S_m and α_a) can be found in Section 2.10.2.2. Similar to the previous bond-slip model, this bond-slip model is used to represent the overall FRP bar-to-concrete interface behaviour rather than that of the adhesive material.

In this study, the bond-slip model given in Equations 4-14 and 4-15 was used for the FE modelling of the beams tested by Mofidi et al. (2012) and Qin et al. (2014), in which the beams were strengthened with sand-coated CFRP bars. However, two

different scenarios were adopted in modelling the beams tested by Valerio and Ibell, (2003), due to the lack of a bespoke bond stress-slip model for the DE AFRP bars. The first scenario was implemented using perfect bond assumption between the concrete and AFRP bars, whereas the bond-slip model developed by Mofidi et al. (2012) was adopted in the second scenario to investigate the influence of the bond-slip model on the predicted shear behaviour of the strengthened beams. A comparison between the results obtained is given in the validation section.

4.3.5 Loading, Support and End Plates

Loading and support plates were used in all beams, whilst end plates were only used in the case of PC beams to avoid stress concentrations in the concrete elements (see Figures 4-22 and 4-26). Such stress concentrations are caused by prestressing force in tendons and may lead to convergence difficulties.

The behaviour of these steel plates in compression and tension was modelled by an elastic-perfectly plastic model combined with von-Mises yield criterion (DIANA user's manual, 2012). The assumed values of elastic modulus, yield stress and Poisson's ratio of were 200000 MPa, 1000 MPa and 0.15, respectively.

4.3.6 Anchorage System

The anchorage system, which was used in the PC beams tested by Zong et al. (2013), consisted of horizontal steel sheets and anchorage bolts as illustrated in Figure 4-4b.

Similar to the loading, support and end plates, the steel material behaviour of the anchorage system was modelled with an elastic-perfectly plastic model, based on the von-Mises yield criterion, with an elastic modulus, yield stress and Poisson's ratio of 200000 MPa, 500 MPa and 0.15, respectively.

4.4 Finite Element Modelling

In the following subsections, the elements used in the development of three-dimensional FE models are briefly described. Further details about these elements can be found elsewhere (DIANA user's manual, 2012).

4.4.1 Concrete

The three-dimensional eight-node isoparametric brick element type, depicted in Figure 4-14, was used for concrete modelling. This brick element has three translational degrees of freedom in each node. The stress field in this element is three dimensional, and both the loading and principal stress can be in any direction (DIANA user's manual, 2012). In order to adopt an appropriate element size, several mesh densities were investigated and the average mesh size of 25-30 mm was selected throughout this study. Moreover, the adopted mesh size is consistent with the recommendation of Bažant and Oh (1983) to use element size of three times d_{a}, as well as the findings of Godat et al. (2012c). Furthermore, the selected mesh size maintains a balance between accuracy and cost of computational time.

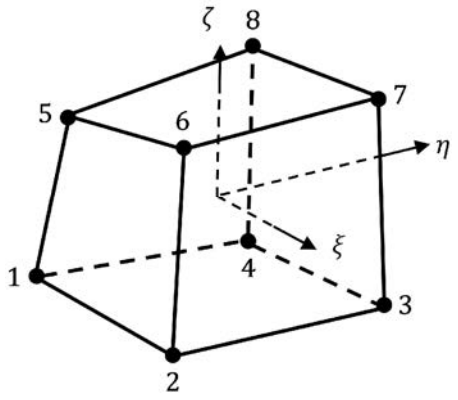

Figure 4-14: Eight-node isoparametric brick element (DIANA user's manual, 2012)

4.4.2 Steel Reinforcement and Prestressing Tendons

There are two common techniques that are usually used for the geometric representation of steel reinforcement and prestressing tendons in three-dimensional FE analysis, namely the discrete bar technique and the embedded bar technique. In the discrete bar technique the reinforcement is represented by truss elements connected to the nodes of concrete elements, whilst truss-like embedded bar elements are used within the concrete elements in the embedded bar technique, as shown in Figure 4-15.

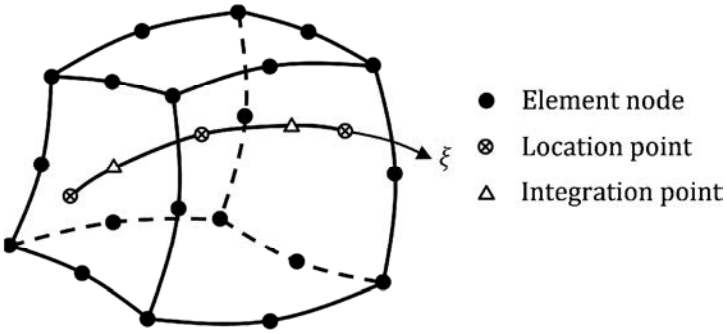

Figure 4-15: Embedded bar in brick element (DIANA user's manual, 2012)

In this study, both the steel reinforcement and tendons were represented by truss-like embedded bar elements. These elements have no degrees of freedom of their own and their strains are calculated from the displacement field of the surrounding concrete elements (DIANA user's manual, 2012).

As mentioned earlier in Section 4.3.2, a perfect bond was assumed between steel reinforcement and the surrounding concrete elements, as no bond failure was observed in the experimental tests used for validating the developed FE models.

4.4.3 FRP Composites

Based on the findings of Godat et al. (2012c) and Dirar et al. (2013a), the geometric modelling of the FRP laminates was carried out using four-node quadrilateral isoparametric curved shell elements, as given in Figure 4-16. These elements are a combination of plate bending and plane stress elements. Moreover, the transverse shear strain fields are automatically modified by the FE package to avoid shear locking (DIANA user's manual, 2012).

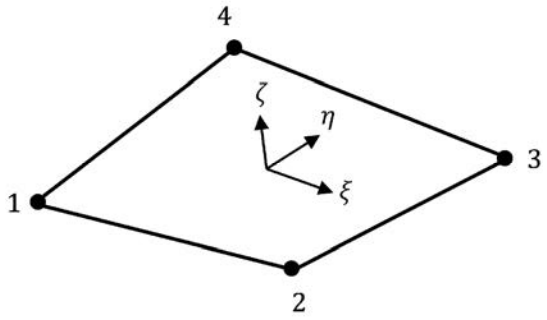

Figure 4-16: Four-node quadrilateral isoparametric curved shell element (DIANA user's manual, 2012)

On the other hand, the FRP bars were represented using three-dimensional two-node truss elements, as depicted in Figure 4-17. These elements have three translational degrees of freedom in each node and are only deformable in the axial direction, whilst bending and shear deformation are not allowed (DIANA user's manual, 2012).

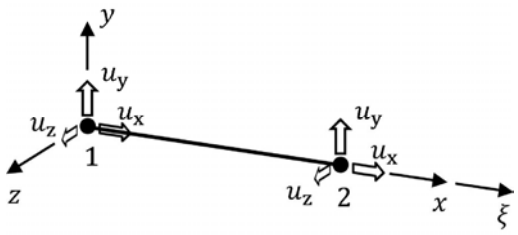

Figure 4-17: Three-dimensional two-node truss element (DIANA user's manual, 2012)

4.4.4 FRP-to-Concrete Interface

The bond zone between the concrete and EB CFRP laminates was simulated using eight-node plane quadrilateral interface elements. This element type, which is illustrated in Figure 4-18, is used to connect two planes in three-dimensional FE models (DIANA user's manual, 2012).

To Model the interface region between the FRP bars and surrounding concrete, four-node three-dimensional interface elements (see Figure 4-19) were employed. This interface element type is used to link a line to an edge of a brick element in three-dimensional FE models (DIANA user's manual, 2012).

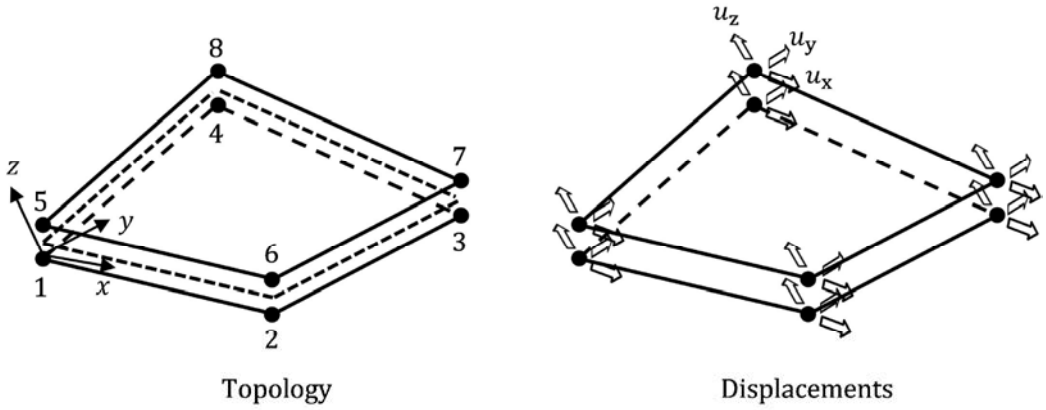

Figure 4-18: Eight-node plane quadrilateral interface element (DIANA user's manual, 2012)

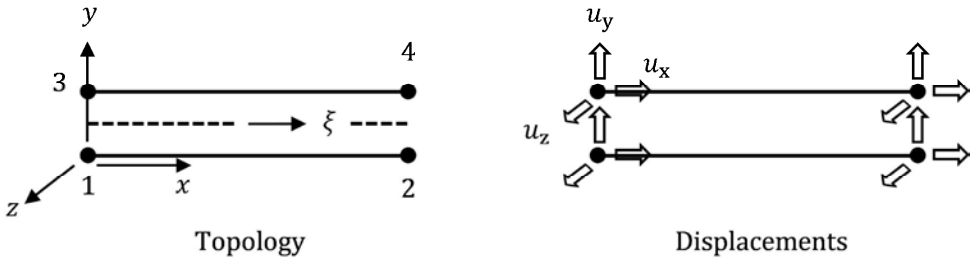

Figure 4-19: Four-node three-dimensional interface element (DIANA user's manual, 2012)

The use of interface elements aims to simulate the transfer of normal and shear stresses from the surrounding concrete elements into the FRP elements. As can be seen from Figure 4-18 and Figure 4-19, each of the interface elements has two sets of duplicated nodes; one set is connected to the concrete elements while the other is linked to the FRP composites elements. The slip between the FRP composites and concrete is determined from the relative displacement between these two sets of nodes, and then the corresponding bond stress is found from the adopted bond-slip constitutive model. Finally, the force to be transferred by the interface element is determined by multiplying the bond stress by the interfacial area.

4.4.5 Loading, Support and End Plates

The end plates were modelled using eight-node isoparametric brick elements shown in Figure 4-14, the same element type used to model the concrete, whereas six-node isoparametric wedge elements were used to model both the loading and support plates. This wedge element type, which is depicted in Figure 4-20, is a three-dimensional element and has three translational degrees of freedom in each node.

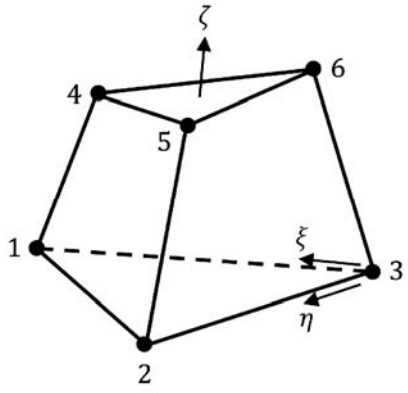

Figure 4-20: Six-node isoparametric solid wedge element (DIANA user's manual, 2012)

4.4.6 Anchorage System

The horizontal steel sheets were modelled using four-node isoparametric curved shell elements, as given in Figure 4-16 (which were used to model the FRP laminates), whereas the anchorage bolts were represented by three-dimensional two-node truss elements (see Figure 4-17). The anchorage bolts, which were embedded in the concrete, were linked to the horizontal steel sheets using high stiffness two-node translation spring elements to prevent any relative displacement.

Two-node translation spring elements, depicted in Figure 4-21, are usually used to simulate the interaction between two points of the FE model.

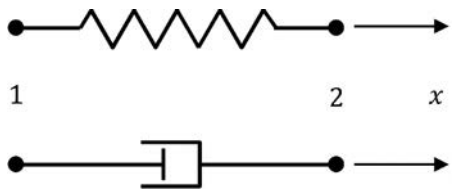

Figure 4-21: Two-node translation spring element (DIANA user's manual, 2012)

4.5 Solution Procedure

The DIANA Phased Analysis Module, which can be used to simulate various stages of construction (DIANA user's manual, 2012), was used in this study to model different construction and loading stages of the tested beams. The FE model may be modified at any phase by the addition or removal of elements or boundary conditions. In nonlinear phased analysis, the results of the last step in a given phase are used as initial values for the first step in the following phase.

For instance, two phases were implemented in the FE modelling of the PC girders. In Phase I, elements representing the EB FRP laminates (along with their anchorage system if applicable) and the FRP-to-concrete interface were set as inactive and the unstrengthened FE model was prestressed (the prestressing load was applied as initial stress in tendons). Phase II included activating of the aforementioned elements, and then the FE model is loaded up to failure. This procedure accurately modelled the physical tests.

For the solution algorithm, an incremental-iterative procedure was adopted to achieve convergence, in which the prestressing (if any) and vertical loads were respectively applied as stress and vertical displacement increments. For each load increment, the Quasi-Newton iterative method (described in Section 3.5.1.2) was employed together with a displacement-based convergence criterion (see Section 3.5.3.2). The displacement norm value of 0.001 was used to specify convergence based on the work carried out by Hee and Jefferson (2008), whereas a maximum iteration number of 1000 was utilised to stop the analysis due to divergence. A similar solution procedure was adopted by Dirar et al. (2013a); moreover, convergence was successfully achieved at every load step using this procedure.

4.6 Validation of the Developed FE models

The experimentally tested beams described in Section 4.2 were used to validate the developed FE models. The available experimental and the relevant FE results are presented and compared in the following subsections to identify the accuracy of the developed FE models.

4.6.1 PC Beams Strengthened in Shear with EB FRP Laminates

4.6.1.1 Kang and Ary (2012)

The double symmetry of the tested girders about both the mid-span and mid-width planes (see Figure 4-1 and Figure 4-2) enabled a quarter-model to be developed as depicted in Figure 4-22. Appropriate boundary conditions were applied by restraining

the movement of the planes of symmetry at mid-span and mid-width in the perpendicular direction, and allowing movement in the vertical direction only.

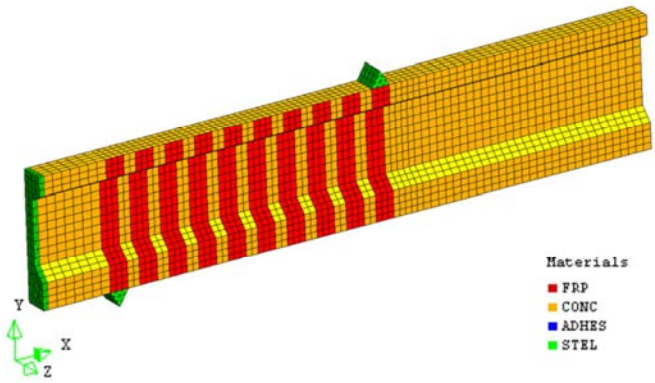

Figure 4-22: FE model of the beams tested by Kang and Ary (2012)

For this series of beams, the comparison between the numerical and experimental results includes the shear force capacity, shear-force versus mid-span deflection curves and crack patterns at failure. No strain gauges were used to measure the CFRP strain during testing. Thus, the CFRP strain predictions are not included.

Table 4-6 gives the experimental shear forces (V_{Exp}) and the FE-predicted shear forces (V_{FE}) at failure, as well as the experimental mid-span deflection (Δ_{Exp}) and the FE-predicted mid-span deflection (Δ_{FE}) at failure. From this table it can be seen that the FE model predicted the experimental shear force capacities of the tested PC girders with a mean predicted/experimental ratio of 1.11 and a standard deviation of 0.10. The mid-span deflections at failure of the tested PC girders were predicted with a mean predicted/experimental ratio of 0.95 and a standard deviation of 0.08.

Table 4-6: Experimental (Kang and Ary, 2012) and FE predicted results

Beam	V_{Exp} (kN)	V_{FE} (kN)	$V_{\mathrm{FE}}/V_{\mathrm{Exp}}$	Δ_{Exp} (mm)	Δ_{FE} (mm)	$\Delta_{\mathrm{FE}}/\Delta_{\mathrm{Exp}}$
Control	117.4	129.5	1.10	12.58	11.33	0.90
IB-05	161.9	162.0	1.00	16.13	14.38	0.89
IB-10	119.2	149.7	1.25	12.34	13.18	1.06

Figure 4-23 presents the shear-force versus mid-span deflection responses for both the experimental and FE work. It should be noted that Figure 4-23 does not show the camber due to prestress. Both the experimental and FE-predicted curves are quasi-linear up to crack formation. After crack formation, the experimental and numerical curves turned nonlinear due to stiffness deterioration. The post-cracking stiffness, i.e. the slope of the shear force-deflection curve after crack formation, was well modelled. Upon further loading, the post-cracking stiffness continued to deteriorate until failure occurred. At failure, there is a sudden drop in load at peak shear force, which is a characteristic of brittle (shear) failure.

As can be seen from Table 4-6 and Figure 4-23, the FE model with a concrete compressive strength of 59 MPa overestimated the shear force at failure for IB-10. It may be argued that shear failure of IB-10 occurred due to discrete major cracks whereas the FE model was based on smeared cracking without explicit attention to modelling fast fracture (see Section 3.2.1 on modelling of cracking in concrete). However, such an argument is at variance with the predicted/experimental shear force capacity ratios of 1.10 and 1.00 for the control and IB-05 girders respectively (see Table 4-6).

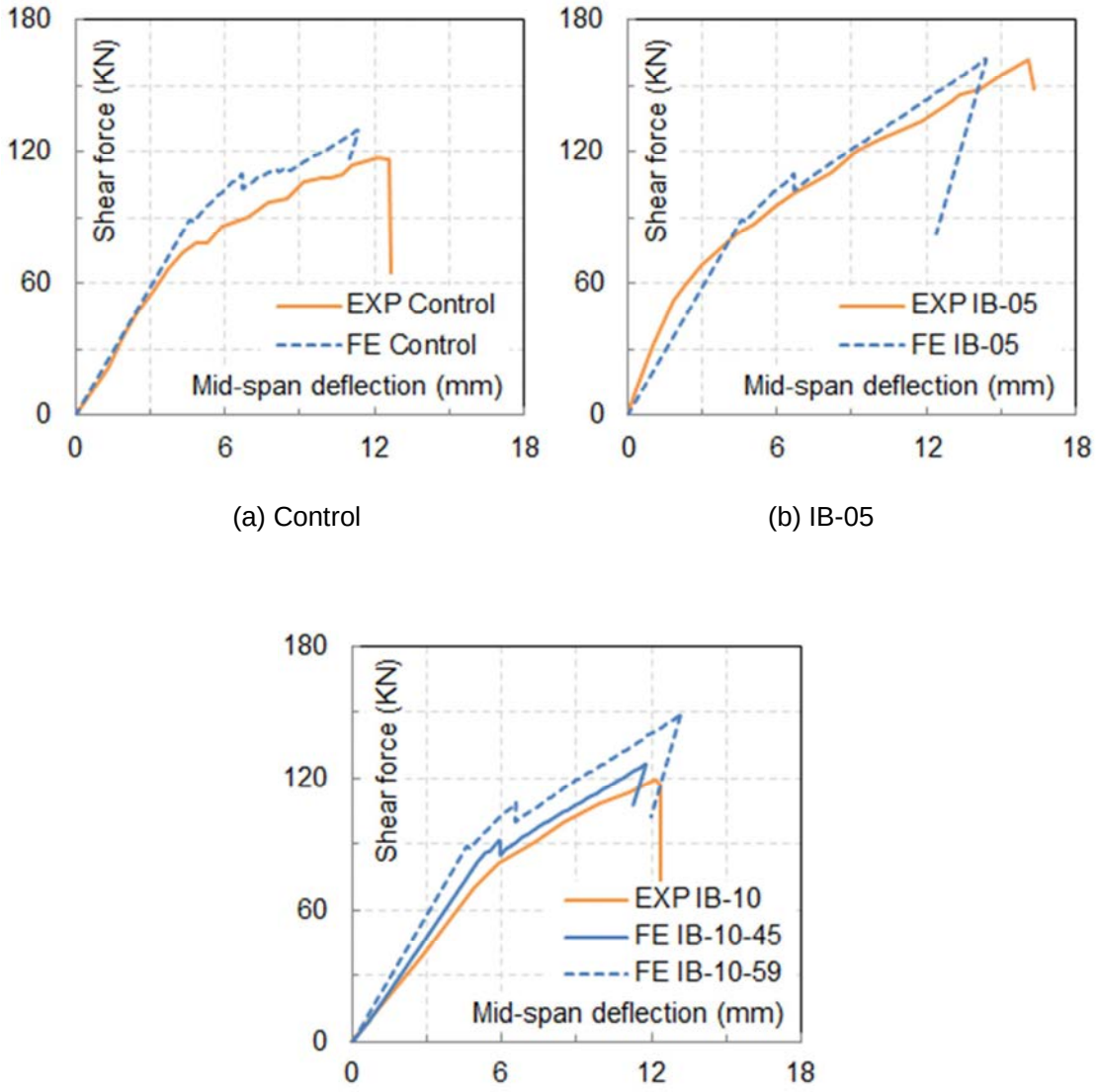

(a) Control

(b) IB-05

(c) IB-10

Figure 4-23: Experimental (Kang and Ary, 2012) and FE predicted shear force-mid span deflection curves

The discrete crack approach, which employs interface elements to introduce a gap in the FE mesh after cracking, is more realistic in modelling shear failure of concrete beams arising from a few shear cracks than the smeared crack approach (as

explained in Section 3.2.1.1). However, the overall structural behaviour can be well modelled using the smeared crack approach (Sagaseta and Vollum, 2009).

A careful analysis of the experimental results (Kang and Ary 2012) shows that IB-10 had a significantly lower initial un-cracked stiffness compared to the other two girders (i.e. Control and IB-05). Furthermore, the EB CFRP strips used to strengthen IB-10 fractured at failure. Nonetheless, the experimental results suggested that the EB CFRP strips did not enhance the shear force capacity of IB-10 over that of the control girder (see Table 4-6). These two contradictory results, together with the observed lower un-cracked stiffness for IB-10, may be reconciled by considering a lower compressive strength of concrete, and consequently lower initial un-cracked stiffness and unstrengthened shear force capacity, for IB-10.

Using a concrete cylinder compressive strength value of 45 MPa gave the best numerical results for IB-10 (see Figure 4-23c) in terms of the initial un-cracked stiffness, cracked stiffness, shear force capacity and mid-span deflection at failure. Therefore, further experimental testing for IB-10 with concrete cylinder compressive strengths of 45 MPa and 59 MPa is required in order to confirm the above explanation.

The experimental crack patterns at failure for the three girders, together with contour plots of the predicted principal tensile strain in the concrete at the predicted failure loads, are shown in Figure 4-24. Moreover, the predicted contour plot of the principal tensile strain of an IB-10 girder using f_c' of 45 MPa is presented in Figure 4-25.

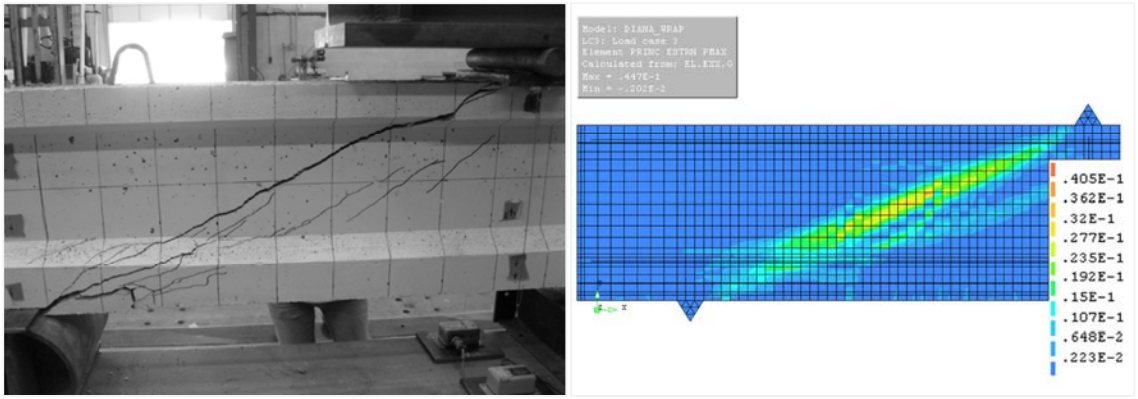

(a) Control

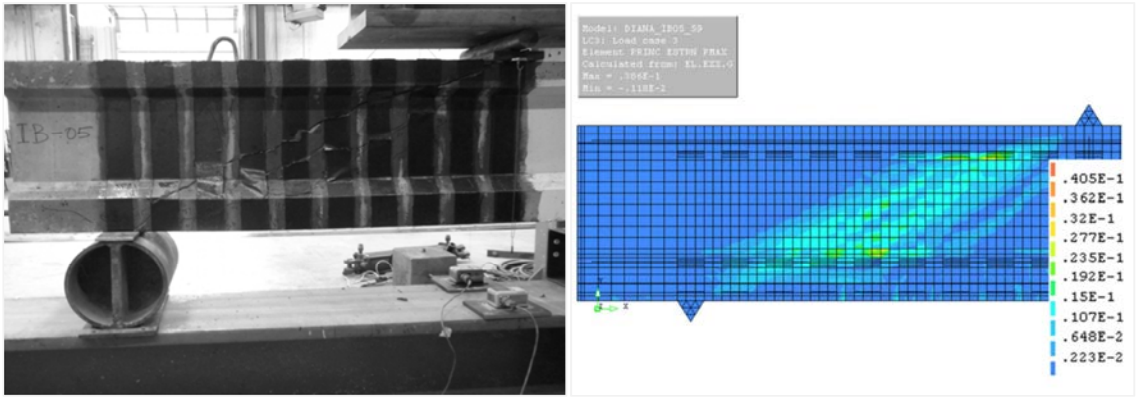

(b) IB-05

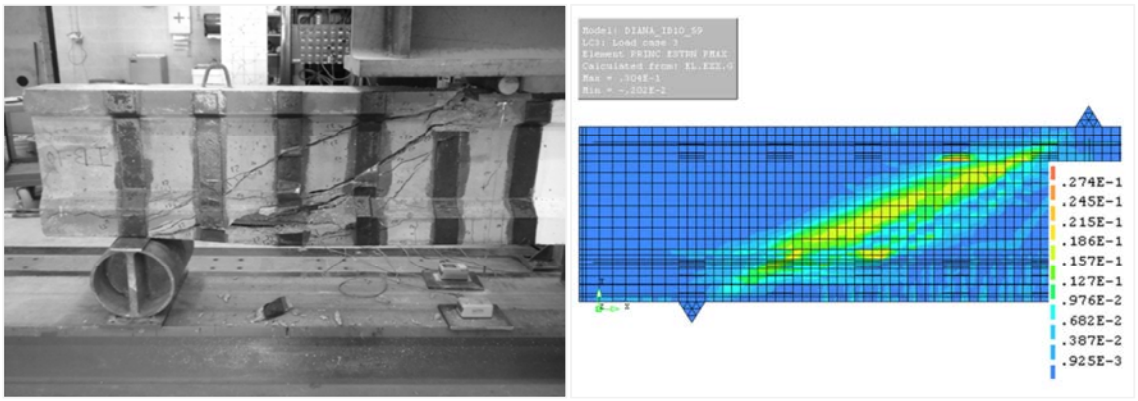

(c) IB-10

Figure 4-24: Experimental (Kang and Ary, 2012) and FE predicted failure modes

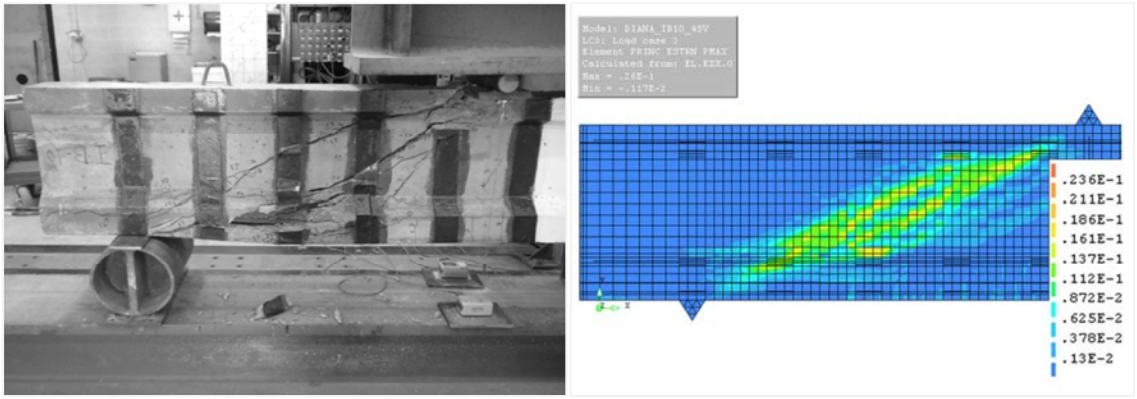

Figure 4-25: Experimental (Kang and Ary, 2012) and FE predicted failure mode of an IB-10 girder using concrete cylinder compressive strength of 45 MPa

It can be seen that the FE model correctly predicted the shear failure mode of the tested girders. The FE model also correctly predicted that the control girder failed due to a major diagonal crack that ran from the support to the loading plate (see Figure 4-24a), whereas the strengthened girders had more distributed diagonal cracks due to the presence of the EB CFRP strips as depicted in Figure 4-24b, Figure 4-24c and Figure 4-25. Once more, the predicted failure mode of an IB-10 girder using f_c' of 45 MPa (i.e. Figure 4-25) was more realistic than the predicted failure mode using f_c' of 59 MPa (see Figure 4-24c).

4.6.1.2 Zong et al. (2013)

For this series of beams, see Figure 4-26, only the advantage of the symmetry about mid-span was taken into account (after considering mid-span symmetry the beam size became small and hence the analysis did not consume time) with appropriate boundary conditions being applied at the plane of symmetry (by allowing movement in the vertical direction, i.e. Y-direction, and restraining it in other directions).

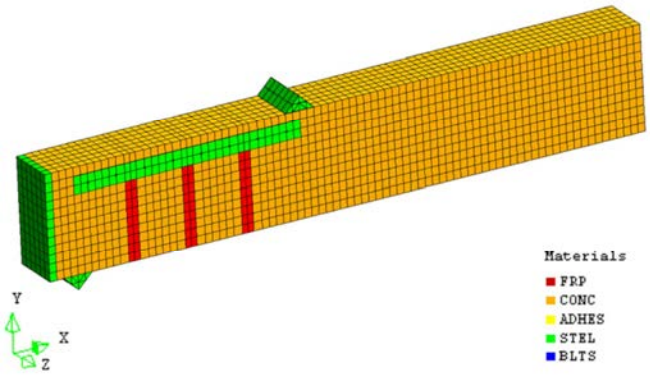

Figure 4-26: FE model of the beams tested by Zong et al. (2013)

Table 4-7 summarises the experimental and the FE predicted shear force capacities of the tested beams with their corresponding mid-span deflections. It can be seen that the FE model predicted the shear force capacities and mid-span deflections at failure of the tested beams respectively, with a mean predicted/experimental ratio of 0.95 (standard deviation of 0.016) and 0.86 (standard deviation of 0.02).

Table 4-7: Experimental (Zong et al., 2013) and FE predicted results

Beam	V_{Exp} (kN)	V_{FE} (kN)	$V_{\mathrm{FE}}/V_{\mathrm{Exp}}$	Δ_{Exp} (mm)	Δ_{FE} (mm)	$\Delta_{\mathrm{FE}}/\Delta_{\mathrm{Exp}}$
PPC0	266.5	251.8	0.95	28.25	24.48	0.87
PPC1	270.5	262.1	0.97	29.02	25.42	0.88
PPC2	284.5	264.3	0.93	30.79	25.48	0.83

The experimental and FE-predicted shear force versus mid-span deflection curves, without including the camber due to prestress, are shown in Figure 4-27. As can be seen, the overall behaviour of the control (PPC0) and strengthened (PPC1 and PPC2) beams was reasonably well predicted by the developed FE model. The FE model predicted a sudden drop in load at peak shear force, which is a characteristic

of shear failure. Moreover, the experimental and FE predicted failure mode of a PPC2 girder is depicted in Figure 4-28. Zong et al. (2013) did not report the crack patterns at failure of PPC0 and PPC1.

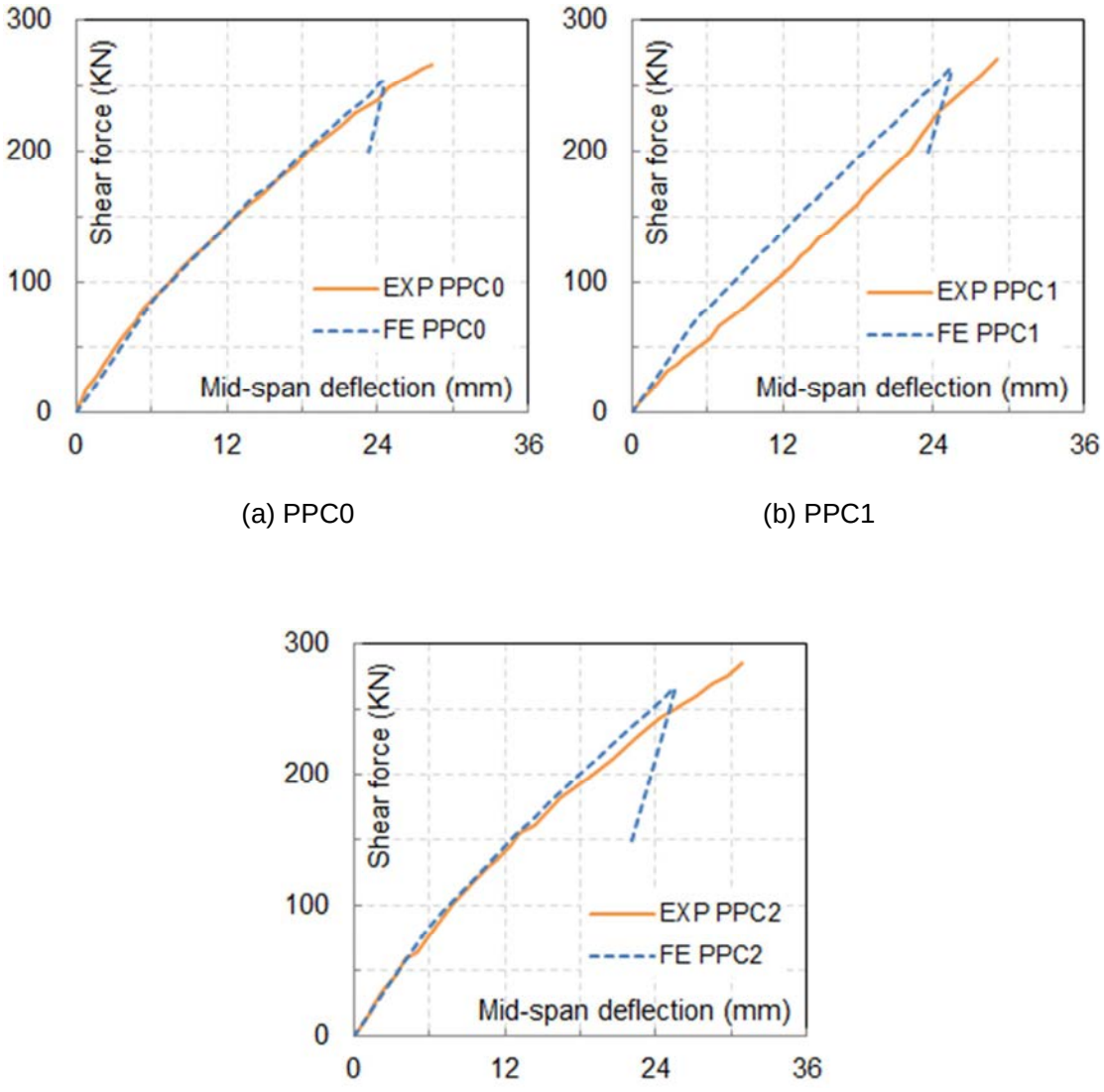

(a) PPC0

(b) PPC1

(c) PPC2

Figure 4-27: Experimental (Zong et al., 2013) and FE predicted shear force-mid span deflection curves

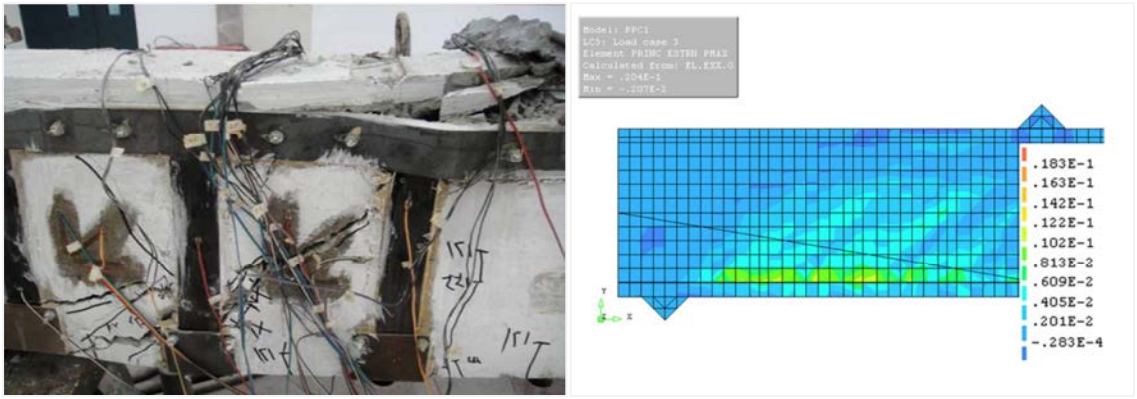

Figure 4-28: Experimental (Zong et al., 2013) and FE predicted failure mode of PPC2 girder

Unlike the experimental work presented by Kang and Ary (2012), this study reported the strain variation in the EB CFRP laminates as well as stress variation in the prestressing tendons of some of the tested beams which were also used for validating the FE model. The experimental and FE-predicted results for the shear force versus maximum strain variation in the EB CFRP laminates of PPC1 and the shear force versus stress increment variation in the prestressing tendons of PPC2 are presented in Figure 4-29 and Figure 4-30 respectively.

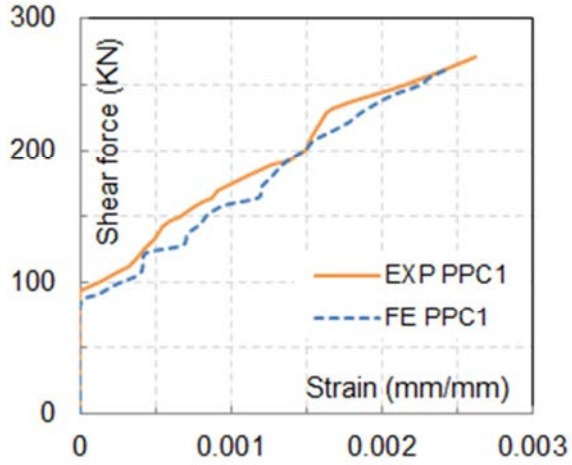

Figure 4-29: Experimental (Zong et al., 2013) and FE predicted variation of the maximum strain in the CFRP sheets of PPC1

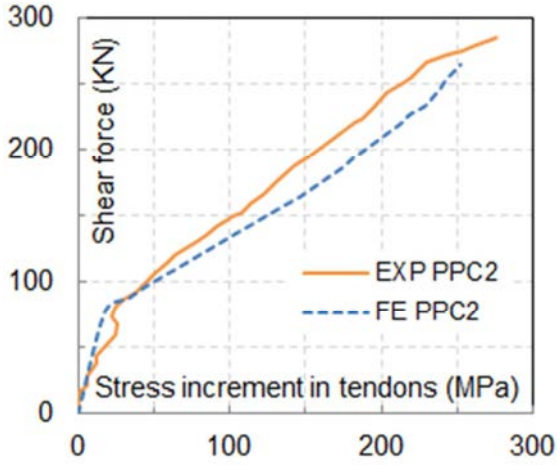

Figure 4-30: Experimental (Zong et al., 2013) and FE predicted stress increment variation in the prestressing tendons of PPC2

Once more, all the presented comparisons (in terms of the shear force-deflection curves, mode of failure, FRP strain and stress variation in tendons) demonstrate the prediction accuracy of the developed FE model.

4.6.2 RC Beams Strengthened in Shear with DE FRP Bars

4.6.2.1 Mofidi et al. (2012)

For this series, the whole beams were modelled as shown in Figure 4-31. The four beams considered, as shown in Section 4.2.2.1, had different steel reinforcement stirrups and DE CFRP ratios. The accuracy of the FE model was identified by comparing the experimental results with the FE predictions, including shear force versus deflection (under loading point) curves, strain variation in steel reinforcement stirrups and strain variation in CFRP bars. Unfortunately, the crack patterns at failure of the modelled beams have not been presented in the original experimental work.

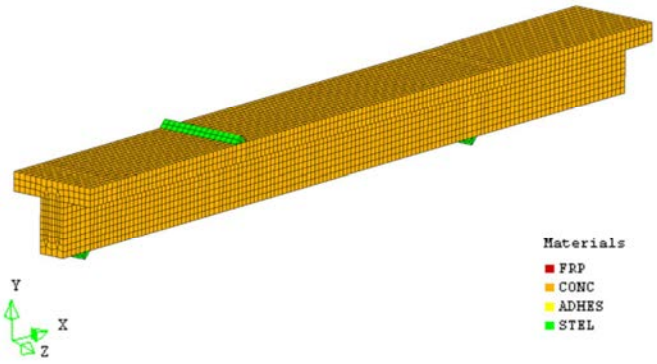

Figure 4-31: FE model of the beams tested by Mofidi et al. (2012)

A summary of the experimental and FE predicted results is presented in Table 4-8, whereas the results in terms of the shear force versus deflection curves are depicted in Figure 4-32.

Table 4-8: Experimental (Mofidi et al., 2012) and FE predicted results

Beam	V_{Exp} (kN)	V_{FE} (kN)	V_{FE}/V_{Exp}	Δ_{Exp} (mm)	Δ_{FE} (mm)	Δ_{FE}/Δ_{Exp}
S0-CON	81.3	80.5	0.99	2.6	2.6	1.00
S0-12d130s	180.8	176.9	0.98	9.8	9.5	0.97
S1-CON	232.2	234.5	1.01	11.9	11.5	0.97
S1-12d260s	266.6	271.5	1.02	15.4	12.5	0.81

The good match between the experimental results and FE predictions is demonstrated in this table. The mean and the standard deviation were 1.0 and 0.016 respectively for the predicted/experimental shear force capacities, whilst they were 0.94 and 0.075 respectively for the predicted/experimental deflections under loading point at failure.

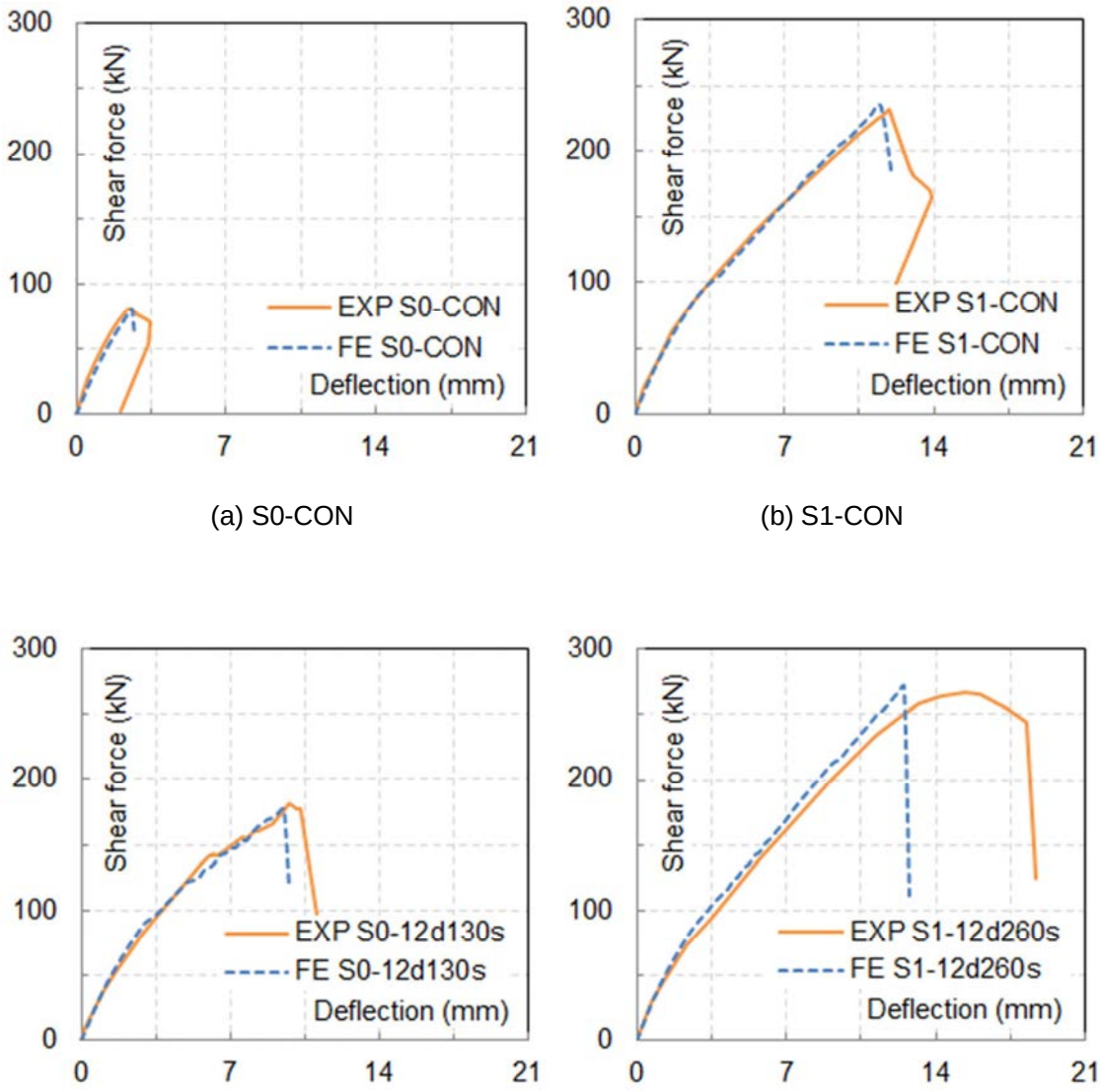

(a) S0-CON (b) S1-CON

(c) S0-12d130s (d) S1-12d260s

Figure 4-32: Experimental (Mofidi et al., 2012) and FE predicted shear force-deflection curves

Moreover, the shear force versus maximum strain results in the steel stirrups and CFRP bars are comparable, as shown in Figure 4-33 and Figure 4-34 respectively. As can be seen, the developed FE model correctly predicted that both the shear stirrups and DE CFRP bars remained passive up to the formation of inclined cracks.

The developed model also correctly predicted the shear forces (50-75 kN) at which the steel and CFRP shear reinforcement started to develop strain. The development of strain in the steel shear links was overall well modelled, whilst the strain in the DE CFRP bars was underestimated. This may be mainly attributed to the smeared crack model used for concrete where the localised cracking in concrete is smeared over a finite region (Godat et al., 2010; Dirar et al., 2013a), or the FRP-to-concrete bond-slip model used, as it is responsible for estimating the interfacial shear stress and consequently the strain in the DE CFRP bars. Nonetheless, the FE model successfully captured the main characteristics of the experimental behaviour which included yielding of shear stirrups (which took place at a strain value of 0.0027 mm/mm), absence of DE CFRP bar debonding and brittle (shear) failure.

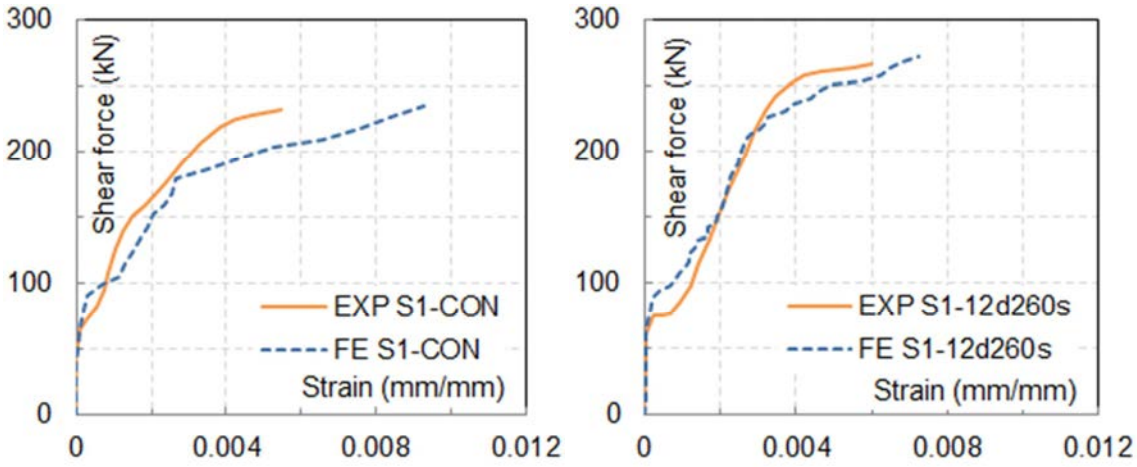

(a) S1-CON (b) S1-12d260s

Figure 4-33: Experimental (Mofidi et al., 2012) and FE predicted shear force-maximum strain variation in the shear stirrups

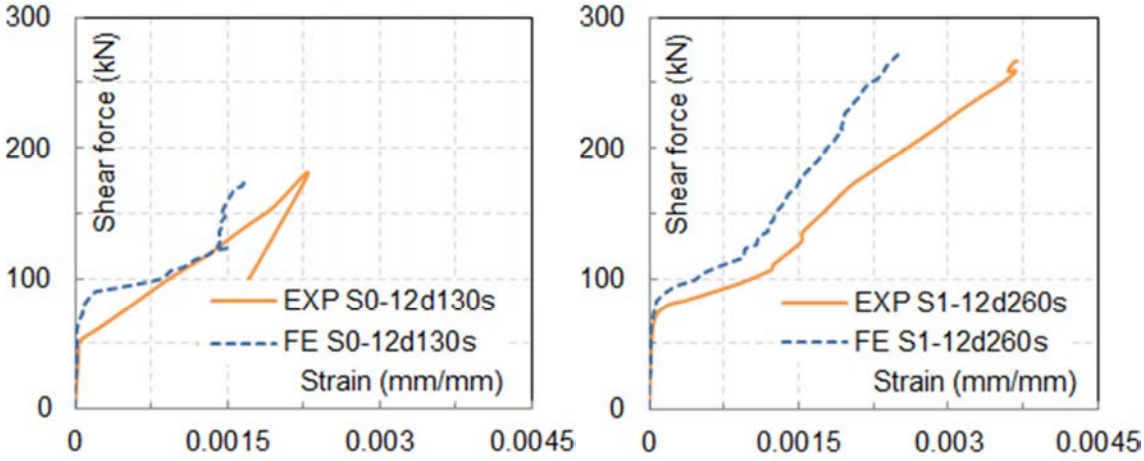

(a) S0-12d130s (b) S1-12d260s

Figure 4-34: Experimental (Mofidi et al., 2012) and FE predicted shear force-maximum strain variation in the DE CFRP bars

In spite of the missing crack patterns at failure in the experimental work however, Mofidi et al. (2012) reported that S1-12d260s failed when parallel diagonal shear cracks, that formed at relatively equal distances with an inclination angle of 37°-42°, opened up and reached the flange of the beam. This description is quite comparable to the predicted principal tensile strain contours at failure shown in Figure 4-35.

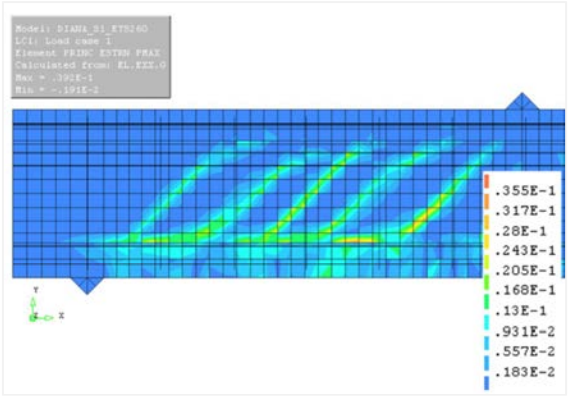

Figure 4-35: FE predicted principal tensile strain contours at failure of S1-12d260s beam

4.6.2.2 Qin et al. (2014)

Two of the beams, one unstrengthened and the other strengthened by DE CFRP bars, tested by Qin et al. (2014) were used to quantify the applicability of the developed FE model. Figure 4-36 presents the FE model of this series of beams.

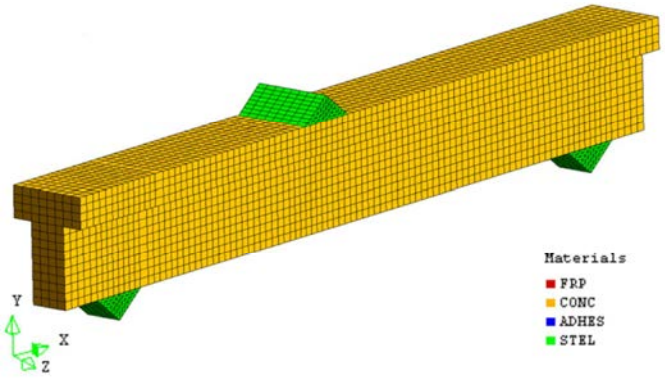

Figure 4-36: FE model of the beams tested by Qin et al. (2014)

As explained in Section 4.3.4, the bond behaviour between the DE FRP bars and concrete for the strengthened beam (i.e. R00) was modelled using the bond-slip model of Mofidi et al. (2012) because sand-coated CFRP bars were used in both studies. A comparison between the obtained FE results, together with the corresponding experimental results, is given in Table 4-9.

Table 4-9: Experimental (Qin et al., 2014) and FE predicted results

Beam	V_{Exp} (kN)	V_{FE} (kN)	$V_{\mathrm{FE}}/V_{\mathrm{Exp}}$	Δ_{Exp} (mm)	Δ_{FE} (mm)	$\Delta_{\mathrm{FE}}/\Delta_{\mathrm{Exp}}$
N00	143.0	133.4	0.93	7.39	6.5	0.88
R00	142.0	150.6	1.06	9.57	7.5	0.78

As can be seen from this table, the FE model predictions were good for shear force capacities; however, the model underestimated deflections under loading point at failure (particularly for the case of R00). The mean V_{FE}/V_{Exp} is 1.0 with a standard deviation of 0.068, whereas the developed FE model predicted the experimental deflection of the tested beams with a mean Δ_{FE}/Δ_{Exp} of 0.83 and a standard deviation of 0.05. The experimental and FE predicted shear force versus deflection under loading point curves are shown in Figure 4-37. The stiffer predicted behaviour of the R00 beam can be attributed to the smeared crack model used for the concrete, i.e. a similar argument to that of the IB-10 girder, or the bond-slip model adopted between the concrete and FRP bars (Arduini et al., 1997; Vecchio and Bucci, 1999).

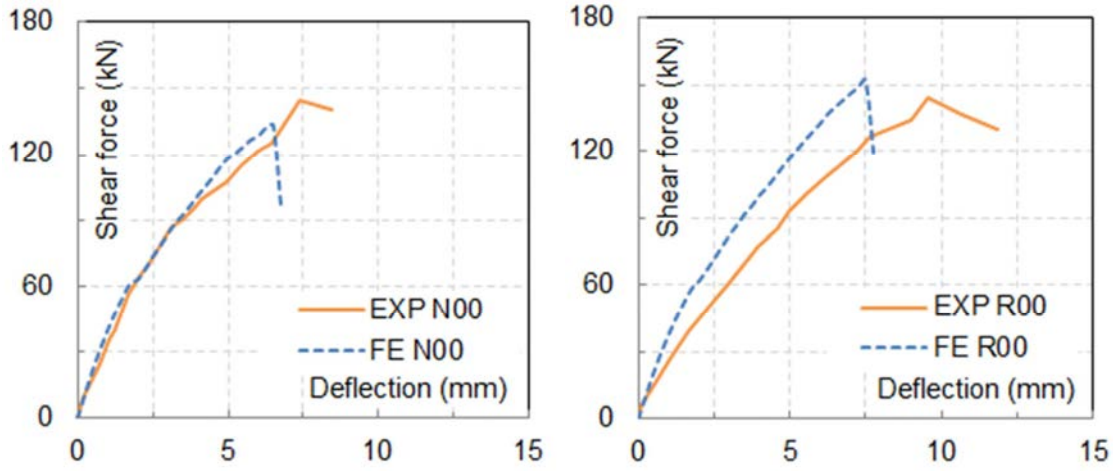

(a) N00 (b) R00

Figure 4-37: Experimental (Qin et al., 2014) and FE predicted shear force-deflection curves

The experimentally tested beams failed in a brittle shear failure with no sign of debonding for the strengthened beam; this behaviour was accurately predicted by the

developed FE model. However, the authors did not report the strain results in the DE FRP bars of the R00 beam, as opposed to the strain variation in steel stirrups which was provided for this beam. The experimental and FE predicted results of the R00 beam in terms of the shear force versus strain in the middle shear stirrup are depicted in Figure 4-38. Moreover, the experimental and FE predicted failure mode are compared in Figure 4-39. Once more, the presented comparisons demonstrate the accuracy of the developed FE model.

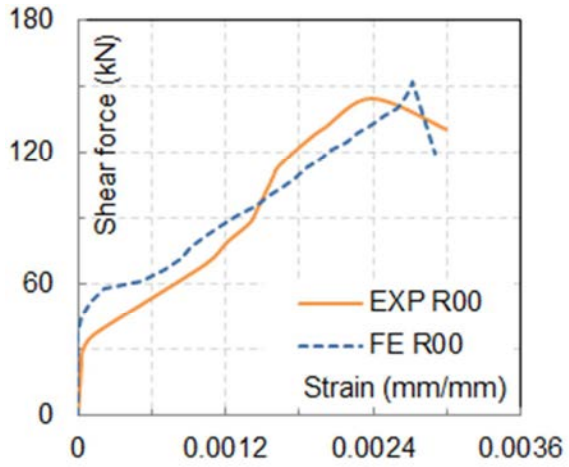

Figure 4-38: Experimental (Qin et al., 2014) and FE predicted shear force-strain curves in the steel stirrups of R00 beam

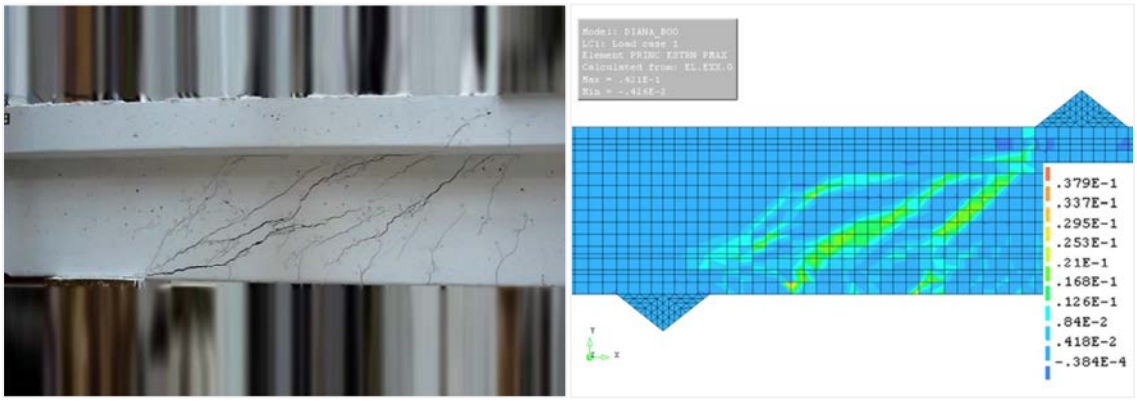

Figure 4-39: Experimental (Qin et al., 2014) and FE predicted failure mode of R00 beam

4.6.2.3 Valerio and Ibell (2003)

The FE model of the RC beams tested by Valerio and Ibell (2003) is illustrated in Figure 4-40. As can be seen, the advantage of the symmetry about the mid-span was taken into account during the modelling of this series of beams with appropriate boundary conditions assigned to the symmetry plane, which involved allowing the movement in vertical direction only.

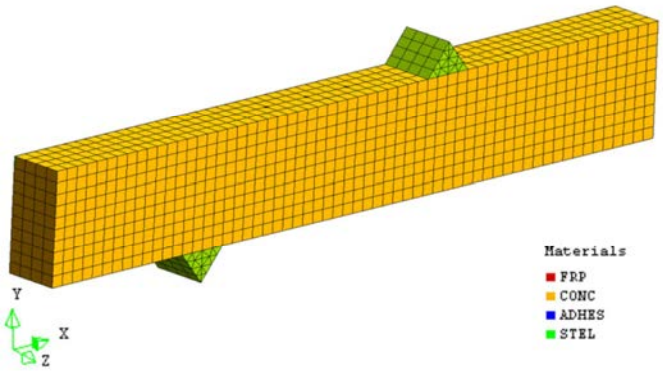

Figure 4-40: FE model of the beams tested by Valerio and Ibell (2003)

As mentioned earlier in Section 4.3.4, two different scenarios were adopted for modelling the bond behaviour between the DE AFRP bars and concrete of the strengthened beams (i.e. Specimens 8, 9 and 10). The experimental as well as the obtained FE results are comparable in Table 4-10. This table shows that the use of the bond-slip model of Mofidi et al. (2012) had insignificant implications on the modelled behaviour, as none of the beams tested by Valerio and Ibell (2003) failed due to debonding of the AFRP bars, which in turn was accurately predicted by the developed FE model. However, the FE predictions with the bond-slip model showed that debonding was initiated near the soffit of Specimen 10 at the final stages of

loading but without reaching the full debonding (i.e. the ultimate slip value of the bond-slip model as given in Figure 4-13). This might explain the small discrepancy in the predictions of Specimen 10 given in Table 4-10. Unfortunately, it was not possible to confirm this finding as the corresponding results were not reported in the experimental work.

Table 4-10: Experimental (Valerio and Ibell, 2003) and FE predicted results

Specimen	V_{Exp} (kN)	V_{FE} (kN)	$V_{\mathrm{FE}}/V_{\mathrm{Exp}}$	Δ_{Exp} (mm)	Δ_{FE} (mm)	$\Delta_{\mathrm{FE}}/\Delta_{\mathrm{Exp}}$
1	22.5	25.39	1.13	12.0	11.8	0.98
8 (perfect bond)	32.0	33.15	1.04	13.0	15.0	1.15
8 (bond-slip)	32.0	33.30	1.04	13.0	15.2	1.16
9 (perfect bond)	32.0	31.90	1.00	13.0	14.3	1.10
9 (bond-slip)	32.0	31.86	1.00	13.0	14.6	1.12
10 (perfect bond)	30.0	32.60	1.09	12.0	14.7	1.22
10 (bond-slip)	30.0	31.54	1.05	12.0	14.2	1.18

The predictions of the developed FE model had a mean $V_{\mathrm{FE}}/V_{\mathrm{Exp}}$ of 1.06 with a standard deviation of 0.05 for the FE model with perfect bond assumption between the DE AFRP bars and concrete, and a mean $V_{\mathrm{FE}}/V_{\mathrm{Exp}}$ of 1.05 with a standard deviation of 0.048 for the FE model considering the bond-slip behaviour. For the deflection results, the FE model had a mean $\Delta_{\mathrm{FE}}/\Delta_{\mathrm{Exp}}$ of 1.11 with a standard deviation of 0.087, and a mean $\Delta_{\mathrm{FE}}/\Delta_{\mathrm{Exp}}$ of 1.11 with a standard deviation of 0.078, respectively for the FE modelling without and with a bond slip model.

In Figure 4-41, a comparison between the experimental and FE predicted (with perfect bond assumption) shear force versus mid-span deflection curves is

presented. The available experimental and the corresponding predicted failure modes of the modelled beams are compared in Figure 4-42. All the presented comparisons clearly demonstrate the accuracy of the developed FE model.

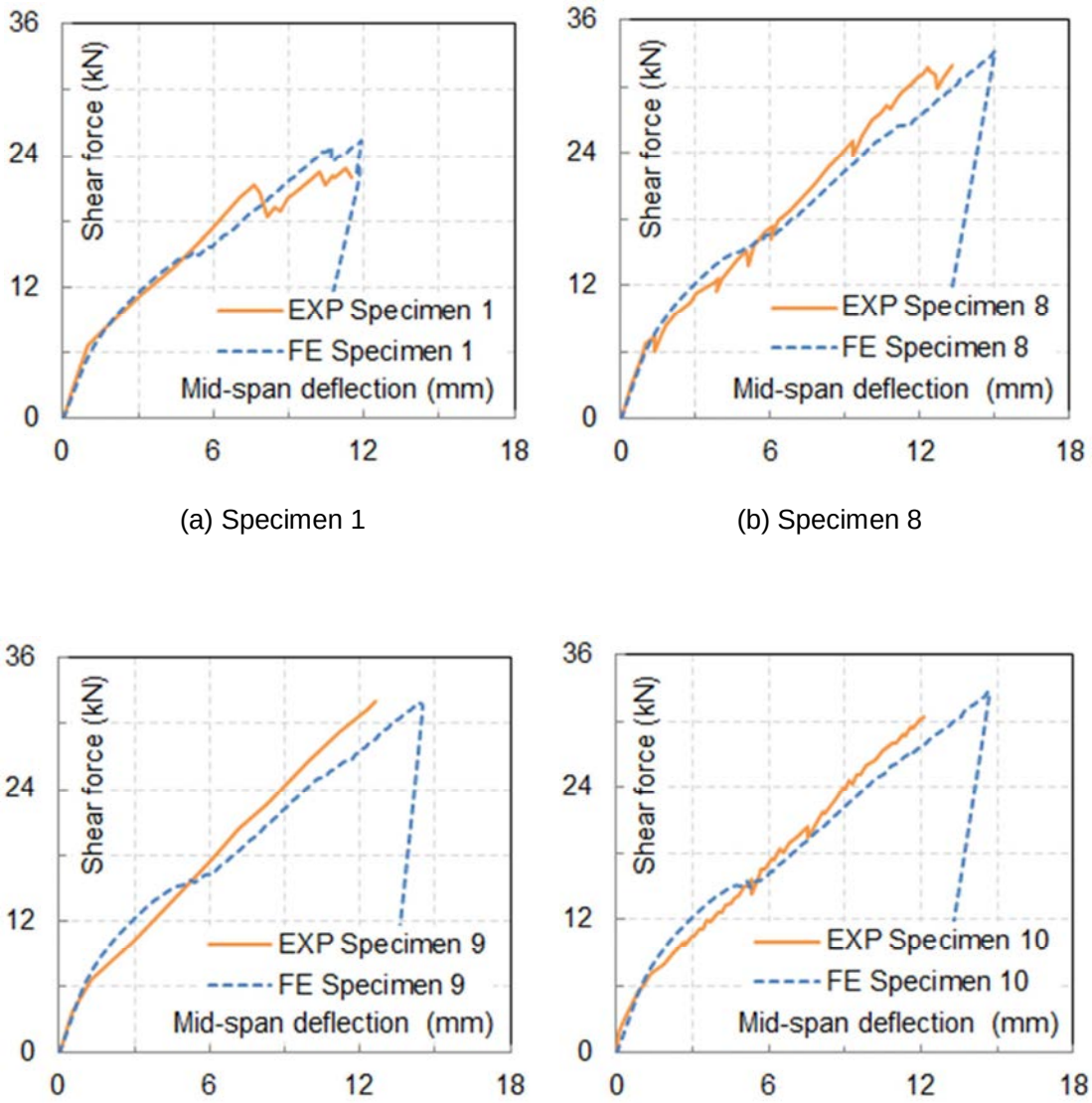

(a) Specimen 1

(b) Specimen 8

(c) Specimen 9

(d) Specimen 10

Figure 4-41: Experimental (Valerio and Ibell, 2003) and FE predicted shear force-deflection curves

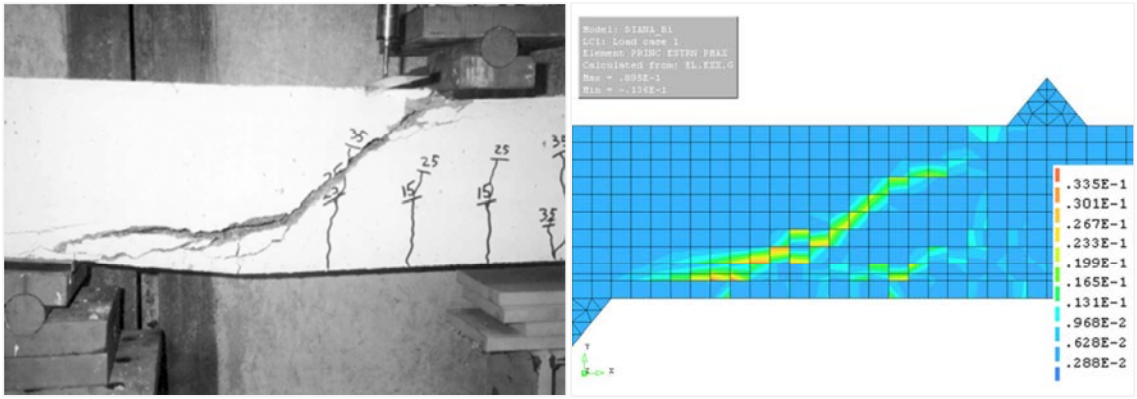

(a) Specimen1

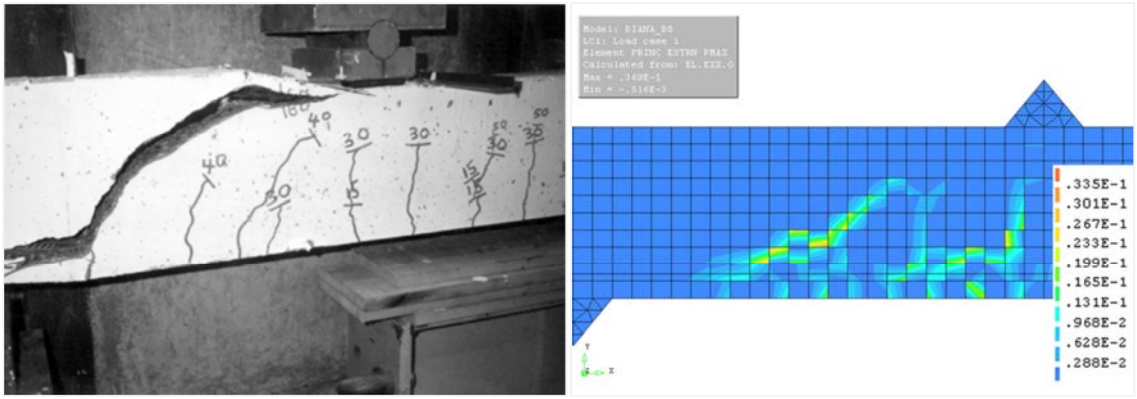

(b) Specimen 8

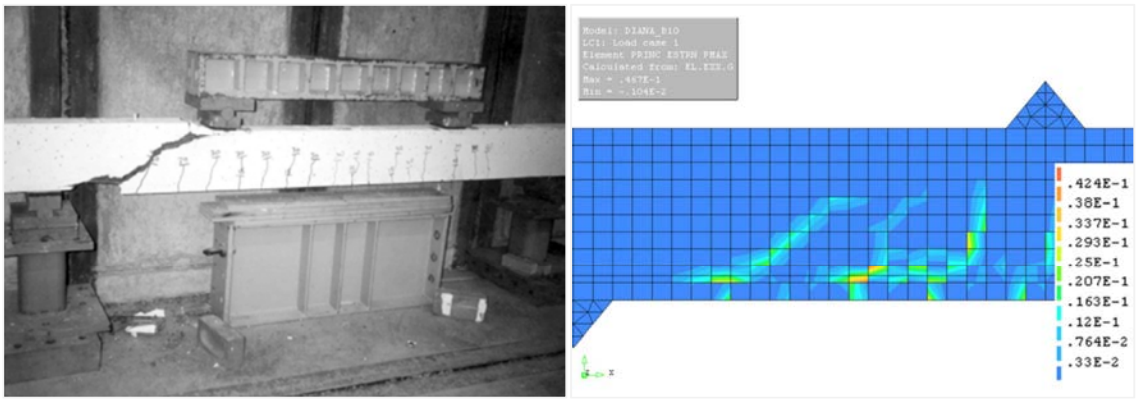

(c) Specimen 10

Figure 4-42: Experimental (Valerio and Ibell, 2003) and FE predicted failure modes

4.7 Concluding Remarks

Chapter Four addressed the development and validation of the FE models. Two three-dimensional nonlinear FE models were developed for predicting the behaviour of PC beams strengthened in shear with EB FRP laminates and RC beams strengthened in shear with DE FRP bars. For validation purposes, the results of five sets of experiments from the literature were used; two of these were conducted on PC beams shear-strengthened with EB CFRP sheets (i.e. Kang and Ary, 2012; Zong et al., 2013), while the remaining three (i.e. Mofidi et al., 2012; Qin et al., 2014; Valerio and Ibell, 2003) were carried out on RC beam shear strengthened using DE FRP bars. These experimental studies have been briefly presented in this chapter.

In addition, this chapter has described in detail the material and geometric modelling used in the developed FE models. The choice of the constitutive models and element types used was carefully selected, mainly based on the findings of previous FE studies as presented in previous chapter. Furthermore, the adopted solution algorithm throughout the numerical analysis has also been presented.

The accuracy of the developed FE models was quantified by comparing the experimental results against the relevant FE predictions. The comparison between the experimental and the FE predicted results included, if any was reported in the experimental investigations, shear force-deflection responses, strain variation in the steel stirrups, strain variation in the FRP reinforcement, stress variation in the prestressed tendons and modes of failure. The mean $V_{\mathrm{FE}}/V_{\mathrm{Exp}}$ values are 1.11 (with a standard deviation of 0.10), 0.95 (with a standard deviation of 0.016), 1.0 (with a

standard deviation of 0.016), 1.0 (with a standard deviation of 0.068), 1.06 (with a standard deviation of 0.05) and 1.05 (with a standard deviation of 0.048) respectively for the beams tested by Kang and Ary (2012), Zong et al. (2013), Mofidi et al. (2012), Qin et al. (2014), Valerio and Ibell (2003) without considering the FRP-to-concrete bond-slip behaviour and Valerio and Ibell (2003) considering the FRP-to-concrete bond-slip behaviour. The mean $\Delta_{\mathrm{FE}}/\Delta_{\mathrm{Exp}}$ values are 0.95 (with a standard deviation of 0.08), 0.86 (with a standard deviation of 0.02), 0.94 (with a standard deviation of 0.075), 0.83 (with a standard deviation of 0.05), 1.11 (with a standard deviation of 0.087) and 1.11 (with a standard deviation of 0.078) respectively for the beams tested by Kang and Ary (2012), Zong et al. (2013), Mofidi et al. (2012), Qin et al. (2014), Valerio and Ibell (2003) without considering the FRP-to-concrete bond-slip behaviour and Valerio and Ibell (2003) considering the FRP-to-concrete bond-slip behaviour.

The overall mean $V_{\mathrm{FE}}/V_{\mathrm{Exp}}$ values are 1.03 (with a standard deviation of 0.11), 1.03 (with a standard deviation of 0.055) and 1.02 (with a standard deviation of 0.051) respectively for PC beams, RC beams (without considering the FRP-to-concrete bond-slip behaviour for the beams tested by Valerio and Ibell, 2003) and RC beams (considering the FRP-to-concrete bond-slip behaviour for the beams tested by Valerio and Ibell, 2003). The overall mean $\Delta_{\mathrm{FE}}/\Delta_{\mathrm{Exp}}$ values are 0.91 (with a standard deviation of 0.073), 0.99 (with a standard deviation of 0.134) and 0.99 (with a standard deviation of 0.13) respectively for PC beams, RC beams (without considering the FRP-to-concrete bond-slip behaviour for the beams tested by Valerio

and Ibell, 2003) and RC beams (considering the FRP-to-concrete bond-slip behaviour for the beams tested by Valerio and Ibell, 2003).

The comparisons presented demonstrate the applicability of the developed FE models, which then were used to carry out further numerical analysis as shown in Chapter Five and Chapter Six.

CHAPTER 5: PARAMETRIC STUDY OF PC GIRDERS STRENGTHENED IN SHEAR BY EB FRP LAMINATES

5.1 Introduction

The nonlinear behaviour of PC girders strengthened in shear using CFRP laminates can be taken into consideration by incorporating appropriate constitutive laws and iterative procedures (You et al, 2011). Nonetheless, numerical studies on CFRP shear-strengthened PC girders are scarce (see Section 3.6.1). Moreover, to date, extensive FE studies examining the influencing parameters on the behaviour of CFRP shear-strengthened PC girders have not been found. This was partially attributed to the complex behaviour of strengthened PC girders (You et al, 2011).

Based on the good predictions of the developed FE model presented in Section 4.6.1, this was used to carry out an extensive parametric study on CFRP shear-strengthened PC girders with and without internal steel stirrups. The parametric study was based on both the experimental studies used for the validation (i.e. Kang and Ary, 2012; Zong et al., 2013) to cover a wide range of influencing variables.

Moreover, the parametric study results were compared, in terms of the shear force gain due to the CFRP laminates, to the predictions of the ACI 440.2R (2008) and TR55 design code (2012) to highlight the parameters that had not been considered in the development of these design guidelines.

All modelled girders reported in this study failed in shear. In order to investigate the effect of a given parameter, only its value was varied while the values of the other parameters were kept unchanged. Moreover, the shear force gain for a given FE model was calculated by subtracting the predicted unstrengthened shear force capacity from the corresponding predicted strengthened shear force capacity. It should be noted that the predicted results reflect the performance of the FE model rather than that of actual girders. Thus, further testing is recommended to confirm the predicted results.

5.2 PC Girders without Internal Steel Stirrups (Kang and Ary, 2012)

The validated FE model was used to examine the effect of the concrete compressive strength, CFRP width-to-spacing ratio, CFRP thickness, girder effective depth, shear span-to-effective depth ratio, level of prestress, tendon profile, pre-cracking and CFRP-to-concrete interface model on the predicted shear strength of the CFRP shear-strengthened PC girders tested by Kang and Ary (2012). Except for the FE models used to investigate the effect of concrete compressive strength, all the FE models considered in this parametric study had a concrete cylinder compressive strength of 59 MPa (i.e. the value reported in the experimental investigation).

5.2.1 Effect of Cylinder Compressive Strength of Concrete

The FE models used to investigate the effect of concrete compressive strength were nominally identical to those validated in Section 4.6.1.1. Concrete cylinder compressive strength values of 30 MPa, 40 MPa, 50 MPa, 59 MPa (i.e. similar to the

average concrete compressive strength of the tested girders) and 70 MPa were considered for the control as well as the strengthened girders.

Figure 5-1a depicts the influence of concrete compressive strength on the predicted shear force capacity. The FE model predicted that the shear force capacity of the PC girders varies approximately linearly with the cylinder compressive strength. The predicted shear force capacity of the unstrengthened, IB-10 and IB-05 PC girders increased by 62.7%, 61.3% and 65.1% respectively when the concrete compressive strength was increased from 30 MPa to 70 MPa. Such significant increases were to be expected because, for PC girders without internal shear reinforcement, the concrete contribution to shear force capacity is significant. Increasing the concrete compressive strength will therefore increase the concrete contribution and enhance shear force capacity.

The variation of predicted shear force gain (i.e. predicted CFRP contribution to shear force capacity) with concrete compressive strength is shown in Figure 5-1b. It can be seen that the increase in concrete compressive strength resulted in a corresponding increase in the predicted CFRP contribution (especially for the case of IB-05 where a higher CFRP reinforcement ratio was used). The predicted CFRP contributions of IB-10 and IB-05 girders increased respectively from 14.32 kN and 20.64 kN to respectively 21.8 kN and 36.2 kN, due to the increase in concrete compressive strength from 30 MPa to 70 MPa. This increase may be attributed to the role of concrete compressive strength in enhancing the bond performance between the EB CFRP reinforcement and the concrete (see Equation 4-10). The average percentage

of CFRP shear contribution was increased by 52.1% and 75.4% for IB-10 and IB-05 girders respectively.

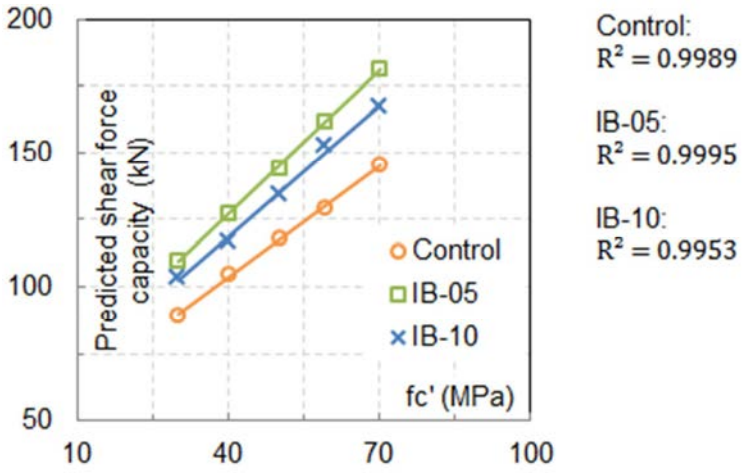

(a)

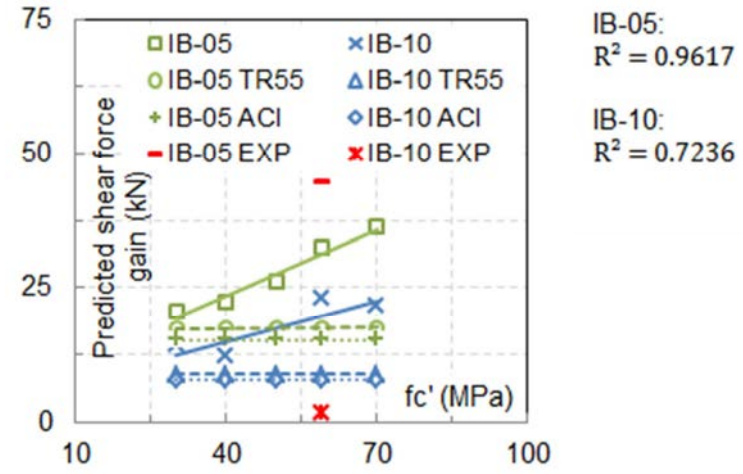

(b)

Figure 5-1: Effect of concrete compressive strength on the predicted (a) shear force capacity and (b) CFRP shear force gain of PC girders without stirrups

In contrast, Figure 5-1b shows that, due to the low elastic modulus of the CFRP sheets used in the tested girders (see Table 4-1), the ACI 440.2R (2008) and TR55 design code (2012) wrongly predicted the effective strain in the CFRP sheets, as the value 0.004 governed in both design guidelines, regardless of the concrete grade used; hence the design guidelines wrongly predicted the governing mode of failure (see Section 2.10.1). Therefore, the design guidelines were unable to predict the influence of concrete grade on the shear force contribution due to the CFRP sheets.

5.2.2 Effect of CFRP Width-to-Spacing Ratio

In order to investigate the effect of CFRP laminates width-to-spacing ratio, a FE model nominally identical to those in the validation section, but with the EB CFRP reinforcement attached to the full shear spans, was developed. Hence, three CFRP width-to-spacing ratios were considered, namely 0.3 (i.e. 76 mm/254 mm), 0.6 (i.e. 76 mm/127 mm) and 1.0 (i.e. continuous CFRP reinforcement).

As can be seen in Figure 5-2, the predicted results suggest that both the shear force capacity and the contribution of the EB CFRP reinforcement increase linearly with the increase in CFRP width-to-spacing ratio. The predicted CFRP contribution increased from 22.9 kN (17.6%) to 44.3 kN (34.2%) when the CFRP width-to-spacing ratio was increased from 0.3 to 1.0. This linear variation between the CFRP contribution and the CFRP width-to-spacing ratio is also adopted by existing design guidelines (i.e. ACI 440.2R, 2008; TR55 design code, 2012). It is based on the truss analogy which models the EB CFRP reinforcement as external shear links that contribute to the

shear resistance by controlling and limiting the progress of inclined cracks. However, the predictions of the design guidelines were much lower than those of the FE model.

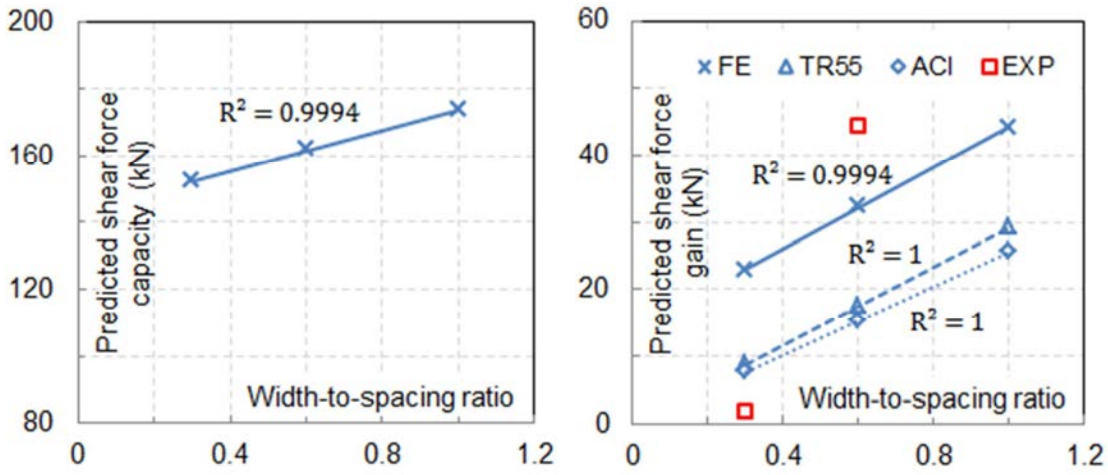

(a) (b)

Figure 5-2: Effect of CFRP width-to-spacing ratio on the predicted (a) shear force capacity and (b) CFRP shear force gain of PC girders without stirrups

5.2.3 Effect of CFRP Thickness

The effect of CFRP thickness was studied by modelling PC girders nominally identical to the strengthened models validated in Section 4.6.1.1. Three CFRP laminates thickness values were considered for each of the strengthened girders, namely 1.25 mm (i.e. similar to the experimental value), 2.50 mm and 3.75 mm. Figures 5-3a and 5-3b show the variation of predicted shear force capacity and predicted CFRP shear contribution (according to the FE model and the design guidelines) with CFRP thickness, respectively.

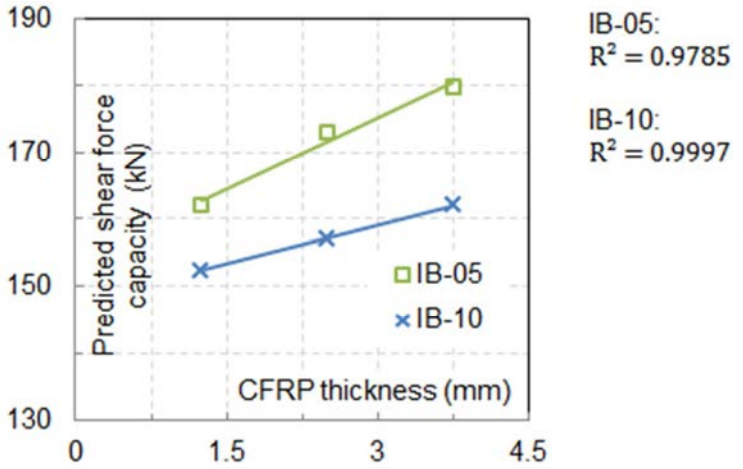

(a)

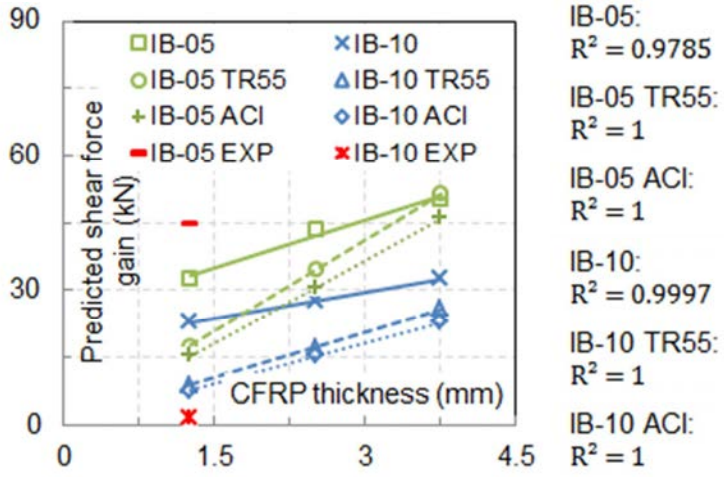

(b)

Figure 5-3: Effect of CFRP thickness on the predicted (a) shear force capacity and (b) CFRP shear force gain of PC girders without stirrups

Similar to the effect of CFRP width-to-spacing ratio, the increase in CFRP thickness enhanced the predicted CFRP shear contribution and consequently the predicted shear force capacity. The FE-predicted CFRP shear contributions of IB-10 and IB-05

girders increased respectively from 22.9 (17.6%) and 32.5 kN (25.1%) to respectively 32.5 kN (25.1%) and 50.2 kN (38.8%), when the CFRP thickness was increased from 1.25 mm to 3.75 mm. This may be attributed to the fact that thicker CFRP reinforcement have higher axial rigidity and therefore provide higher resistance to crack propagation. This trend in CFRP shear contribution (i.e. the increase in predicted shear force capacity with the increase in CFRP thickness) was comparably predicted by existing design guidelines. Once more, the predictions of the ACI 440.2R (2008) and TR55 design code (2012) were in general lower than those predicted by the FE model, as depicted in Figure 5-3b.

5.2.4 Shear Span-to-Effective Depth Ratio (a/d)

It was aforementioned in Section 2.8.3 that the results obtained from the published literature investigating the effect of the a/d ratio on the EB CFRP laminates shear contribution are contradictory. Moreover, the whole a/d ratio range, within which a shear failure is expected to dominate if the flexural capacity is sufficient, has not been fully investigated. To this end, FE models nominally identical to those validated in Section 4.6.1.1, but with varying shear spans, were developed. Shear span-to-effective depth ratios in the range of 2.5-5.5 were considered in this series of girders.

The influence of a/d ratio on the predicted shear force capacity is presented in Figure 5-4a. The results in this figure, which are in accordance with the findings of Kani et al. (1979) for RC beams, reveal that the higher the a/d ratio, the lower the shear force capacity. This reduction may be related to the shift from arch-action, which provides higher resistance, to beam-action.

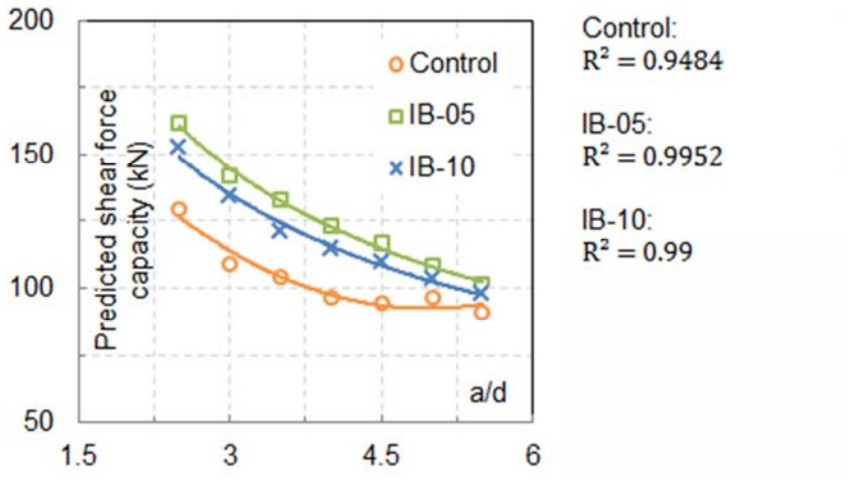

(a)

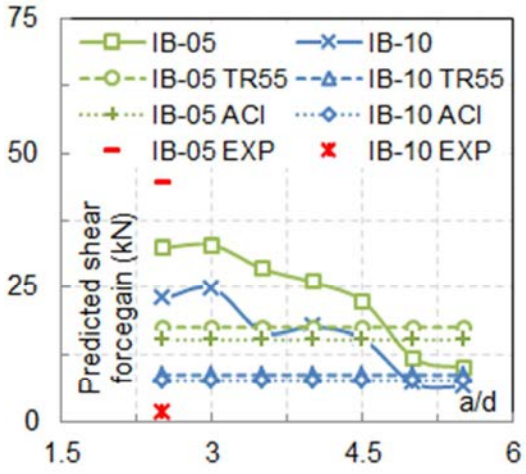

(b)

Figure 5-4: Effect of shear span-to-effective depth ratio on the predicted (a) shear force capacity and (b) CFRP shear force gain of PC girders without stirrups

Figure 5-4b presents the influence of a/d ratio on the predicted CFRP shear contribution. The general trend that can be observed in Figure 5-4b is that the predicted CFRP shear contribution decreased with the increase in a/d ratio. The

CFRP shear contributions of series IB-05 and IB-10 decreased by 69% and 71.5%, respectively when a/d ratio was increased from 2.5 to 5.5. Similar trend was recently reported by Sayed et al. (2013) for RC beams strengthened in shear with EB CFRP sheets. This finding is important because current design guidelines, i.e. the ACI 440.2R (2008) and the TR55 design code (2012), do not capture the effect of a/d ratio on the CFRP shear contribution, as depicted in Figure 5-4b.

5.2.5 Effective Girder Depth (Size Effect)

Effective depth of girders is a major factor affecting both the shear force capacity and behaviour of concrete girders. However, its influence on the shear force capacity of CFRP-strengthened PC girders has not been fully investigated. In concrete members without internal shear reinforcement, the increase in effective depth is associated with a strong size effect (see Section 2.4.1). To investigate the influence of girder size, additional FE models were developed for the control, IB-10 and IB-05 girders with effective depths of 343 mm (i.e. 0.75d) and 686 mm (i.e. 1.5d). Other parameters; such as the a/d ratio, mesh density, prestressing tendons ratio, longitudinal steel ratio and FRP reinforcement ratio; were kept constant. Moreover, the girder width has no or very limited influence on the shear behaviour (Kani, 1967) and therefore was not considered for this series of girders.

Figure 5-5a shows that the predicted shear stress at failure drops significantly with the increase in effective girder depth, suggesting a strong size effect in both unstrengthened and CFRP-strengthened PC girders without internal shear reinforcement. The shear stress at failure for the control, IB-10 and IB-05 series

decreased by 25.2%, 23.3% and 25.2%, respectively when the effective depth was increased from 343 mm to 686 mm. As explained in Section 2.4.1, this reduction may be attributed to wider shear cracks in deeper sections (Collins et al., 2008).

The influence of effective girder depth on the percentage gain in shear force and the predicted shear force contribution due to the CFRP laminates are presented in Figure 5-5b and Figure 5-5c respectively. From these figures it can be seen that for effective depths lower than 457 mm, the percentage of shear force gain and the predicted shear force contribution due to the CFRP laminates increase with the increase in effective beam depth. It seems that size effect is likely to be negligible within such relatively low effective depth values. Hence the increase in effective girder depth leads to a corresponding increase in the CFRP effective bond length which, in turn, enhances the CFRP contribution (Triantafillou, 1998; Dirar et al. 2012).

On the other hand, for girders with effective depths higher than 457 mm, the percentage of CFRP shear force gain as well as the predicted CFRP shear force contribution of beams with lower CFRP ratio tend to decrease with the increase in effective beam depth. This reduction may be related to size effect as effective bond length of the bonded CFRP laminates does not increase proportionally to the beam size increase (Bousselham and Chaallal, 2013). However, the predictions of the ACI 440.2R (2008) and the TR55 design code (2012) presented in Figure 5-5c suggest that the CFRP shear force contribution increases linearly with the increase in beam effective depth without accounting for the size effect. Therefore further experimental testing is required to confirm the predicted results.

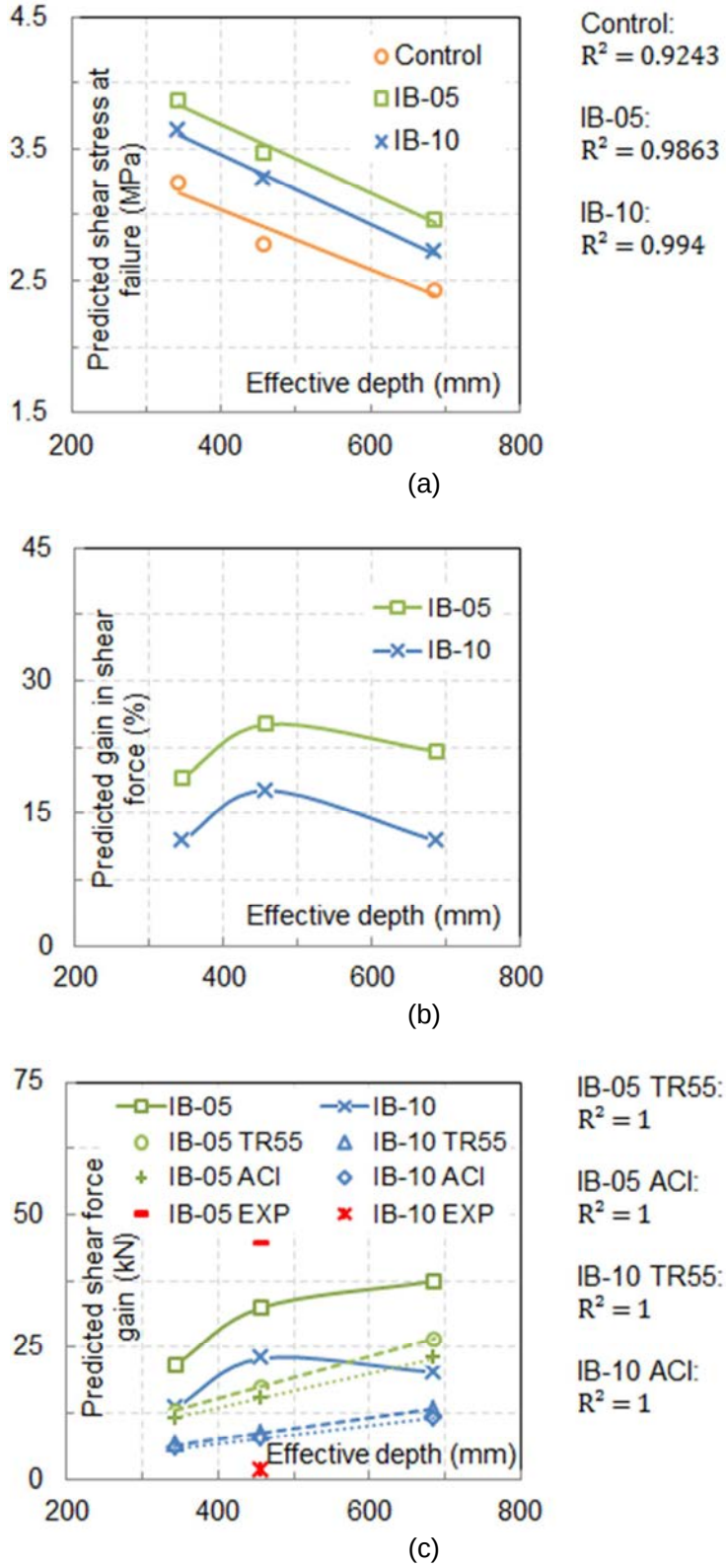

Figure 5-5: Effect of beam depth on the predicted (a) shear stress at failure, (b) shear force gain percentage due to CFRP and (c) CFRP shear force gain of PC girders without stirrups

5.2.6 Effect of Prestress

In order to investigate the effect of axial prestress, FE models nominally identical to those validated in Section 4.6.1.1, but with different levels of prestress in the tendons, were developed. Three levels of prestress in the tendons were considered, namely 830 MPa, 1075 MPa and 1325 MPa. These prestress levels represented 50%, 65% and 80% of the tendon yield strength respectively.

Except for the FE model for IB-10 with a prestress level of 1328 MPa, Figure 5-6a shows that the predicted shear force capacity is marginally enhanced by the increase in axial prestress. The percentage increase in the predicted shear force capacity of the modelled girders varied from 3.97% to 6.75% when the tendon prestress level was increased from 830 MPa to 1328 MPa. This marginal increase might be attributed to the fact that the axial prestress reduces crack widths and consequently enhances the concrete contribution to shear force capacity.

The variation of predicted CFRP shear contribution with prestress level is presented in Figure 5-6b. Except for the FE model for IB-10 with a prestress level of 1328 MPa, the change in prestress level did not have a significant effect on the predicted CFRP contribution. The marginal increase in the predicted shear force capacity of the strengthened girders (see Figure 5-6a) is therefore caused by the increase in predicted concrete contribution as explained earlier rather than of that due to the CFRP contribution. Figure 5-6b also shows that the predictions of both the ACI 440.2R (2008) and the TR55 design code (2012) were realistic by not considering the influence of the prestressing force on the CFRP shear force contribution.

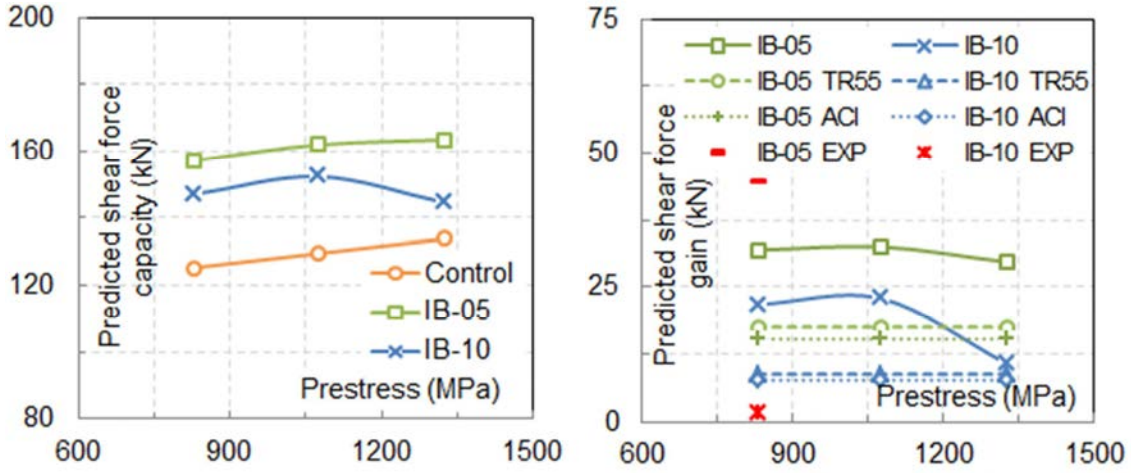

(a) (b)

Figure 5-6: Effect of prestress level on the predicted (a) shear force capacity and (b) CFRP shear force gain of PC girders without stirrups

5.2.7 Effect Tendon Profile

For simply supported beams, it is well known that when a parabolic or harped tendon profile is used, a resultant upward force, which may enhance the shear force capacity, acts on the concrete section. Therefore, the effect of tendon profile was investigated by developing FE models nominally identical to those validated in Section 4.6.1.1 but with a double-harped tendon profile. At girders ends, the tendons were positioned at the concrete centroid. They descended linearly to the level of the straight tendon at loading points (see Figure 5-7).

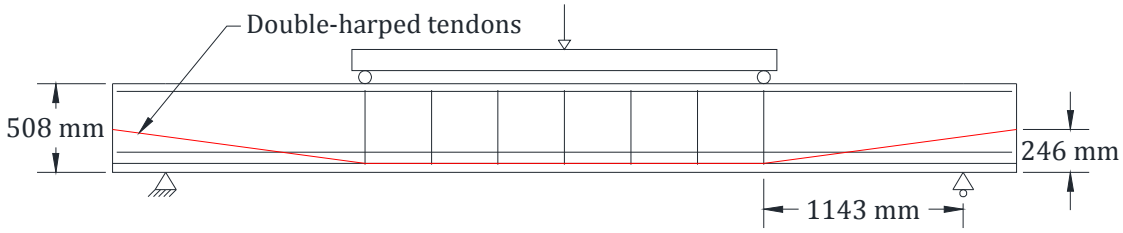

Figure 5-7: PC I-girder with a double-harped tendon profile

The predicted shear force capacities of the control, IB-10 and IB-05 girders with a double-harped tendon profile were 154.9 kN, 169.5 kN and 180.0 kN respectively. This represents an increase of 19.6%, 11.2% and 11.1%, respectively over the predicted shear strength of the corresponding girders with a straight tendons profile.

On the other hand, the predicted CFRP shear contributions of IB-10 and IB-05 girders with a double-harped tendon profile were 14.6 kN and 25.1 kN, respectively whereas the predicted CFRP contributions for the corresponding girders with a straight tendon profile were 22.9 kN and 32.5 kN, respectively. This result indicates that, for the girders with a double-harped tendon profile, the concrete contribution increased whereas the CFRP contribution decreased. However, both the ACI 440.2R (2008) and the TR55 design code (2012) do not account for the effect of tendon profile on the CFRP shear contribution. Further research is required to better understand the interaction between tendon profile and the CFRP contribution to shear force capacity.

5.2.8 Effect of Pre-Cracking

EB CFRP reinforcement may be used to strengthen cracked PC members. Hence, it is important to investigate the effect of precracking on shear force capacity of CFRP-strengthened PC girders. To accomplish this, six FE models nominally identical to those for IB-05 and IB-10, were developed. The nonlinear analysis of these models included three calculation phases. In Phase I, the unstrengthened FE models, with the elements representing the EB CFRP reinforcement and the FRP-to-concrete interface set as inactive, were prestressed. Phase II included loading the unstrengthened FE models to 75%, 85% or 95% of their unstrengthened shear force capacity. Phase III included activating the elements representing the EB CFRP reinforcement and the FRP-to-concrete interface, and then loading the FE models up to failure.

Figure 5-8 presents the obtained results in terms of the variation of predicted shear force capacity with normalised pre-crack load (pre-cracking level). It can be seen that, up to a pre-cracking level of 85%, there was no significant effect on the predicted shear strength. Comparable results were reported by Dirar et al. (2012) for CFRP-strengthened RC beams where it was found that a pre-cracking level of 70% had insignificant effect on the shear force capacity. At a pre-cracking level of 95%, the EB CFRP strips enhanced the shear force capacity of IB-10 and IB-05 girders by 5.5 kN (4.2%) and 3.98 kN (3.1%), respectively. Failure was governed by excessive opening of the existing diagonal cracks. The results imply that EB CFRP reinforcement can be effectively used to retrofit cracked PC girders.

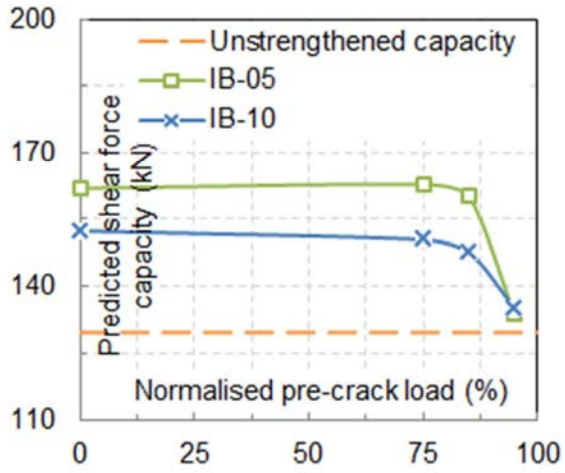

Figure 5-8: Effect of pre-cracking level on the predicted shear force capacity

5.2.9 Effect of CFRP-to-Concrete Bond-Slip Model

The CFRP-to-concrete bond-slip model plays an important role in FE modelling of concrete structures strengthened with EB CFRP reinforcement. In addition to the bond-slip model adopted in the validation (Sato and Vecchio, 2003), the simplified bond-slip model proposed by Lu et al. (2005) was considered. The latter model assumes that the bond stress varies nonlinearly with slip (for more details see Lu et al., 2005). For approximately equal values of peak bond stress and interfacial fracture energy, the shear force versus deflection curves predictions of the two bond-slip models were identical as shown in Figure 5-9 suggesting that the shape of the bond-slip model had no influence on the overall behaviour. Similar findings were reported by Niu and Wu (2006).

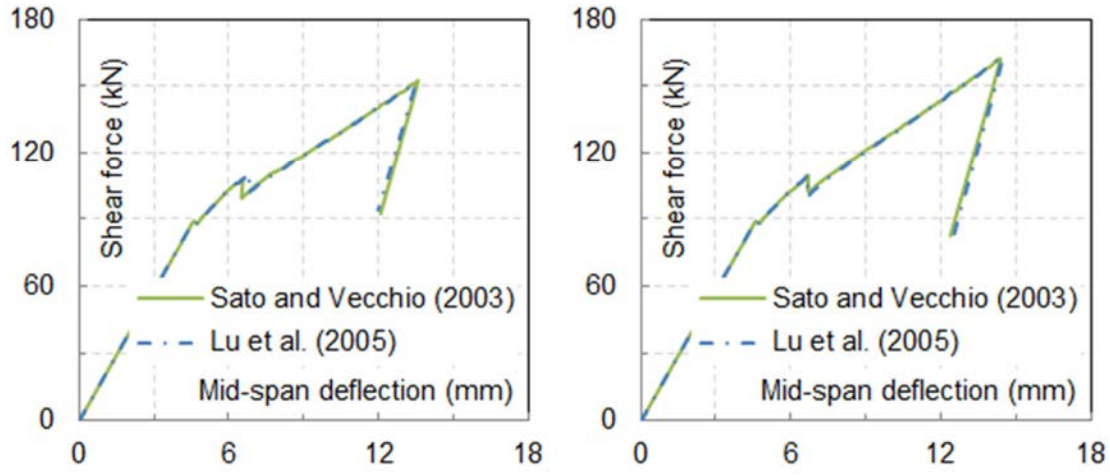

(a) IB-10 (b) IB-05

Figure 5-9: Effect of CFRP-to-concrete bond-slip model shape

5.3 PC Girders with Internal Steel Stirrups (Zong et al., 2013)

The developed FE model was also used to investigate the effect of concrete compressive strength, a/d ratio, effective beam depth and interaction between internal steel and EB CFRP shear reinforcement on the behaviour of the strengthened PC girders with internal steel stirrups tested by Zong et al. (2013). The previous parametric study presented in Section 5.2 showed that neither the shear force capacity nor the shear force gain was significantly influenced by the effective prestress. Hence, the effect of prestress level was not considered in this parametric study and consequently all modelled beams were variants of PPC0 and PPC2.

In order to ensure that the modelled beams considered in the parametric study would fail in shear, their flexural-to-shear strength ratio was increased by increasing the

yield strength value of the steel compression and tension reinforcement to 520 MPa, increasing the diameter of the compression reinforcement from 14 to 25 mm, and changing the tendon profile from double-harped to straight. Furthermore, unless otherwise stated, the modelled beams had a concrete cylinder compressive strength of 44 MPa and steel stirrups spacing of 266 mm c/c.

5.3.1 Effect of Cylinder Compressive Strength of Concrete

Concrete cylinder compressive strength values of 44, 55 and 65 MPa were considered. Both the predicted shear force capacity and the predicted shear force gain due to the EB CFRP sheets increased approximately linearly with the increase in concrete compressive strength, for both the unstrengthened PC girders (PPC0N) and strengthened PC girders (PPC2N), as can be seen respectively in Figure 5-10a and Figure 5-10b. Comparable results were reported in Section 5.2.1 for CFRP shear-strengthened PC beams without internal shear reinforcement.

The predicted shear force capacity of PPC0N and PPC2N increased by 35% and 30% respectively when the concrete compressive strength was increased from 44 MPa to 65 MPa. The corresponding increase in predicted shear force gain due to the EB CFRP sheets was 12%. Once more, this increase may be attributable to the enhancement in bond performance between the concrete and EB CFPR sheets as a result of the increase in concrete strength, as shown in Equation 4-10.

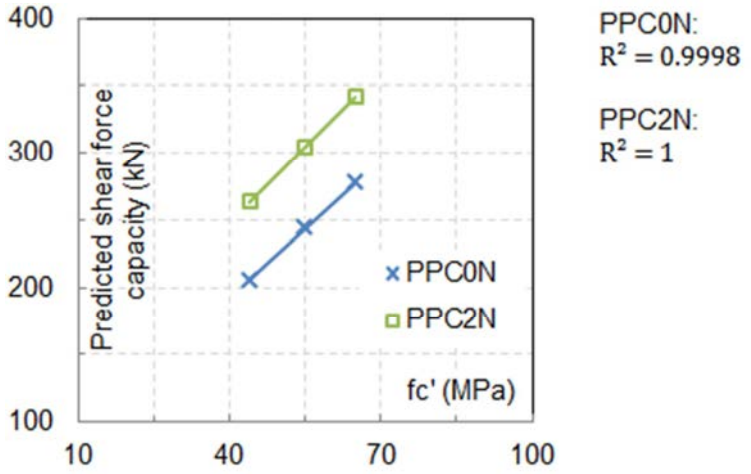

(a)

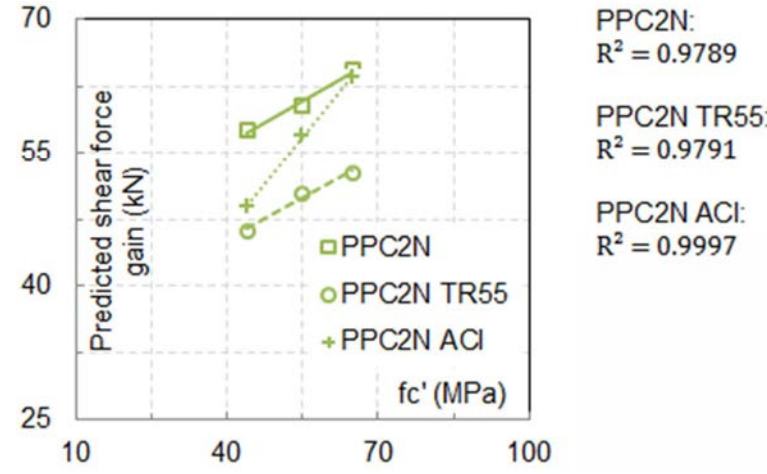

(b)

Figure 5-10: Effect of concrete compressive strength on the predicted (a) shear force capacity and (b) CFRP shear force gain of PC girders with stirrups

Unlike the parametric study carried out on PC girders without stirrups, both the ACI 440.2R (2008) and TR55 design code (2012) were able to capture the influence of concrete grade on the CFRP shear force contribution for this series of PC girders,

where the CFRP contribution increased linearly with the increase in concrete compressive strength, as depicted in Figure 5-10b. This might be mainly attributed to the higher elastic modulus of FRP sheets used in this series of beams, which led to the correct prediction of the debonding failure mode (see Equations 2-5 and 2-13).

5.3.2 Shear Span-to-Effective Depth Ratio (a/d)

In order to study the influence of the a/d ratio on the shear behaviour of this series of PC girders, FE models with a/d ratios in the range of 2.42-3.63 were developed. The desired a/d ratios were obtained by increasing the shear spans by shifting the supports to the outside (see Figure 4-4). It should be mentioned that FE models having a/d ratios higher than 3.63 were failed in flexure; thus, their results have not been reported on here. The effect of a/d ratio on the predicted shear force capacity and the CFRP shear contribution are given respectively in Figures 5-11a and 5-11b.

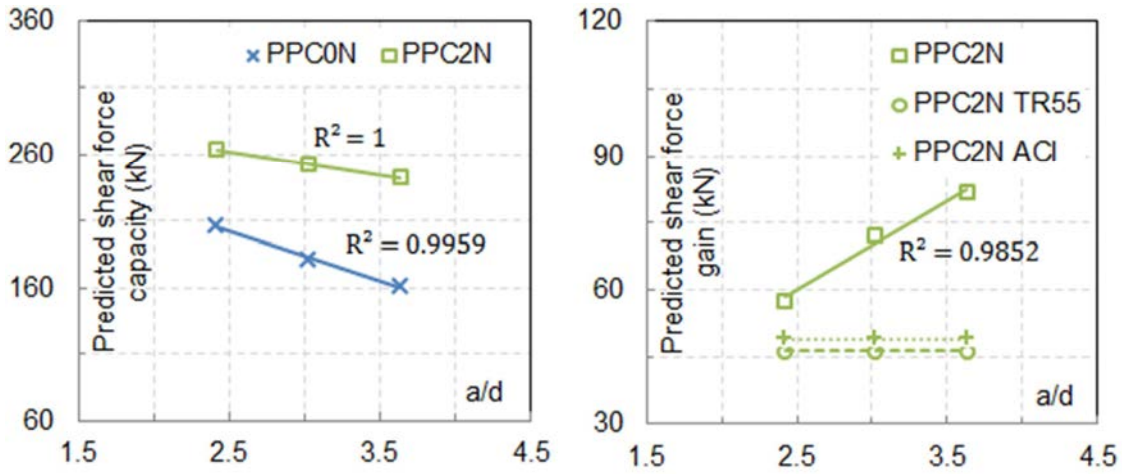

(a) (b)

Figure 5-11: Effect of shear span-to-effective depth ratio on the predicted (a) shear force capacity and (b) CFRP shear force gain of PC girders with stirrups

Similar to what has been obtained for the PC girders without steel stirrups, Figure 5-11a shows that the a/d ratio has a detrimental effect on the predicted shear force capacity of both the unstrengthened and strengthened girders. Once more, this reduction, which is in accordance with the results of Kani et al. (1979) for RC beams, might be related to the shifting from arch-action to beam-action as a result of increasing a/d ratio of the beam.

However, Figure 5-11b shows an unexpected influence of the a/d ratio on the shear force contribution due to the EB CFRP sheets to that of the previous parametric study (see Figure 5-4b). It can be seen in Figure 5-11b that the increase in a/d ratio resulted in a corresponding increase in the CFRP shear contribution. The CFRP shear contribution increased by 42% when a/d ratio was increased from 2.42 to 3.63. A similar trend was reported in the published literature (e.g. Khalifa and Nanni, 2002; Bousselham and Chaallal, 2004; Bousselham and Chaallal, 2006; Ary and Kang, 2012). Therefore, tests with a wider range of a/d ratio are required to confirm this finding. Again, the ACI 440.2R (2008) and the TR55 design code (2012) failed to simulate the influence of a/d ratio on the CFRP shear contribution.

5.3.3 Effective Girder Depth (Size Effect)

FE models with effective depths of 330 mm (i.e. d), 495 mm (i.e. 1.5d) and 660 mm (i.e. 2.0d) were considered to investigate the influence of effective beam depth, whereas other parameters; such as the a/d ratio, mesh density, prestressing tendons ratio, longitudinal steel ratio, shear stirrups ratio and FRP reinforcement ratio; were kept constant. Moreover, in this series of PC girders, the effect of girder

width was not considered as a varying parameter. The variation of predicted shear stress at failure, percentage of shear force gain due to the EB CFRP laminates and CFRP shear contribution with effective beam depth are presented in Figures 5-12a, 5-12b and 5-12c, respectively.

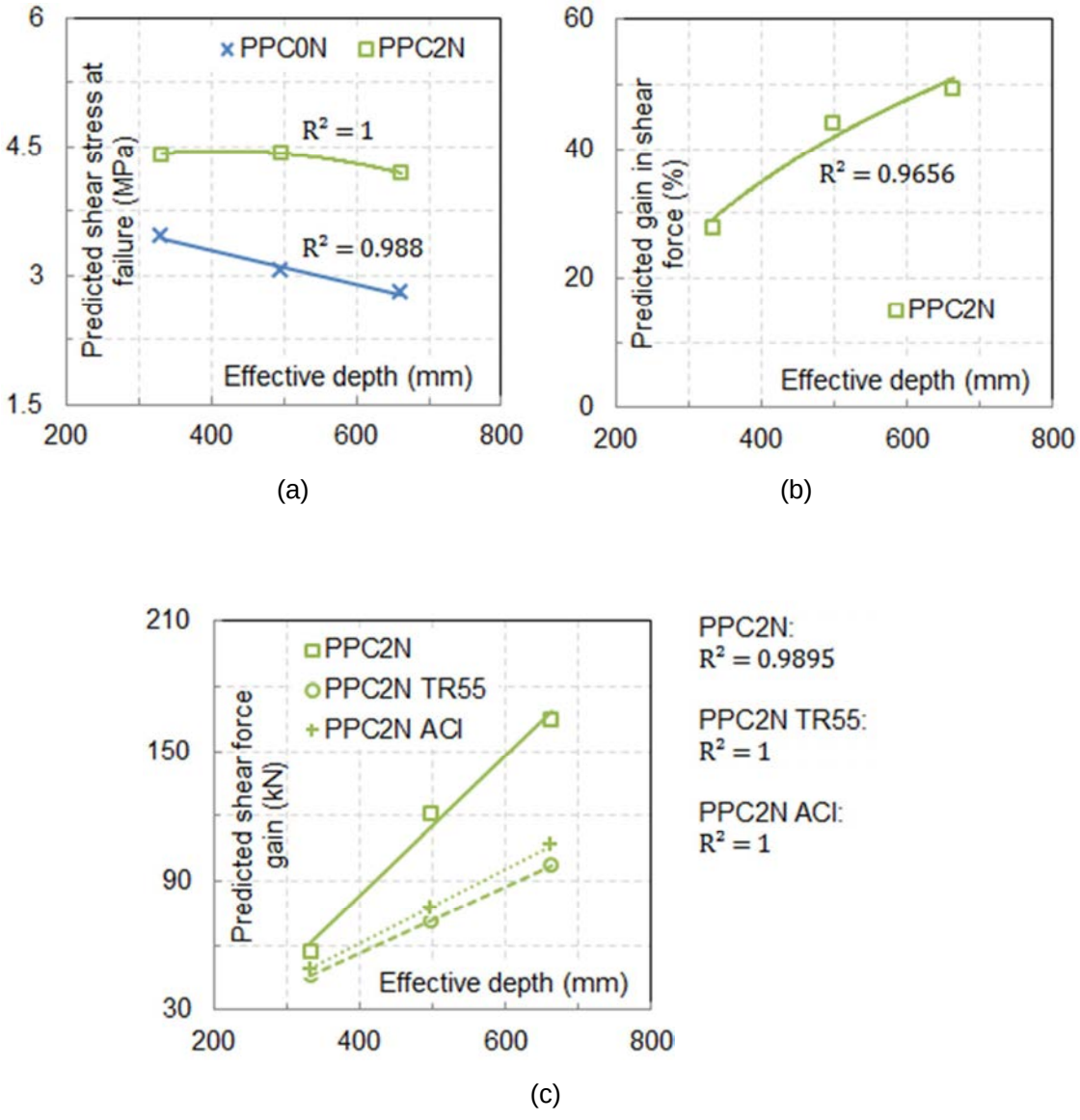

Figure 5-12: Effect of beam depth on the predicted (a) shear stress at failure, (b) shear force gain percentage due to CFRP and (c) CFRP shear force gain of PC girders with stirrups

Figure 5-12a shows that the predicted shear stress at failure of PPC0N and PPC2N decreased by 19% and 5%, respectively with the increase in effective beam depth from 330 mm to 660 mm. As mentioned earlier, this reduction is attributable to size effect which is caused by wider shear cracks in large beams (Collins et al., 2008). Of note is that the EB CFRP sheets helped mitigate size effect in the strengthened beams (i.e. PPC2N).

Figure 5-12b shows that the predicted percentage of shear force gain increased from 28% to 49.5% with the increase in effective beam depth from 330 mm to 660 mm. This enhancement can be attributed to the fact that increasing the effective beam depth increases the effective bond length of the EB CFRP sheets which, in turn, enhances the shear contribution due to the CFRP (Triantafillou, 1998; Dirar et al. 2012).

Moreover, the shear force gain due to the EB CFRP sheets increased approximately linearly, from 57.6 kN to 165.3 kN, with the increase in effect beam depth as shown in Figure 5-12c. This result is contradictory to what was found in the previous parametric study and might be attributed to the fact that the U-shape CFRP sheets in this series of girders were sufficiently anchored from the free ends. Therefore, the effectiveness of the EB CFRP laminates became independent of size effect (Triantafillou, 1998; Leung et al., 2007). This behaviour, i.e. the linear increase in the CFRP shear force gain with the increase in effect beam depth, can be predicted by both the ACI 440.2R (2008) and the TR55 design code (2012), as illustrated in Figure 5-12c.

5.3.4 Interaction between Internal Steel and EB CFRP Reinforcement

The variation of predicted shear force gain due to the EB CFRP sheets with the quantity $E_s\rho_s/E_f\rho_f$ (i.e. the internal steel-to-CFRP axial rigidity ratio) is depicted in Figure 5-13. It can be seen that the predicted shear force gain is inversely proportional to the $E_s\rho_s/E_f\rho_f$. As explained in Section 2.8.5, this may be explained by the fact that cracks become more distributed as the value of $E_s\rho_s/E_f\rho_f$ increases, due to increase in the internal steel stirrups ratio. These more distributed cracks reduce the anchorage length of the EB CFRP reinforcement and consequently their contribution to shear force capacity (Pellegrino and Modena, 2002).

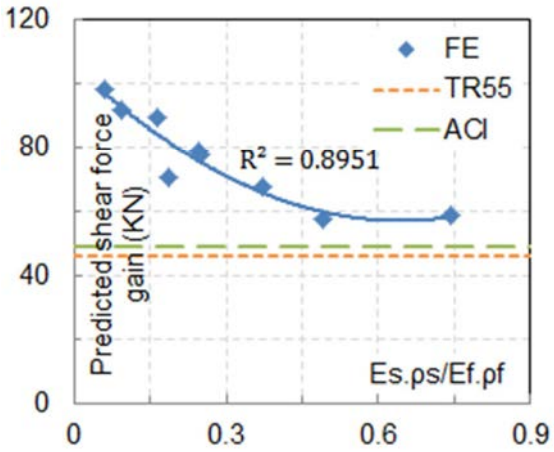

Figure 5-13: Interaction between steel reinforcement stirrups and EB CFRP sheets

Once more, Figure 5-13 shows that both the ACI 440.2R (2008) and the TR55 design code (2012) do not account for the influence of this significant parameter as shear stirrups are usually existing in PC girders.

5.4 Concluding Remarks

In this chapter, the developed three-dimensional nonlinear FE model for PC girders strengthened in shear with EB CFRP strips has been used to carry out an extensive parametric study to investigate the effect of the concrete compressive strength, CFRP width-to-spacing ratio, CFRP thickness, shear span-to-effective depth ratio, girder effective depth, level of prestress, tendon profile, precracking, CFRP-to-concrete interface model and interaction between internal steel stirrups and EB CFRP shear reinforcement on the predicted shear behaviour of the modelled beams. Moreover, a comparison between the FE predicted shear force gain due to the EB CFRP laminates and the corresponding results obtained from both the ACI 440.2R (2008) and the TR55 design code (2012) has been presented to reveal the influencing factors that are not being considered by these design guidelines.

Based on the numerical results obtained, the following conclusions can be drawn for PC girders without internal steel stirrups:

1- The concrete compressive strength had a significant influence on both the concrete and CFRP contributions to predicted shear force capacity. The percentage increase in predicted shear force capacity and CFRP contribution ranged respectively from 61.3% to 65.1% and from 52.1% to 75.4%, when the concrete compressive strength was increased from 30 to 70 MPa.

2- The predicted CFRP contribution increased from 22.9 kN (17.6%) to 44.3 kN (34.2%) when the CFRP width-to-spacing ratio was increased from 0.3 to 1.0.

3- The increase in the CFRP thickness enhanced the predicted CFRP contribution and consequently the predicted shear force capacity. The percentage of CFRP contribution to shear force capacity ranged from 17.6% to 38.8%.

4- The increase in a/d ratio affected inversely both the predicted shear force capacity and CFRP shear force contribution. The predicted CFRP shear contributions averagely decreased by 69-71.5% when the a/d ratio was increased from 2.5 to 5.5.

5- A strong size effect was predicted for both the unstrengthened and CFRP-strengthened PC girders without internal shear reinforcement. The percentage reduction in predicted shear stress at failure ranged from 23.3% to 25.2% when the effective depth was increased from 343 mm to 686 mm, whereas both the rate of increase in the percentage shear force gain and the rate of CFRP shear contribution tend to decrease for beams having an effective depth of 457 mm or more.

6- The level of prestress in the tendons did not significantly influence either the predicted CFRP contribution or the predicted shear force capacity.

7- The change in tendon profile from a straight to double-harped shape increased the predicted total shear force capacity by 11.1-19.6%, but it had a detrimental effect on the predicted CFRP contribution to shear force capacity.

8- Pre-cracking loads of up to 85% of the unstrengthened shear force capacity did not have a significant effect on the predicted strengthened capacity. At higher pre-cracking load levels, the predicted CFRP shear contribution was insignificant.

9- For approximately equal values of peak bond stress and interfacial fracture energy, the shape of the CFRP-to-concrete bond-slip model had no influence on the overall behaviour of the modelled girders.

10- It can be observed that the predictions of the ACI 440.2R (2008) and the TR55 design code (2012) are systematically lower than those of the FE model. It is very difficult to identify whether the design guidelines are underestimating the shear strength enhancement or the FE model is overestimating it, unless physical tests are carried out. In addition, the results showed that, for this series of PC girders, both the ACI 440.2R (2008) and the TR55 design code (2012) did not capture correctly the effect of concrete compressive strength, a/d ratio and tendon profile on the shear force contribution due to the EB CFRP laminates. However, the predicted CFRP shear contribution was linearly increased with the increase in beam depth without accounting for the size effect. Moreover, the inaccuracy of the ACI 440.2R (2008) and the TR55 design code (2012) has been pointed out by several researchers (e.g. Dirar et al., 2012; Belarbi and Acun, 2013).

For the PC girders with internal steel stirrups, the main obtained conclusions were as follows:

1- The FE-predicted results suggest that increasing the concrete cylinder compressive strength from 44 to 65 MPa increases both the shear force capacity of the beams and the CFRP contribution to shear force capacity by 30-35% and 12%, respectively. This behaviour is in agreement with what was observed for PC girders without stirrups.

2- Similar to the PC girders without steel stirrups, the increase in a/d ratio resulted in a reduction in the predicted shear force capacity, due to the shifting from arch-action to beam-action, for both the unstrengthened and strengthened girders. However, unlike the previous parametric study, the increase in a/d ratio from 2.42 to 3.63 led to an increase in the CFRP shear contribution, which increased by 42% for this series of PC girders.

3- The predicted shear stress at failure of the unstrengthened and CFRP-strengthened beams decreased by 19% and 5% respectively with the increase in effective beam depth from 330 mm to 660 mm (suggesting that the CFRP sheets were able to cut down the size effect of the modelled girders), whereas both the predicted percentage of shear force gain due to the CFRP and the CFRP contribution to shear force capacity increased from 28% to 49.5% and by 187% (i.e. from 57.6 kN to 165.3 kN) respectively. This finding is contradictory to what was observed in the previous parametric study, which might be attributed to the anchorage system used in this series of girders.

4- The increase in the internal steel-to-CFRP axial rigidity ratio (i.e. $E_s\rho_s/E_f\rho_f$) had a detrimental effect on shear force gain provided by the EB CFRP sheets. This behaviour might be attributed to more distributed cracks which developed in beams with higher internal steel stirrups ratios; thus, the anchorage length of the EB CFRP sheets, and in turn the CFRP contribution to shear force capacity, is reduced.

5- For the CFRP shear contribution predictions of the ACI 440.2R (2008) and the TR55 design code (2012), the graphs presented revealed that both design guidelines were not able to simulate the influence of the a/d ratio and the internal steel-to-EB CFRP reinforcement interaction of this series of PC girders, whereas, unlike the parametric study conducted on PC I-girders without steel stirrups, both design guidelines showed a comparable trend to the FE-predicted influence of concrete compressive strength and effective depth of beams. The better prediction of the concrete compressive strength effect can be attributed to the correct prediction of the debonding failure mode in this series of modelled PC girders. Once more, the predictions of the ACI 440.2R (2008) and the TR55 design code (2012) were lower than the FE predictions.

CHAPTER 6: PARAMETRIC STUDY AND DESIGN MODEL FOR RC BEAMS STRENGTHENED IN SHEAR WITH DE FRP BARS

6.1 Introduction

After validating the FE model for RC beams strengthened in shear with DE FRP bars against experimental data from the literature, as demonstrated in Section 4.6.2, the model was then used to carry out a numerical parametric study to investigate the influence of the main parameters affecting FRP DE shear strengthening that have not been fully investigated in previous studies. The parametric study presented in this chapter was based on the set of beams tested by Mofidi et al. (2012) because it is the only set that included RC beams with different steel shear reinforcement ratios (0% and 0.38%). Furthermore, this set included RC beams with a T-shaped cross-section which adequately simulates the common slab-on-beam construction method. Thus, it allows a more realistic parametric study to be carried out.

In addition, this chapter presents a comparison between the FE predicted shear force gain due to the DE FRP bars and the predicted shear force gain by TR55 design code (2012), as well as the design model proposed by Mofidi et al. (2012). This was done to assess the prediction accuracy of these design models and to reveal the parameters influencing the shear contribution of DE FRP bars that are not

considered by such models. All safety factors were set equal to 1 for the purpose of comparison. Finally, an improved design model, based on the results of the FE prediction, is presented and demonstrated to be an improvement upon existing design models.

6.2 Variables of the Parametric Study

The parametric study presented in this section includes the effect of concrete compressive strength, shear span-to-effective depth ratio, effective beam depth, internal steel-to-DE FRP reinforcement interaction and orientation of DE FRP bars (i.e. vertical versus inclined) on the predicted shear force capacity of RC T-beams shear-strengthened with DE FRP bars.

Similar to previous parametric studies carried out on PC girders in Chapter Five, the effect of each parameter was studied solely through changing its value, whereas the other parameters were kept unchanged. Moreover, the shear force gain was calculated by subtracting the predicted unstrengthened shear force capacity from the corresponding predicted strengthened shear force capacity.

6.2.1 Effect of Cylinder Compressive Strength of Concrete

The effect of concrete compressive strength on the predicted shear force capacity was investigated by modelling beams nominally identical to S0-CON, S0-12d130s, S1-CON and S1-12d260s (see Section 4.2.2.1). For each beam, concrete cylinder compressive strength values of 25, 35, 45, 55 and 65 MPa were considered.

Figure 6-1a and Figure 6-1b present the effect of concrete cylinder compressive strength on the predicted shear force capacity and the predicted shear force gain due to the DE FRP bars respectively. Some of the FE models for S1-CON and S1-12d260s failed in flexure and their predictions were discarded. All the remaining predictions presented in Figure 6 are for FE models that failed in shear.

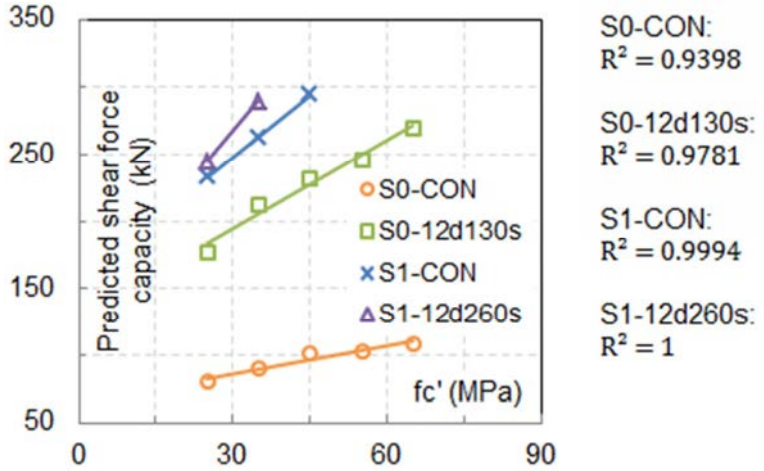

(a)

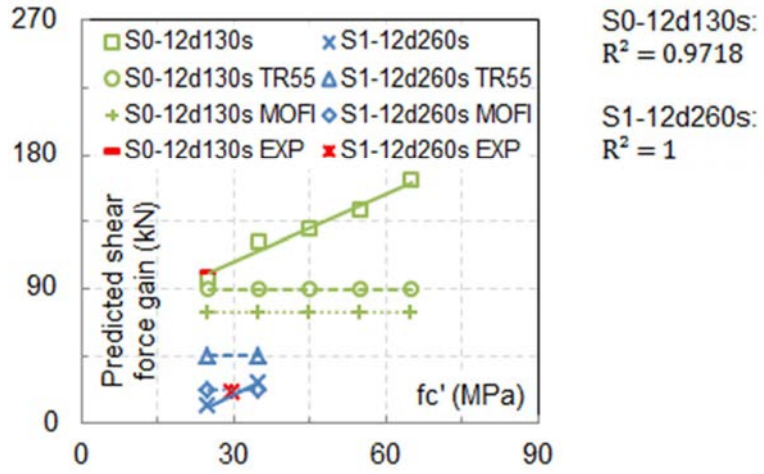

(b)

Figure 6-1: Effect of concrete compressive strength on the predicted (a) shear force capacity and (b) shear force gain due to DE FRP bars

Figure 6-1a shows that the predicted shear force capacity increased approximately linearly with the increase in concrete compressive strength. The predicted shear force capacity increased by 33.8% and 52.8% for the unstrengthened (S0-CON) and strengthened (S0-12d130s) beams without steel shear reinforcement, respectively, when the concrete cylinder compressive strength was increased from 25 to 65 MPa. For the unstrengthened beam with steel shear reinforcement (S1-CON), the predicted shear force capacity increased by 26.1% when the concrete cylinder compressive strength was increased from 25 to 45 MPa. The predicted shear force capacity increased by 18.3% for the strengthened beam with steel shear reinforcement (S1-12d260s) when the concrete cylinder compressive strength was increased from 25 to 35 MPa. Such increases in the shear force capacities may be attributable to the enhancement in the concrete shear force contribution due to the increase in concrete compressive strength.

It can be seen in Figure 6-1b that the higher the concrete cylinder compressive strength, the higher the predicted shear strength enhancement due to the DE FRP bars. Due to the good bond between the concrete and DE FRP bars, which is represented by the bond-slip model, bond failure does not occur. The weakest link becomes the concrete next to the FRP-to-concrete interface. Increasing the concrete compressive strength results in a corresponding increase in the concrete tensile strength and this, in return, improves the DE FRP contribution. The predicted shear contribution of the DE FRP bars increased from 96.4 kN to 162.6 kN for the beams without steel stirrups when the concrete cylinder compressive strength was increased from 25 to 65 MPa. For the beams with steel stirrups, the predicted shear force gain

due to the DE FRP bars increased from 11.2 kN to 26.8 kN when the concrete cylinder compressive strength was increased from 25 to 35 MPa. These findings are in accordance with the results presented in Chapter Five for PC girders strengthened in shear with EB CFRP sheets.

As demonstrated in Figure 6-1b, neither the TR55 design model (2012) nor the design model proposed by Mofidi et al. (2012) considers the influence of concrete compressive strength on shear strength enhancement provided by DE FRP bars.

6.2.2 Shear Span-to-Effective Depth Ratio (a/d)

The results of a recent investigation carried out by Sayed et al. (2013) on strengthened RC beams, in addition to the parametric studies conducted on strengthened PC girders which have been presented in Chapter Five, showed that the shear contribution of EB CFRP sheets is significantly influenced by the a/d ratio of the beam. On the other hand, the effect of a/d on the shear contribution of DE FRP bars has not been investigated.

The influence of a/d ratio on the behaviour of RC beams strengthened in shear with DE FRP bars was investigated in this study by developing FE models nominally identical to S0-CON, S0-12d130s, S1-CON and S1-12d260s. For each modelled beam, a/d ratios in the range from 2.6 to 4.1 were considered. FE models with a/d ratios higher than 4.1 failed in flexure and thus their predictions were discarded.

The effect of a/d ratio on the predicted shear force capacity of the beams is depicted in Figure 6-2a. It can be seen that the increase in a/d ratio resulted in a reduction in predicted shear force capacity. This observation is compatible with the findings of Kani et al. (1979) for RC beams, as well as the parametric studies presented in the previous chapter for PC beams strengthened in shear with EB CFRP sheets. When the a/d ratio was increased from 2.6 to 4.1, the predicted shear force capacity decreased by 17.9% and 25.2% for S0-CON and S1-CON respectively, whereas it reduced by 28.1% and 28.3% for S0-12d130s and S1-12d260s respectively. This reduction may be attributable to the shift from arch-action, which provides higher resistance, to beam-action. The relatively higher reduction in the predicted shear force capacity of the strengthened beams (i.e. S0-12d130s and S1-12d260s) may be explained by the influence of the a/d ratio on shear force contribution due to DE FRP bars, as presented in Figure 6-2b.

It should be noted that in order to eliminate the variation in concrete compressive strength between S1-CON and S1-12d260s beams, additional S1-CON beams having a concrete compressive strength value of 29.6 MPa were modelled. Thus, the results of each series of beams in Figure 6-2b were obtained by subtracting the unstrengthened shear force capacity from the strengthened shear force capacity of beams having the same concrete compressive strength value. The results of this show that the higher the a/d ratio, the lower the predicted shear contribution of DE FRP bars. The predicted shear force gain due to DE FRP bars decreased approximately linearly by 36.4% and 64.4%%, for S0-12d130s and S1-12d260s series respectively, as a result of increasing the a/d ratio from 2.6 to 4.1. This

outcome is compatible with the findings of Sayed et al. (2013) for RC beams and the parametric study carried out on PC girders without stirrups (see Section 5.2.4). This reduction may be attributed to the change in the shear resisting mechanism.

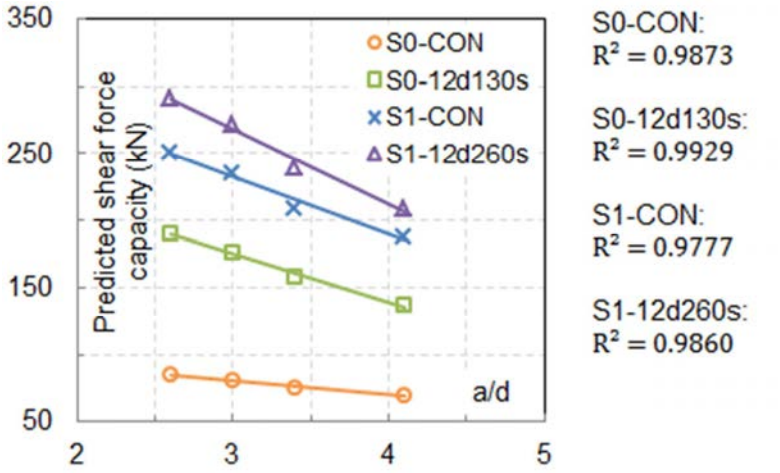

(a)

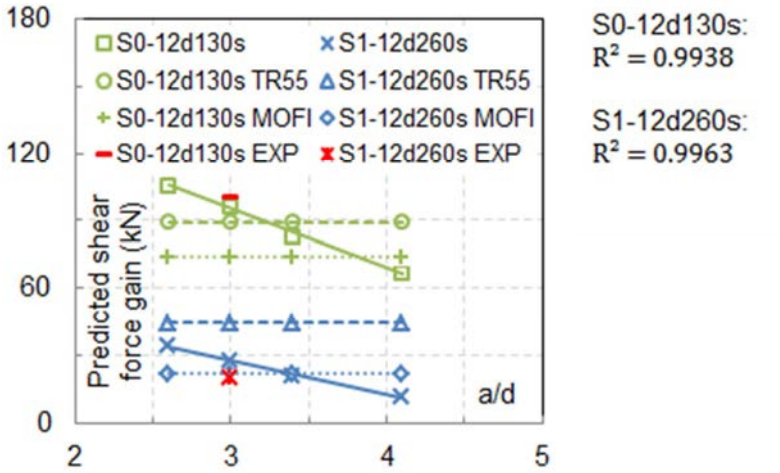

(b)

Figure 6-2: Effect of shear span-to-effective depth ratio on the predicted (a) shear force capacity and (b) shear force gain due to DE FRP bars

As shown in Figure 6-2b, both the TR55 design model (2012) and the design model suggested by Mofidi et al. (2012) do not take into account the effect of a/d ratio on the shear contribution of the DE FRP bars. This shortcoming needs urgent attention since a/d ratio is one of the key parameters governing the strengthened behaviour.

6.2.3 Effective Beam Depth (Size Effect)

The parametric studies presented in Chapter Five addressed the effect of the depth of PC girders strengthened in shear with EB CFRP sheets, and revealed that the effective beam depth can have a significant influence on the shear contribution of concrete as well as that of EB FRP sheets. The effect of beam depth has not been fully investigated for beams strengthened with DE FRP bars.

Due to the absence of such a study, the influence of effective beam depth on the strength of beams strengthened in shear with DE FRP bars was considered in the current parametric study. In addition to the FE models developed for S0-CON, S0-12d130s, S1-CON and S1-12d260s beams tested by Mofidi et al. (2012), which had an effective depth of 350 mm (i.e. $1.0\,d$), FE models with effective depths of 525 mm (i.e. $1.5\,d$) and 700 mm (i.e. $2\,d$) were developed for each series in order to investigate the effect of beam depth. Other parameters (e.g. a/d ratio, mesh density, longitudinal steel ratios, shear reinforcement ratio and DE FRP bars ratio) were kept unchanged. Unlike the effect of beam depth investigated on PC girders in Sections 5.2.5 and 5.3.3, the effect of beam width was considered for this series of beams in order to eliminate any effect that may arise from the slab (top flange) on the shear

behaviour. Therefore, the web and flange dimensions of the beams were changed proportionally with the change in beam depth.

The influence of beam depth on the predicted shear stress at failure is depicted in Figure 6-3a. It can be seen that the predicted shear stress decreases with increasing effective beam depth. The predicted shear stress at failure decreased respectively by 19.1%, 20.7%, 25.2% and 20.5% for S0-CON, S0-12d130s, S1-CON and S1-12d260s, when the effective depth of the beams was doubled. This result is consistent with the findings of previous parametric studies presented in Chapter Five and may be explained by the wider shear cracks in deeper sections.

Figure 6-3b presents the effect of effective beam depth on the shear strength enhancement percentage. Similar to the effect of a/d ratio, the variation in concrete compressive strength between S1-CON and S1-12d260s beams was eliminated by modelling additional S1-CON beams having a concrete compressive strength value of 29.6 MPa. The figure shows that the percentage of the predicted shear force gain decreased from 119.7% and 12.2% to 115.3% and 9.5% for series S0-12d130s and S1-12d260s, respectively, when the effective depth of the beams was doubled. This result is important because it suggests that beam depth does not significantly affect the shear strength enhancement offered by the DE FRP bars.

Figure 6-3c compares the FE-predicted shear strength enhancement results with the predictions of both the TR55 design model (2012) and the design model proposed by Mofidi et al. (2012). It can be seen that the predicted shear strength enhancement

increases with the increase in effective beam depth. This may be explained by the increase in effective bond length in large beams (Dirar et al., 2012).

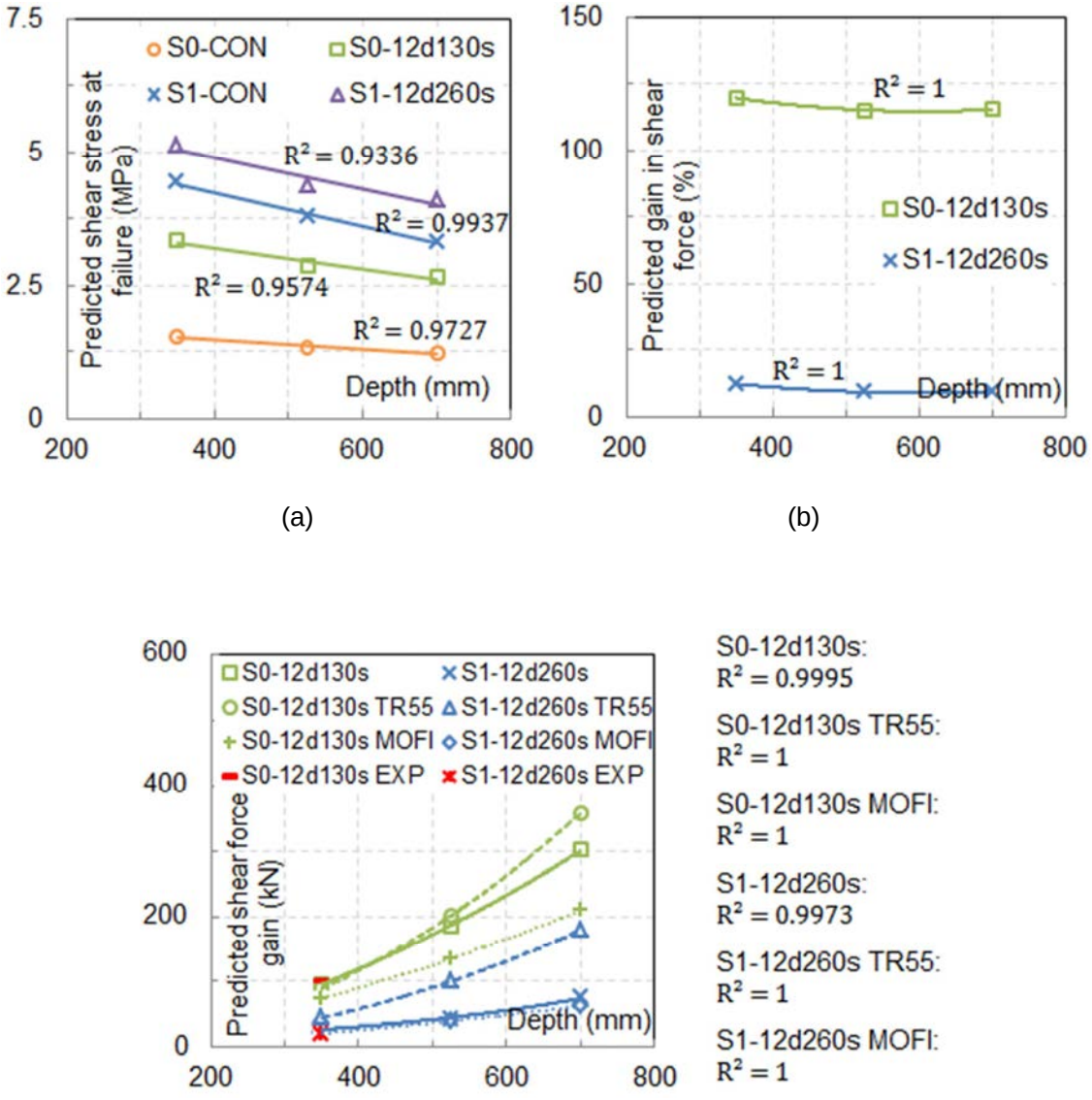

Figure 6-3: Effect of beam depth on the predicted (a) shear stress at failure, (b) shear force gain percentage due to DE FRP bars and (c) DE FRP bars shear force gain

It can also be noted from Figure 6-3c that the TR55 (2012) predictions were comparable to the FE-predicted results for strengthened beams without stirrups (i.e. S0-12d130s) only, whereas the predictions of the design model of Mofidi et al. (2012) were comparable to the FE-predicted results for strengthened beams with stirrups (i.e. S1-12d260s) only. According to the FE results, the gain in shear force increased from 96.4 kN to 302.2 kN and from 28 kN to 75.3 kN for series S0-12d130s and S1-12d260s, respectively, when the effective depth of beams was doubled. The corresponding increases predicted by the TR55 design model (2012) and the design model of Mofidi et al. (2012) were respectively from 89.8 kN to 357.7 kN and from 73.8 kN to 208.7 kN for S0-12d130s series, whereas the shear force gain predicted by both models increased respectively from 44.7 kN to 178.8 kN and from 22.1 kN to 62.6 kN for S1-12d260s series as a result of the increase in beam depth from 350 mm to 700 mm. The values predicted by the TR55 (2012), especially for S1-12d260s, seem unrealistically high. This may be attributable to the relatively high average bond stress value allowed by the TR55 (2012) which leads to overestimating the DE FRP bars contribution. Further testing is recommended to confirm the predicted results.

6.2.4 Interaction between Internal Steel and DE FRP Reinforcement

It was mentioned in Section 2.8.5, and demonstrated in Section 5.3.4, that the presence of steel stirrups is one of the substantial parameters influencing the shear contribution of EB FRP sheets (Khalifa and Nanni, 2002; Ary and Kang, 2012). The interaction between steel stirrups and DE FRP bars was examined by developing FE models nominally identical to S1-12d260s but with different steel stirrup-to-DE FRP bar ratios.

The FE results obtained are presented in Figure 6-4 in terms of predicted shear force gain due to DE FRP bars versus steel stirrup-to-DE FRP bar axial rigidity ratio (i.e. $E_s\rho_s/E_f\rho_f$). The FE results show that the predicted shear contribution of the DE FRP bars is inversely proportional to $E_s\rho_s/E_f\rho_f$. This observation is consistent with the findings of Ary and Kang (2012) for RC beams, as well as the FE-predicted results shown in Section 5.3.4 for PC girders strengthened in shear with EB FRP sheets, and might be explained by the fact that the increase in steel stirrup ratio increases the number of distributed cracks, and consequently, reduces the bond length.

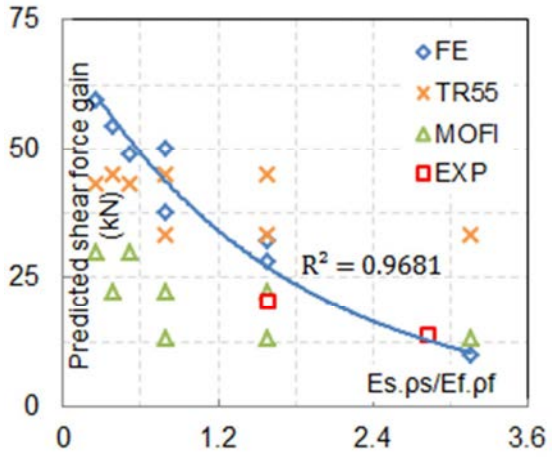

Figure 6-4: Interaction between steel stirrups and DE FRP bars

Figure 6-4 shows that both the TR55 design model (2012) and the design model of Mofidi et al. (2012) do not consider the interaction between steel stirrups and DE FRP bars. Consequently, both design models might overestimate shear strength enhancement for beams with high steel stirrup ratios. It should be noted that the variation in predicted shear force gain using these design models was due to changing the FRP bar diameter (and consequently ρ_f), which had been done to

achieve the desired $E_s\rho_s/E_f\rho_f$ range, rather than the change in steel stirrup ratio. Further tests are required to confirm this result.

6.2.5 Effect of DE FRP Bar Orientation

The effect of DE FRP bar orientation was investigated by modelling beams nominally identical to S0-12d130s and S1-12d260s. For each modelled beam, the DE FRP bars were inclined at either 45° or 90° to the longitudinal beam axis.

The FE-predicted results are given in Table 6-1. From this table it can be seen that the predicted shear force gain due to the DE FRP bars increased by 22.9% and 41.4% for beams without (S0-12d130s) and with (S1-12d260s) internal steel stirrups, respectively when the DE FRP bar inclination angle was changed from 90° to 45°. This result is in broad agreement with the findings of Barros and Dalfré (2013) who reported that DE steel bars inclined at 45° were more effective than vertical ones. The higher strength enhancement offered by inclined DE bars may be attributable to two reasons. First, inclined DE bars are less susceptible to debonding issues due to the higher anchorage length. Second, for the same values of A_f, b_w and s_b; the shear reinforcement ratio of inclined DE bars ($A_f/b_w s_b \sin\alpha$), where α is the DE bar inclination angle, is higher than that of vertical bars ($A_f/b_w s_b$). Thus, inclined DE bars offer higher resistance to crack opening than vertical DE bars.

According to the design model suggested by Mofidi et al. (2012), the increase in FRP shear force contribution due to the change in the bars orientation was 41.4% for all beams. Moreover, Table 6-1 shows that the TR55 design model (2012) does not

consider the influence of DE FRP bar orientation on shear strength enhancement. However, the TR55 design model (2012) recommends using FRP bars perpendicular to the longitudinal axis of beams which is more practical in shear strengthening. Therefore, it was not possible to compare between the FE results for beams with inclined DE FRP bars and the corresponding TR55 predictions.

Table 6-1: Effect of DE FRP bar orientation on shear force gain

Beam	FE (kN)		Increase (%)	TR55 (kN)		Increase (%)	MOFI (kN)		Increase (%)
	90°	45°		90°	45°		90°	45°	
S0-12d130s	96.4	118.5	22.9	89.4	89.4	0	73.8	104.3	41.4
S1-12d260s	28.0	39.6	41.4	44.7	44.7	0	22.1	31.3	41.4

6.3 Proposed Design Model for DE FRP bars

From reviewing the published literature it can be seen that several analytical models and design guidelines have been proposed for determining the shear force contribution of EB FRP sheets (Belarbi et al., 2011; Belarbi and Acun, 2013). On the other hand, only the two design models, presented in Section 2.10.2, are available for determining the shear force gain due to DE FRP bars. This can be partly attributed to the limited research carried out on this relatively new method of shear strengthening.

The comparisons presented in Section 6.2 reveal that the current design models, i.e. the TR55 design model (2012) and the design model developed by Mofidi et al. (2012), failed to account for the influence of concrete compressive strength, a/d ratio

and existence of internal steel stirrups on shear strength enhancement. Hence, the prediction accuracy of these design guidelines is questionable. Therefore, development of a more accurate and practical design model for determining shear force gain due to DE FRP bars is addressed and presented in the following subsections. The developed design model is mainly based on the findings of the parametric study reported in Section 6.2 in order to take into account the effect of major influencing parameters.

6.3.1 Development of Design Model

In the TR55 design code (2012), as well as the design model developed by Mofidi et al. (2012), the DE FRP bars contribution to shear resistance (V_{f}) is based on a 45° truss analogy. Hence, V_{f} is given by:

$$V_{\mathrm{f}} = \varepsilon_{\mathrm{fe}} E_{\mathrm{fd}} A_{\mathrm{f}} \frac{h}{s_{\mathrm{b}}} \tag{6-1}$$

The equation given above represents the shear force ($\varepsilon_{\mathrm{fe}} E_{\mathrm{fd}} A_{\mathrm{f}}$) resisted by one DE FRP bar multiplied by the number of DE FRP bars intersecting a 45° diagonal shear crack, as shown in Figure 6-5. However, it can be seen that Equation 6-1 assumes that all bars within the length h (i.e. strengthened depth) are fully effective. This is incorrect because some bars will have a short anchorage length. Based on the simplified pull-out test of an FRP bar embedded in a concrete block as shown in Figure 6-6, a certain anchorage length is required for a bar to be fully effective. Hence, an anchorage length (i.e. $l_{\mathrm{b,max}}$) should be subtracted from each end of the

length of strengthened depth to ensure that the bars located within the remaining length ($h - 2l_{\mathrm{b,max}}$) are effective. From Figure 6-6, $l_{\mathrm{b,max}}$ can be determined by equalling the externally applied pull-out force (F_{ult}) at the FRP bar free end at failure with the internal force generated by the interfacial shear stress along the required anchorage length as follows:

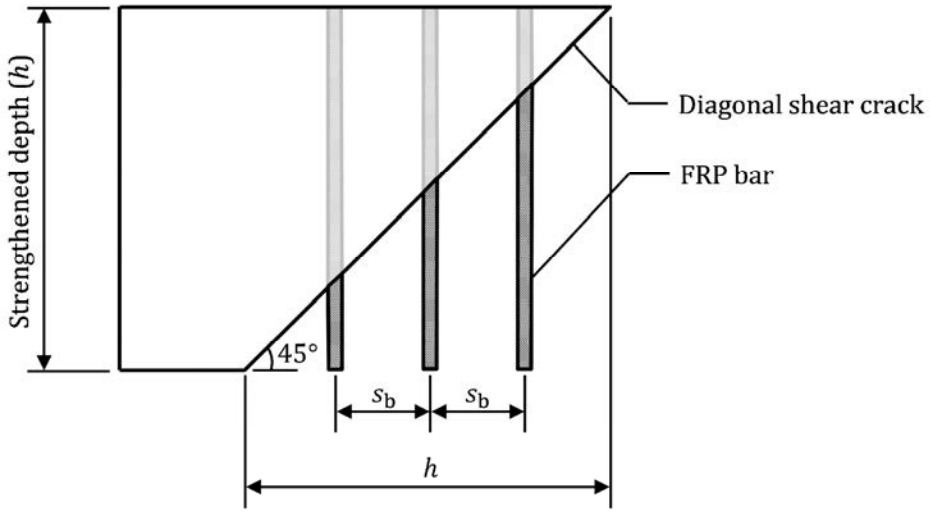

Figure 6-5: DE FRP bars intersecting a 45° diagonal shear crack

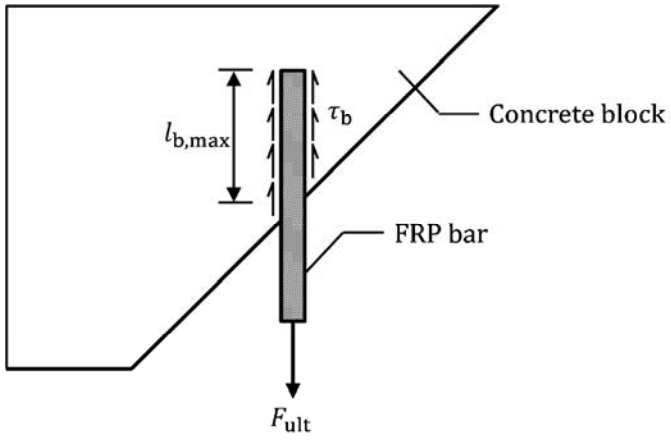

Figure 6-6: Simplified pull-out test

$$F_{\mathrm{ult}} = \varepsilon_{\mathrm{fe}} E_{\mathrm{fd}} A_{\mathrm{f}} = \pi d_{\mathrm{b}} \tau_{\mathrm{b}} l_{\mathrm{b,max}} \tag{6-2}$$

then $l_{\mathrm{b,max}}$ can be calculated after rearranging the equation above, as follows:

$$l_{\mathrm{b,max}} = \frac{\varepsilon_{\mathrm{fe}} E_{\mathrm{fd}} A_{\mathrm{f}}}{\pi d_{\mathrm{b}} \tau_{\mathrm{b}}} \tag{6-3}$$

It can be seen that the equation obtained is the same as Equation 2-16 when the partial safety factor for the adhesive material (γ_{A}) is taken as equal to 1.

After subtracting two times $l_{\mathrm{b,max}}$ from h in Equation 6-1, it leads to:

$$V_{\mathrm{f}} = \frac{\varepsilon_{\mathrm{fe}} E_{\mathrm{fd}} A_{\mathrm{f}}}{s_{\mathrm{b}}} \left(h - 2 \frac{\varepsilon_{\mathrm{fe}} E_{\mathrm{fd}} A_{\mathrm{f}}}{\pi d_{\mathrm{b}} \tau_{\mathrm{b}}} \right) \tag{6-4}$$

The term given between two parentheses in Equation 6-4 represents W_{eff} (see Equation 2-15), when γ_{A} is taken as 1. Hence, Equation 6-4 can be rearranged and given by the following formula:

$$\frac{V_{\mathrm{f}}}{E_{\mathrm{fd}} A_{\mathrm{f}}} = \frac{\varepsilon_{\mathrm{fe}} W_{\mathrm{eff}}}{s_{\mathrm{b}}} \tag{6-5}$$

Equation 6-5 can be written as follows:

$$V_{\mathrm{f}} = \varepsilon_{\mathrm{fe}}^{*} E_{\mathrm{fd}} A_{\mathrm{f}} \tag{6-6}$$

where ε_{fe}^{*} is a parameter equal to the effective strain in DE FRP bars multiplied by the number of effective bars intersecting a 45° diagonal shear crack.

Equation 6-6 is adopted by TR55 (2012) for determining V_f. It should be mentioned that the lack of adequate formulae for computing ε_{fe}^{*}, which might be attributed to limited experimental tests, limits the accuracy of TR55 (2012). Hence, an expression for ε_{fe}^{*} was derived using the results presented in Section 6-2. The nonlinear regression capability of IBM SPSS statistics software (version 22) was used to obtain the new expression for ε_{fe}^{*} which takes into account the effect of concrete compressive strength, shear span-to-effective depth ratio, effective beam depth and interaction between DE FRP bars and steel stirrups. The nonlinear regression analysis of the new expression for ε_{fe}^{*} is given in Appendix A. The new expression, which has an R-squared value of 0.984, is given by:

$$\varepsilon_{fe}^{*} = 4.2 \times 10^{-7} \sqrt{\frac{f_c' E_{fd}}{s_b}} \frac{(d)^{1.5}\, e^{-336\rho_s}}{(a/d)(A_f)^{0.7}} \tag{6-7}$$

where ρ_s can be determined from the total area of steel stirrup legs (A_v), stirrups spacing (s) and web width (b_w), as follows:

$$\rho_s = \frac{A_v}{b_w s} \tag{6-8}$$

In many RC structures, it is more practical to drill vertical holes and use vertical DE FRP bars. Hence, similar to the TR55 (2012) philosophy, the proposed model should be used for vertically embedded bars. It must also be noted that the proposed model is valid for CFRP and AFRP bars only, as the FE model was validated solely for these FRP bar types.

6.3.2 Validation of the Proposed Design Model

As mentioned in Section 6.3.1, the development of the proposed equation was based on the FE results presented in Section 6.2. It is therefore important that the developed design model be validated against various experimental results to quantify its accuracy. A comparison between the experimentally measured $V_{\mathrm{f,exp}}$ and the predicted results using the developed equation, the TR55 design model (2012) and the design model developed by Mofidi et al. (2012) is presented in this section.

The results obtained are presented in Table 6-2 as well as in Figure 6-7 as scatter plots between the experimental and predicted shear force gain due to DE FRP bars. It should be mentioned that only RC beams which failed experimentally in shear were considered in this comparison. Hence, published results of experimentally tested beams which failed in flexure or due to premature failure mode were discarded.

Table 6-2: A comparison between experimentally measured and predicted shear force contributions due to DE FRP bars

Beam	Properties of the tested beam							Shear contribution of DE FRP bars						
	d mm	a/d ratio	f_c' MPa	ρ_s	A_f mm^2	s_b mm	E_{fd} MPa	Exp. ($V_{f,exp}$) kN	Eq. 6-6 ($V_{f,Eq6\cdot6}$) kN	TR55 ($V_{f,TR55}$) kN	MOFI ($V_{f,Mofi}$) kN	$\frac{V_{f,Eq6\cdot6}}{V_{f,exp}}$ [x]	$\frac{V_{f,TR55}}{V_{f,exp}}$ [+]	$\frac{V_{f,Mofi}}{V_{f,exp}}$ [*]
S0-12d130s [1]	350	3	25	0	127	130	148000	99.50	97.90	89.42	73.77	0.98	0.90	0.74
S1-9d260s [1]	350	3	29.6	0.0038	71	260	148000	14.00	17.88	35.26	14.31	1.27	2.52	1.02
S1-12d260s [1]	350	3	29.6	0.0038	127	260	148000	20.30	21.29	44.70	22.13	1.04	2.20	1.09
R00 [2]	295	3.05	17.4	0.0029	78	275	124000	11.80	10.59	27.53	18.62	0.90	2.33	1.58
Specimen 8 [3]	189	3.17	47.2	0	78.5	200	60000	8.40	9.10	13.19	11.48	1.08	1.57	1.37
Specimen 9 [3]	189	3.17	47.2	0	44.2	200	60000	8.40	7.66	8.48	7.47	0.91	1.01	0.89
Specimen 10 [3]	189	3.17	47.2	0	78.5	300	60000	6.40	7.43	8.79	7.66	1.16	1.37	1.20
SSB R3d-C6@0.7d [4]	150	3	48	0	28	105	124000	22.90	20.63	12.13	11.65	0.90	0.53	0.51
SSB R3d-C6@0.5d [4]	150	3	48	0	28	75	124000	27.00	24.41	16.98	16.31	0.91	0.63	0.60
2S-C180-90 [5]	360	2.5	29.7	0.001	50.2	180	160000	77.10	68.60	41.26	29.28	0.89	0.53	0.38

[1] Tested by Mofidi et al. (2012); [2] Tested by Qin et al. (2014); [3] Tested by Valerio and Ibell (2003); [4] Tested by Valerio et al. (2009); [5] Tested by Breveglieri et al. (2015)

[x] Mean $V_{f,Eq6\cdot6}/V_{f,exp}$ value is 1.004 with standard deviation of 0.125

[+] Mean $V_{f,TR55}/V_{f,exp}$ value is 1.359 with standard deviation of 0.727

[*] Mean $V_{f,Mofi}/V_{f,exp}$ value is 0.938 with standard deviation of 0.367

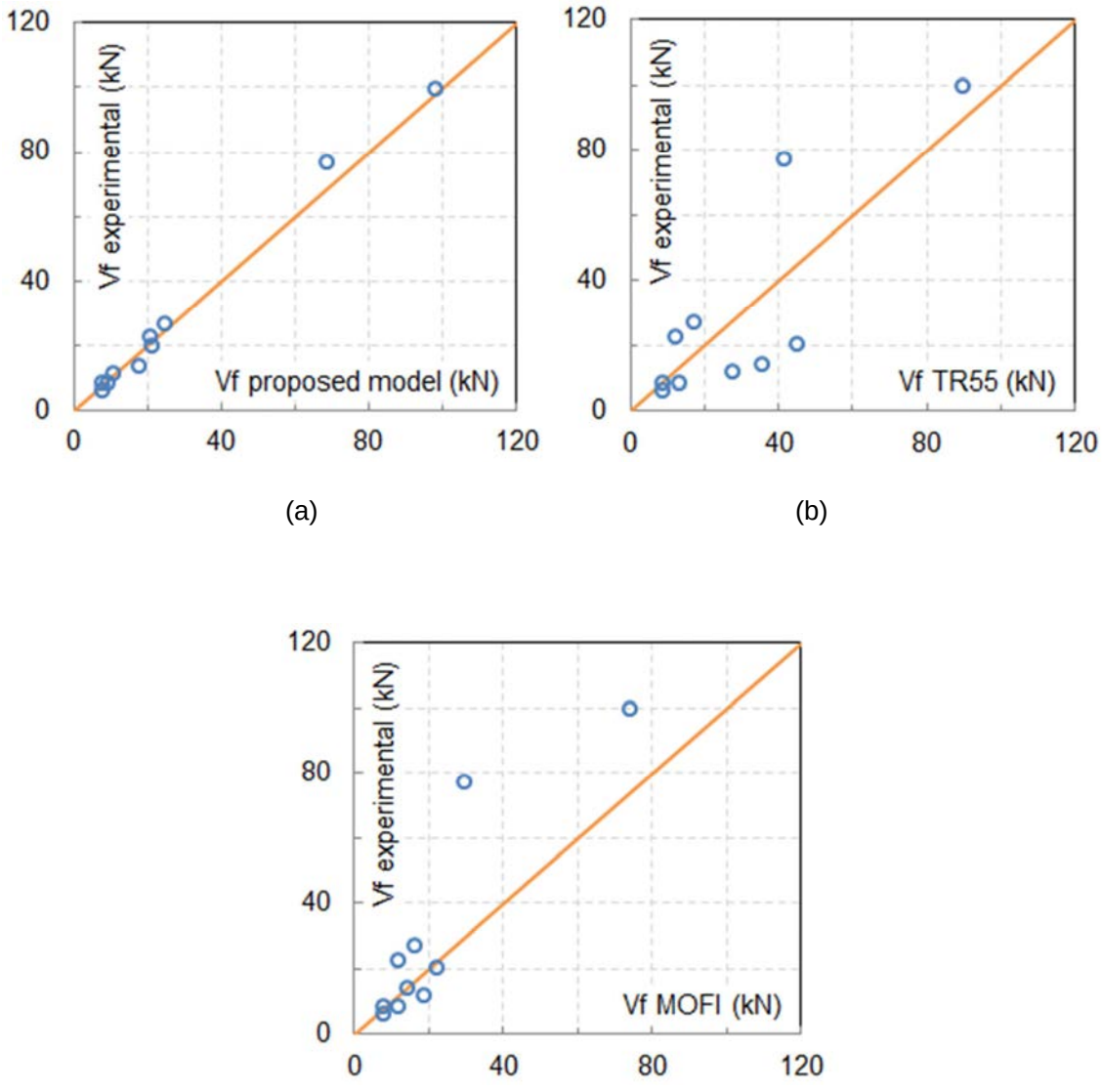

Figure 6-7: Scatter plots for experimental versus predicted shear force contributions of DE FRP bars using (a) proposed model, (b) TR55 design model (2012) and (c) design model of Mofidi et al. (2012)

The results presented above clearly demonstrate the accuracy of the developed equation. From Table 6-2, it can be seen that the predicted shear force gain due to DE FRP bars using Equation 6-6 was much more accurate compared to the

corresponding predictions obtained from the TR55 design model (2012) and the design model of Mofidi et al. (2012). This can be attributed to the fact that Equation 6-6 takes into account the influence of various parameters which had been investigated in Section 6-2. The developed equation has a mean predicted-to-experimental ratio of 1.004 and a standard deviation of 0.125, whereas the mean TR55 predicted-to-experimental ratio is 1.359 with a standard deviation value of 0.727 and the mean predicted-to-experimental ratio for Mofidi's model is 0.938 with a standard deviation of 0.367.

Notwithstanding the accuracy of the proposed model, it is acknowledged that the results used for comparison were very limited. Hence, further experimental results are required to confirm the applicability of the developed equation.

6.4 Concluding Remarks

The developed FE model for RC beams strengthened in shear with DE FRP bars has been used to conduct a wide-ranging parametric study to investigate the influence of concrete compressive strength, a/d ratio, effective beam depth, internal steel-to-DE FRP reinforcement interaction and DE FRP bar orientation on the predicted behaviour of RC beams strengthened in shear using DE FRP bars. The FE-predicted shear force gain due to DE FRP bars has been compared with the predictions of the TR55 design model (2012) and the design model of Mofidi et al. (2012). The results obtained showed that:

1- The predicted shear strength enhancement was positively influenced by the increase in concrete compressive strength. The increase in predicted shear strength and shear force gain due to DE FRP bars was relatively linear with the increase cylinder compressive strength of concrete. Furthermore, the increase in concrete compressive strength resulted in a change in the failure mode of some FE models, from shear to flexure failure.

2- The effect of a/d ratio was significant. The increase in a/d ratio from 2.6 to 4.1 resulted in a reduction in predicted shear contribution of DE FRP bars by 36.4% and 64.4% respectively for beams without and with steel reinforcement stirrups, whereas it reduced predicted shear force capacity by 17.9-25.2% and 28.1-28.3% respectively for unstrengthened and strengthened beams. The relatively high reduction for strengthened beams can be attributed to the negative influence of a/d ratio on predicted shear force contribution due to DE FRP bars.

3- The predicted shear stress at failure decreased when the beam size was doubled. This reduction was in the range of 19.1-25.2%. However, beam size did not have a significant influence on predicted shear force gain percentage. This implies that the size effect was very limited for this type of shear strengthening. The results obtained showed that shear force contribution due to DE FRP bars was increased proportionally with the increase in beam depth, which may be attributed to the increase in bond length provided by larger beams.

4- The predicted shear contribution due to DE FRP bars was significantly influenced by the quantity $E_s\rho_s/E_f\rho_f$. The obtained results showed that the higher the $E_s\rho_s/E_f\rho_f$, the lower the predicted shear contribution of DE FRP bars. This might be attributed to the increase in distributed crack number as a result of the increase in steel stirrups ratio, which in turn reduces the available anchorage length.

5- The use of 45° inclined DE FRP bars, compared with vertical DE FRP bars, enhanced predicted shear force capacity for beams with and without steel stirrups. It increased predicted shear force gain due to DE FRP bars by 22.9% and 41.4% for beams without and with steel stirrups respectively.

6- Compared to the FE results, neither the TR55 design model (2012) nor the design model of Mofidi et al. (2012) consider the effect of concrete compressive strength, a/d ratio and existence of internal steel stirrups on shear force gain due to DE FRP bars. However, in some cases, the predictions of design models showed a comparable trend for the influence of beam depth to that of the FE model. For the effect of DE FRP bar orientation, only the design model of Mofidi et al. (2012) predicted an increase in FRP shear force gain when the DE FRP bar inclination angle was changed from 90° to 45°; this increase was 41.4% for all beams.

7- Finally, it is noteworthy that the presented FE predictions reflect the performance of the developed model. Further experimental tests are therefore needed to confirm the FE predictions.

This chapter also has addressed the development of a new design model for determining the shear force contribution due to DE FRP bars. A new expression for ε_{fe}^{*} was derived using the nonlinear regression capability in the statistics package IBM SPSS (version 22). The obtained formula has an R-squared value of 0.984 and takes into consideration the effect of concrete compressive strength, shear span-to-effective depth ratio, effective beam depth and internal steel-to-DE FRP reinforcement interaction. The developed design model is valid only for vertical DE CFRP and AFRP bars.

The developed design model was then used to predict the experimental shear force gain due to DE FRP bars for 10 strengthened RC beams from the published literature. The results showed that the predictions of the proposed equation were more accurate when compared to those of TR55 (2012) and the design model of Mofidi et al. (2012). The mean predicted/experimental shear force gain ratios were 1.004, 1.359 and 0.938 respectively for the proposed equation, the TR55 design model (2012) and the design model of Mofidi et al. (2012), with standard deviation values of 0.125, 0.727 and 0.367 respectively.

Due to limited research work published on the DE shear strengthening method, the results used for comparison were very limited. Therefore, further experimental results are highly recommended to further quantify the applicability of the developed equation.

CHAPTER 7: CONCLUSIONS AND RECOMMENDATIONS

7.1 Introduction

In this research, nonlinear finite element modelling has been used to study the shear behaviour of PC and RC beams strengthened in shear with EB CFRP sheets or DE CFRP bars respectively. The objectives of this research are:

1- To develop and validate FE models capable of simulating the overall behaviour of shear-strengthened PC and RC beams with EB CFRP sheets or DE FRP bars respectively;

2- To use the developed FE models to investigate the effect of the main parameters influencing the shear behaviour of beams in terms of shear force capacity and shear strength enhancement;

3- To quantify the accuracy of current design models for shear strengthening with EB FRP sheets and DE FRP bars; and

4- To develop a new design equation for shear strengthening of RC beams with DE FRP bars.

Two FE models were developed and validated. In both FE models, which were implemented in DIANA FE package Version 9.4.4 (DIANA user's manual, 2012),

representative constitutive models, appropriate elements types and robust analysis procedures were adopted in order to accurately simulate the overall behaviour of experimentally tested beams. The accuracy of the developed FE models was established through comparing published experimental results with the corresponding FE-predicted results. The comparisons included failure loads, shear force-deflection curves, strain variation in steel stirrups, strain variation in FRP composites, stress variation in the prestressed tendons and crack patterns at failure (i.e. mode of failure). The developed FE models were then used to investigate the effect of various influencing parameters on the shear behaviour of FE models nominally identical to the experimentally tested beams. This chapter presents a summary of the findings obtained throughout this study in addition to some recommendations for future research.

7.2 Conclusions

The results of this research came to the following conclusions:

1- FE modelling of the behaviour of FRP shear-strengthened PC and RC beams has received much less attention than physical testing. Furthermore, controversial findings have been reported for shear contribution due to FRP composites.

2- Current design guidelines for determining shear contribution due to FRP composites, especially for shear strengthening with DE FRP bars, are still far from being classified as fully developed.

3- The FEM can accurately simulate the overall behaviour of FRP shear-strengthened PC and RC beams if representative constitutive models, appropriate elements types and robust analysis procedures are used.

4- For PC girders strengthened in shear with EB CFRP laminates, the effect of concrete compressive strength, CFRP width-to-spacing ratio, CFRP thickness, shear span-to-effective depth ratio, effective beam depth, level of prestress, tendon profile, precracking, CFRP-to-concrete interface model and internal steel-to-EB CFRP shear reinforcement interaction on shear behaviour was investigated. For I-shaped PC girders without internal steel stirrups, the predicted shear force capacity was only reduced by increasing the shear span-to-effective depth ratio and pre-cracking loads more than 85% of the unstrengthened shear force capacity. A significant size effect was predicted for both the unstrengthened and CFRP-strengthened girders. The predicted shear strength enhancement was increased by the increase in concrete compressive strength, CFRP width-to-spacing ratio and CFRP thickness, but decreased by increasing shear span-to-effective depth ratio and changing tendon profile from straight to double-harped shape. The rate of increase in percentage of shear force gain and CFRP shear contribution tended to decrease for beams having an effective depth of 457 mm or more. The CFRP-to-concrete bond-slip model shape and level of prestress in tendons had no significant influence on shear strength enhancement. For rectangular PC beams with internal steel stirrups, the shear force capacity was increased by increasing concrete cylinder compressive strength, whilst it was decreased by increasing shear span-to-effective depth ratio. The predicted shear stresses at

failure suggest that the CFRP sheets were able to cut down the size effect. Predicted shear strength enhancement was positively influenced by the increase in concrete compressive strength, shear span-to-effective depth ratio and effective beam depth, but adversely affected by the increase in internal steel-to-EB CFRP axial rigidity ratio. The shear strength enhancement predictions of ACI 440.2R (2008) and TR55 (2012) were inconsistent with the corresponding FE predictions for the effect of concrete compressive strength, shear span-to-effective depth ratio, effective beam depth and tendon profile of PC I-girders without internal stirrups. However, for rectangular PC beams with internal steel stirrups, ACI 440.2R (2008) and TR55 (2012) failed to simulate the influence of shear span-to-effective depth ratio and internal steel-to-EB CFRP shear reinforcement ratio.

5- The effect of concrete compressive strength, shear span-to-effective depth ratio, effective beam depth, steel stirrup-to-DE FRP bar ratio and DE FRP bar orientation on the behaviour of RC beams shear-strengthened with DE FRP bars was numerically studied. The predicted shear force capacity was positively influenced by the increase in concrete compressive strength and the use of 45° inclined (compared with vertical) DE FRP bars, but negatively influenced by the increase in shear span-to-effective depth ratio. The predicted shear stress at failure was decreased by increasing effective beam depth. The predicted shear strength enhancement was increased by the increase in concrete compressive strength and effective beam depth, but decreased by increasing shear span-to-effective depth ratio and steel stirrup-to-DE FRP bar ratio. The increase in effective beam depth did not have a

substantial influence on the percentage shear strength enhancement offered by the DE FRP bars. Comparisons between the FE predictions and the predictions obtained by TR55 (2012) and the design model of Mofidi et al. (2012) showed that the aforementioned analytical design models failed to represent the effect of concrete compressive strength, shear span-to-effective depth ratio and steel stirrup-to-DE FRP bar ratio on the shear strength enhancement. Both design models predicted that the increase in effective depth would result in a corresponding increase in shear strength enhancement; however, the predictions of TR55 (2012) were generally much higher than the corresponding FE results. Furthermore, TR55 (2012) did not consider the influence of DE FRP bar orientation, whereas the design model of Mofidi et al. (2012) predicted a constant percentage increase in shear strength enhancement due to the change in bar orientation.

6- Based on the FE parametric study for RC beams shear-strengthened with DE FRP bars, an analytical design model for determining the shear contribution due to DE FRP bars was developed using nonlinear regression analysis. The new design model takes into consideration the effect of concrete compressive strength, shear span-to-effective depth ratio, effective beam depth and the existence of internal steel stirrups. The developed model had a mean predicted-to-experimental shear strength enhancement ratio of 1.004 with a standard deviation of 0.125, whereas the mean predicted-to-experimental shear strength enhancement ratios for the TR55 (2012) and the design model of Mofidi et al. (2012) were 1.359 and 0.938, respectively, with standard deviations of 0.727 and 0.367, respectively.

7.3 Recommendations for Future Work

This research work has presented significant data on concrete beams strengthened in shear using FRP composites, and covered several knowledge gaps in this area. However, the following topics are highly recommended for future research in order to better understand shear behaviour of FRP-strengthened beams:

1- For both PC and RC beams, the presented results suggest that shear strength enhancement can be influenced by parameters not covered by existing design guidelines (e.g. ACI 440.2R, 2008; TR55 design model, 2012; the design model of Mofidi et al., 2012). Therefore, further experimental testing is highly recommended to confirm the FE-predicted results, increase the database of beams strengthened in shear with FRP reinforcement and further evaluate, and where needed improve, the accuracy of existing design models.

2- The main problem with shear strengthening of I-shaped concrete beams with EB FRP sheets is debonding failure at internal corners. Numerous attempts have been made to resolve this issue by using anchors at these corners, but this solution requires high quality workmanship and may encourage other premature modes of failure such as failure in the anchorage system itself (You et al., 2011). The DE technique has the potential to overcome this shortcoming. Therefore, investigating shear strengthening of I-girders with DE FRP bars, both experimentally and numerically, is of great importance.

3- All beams considered in this study had shear span-to-effective depth ratios of approximately 2.5 or more. Studies on the shear behaviour of FRP-

strengthened concrete beams with shear span-to-effective depth ratios of less than 2.5 (i.e. deep beams) are limited. It is well known, as explained in Chapter Two, that shear behaviour of beams is significantly dependent on this parameter. Thus, investigating the behaviour of FRP-shear strengthened deep beams is highly recommended to evaluate the effectiveness of FRP shear strengthening of such beams and expand the available database and knowledge.

4- Although the effect of FRP-to-concrete bond-slip model was not significant in the case of DE shear-strengthened RC beams considered in this study, the development of a practical bond-slip model is still required for more accurate FE models.

APPENDIX A: NONLINEAR REGRESSION ANALYSIS

```
* NonLinear Regression.

MODEL PROGRAM  A=1 B=1 C=1 D=1 E=1 F=1 G=1 H=1.

COMPUTE  PRED_=A * (SQRT(fc * Ef)) * (Deff ** 1.5) * (1 / (A_D)) * ((EXP( - 0.6 * S_F)) **
B) * (1 /( Afrp ** 0.7)) * (1/ (Sf ** 0.5)).

NLR VFEA

  /OUTFILE='C:\Users\Michael\AppData\Local\Temp\spss1700\SPSSFNLR.TMP'

  /PRED PRED_

  /CRITERIA SSCONVERGENCE 1E-8 PCON 1E-8.
```

Input

	VFEA	fc	A_D	S_F	Deff	Sf	Ef	Afrp
1	.005129	25.00	3.00	.00000	350.00	130.00	148000.00	127.00
2	.006487	35.00	3.00	.00000	350.00	130.00	148000.00	127.00
3	.006939	45.00	3.00	.00000	350.00	130.00	148000.00	127.00
4	.007598	55.00	3.00	.00000	350.00	130.00	148000.00	127.00
5	.008649	65.00	3.00	.00000	350.00	130.00	148000.00	127.00
6	.000598	25.00	3.00	.00376	350.00	260.00	148000.00	127.00
7	.001426	35.00	3.00	.00376	350.00	260.00	148000.00	127.00
8	.005613	25.00	2.60	.00000	350.00	130.00	148000.00	127.00
9	.004412	25.00	3.40	.00000	350.00	130.00	148000.00	127.00

	VFEA	fc	A_D	S_F	Deff	Sf	Ef	Afrp
10	.003569	25.00	4.10	.00000	350.00	130.00	148000.00	127.00
11	.001825	29.60	2.60	.00376	350.00	260.00	148000.00	127.00
12	.001133	29.60	3.40	.00376	350.00	260.00	148000.00	127.00
13	.000650	29.60	4.10	.00376	350.00	260.00	148000.00	127.00
14	.005297	29.60	3.00	.00094	350.00	260.00	148000.00	63.50
15	.003404	29.60	3.00	.00188	350.00	260.00	148000.00	63.50
16	.001031	29.60	3.00	.00376	350.00	260.00	148000.00	63.50
17	.002899	29.60	3.00	.00094	350.00	260.00	148000.00	127.00
18	.001995	29.60	3.00	.00188	350.00	260.00	148000.00	127.00
19	.001490	29.60	3.00	.00376	350.00	260.00	148000.00	127.00
20	.002112	29.60	3.00	.00094	350.00	260.00	148000.00	190.50
21	.001727	29.60	3.00	.00188	350.00	260.00	148000.00	190.50
22	.004348	25.00	3.00	.00000	525.00	195.00	148000.00	285.75
23	.004019	25.00	3.00	.00000	700.00	260.00	148000.00	508.00
24	.001039	29.60	3.00	.00376	525.00	390.00	148000.00	285.75
25	.001001	29.60	3.00	.00376	700.00	520.00	148000.00	508.00

Nonlinear Regression Analysis

Notes

Output Created		25-AUG-2015 17:42:26
Comments		
Input	Data	C:\Users\Michael\Desktop\EQ\FIN.sav
	Active Dataset	DataSet1
	Filter	<none>
	Weight	<none>
	Split File	<none>
	N of Rows in Working Data File	25
Missing Value Handling	Definition of Missing	User-defined missing values are treated as missing.
	Cases Used	Statistics are based on cases with no missing values for any variable used. Predicted values are calculated for cases with missing values on the dependent variable.
Syntax		MODEL PROGRAM A=1 B=1 C=1 D=1 E=1 F=1 G=1 H=1. COMPUTE PRED_=A * (SQRT(fc * Ef)) * (Deff ** 1.5) * (1 / (A_D)) * ((EXP(- 0.6 * S_F)) ** B) * (1 /(Afrp ** 0.7)) * (1/ (Sf ** 0.5)). NLR VFEA /PRED PRED_ /CRITERIA SSCONVERGENCE 1E-8 PCON 1E-8.
Resources	Processor Time	00:00:00.02
	Elapsed Time	00:00:00.01
Files Saved	Parameter Estimates File	C:\Users\Michael\AppData\Local\Temp\spss1700\SPSSFNLR.TMP

Iteration History[b]

Iteration Number[a]	Residual Sum of Squares	Parameter							
		A	B	C	D	E	F	G	H
1.0	3625580497.025	1.000	1.000	1.000	1.000	1.000	1.000	1.000	1.000
1.1	.000	4.113E-7	1.000	1.000	1.000	1.000	1.000	1.000	1.000
2.0	.000	4.113E-7	1.000	1.000	1.000	1.000	1.000	1.000	1.000
2.1	.000	4.127E-7	332.529	1.000	1.000	1.000	1.000	1.000	1.000
3.0	.000	4.127E-7	332.529	1.000	1.000	1.000	1.000	1.000	1.000
3.1	.000	4.191E-7	521.448	1.000	1.000	1.000	1.000	1.000	1.000
4.0	.000	4.191E-7	521.448	1.000	1.000	1.000	1.000	1.000	1.000
4.1	.000	4.198E-7	559.338	1.000	1.000	1.000	1.000	1.000	1.000
5.0	.000	4.198E-7	559.338	1.000	1.000	1.000	1.000	1.000	1.000
5.1	.000	4.197E-7	559.857	1.000	1.000	1.000	1.000	1.000	1.000
6.0	.000	4.197E-7	559.857	1.000	1.000	1.000	1.000	1.000	1.000
6.1	.000	4.197E-7	559.846	1.000	1.000	1.000	1.000	1.000	1.000

Derivatives are calculated numerically.[b]

a. Major iteration number is displayed to the left of the decimal, and minor iteration number is to the right of the decimal.

b. Run stopped after 12 model evaluations and 6 derivative evaluations because the relative reduction between successive residual sums of squares is at most SSCON = 1.00E-008.

Parameter Estimates

Parameter	Estimate	Std. Error	95% Confidence Interval	
			Lower Bound	Upper Bound
A	4.197E-7	.000	4.033E-7	4.362E-7
B	559.846	38.290	479.062	640.630
C	1.000	.000	1.000	1.000
D	1.000	.000	1.000	1.000
E	1.000	.000	1.000	1.000
F	1.000	.000	1.000	1.000
G	1.000	.000	1.000	1.000
H	1.000	.000	1.000	1.000

Correlations of Parameter Estimates

	A	B	C	D	E	F	G	H
A	1.000	.343	.	.	.	.	.	.
B	.343	1.000	.	.	.	.	.	.
C	.	.	.	.	.	.	.	.
D	.	.	.	.	.	.	.	.
E	.	.	.	.	.	.	.	.
F	.	.	.	.	.	.	.	.
G	.	.	.	.	.	.	.	.
H	.	.	.	.	.	.	.	.

ANOVA[a]

Source	Sum of Squares	df	Mean Squares
Regression	.000	8	.000
Residual	.000	17	.000
Uncorrected Total	.000	25	
Corrected Total	.000	24	

Dependent variable: VFEA[a]

a. R squared = 1 - (Residual Sum of Squares) / (Corrected Sum of Squares) = .984.

REFERENCES

ACI Committee 440 (2007) **Report on Fiber-Reinforced Polymer (FRP) Reinforcement for Concrete Structures**. ACI 440R-07. USA: Farmington Hills

ACI Committee 440 (2008) **Guide for the Design and Construction of Externally Bonded FRP Systems for Strengthening Concrete Structures**. ACI 440.2R-08. USA: Farmington Hills

ACI Committee 446 (1997) **Finite Element Analysis of Fracture in Concrete Structures: State-of-the-Art**. ACI 446.3R-97. USA: Farmington Hills

Adhikary, B.B. and Mutsuyoshi, H. (2004) Behavior of Concrete Beams Strengthened in Shear with Carbon-Fiber Sheets. **ASCE Journal of Composites for Construction**, 8 (3): 258-264

Advisory Council of ASCE (2013) **Report Card for America's Infrastructure**. [online]. Available from: http://dx.doi.org/10.1061/9780784478837 [Accessed 11 May 2015]

Agapay, A. (2003) **Test of Prestressed Concrete T-Beams Retrofitted for Shear and Flexure Using Carbon Fiber Reinforced Polymers**. MSc thesis, University of Hawaii

Ahmed, S.M. and Gunasekaran, U. (2014) Testing and Evaluation of Reinforced Concrete Beam-Column-Slab Joint. **GRAĐEVINAR**, 66 (1): 21-36

Al-Mahaidi, R., Lee, K. and Taplin, G. (2001). "Behavior and Analysis of RC T-Beams Partially Damaged in Shear and Repaired with CFRP Laminates." In **Structures 2001: A Structural Engineering Odyssey. Washington, D.C., 21-23 May.**

Altin, S., Anil, Ö. and Kara, M.E. (2005) Improving Shear Capacity of Existing RC Beams Using External Bonding of Steel Plates. **Engineering Structures**, 27 (5): 781-791

Arduini, M., Tommaso, A.D. and Nanni, A. (1997) Brittle Failure in FRP Plate and Sheet Bonded Beams. **ACI Structural Journal**, 94 (4): 363-370

Ary, M.I. and Kang, T.H.-K. (2012) Shear-Strengthening of Reinforced & Prestressed Concrete Beams Using FRP: Part I - Review of Previous Research. **International Journal of Concrete Structures and Materials**, 6 (1): 41-47

ASCE-ACI Committee 426 (1973) The Shear Strength of Reinforced Concrete Members. **Journal of the Structural Division**, 99 (6): 1091-1187

ASCE-ACI Committee 445 (1998) Recent Approaches to Shear Design of Structural Concrete. **Journal of Structural Engineering**, 124 (12): 1375-1417

Asferg, J.L. (2006) **Modeling of Concrete Fracture Applying the eXtended Finite Element Method**. PhD thesis, Technical University of Denmark

Bakis, C.E., Bank, L.C., Brown, V.L. et al. (2002) Fiber-Reinforced Polymer Composites for Construction—State-of-the-Art Review. **ASCE Journal of Composites for Construction**, 6 (2): 73-87

Barnes, R.A., Baglin, P.S., Mays, G.C. et al. (2001) External Steel Plate Systems for the Shear Strengthening of Reinforced Concrete Beams. **Engineering Structures**, 23 (9): 1162-1176

Barros, J.A.O. and Dalfre, G.M. (2013) Assessment of the Effectiveness of the Embedded Through-Section Technique for the Shear Strengthening of Reinforced Concrete Beams. **Strain**, 49 (1): 75-93

Bathe, K.-J. (1996) **Finite Element Procedures**. New Jersey: Prentice Hall International.

Bažant, Z.P. and Cao, Z. (1986) Size Effect of Shear Failure in Prestressed Concrete Beams. **ACI Journal Proceedings**, 83 (2): 260-268

Bažant, Z.P. and Kim, J.-K. (1984) Size Effect in Shear Failure of Longitudinally Reinforced Beams. **ACI Journal Proceedings**, 81 (5): 456-468

Bažant, Z.P. and Oh, B.H. (1983) Crack Band Theory for Fracture of Concrete. **Materials and Structures**, 16 (3): 155-177

Bažant, Z.P. and Sun, H.-H. (1987) Size Effect in Diagonal Shear Failure: Influence of Aggregate Size and Stirrups. **ACI Materials Journal**, 84 (4): 259-272

Belarbi, A. and Acun, B. (2013) FRP Systems in Shear Strengthening of Reinforced Concrete Structures. **Procedia Engineering**, 57: 2-8

Belarbi, A., Bae, S.-W., Ayoub, A. et al. (2011) **Design of FRP Systems for Strengthening Concrete Girders in Shear**. NCHRP Report No. 678. Washington, D.C.: Transportation Research Board

Belytschko, T. and Black, T. (1999) Elastic Crack Growth in Finite Elements with Minimal Remeshing. **International Journal for Numerical Methods in Engineering**, 45 (5): 601-620

Bentz, E.C., Vecchio, F.J. and Collins, M.P. (2006) Simplified Modified Compression Field Theory for Calculating Shear Strength of Reinforced Concrete Elements. **ACI Structural Journal**, 103 (4): 614-624

Berset, J.-D. (1992) **Strengthening of Reinforced Concrete Beams for Shear Using FRP Composites**. MSc thesis, Massachusetts Institute of Technology

Bousselham, A. and Chaallal, O. (2004) Shear Strengthening Reinforced Concrete Beams with Fiber-Reinforced Polymer: Assessment of Influencing Parameters and Required Research. **ACI Structural Journal**, 101 (2): 219-227

Bousselham, A. and Chaallal, O. (2006) Behavior of Reinforced Concrete T-Beams Strengthened in Shear with Carbon Fiber-Reinforced Polymer—An Experimental Study. **ACI Structural Journal**, 103 (3): 339-347

Bousselham, A. and Chaallal, O. (2013) Experimental Investigations on the Influence of Size on the Performance of RC T-Beams Retrofitted in Shear with CFRP Fabrics. **Engineering Structures**, 56: 1070-1079

Breveglieri, M., Aprile, A. and Barros, J.A.O. (2015) Embedded Through-Section Shear Strengthening Technique Using Steel and CFRP Bars in RC Beams of Different Percentage of Existing Stirrups. **Composite Structures**, 126: 101-113

Carolin, A. (2001) **Strengthening of Concrete Structures with CFRP - Shear Strengthening and Full-Scale Applications**. PhD thesis, Lulea University of Technology

Carolin, A. and Täljsten, B. (2005) Experimental Study of Strengthening for Increased Shear Bearing Capacity. **ASCE Journal of Composites for Construction**, 9 (6): 488-496

Chaallal, O., Mofidi, A., Benmokrane, B. et al. (2011) Embedded Through-Section FRP Rod Method for Shear Strengthening of RC Beams: Performance and

Comparison with Existing Techniques. **ASCE Journal of Composites for Construction**, 15 (3): 374-383

Chaallal, O., Shahawy, M. and Hassan, M. (2002) Performance of Reinforced Concrete T-Girders Strengthened in Shear with Carbon Fiber-Reinforced Polymer Fabric. **ACI Structural Journal**, 99 (3): 335-343

Chen, G.-M. (2010) **Behaviour and Strength of RC Beams Shear-Strengthened with Externally Bonded FRP Reinforcement**. PhD thesis, The Hong Kong Polytechnic University

Chen, G.M., Chen, J.F. and Teng, J.G. (2012) On the Finite Element Modelling of RC Beams Shear-Strengthened with FRP. **Construction and Building Materials**, 32: 13-26

Chen, W.-F. (2007) **Plasticity in Reinforced Concrete**. USA: J. Ross Publishing.

Chen, W.-F. and Han, D.J. (1988) **Plasticity for Structural Engineers**. New York: Springer-Verlag Inc.

Collins, M.P., Bentz, E.C., Sherwood, E.G. et al. (2008) An Adequate Theory for the Shear Strength of Reinforced Concrete Structures. **Magazine of Concrete Research**, 60 (9): 635-650

Collins, M.P. and Mitchell, D. (1980) Shear and Torsion Design of Prestressed and Non-Prestressed Concrete Beams. **PCI Journal**, 25 (5): 32-100

Concrete Society (2000) **Design Guidance for Strengthening Concrete Structures Using Fibre Composite Materials**. Technical Report TR55. Crowthorne: The Concrete Society

Concrete Society (2012) **Design Guidance for Strengthening Concrete Structures Using Fibre Composite Materials**. Technical Report TR55. Camberley: The Concrete Society

Cosenza, E., Manfredi, G. and Realfonzo, R. (1997) Behavior and Modeling of Bond of FRP Rebars to Concrete. **ASCE Journal of Composites for Construction**, 1 (2): 40-51

Cosenza, E., Manfredi, G. and Realfonzo, R. (2002) Development Length of FRP Straight Rebars. **Composites Part B: Engineering**, 33 (7): 493-504

Deaton, J.B. (2013) **Nonlinear Finite Element Analysis of Reinforced Concrete Exterior Beam-Column Joints with Nonseismic Detailing**. PhD thesis, Georgia Institute of Technology

Devalapura, R.K. and Tadros, M.K. (1992) Stress-Strain Modeling of 270 ksi Low-Relaxation Prestressing Strands. **PCI Journal**, 37 (2): 100-106

Dirar, S. (2010) **Shear Strengthening of Pre-Cracked Reinforced Concrete T-Beams Using Carbon Fibre**. PhD thesis, University of Cambridge

Dirar, S., Lees, J. and Morley, C. (2012) Precracked Reinforced Concrete T-Beams Repaired in Shear with Bonded Carbon Fiber-Reinforced Polymer Sheets. **ACI Structural Journal**, 109 (2): 215-224

Dirar, S., Lees, J.M. and Morley, C. (2013a) Phased Nonlinear Finite-Element Analysis of Precracked RC T-Beams Repaired in Shear with CFRP Sheets. **ASCE Journal of Composites for Construction**, 17 (4): 476-487

Dirar, S., Lees, J.M. and Morley, C.T. (2013b) Precracked Reinforced Concrete T-Beams Repaired in Shear with Prestressed Carbon Fiber-Reinforced Polymer Straps. **ACI Structural Journal**, 110 (5): 855-866

Doran, D. and Cather, B. (2014) **Construction Materials Reference Book**. 2nd ed. New York: Routledge.

Eshwar, N., Nanni, A. and Ibell, T.J. (2008) Performance of Two Anchor Systems of Externally Bonded Fiber-Reinforced Polymer Laminates. **ACI Materials Journal**, 105 (1): 72-80

fib (1993) **CEB-FIP Model Code 1990**. CEB Bulletin No. 213/214. London: Thomas Telford Services Ltd

fib (2001) **Externally Bonded FRP Reinforcement for RC Structures: Technical Report on the Design and Use of Externally Bonded Fibre Reinforced Polymer Reinforcement (FRP EBR) for Reinforced Concrete Structures**. Technical Report Volume 14 of Bulletin. Switzerland: Fédération Internationale du Béton

fib (2008) **Practitioners' Guide to Finite Element Modelling of Reinforced Concrete Structures**. Technical Report Volume 45 of Bulletin. Switzerland: Fédération Internationale du Béton

fib (2012) **Model Code 2010 - Final draft: Volume 1**. Technical Report Volume 65 of Bulletin. Switzerland: Fédération Internationale du Béton

Fu, F. (2015) **Advanced Modelling Techniques in Structural Design**. United Kingdom: John Wiley & Sons Ltd.

Gale, L. and Ibell, T.J. (2000) Effects of Compression Reinforcement on the Shear Strength of Reinforced Concrete Bridge Beams. **Magazine of Concrete Research**, 52 (4): 275-285

Godat, A. (2008) **Finite Element Modelling of Externally Shear-Strengthened Beams Using Fibre Reinforced Polymers**. PhD thesis, University of Sherbrooke

Godat, A., Chaallal, O. and Neale, K.W. (2013) Nonlinear Finite Element Models for the Embedded Through-Section FRP Shear-Strengthening Method. **Computers and Structures**, 119: 12-22

Godat, A., L'Hady, A., Chaallal, O. et al. (2012a) Bond Behavior of the ETS FRP Bar Shear-Strengthening Method. **ASCE Journal of Composites for Construction**, 16 (5): 529-539

Godat, A., Labossière, P. and Neale, K.W. (2012b) Numerical Investigation of the Parameters Influencing the Behaviour of FRP Shear-Strengthened Beams. **Construction and Building Materials**, 32: 90-98

Godat, A., Labossière, P., Neale, K.W. et al. (2012c) Behavior of RC Members Strengthened in Shear with EB FRP: Assessment of Models and FE Simulation Approaches. **Computers and Structures**, 92–93: 269-282

Godat, A., Neale, K.W. and Labossière, P. (2007) Numerical Modeling of FRP Shear-Strengthened Reinforced Concrete Beams. **ASCE Journal of Composites for Construction**, 11 (6): 640-649

Godat, A., Qu, Z., Lu, X.Z. et al. (2010) Size Effects for Reinforced Concrete Beams Strengthened in Shear with CFRP Strips. **ASCE Journal of Composites for Construction**, 14 (3): 260-271

Gopalaratnam, V.S. and Shah, S.P. (1985) Softening Response of Plain Concrete in Direct Tension. **ACI Journal Proceedings**, 82 (3): 310-323

Greunen, J.V. and Scordelis, A.C. (1983) Nonlinear Analysis of Prestressed Concrete Slabs. **ASCE Journal of Structural Engineering**, 109 (7): 1742-1760

Hee, S.C. and Jefferson, A.D. (2008) A New Model for Simulating Cracks in Cementitious Composites. **Engineering and Computational Mechanics**, 161 (1): 3-16

Hendriks, M.A.N. and Rots, J.G. (2002) **Finite Elements in Civil Engineering Applications: Proceedings of the Third Diana World Conference, Tokyo, Japan, 9-11 October 2002**. Tokyo: A. A. Balkema. pp. 17-28

Holicky, M., Markova, J. and Sykora, M. (2010) "Assessment of Deteriorating Reinforced Concrete Road Bridges." In Bris, R., Soares, C.G. and Martorell, S. (ed.) **Reliability, Risk, and Safety: Theory and Applications.** London: Taylor and Francis. pp. 1377-1383

Hutchinson, R.L. (1999) **The Use of Externally Bonded CFRP Sheets for Shear Strengthening of I-Shaped Prestressed Concrete Bridge Girders**. PhD thesis, University of Manitoba

Ibell, T.J., Morley, C.T. and Middleton, C.R. (1996) **Background to and Developments in Shear in Reinforced Concrete**. Technical Report No. CUED/D-Struct/TR 151. Cambridge: University of Cambridge

Jalali, M., Sharbatdar, M.K., Chen, J.-F. et al. (2012) Shear Strengthening of RC Beams Using Innovative Manually Made NSM FRP Bars. **Construction and Building Materials**, 36: 990-1000

Jeong, J.-P. and Kim, W. (2014) Shear Resistant Mechanism into Base Components: Beam Action and Arch Action in Shear-Critical RC Members. **International Journal of Concrete Structures and Materials**, 8 (1): 1-14

Kaliakin, V.N., Chajes, M.J. and Januszka, T.F. (1996) Analysis of Concrete Beams Reinforced with Externally Bonded Woven Composite Fabrics. **Composites Part B: Engineering**, 27 (3-4): 235-244

Kang, T.H.-K. and Ary, M.I. (2012) Shear-Strengthening of Reinforced & Prestressed Concrete Beams Using FRP: Part II - Experimental Investigation. **International Journal of Concrete Structures and Materials**, 6 (1): 49-57

Kani, G.N.J. (1964) The Riddle of Shear Failure and Its Solution. **ACI Journal Proceedings**, 61 (4): 441-468

Kani, G.N.J. (1966) Basic Facts Concerning Shear Failure. **ACI Journal Proceedings**, 63 (6): 675-692

Kani, G.N.J. (1967) How Safe are Our Large Reinforced Concrete Beams? **ACI Journal Proceedings**, 64 (3): 128-141

Kani, M.W., Huggins, M.W., Kani, G. et al. (1979) **Kani on Shear in Reinforced Concrete**. Toronto: University of Toronto.

Kaw, A.K. (2006) **Mechanics of Composite Materials**. 2nd ed. Boca Raton: Taylor & Francis Group.

Kesse, G. (2003) **Concrete Beams with External Prestressed Carbon FRP Shear Reinforcement**. PhD thesis, University of Cambridge

Khalifa, A., Alkhrdaji, T., Nanni, A. et al. (1999) Anchorage of Surface Mounted FRP Reinforcement. **Concrete International: Design and Construction**, 21 (10): 49-54

Khalifa, A., Gold, W.J., Nanni, A. et al. (1998) Contribution of Externally Bonded FRP to Shear Capacity of Flexural Members. **ASCE Journal of Composites for Construction**, 2 (4): 195-203

Khalifa, A. and Nanni, A. (2002) Rehabilitation of Rectangular Simply Supported RC Beams with Shear Deficiencies Using CFRP Composites. **Construction and Building Materials**, 16 (3): 135-146

Kim, Y., Quinn, K., Satrom, N. et al. (2012) **Shear Strengthening of Reinforced and Prestressed Concrete Beams Using Carbon Fiber Reinforced Polymer (CFRP) Sheets and Anchors**. Report No. FHWA/TX-12/0-6306-1. Austin: Texas Department of Transportation

Kotsovos, M.D. (1987) Shear Failure of Reinforced Concrete Beams. **Engineering Structures**, 9 (1): 32-38

Kuchma, D.A. and Collins, M.P. (1998) Advances in Understanding Shear Performance of Concrete Structures. **Progress in Structural Engineering and Materials**, 1 (4): 360-369

Kwak, H.-G. and Filippou, F.C. (1990) **Finite Element Analysis of Reinforced Concrete Structures under Monotonic Loads**. Report No. UCB/SEMM-90/14. Berkeley: California Department of Transportation

Leung, C.K.Y., Chen, Z., Lee, S. et al. (2007) Effect of Size on the Failure of Geometrically Similar Concrete Beams Strengthened in Shear with FRP Strips. **ASCE Journal of Composites for Construction**, 11 (5): 487-496

Lorenzis, L.D. and Teng, J.G. (2007) Near-Surface Mounted FRP Reinforcement: An Emerging Technique for Strengthening Structures. **Composites Part B: Engineering**, 38 (2): 119-143

Lu, X.Z., Teng, J.G., Ye, L.P. et al. (2005) Bond-Slip Models for FRP Sheets/Plates Bonded to Concrete. **Engineering Structures**, 27 (6): 920-937

Madenci, E. and Guven, I. (2015) **The Finite Element Method and Applications in Engineering Using ANSYS**. 2nd ed. New York: Springer.

Mander, J.B., Priestley, M.J.N. and Park, R. (1988) Observed Stress-Strain Behavior of Confined Concrete. **ASCE Journal of Structural Engineering**, 114 (8): 1827-1849

Mang, H.A., Lackner, R., Meschke, G. et al. (2003) "Chapter 3.10: Computational Modeling of Concrete Structures." In Milne, I., Ritchie, R.O. and Karihaloo, B. (ed.) **Comprehensive Structural Integrity**. Elsevier Science Ltd. pp. 541-606

Middleton, C.R. (1997) Concrete Bridge Assessment: An Alternative Approach. **The Structural Engineer**, 75 (23/24): 403-409

Middleton, C.R. (2004). "Bridge Management and Assessment in the UK." In **5th Austroads Bridge Conference. Sydney, 19-24 May.**

Miller, A., Rosenboom, O. and Rizkalla, S. (2007). "Repair of Prestressed Concrete Bridge Girders with FRP." In **FRPRCS-8. Patras, 16-18 July.**

Moës, N., Dolbow, J. and Belytschko, T. (1999) A Finite Element Method for Crack Growth without Remeshing. **International Journal for Numerical Methods in Engineering**, 46 (1): 131-150

Mofidi, A., Chaallal, O., Benmokrane, B. et al. (2012) Experimental Tests and Design Model for RC Beams Strengthened in Shear Using the Embedded Through-Section FRP Method. **ASCE Journal of Composites for Construction**, 16 (5): 540-550

Moradi, S. and Alam, M.S. (2015) Finite-Element Simulation of Posttensioned Steel Connections with Bolted Angles under Cyclic Loading. **ASCE Journal of Structural Engineering**, 142 (1): 04015075

Morsch, E. (1909) **Der Eisenbetonbau (Published in English as Concrete-Steel Construction)**. 3rd ed. New York: Engineering News Publishing.

Moslehy, Y. (2010) **Constitutive Relationships and Smart Aggregate-Based Damage Evaluation of FRP Retrofitted Concrete Membrane Elements**. PhD thesis, University of Houston

Murphy, M., Belarbi, A. and Bae, S.-W. (2012) Behavior of Prestressed Concrete I-Girders Strengthened in Shear with Externally Bonded Fiber-Reinforced-Polymer Sheets. **PCI Journal**, 57 (3): 63-82

Nanni, A., Ludovico, M.D. and Parretti, R. (2004) Shear Strengthening of a PC Bridge Girder with NSM CFRP Rectangular Bars. **Advances in Structural Engineering**, 7 (4): 97-109

Ngo, D. and Scordelis, A.C. (1967) Finite Element Analysis of Reinforced Concrete Beams. **ACI Journal Proceedings**, 64 (3): 152-163

Nielsen, M.P., Braestrup, M.W. and Bach, F. (1978). "Rational Analysis of Shear in Reinforced Concrete Beams." In **IABSE Proceedings P-15/78. Zürich.**

Nilson, A.H. (1968) Nonlinear Analysis of Reinforced Concrete by the Finite Element Method. **ACI Journal Proceedings**, 65 (9): 757-766

Nilson, A.H. (1987) **Design of Prestressed Concrete**. 2nd ed. Canada: John Wiley & Sons Inc.

Niu, H. and Wu, Z. (2006) Effects of FRP-Concrete Interface Bond Properties on the Performance of RC Beams Strengthened in Flexure with Externally Bonded

FRP Sheets. **ASCE Journal of Materials in Civil Engineering**, 18 (5): 723-731

Park, H. and Kim, J.-Y. (2005) Plasticity Model using Multiple Failure Criteria for Concrete in Compression. **International Journal of Solids and Structures**, 42 (8): 2303-2322

Park, R. and Paulay, T. (1975) **Reinforced Concrete Structures**. Canada: John Wiley & Sons Inc.

Pellegrino, C. and Modena, C. (2002) Fiber Reinforced Polymer Shear Strengthening of Reinforced Concrete Beams with Transverse Steel Reinforcement. **ASCE Journal of Composites for Construction**, 6 (2): 104-111

Petty, D.A., Barr, P.J., Osborn, G.P. et al. (2011) Carbon Fiber Shear Retrofit of Forty-Two-Year-Old AASHTO I-Shaped Girders. **ASCE Journal of Composites for Construction**, 15 (5): 773-781

Punmia, B.C., Jain, A.K. and Jain, A.K. (2007) **Limit State Design of Reinforced Concrete**. New Delhi: Laxmi Publications.

Qin, S., Dirar, S., Yang, J. et al. (2014) CFRP Shear Strengthening of Reinforced-Concrete T-Beams with Corroded Shear Links. **ASCE Journal of Composites for Construction**, 19 (5): 04014081

Rajagopalan, N. (2002) **Prestressed Concrete**. UK: Alpha Science International Ltd.

Rashid, Y.R. (1968) Ultimate Strength Analysis of Prestressed Concrete Pressure Vessels. **Nuclear Engineering and Design**, 7 (4): 334-344

Raval, S.S. and Dave, U.V. (2013) Effectiveness of Various Methods of Jacketing for RC Beams. **Procedia Engineering**, 51: 230-239

Reed, C.E. and Peterman, R.J. (2004) Evaluation of Prestressed Concrete Girders Strengthened with Carbon Fiber Reinforced Polymer Sheets. **ASCE Journal of Bridge Engineering**, 9 (2): 185-192

Remmel, G. (1994) **Zum Zug- und Schubtragverhalten von Bauteilen aus hochfestem Beton**. Report No. 444. Berlin: Deutscher Ausschuss für Stahlbeton

Ritter, K.W. (1899) Die Bauweise Hennebique (The Hennebique Construction Method). **Schweizerische Bauzeitung**, 33 (7): 59-61

Rots, J.G. and Blaauwendraad, J. (1989) Crack Models for Concrete, Discrete or Smeared? Fixed, Multi-Directional or Rotating?. **HERON**, 34 (1): 1-59

Rust, W. (2015) **Non-Linear Finite Element Analysis in Structural Mechanics**. Switzerland: Springer International Publishing.

Sagaseta, J. and Vollum, R.L. (2009) Non-Linear Finite Element Analysis of Shear Critical High Strength Concrete Beams. **ACEE**, 2 (4): 95-106

Sato, Y. and Vecchio, F.J. (2003) Tension Stiffening and Crack Formation in Reinforced Concrete Members with Fiber-Reinforced Polymer Sheets. **ASCE Journal of Structural Engineering**, 129 (6): 717-724

Sayed, A.M., Wang, X. and Wu, Z. (2013) Modeling of Shear Capacity of RC Beams Strengthened with FRP Sheets Based on FE Simulation. **ASCE Journal of Composites for Construction**, 17 (5): 687-701

Schlaich, J., Schafer, K. and Jennewein, M. (1987) Toward a Consistent Design of Structural Concrete. **PCI Journal**, 32 (3): 74-150

Schnerch, D.A. (2001) **Shear Behavior of Large-Scale Concrete Beams Strengthened with Fibre Reinforced Polymer (FRP) Sheets**. MSc thesis, University of Manitoba

Selby, R.G. and Vecchio, F.J. (1997) A Constitutive Model for Analysis of Reinforced Concrete Solids. **Canadian Journal of Civil Engineering**, 24 (3): 460-470

Shumacher, E.G. (1961) **Ultimate Strength of Prestressed Concrete Beams in Shear**. PhD thesis, University of Leeds

Silhavy, R., Silhavy, P., Prokopova, Z. et al. (2012) **Computer Software and Hardware Applications**. Czech Republic: Silhavy sro.

Stratford, T. and Burgoyne, C. (2003) Shear Analysis of Concrete with Brittle Reinforcement. **ASCE Journal of Composites for Construction**, 7 (4): 323–330

Swamy, R.N. and Andriopoulos, A.D. (1974) Contribution of Aggregate lnterlock and Dowel Forces to the Shear Resistance of Reinforced Beams with Web Reinforcement. **ACI Special Publication**, 42: 129-166

Taljsten, B. (2003) Strengthening Concrete Beams for Shear with CFRP Sheets. **Construction and Building Materials**, 17 (1): 15-26

Taylor, H.P.J. (1974) The Fundamental Behavior of Reinforced Concrete Beams in Bending and Shear. **ACI Special Publication**, 42: 43-78

Teng, J.G., Lam, L. and Chen, J.F. (2004) Shear Strengthening of RC Beams with FRP Composites. **Progress in Structural Engineering and Materials**, 6 (3): 173-184

Thorenfeldt, E., Tomaszewicz, A. and Jensen, J.J. (1987). "Mechanical Properties of Highstrength Concrete and Applications in Design." In **Utilization of High-Strength Concrete. Stavanger, 15-18 June.**

TNO DIANA BV (2012) **DIANA User's Manual (Release 9.4.4)**. Delft, The Netherlands: TNO DIANA BV.

Triantafillou, T.C. (1998) Shear Strengthening of Reinforced Concrete Beams Using Epoxy-Bonded FRP Composites. **ACI Structural Journal**, 95 (2): 107-115

Tsai, S.W. (1963) **Structural Behavior of Composite Materials**. First Quarterly Technical Report No. U-2122. Washington, D.C.: NASA

Valerio, P. (2009) **Realistic Shear Assessment and Novel Strengthening of Existing Concrete Bridges**. PhD thesis, University of Bath

Valerio, P. and Ibell, T.J. (2003) Shear Strengthening of Existing Concrete Bridges. **Structures and Buildings**, 156 (1): 75-84

Valerio, P., Ibell, T.J. and Darby, A.P. (2009) Deep Embedment of FRP for Concrete Shear Strengthening. **Structures and Buildings**, 162 (5): 311-321

Van der Linde, W.B. (2015) **Structural Reliability of Seismic Design Methodologies for Shear Walls and Distributors in RC Buildings - APPENDICES**. MSc thesis, Delft University of Technology

Vecchio, F.J. and Bucci, F. (1999) Analysis of Repaired Reinforced Concrete Structures. **ASCE Journal of Structural Engineering**, 125 (6): 644-652

Vecchio, F.J. and Collins, M.P. (1986) The Modified Compression-Field Theory for Reinforced Concrete Elements Subjected to Shear. **ACI Journal Proceedings**, 83 (2): 219-231

Vecchio, F.J. and Collins, M.P. (1993) Compression Response of Cracked Reinforced Concrete. **ASCE Journal of Structural Engineering**, 119 (12): 3590-3610

Walraven, J.C. (1978) **Influence of Member Depth on the Shear Strength of Lightweight Concrete Beams without Shear Reinforcement**. Report No. 5-78-4. Stevin Laboratory: Delft University of Technology.

Walraven, J. and Lehwalter, N. (1994) Size Effects in Short Beams Loaded in Shear. **ACI Structural Journal**, 91 (5): 585-593

Wang, P.T., Shah, S.P. and Naaman, A.E. (1978) Stress-Strain Curves of Normal and Lightweight Concrete in Compression. **ACI Journal Proceedings**, 75 (11): 603-611

Wong, R.S.Y. and Vecchio, F.J. (2003) Towards Modeling of Reinforced Concrete Members with Externally Bonded Fiber-Reinforced Polymer Composites. **ACI Structural Journal**, 100 (1): 47-55

Xanthakos, P.P. (1996) **Bridge Strengthening and Rehabilitation**. New Jersey: Prentice Hall PTR.

You, Y.-M., Ayoub, A. and Belarbi, A. (2011) Three-Dimensional Nonlinear Finite-Element Analysis of Prestressed Concrete Beams Strengthened in Shear with FRP Composites. **ASCE Journal of Composites for Construction**, 15 (6): 896-907

Zakaria, M., Ueda, T., Wu, Z. et al. (2009) Experimental Investigation on Shear Cracking Behavior in Reinforced Concrete Beams with Shear Reinforcement. **Journal of Advanced Concrete Technology**, 7 (1): 79-96

Zienkiewicz, O.C. and Taylor, R.L. (2000) **The Finite Element Method - Volume 2: Solid Mechanics**. 5th ed. Oxford: Butterworth-Heinemann.

Zong, Z.-H., Cheng, Y., Huang, X.-Y. et al. (2013) Experimental Study on Shear Properties of Reinforced Concrete (RC) and Partial Prestressed Concrete (PPC) Beams Strengthened with Externally Bonded CFRP Strips. **Engineering Mechanics**, 30 (6): 236-246